THE POTENTIAL OF MULTI-SENSOR SATELLITE DATA FOR APPLICATIONS IN ENVIRONMENTAL MONITORING WITH SPECIAL EMPHASIS ON LAND COVER MAPPING, DESERTIFICATION MONITORING AND FIRE DETECTION

Dissertation zur Erlangung des Doktorgrades der Fakultät für Biologie der Ludwig-Maximilians-Universität München

vorgelegt von

Shengli Huang

Department II – GeoBio-Center
Ludwig-Maximilians-Universität
Großhadener Str. 2
82152 Planegg-Martinsried
Deutschland

1. Gutachter: Prof. Dr. Florian Siegert
2. Gutachter: Prof. Dr. Sebastian Diehl

Tag der mündlichen Prüfung: 08.04.2005

SUMMARY

Unprecedented pressure on the physical, chemical and biological systems of the Earth results in environment problems locally and globally, therefore the detection and understanding of environmental change based on long-term environmental data is very urgent. In developing countries/regions, because the natural resources are depleted for development while environmental awareness is poor, environment is changing faster. The insufficient environmental investment and sometimes infeasible ground access make the environment information acquisition and update inflexible through standard methods. With the main advantages of global observation, repetitive coverage, multispectral sensing and low-cost implementation, satellite remote sensing technology is a promising tool for monitoring environment, especially in the less developed countries.

Multi-sensor satellite images may provide increased interpretation capabilities and more reliable results since data with different characteristics are combined and can achieve improved accuracies, better temporal coverage, and better inference about the environment than could be achieved by the use of a single sensor alone. The objective of this thesis is to demonstrate the capability and technique of the multi-sensor satellite data to monitor the environment in developing countries. Land cover assessment of Salonga national park in the democratic republic of Congo of Africa, desertification monitoring in North China and tropical/boreal wildland fire detection in Indonesia/Siberia were selected as three cases in this study for demonstrating the potential of multi-sensor application to environment monitoring.

Chapter 2 demonstrates the combination of Landsat satellite images, Global Position System (GPS) signals, aerial videos and digital photos for assessing the land cover of Salonga national park in Congo. The purpose was to rapidly assess the current status of Salonga national park, especially its vegetation, and investigated the possible human impacts by shifting cultivation, logging and mining. Results show that the forests in the Salonga national park are in very good condition. Most of the area is covered by undisturbed, pristine evergreen lowland and swamp forests. No logging or mining activity could be detected.

Chapter 3 demonstrates the one full year time series SPOT VEGETATION with coarse resolution of 1 km and the ASTER images with higher resolution of 15 meters as well as Landsat images for land cover mapping optimised for desertification monitoring in North-China. One point six million km^2 were identified as risk areas of desertification. Results show within a satellite based multi-scale monitoring system SPOT VEGETATION imagery can be very useful to detect large scale dynamic environmental changes and desertification processes which then can be analysed in more detail by high resolution imagery and field surveys.

Chapter 4 demonstrates the detection of tropical forest fire and boreal forest fire. Firstly, the ENVISAT ASAR backscatter dynamics and ENVISAT full resolution MERIS characteristics of fire scars were investigated in Siberian boreal forest, and results show these two sensors are very useful for fire monitoring and impact assessment. Secondly, the general capability and potential of ENVISAT multi-sensor of MERIS, AATSR, ASAR as well as NOAA-AVHRR and MODIS for tropical forest fire event monitoring and impact assessment in tropical Indonesia were investigated, and results show the capability of ENVISAT to acquire data from different sensors simultaneously or within a short period of time greatly enhances the possibilities to monitor fire occurrence and assess fire impact. Finally, the multi-sensor technology was applied to the disastrous boreal forest fire event of 2003 around East and West Lake Baikal in Siberia, and results show that 202,000 km^2 burnt in 2003 within the study area of 1,300,000 km^2, which is more than the total burnt area between 1996-2002. 71.4% of the burnt areas were forests, and 11.6% were wetlands or bogs. In total 32.2% of the forest cover has been burnt at least once from 1996 to 2003, 14% of the area has been affected at least twice by fire.

These demonstrations show that in spite of the two disadvantages of indirect satellite measurements and the difficulty of detecting the cause of environment change, multi-sensor satellite technology is very useful in environment monitoring. However more studies on multi-sensor data fusion methods are needed for integrating the different satellite data from various sources. The lack of personnel skilled in remote sensing is a severe deficiency in developing countries, so the technology transfer from the developed countries is needed.

ACKNOWLEDGEMENTS

I am very grateful to many individuals who have helped and supported me through my doctoral study in Munich University (Ludwig-Maximilians-Universität München, LMU). First of all, I would like to express my thanks to professor Dr. Florian Siegert for advising this thesis and mentoring me throughout my three years at Munich university and remote sensing solutions Gmbh. Were it not for his excellent guidance and encouragement, his patience in discussing my questions, his original suggestions for some solutions during my Ph.D. work, I would not have finished the Ph.D. work smoothly. His broad knowledge and deep insights have been an important resource to my accomplishment.

I would like to thank ESA/ESRIN for free ENVISAT data provision in the framework of ENVISAT AO 689 (08-03/ENVISAT-Siberia), to the EU 5th Framework Programme (INCO-DEV project STRAPEAT) for field data collection in Indonesia, to European Commission Joint Research Centre for SPOT VEGETATION data provision. Additionally, thanks to Don Cahoon for providing data for the comparative assessment of the 1987 fires and Chris Schmullius for providing forest cover maps.

How to thank the many colleagues in the company of remote sensing solutions Gmbh who have helped me in very substantial ways? Ruth Leska, Andreas Langner, Annette Bechteler, Oelaf Kranz, Robert Lanz, Stefan Einsiedel, Cornelia Merk, Jukka Miettinen, Michael Schulze-Horsel have helped me so much in both research work and daily life. In processing data, searching literatures, repairing hardware/software, visa application, living place searching, they provided unbelievable help in all aspects. My work and life here in Germany would have been a hundred times harder if not for their excellent contributions. Special thanks to René Beuchle, who is now in Global Vegetation Monitoring Unit (GVM) of Institute for Environment and Sustainability (IES) in Joint Research Centre of the European Commission (JRC), for his advice and help before he left the company. Thanks also to Dr. Steffen Kuntz for his initial help when I began the study.

Throughout my time at Munich, I have had several very positive interactions with other scientists who helped me in project implement, publication cooperation, course training, data dissemination, ground survey and academic conference. Thanks to all these people: Claudia Roeben (Zoology institute, Department Biologie II, Munich university, Germany), Claudius Mott (Lehrstuhl für Landnutzungsplanung und Naturschutz der Technical university Munich, Limnologische Station Iffeldorf, Germany), Gernot Ruecker (ZEBRIS GbR, Germany), Johann G. Goldammer (The Global Fire Monitoring Center, Fire Ecology Research Group, Max Planck Institute for Chemistry, Germany), Anatoly Sukhinin (Sukachev Institute of Forest Research Akademgorodok, Krasnoyarsk, Russia), Adi

Jaya (University of Palangka Raya, Indonesia), Hans-Jurgen STIBIG and Etienne Bartholome (Joint Research Centre of the European Commission, Italy), Sabrina Bonaventura (Europeau Space Agency, Italy), Maurizio Santoro (Institute of Geography, Department of Geoinformatics, Friedrich-Schiller-University Jena, Germany), Andreas Wimmer (Joannum Research, Institute for Digital Image Processing, Austria), Lenny Christy and Nanang Hayani (Integrated Forest Fire Management Project (IFFM)/GTZ, Indonesia). Thanks also to my former Chinese supervisor and colleague, professor Jiulin Sun and Mrs. Yanzhen Yue (Geography institute of Chinese Academy of Sciences) and professor Zengyuan Li (Chinese Academy of Forestry).

Last but definitely not least, many many thanks to family, relatives and friends. To my wife for her genuine love, her unselfish support and her hard but excellent care for our daughter while I am far away from home. Without her position as a backbone in our family in remote China, it is impossible for me to finish the thesis. To my father and mother in law for their encouragement and support in these three years. To my foreign friends Alexander, Noemi, Christopher as well as Chinese friends Zhu Hao, Zhou Jiayang, Yang Feikun, Zhu Feng and so on for their friendship.

I dedicate this thesis to my family and friends for their love and support. May all the nice people who are acknowledged here be happy every day.

20 December 2004

Shengli Huang

TABLE OF CONTENTS

CHAPTER 1---INTRODUCTION

Environmental monitoring at all geographical scales is urgently needed for understanding the environmental change caused by the unprecedented pressure on the Earth, especially in developing countries. With the main advantages of global observation, repetitive coverage, multispectral sensing and low-cost implementation, satellite remote sensing technology is a promising tool for monitoring environment. However, for many applications the information provided by individual sensors are incomplete, inconsistent, or imprecise while multi-sensor satellite images are more useful because multi-sensor images give a more complete view of the observed objects in spectral, spatial and temporal dimension. The objective of this thesis was to investigate the potential of multisensor satellite remote sensing to monitor and assess the changing environment in developing countries. The thesis focused on three different issues of global importance: land cover mapping, desertification monitoring, and wildland fire detection.

1-1. Environmental monitoring by satellites

Over the last 200 years, unprecedented pressure has resulted in environmental problems on the physical, chemical and biological systems which support life on Earth (Singh, 1996). The increasing pace and extent of environmental change over the last decades of the 20th century has given a new urgency and relevance to the detection and understanding of environmental change (Parr *et al*., 2003). Concerns over issues such as biodiversity loss, atmospheric pollution, desertification, global fire burning, land use change, sustainable development and climate change have highlighted the need for environmental monitoring (Urquhart *et al*., 1998; Oldfield and Dearing, 2003). Jacobson and Price (1990) identified seven topics of research central to understanding the interactions of human activities and the environment and stated: "Research must be conducted at all geographical scales and should include the past as well as the present and the future." This task is especially important in developing countries.

Developing countries/regions account for nearly 80% of the human population in the world. The challenge for the developing countries clearly lies in the economic development and poverty alleviation but not in the protection of the environment. The poor people depend on natural resources for their livelihoods while there is rarely environmental awareness, thus resulting in the depletion of natural resources and damage to the environment (Wehrmeyer and Mulugetta, 1999). For example nearly 14 million hectares of natural tropical forests are destroyed every year mainly in tropical developing countries (Wehrmeyer and Mulugetta, 1999). This massive and irreversible destruction is mainly due to the expansion of the agricultural frontier in order to accommodate growing numbers of

people in extreme poverty or agricultural production for the rich countries (Centeno, 2002). To know the environment status and protect it, long-term data, including the environmental information of where, when, what, how and why, are required and need to be updated frequently.

A wealth of high-quality long-term data about the environment are being gathered worldwide and these data are vital for informing us about the state of the Earth's terrestrial land. Environment change quickly with the human activities, and most environmental monitoring applications hinge on the timely availability of data on the state and evolution of the system of interest (Verstraete *et al*., 1996). However, due to the poor environmental awareness, fund shortage and technological obstacles, the environment monitoring in developing countries/regions is far away from the need, and sometimes the unstable political situation such as war hinders the monitoring activities *in situ* (Wehrmeyer and Mulugetta, 1999), therefore the environmental data are always absent and difficult to update.

Satellite remote sensing technology provides a promising tool for environmental monitoring, especially in developing countries. On 4 October 1957, the form Soviet Union launched the first successful Earth satellite, Sputnik 1, and provided first space views of our planet's surface and atmosphere. After 123 days the first successful U.S. satellite, Explorer 1, was launched. On 23 July 1972 Landsat 1, called Earth Resources Technology Satellite (ERTS), was launched. Landsat program was designed for land remote sensing with extremely high resolution with 80 m in first satellite and up to 30 m and 15 m in the lasted one. Since 1972 when the first of the Landsat series of satellites was launched, the science of remote sensing has developed rapidly and plentiful satellite systems have been launched. Stoney (2002) summarized the technical characteristics of 31 land observation satellites by the year 2000 and described the 37 satellites planned for the period from 2000 through 2006.

Satellite remote sensing is the science and art of obtaining information about an object, area, or phenomenon through the analysis of data acquired by a device that is not in contact with the object, area, or phenomenon under investigation (Lilesand and Kiefer, 1994). Remote sensing depends upon measuring some kind of energy that is emitted, transmitted, or reflected from an object in order to determine certain physical properties of the object (Lilesand and Kiefer, 1994). Although detailed measurements could and should be acquired *in situ*, remote sensing from space platforms appears to be the only economically feasible way to repetitively gather information over large areas with a high spatial, spectral, and temporal resolution (Verstraete *et al*., 1996). Various international committees have identified satellite remote sensing as a unique and essential tool to repetitively acquire environmental data at spatial, temporal, and spectral resolutions appropriate to investigate environmental issues (IGBP, 1992).

Depending on the particular needs, data can be acquired over a range of spatial scales from local to global, with a spatial resolution of 1 m to 100 km. Some of these data have been acquired over a period of many years with a temporal resolution from hours to a few weeks, in a variety of spectral bands. It is becoming increasingly recognized that remote sensing in conjunction with ground-based observations would provide the best approach to implement some environmental activities (Singh, 1996). The United Nations Conference on Environment and Development (UNCED) clearly envisaged that: "Countries and international organizations should make use of new techniques of data collection, including satellite based remote sensing." (UNCED, 1992). It is the advantage of satellite remote sensing technique that makes it promising in environmental monitoring.

Remotely sensed satellite data and images of the Earth have several important advantages compared to ground observations:

1.) Synoptic view to achieve global observation. Satellite images are 'big-picture' views of large areas of the surface, which may be difficult (slow, expensive, dangerous, politically awkward) to measure *in situ*, in a short period of time, allowing a virtually instantaneous 'snapshot' to be obtained. It is the only practical way to obtain data from inaccessible regions, e.g. primitive forest. The positions, distribution, and spatial relationships of features are clearly evident from space.

2.) Repetitive coverage to obtain uniform and reproducible, periodical and continuous observation. Repeated images of the same regions, taken at regular intervals over periods of days, years, and decades, provide data bases for recognizing and measuring environmental changes. This is crucial for understanding where, when, and how the modern environment is changing.

3.) Multispectral data. Satellite sensors are designed to operate in many different portions of the electromagnetic spectrum. Ultraviolet, visible, infrared, and microwave energy coming from the Earth's surface or atmosphere contain a wealth of information about material composition and physical conditions.

4.) Low-cost data. Near-global, repetitive collection of data is far cheaper using satellite sensors than collecting the same type and quantity of data through conventional ground surveys. It is a relatively cheap and rapid method of acquiring up-to-date information over a large geographical area and constructing base maps in the absence of detailed land surveys.

5.) Digital processing. Most remote sensing systems now generate digital data which can be easily manipulated in a computer and combined with other geographic coverage in the Geographical Information System (GIS) as well as being shared.

6.) Feasible validation. The satellite measurements can be calibrated by using simultaneously observed ground truth data.

All these advantages prompt the satellite remote sensing to be used widely. In many different research fields satellite remote sensing has been applied to monitor and assess the status and condition of the environment. The terrestrial sciences community has made extensive use of satellite image data for mapping land cover, estimating geophysical and biophysical characteristics of terrain features, and monitoring environment changes. Ehrlich *et al*. (1994) reviewed many of the reported findings associated with defining the capabilities of National Oceanic and Atmospheric Administration's (NOAA) AVHRR 1 km data to provide global land cover information; Goward (1989) discussed the current and future role of satellite image data for contributing to studies of bioclimatology; Tucker *et al*. (1991) used coarse-resolution satellite image data for monitoring continental-scale climate-related phenomena; Colwell and Sadowski (1993) used high-resolution satellite data for monitoring regional patterns and rates of forest resource utilization; Freeman and Fox (1994) discussed the semi-operational use of satellite image data by several forest assessment programs.

Satellite data have been used in many earth observation programmes. In 1983, the planning for the National Aeronautics and Space Administration (NASA) Earth Observing System (EOS) began. In 1988 and 1989 an announcement of opportunity was issued (Asrar and Dokken, 1993). Following this activity, many sensors are operational such as Moderate Resolution Imaging Spectroradiometer (MODIS), Advanced Spaceborne Thermal Emission and Reflection (ASTER) etc. Using the available satellite data, humans understand the environment of our Earth much better than before. At global scale, Intergovernmental Panel on Climate Change (IPCC) takes seven major geophysical and biological phenomena to monitor: water and energy cycles, oceans, chemistry of the troposphere and lower stratosphere, land surface hydrology and ecosystem processes, glaciers and polar ice sheets, chemistry of the middle and upper stratosphere, and solid earth. Satellite data are key information for these activities (Hobish, 2002). The central goal of the United States Global Change Research Program (USGCRP) is to establish the scientific basis in support of national and international policy-making relating to natural and human-induced changes in the global Earth system with satellite as a key information source (Running *et al*., 1994; CEES 1992). In addition, coarse resolution satellite data have been used extensively to map global or regional land cover using Advanced Very High Resolution Radiometer (AVHRR), MODIS, SPOT VEGETATION etc. (Cihlar, 2000; DeFries and Townshend, 1999; Loveland *et al*., 2000; Hansen *et al*., 2000; Friedl *et al*., 2002; Strahler *et al*., 1999). At regional or country scale, the National Land Cover Project of China collected Landsat 7 ETM+ images acquired in 1999 and 2000 and generated a thematic map of land cover/use with 25 types at a scale of 1:100,000 (Boles *et al*., 2004).

Currently there are hundreds of instruments (approximately 320 to be investigated by author) available for studying the Earth including land, ocean, atmosphere etc. (**Appendix 1** lists some most widely used sensors in land applications). These satellite sensors can be categorized as Landsat-like

(having the middle resolution, broad area and multispectral coverage characteristic of the current satellites as Landsat, SPOT), High Resolution (providing an order of magnitude improvement in ground resolution, at the expense of less area and multispectral capability**),** Hyperspectral (providing near continuous radiometry over the visible, near infrared and short wave infrared spectrum.**),** and Radar (all weather capability) systems (Stoney, 2002**).** Each sensor has its own characteristics in ground resolution, temporal resolution, spectral resolution, coverage swath and so on. **Fig. 1-1**, **Fig. 1-2** and **Fig. 1-3** illustrate these different parameters.

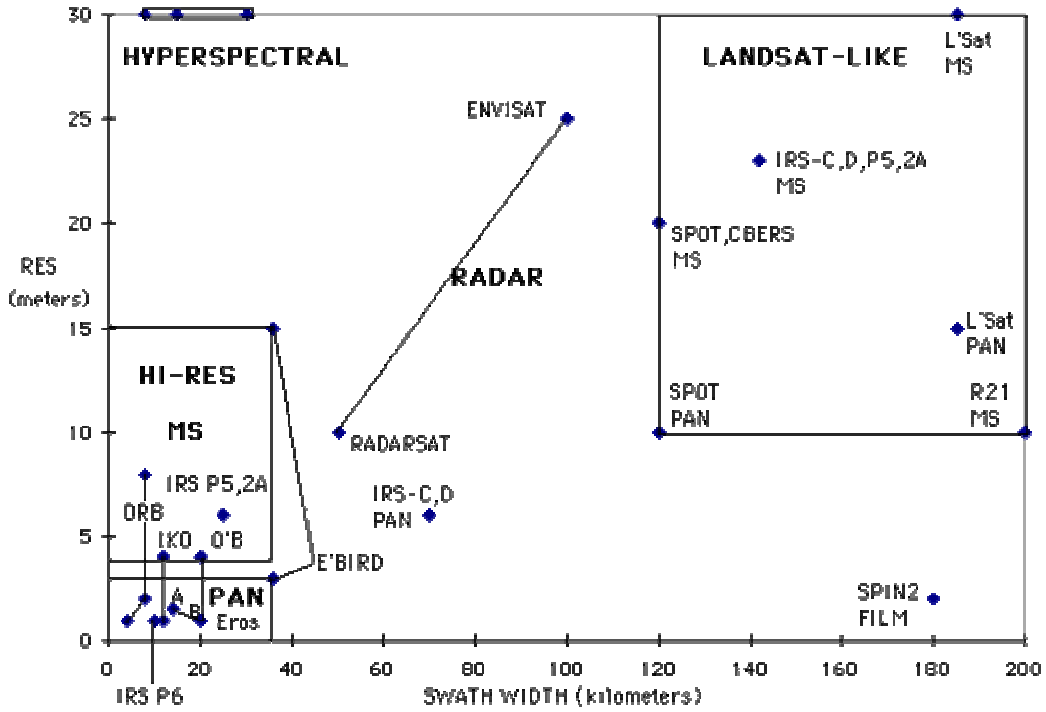

Fig. 1-1. Difference in coverage and resolution of the selected satellites sensors (Source: Stoney, 2002)

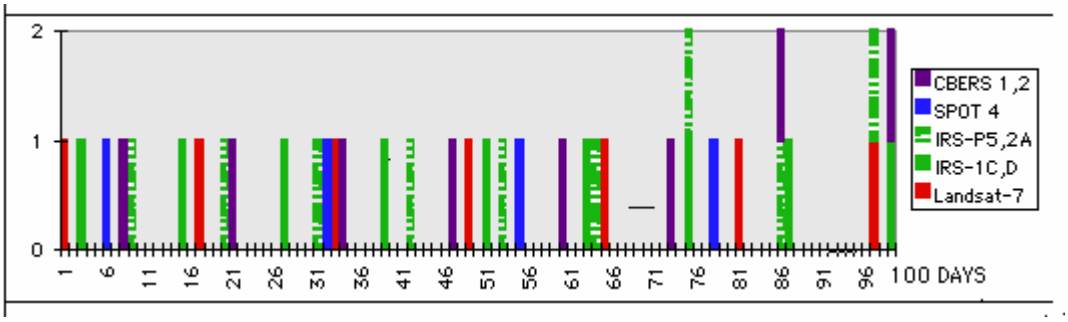

Fig. 1-2. An example showing repeat frequency over a randomly selected 100-day period (Source: Stoney, 2002)

SPECTRAL SPATIAL RESOLUTION SUMMARY

PROGRAM	SENSOR TYPES	RESOLUTION IN METERS								
		THEMATIC MAPPER BANDS								
		PAN		VNIR			SWIR		TIR	RADAR
			1	2	3	4	5	7	6	res,band
LANDSAT-LIKE										
IRS-1C,D	M&P	6		23	23	23	70			
IRS-P5, IRS-2A	M			6,23	6,23	6,23	23			
Spot 4	M&P	10		20	20	20	20			
CBERS	M&P	20, 80	20	20	20	20	80	80	160	
Landsat 7	M&P	15	30	30	30	30	30	30	60	
EOS AM-1	M			15	15	15	6 bands @ 3(		5@90	
Resource 21	M		10	10	10	10	20			
HIGH RESOLUTION										
EarthWatch	M&P	3		15	15	15				
SpaceImaging	M&P	1	4	4	4	4				
EarthWatch	M&P	1	4	4	4	4				
Orbimage	M&P	1&2	8	8	8	8				
SPIN-2	P(f)	2,10								
West Ind. Space	P	1.5								
West Ind. Space	P	1								
IRS-P6 (CARTOSAT-1	P	2.5								
HYPERSPECTRAL										
TRW Lewis	H&P	5		128 bands @ 30			256 bands @ 30			
EO-1	H&M			128 bands @ 30			256 bands @ 30			
HRST	H	5		210 bands @ 30						
ARIES	H	10		32 bands @ 30				32@30		
RADAR										
Radarsat	R								10-100	C
ENVISAT	R								25	C

Fig. 1-3. Resolution of each band listed under their Landsat 7 band counterparts (Source: Stoney, 2002)

The combination of these parameters results in advantages and disadvantages of each sensor in different applications. For example, optical image is very vivid for ground surface, but cloud and haze impede its application. High ground resolution satellite images normally can detect the Earth surface in detail, but the long repeat cycle and narrow coverage swath are commonly not suitable for real-time monitoring and large scale mapping. Visible and near infrared bands are good for vegetation monitoring, but surface temperature and fire detection can be better achieved from thermal bands.

Because of the limited capability of single sensor in the dimension of ground resolution, spectral coverage, wide swath and repeat cycles, the information provided by individual sensors are incomplete, inconsistent, or imprecise for many applications (Varshney, 1997; Hall and Llinas, 1997; Pohl and Genderen, 1998). Many studies show that multi-sensor satellite images are more useful in environment monitoring including land cover, desertification monitoring and fire detection because multi-sensor images vary in spectral, spatial and temporal resolution and give a more complete view of the observed objects. In recent years multi-sensor data fusion has been extensively investigated by researchers in remote sensing (e.g. Haack and Bechdol, 1999). It was demonstrated that multi-sensor fusion techniques could be used to improve rectification accuracies, to depict greater cartographic detail, and to enhance spatial resolution in multi-sensor image data sets (Ehlers, 1991). The reason for

the success is that multi-sensor fused images may provide increased interpretation capabilities and more reliable results since data with different characteristics are combined and can achieve improved accuracies and better inference, by decreasing the uncertainty related to the single sources, about the environment than could be achieved by the use of a single sensor alone (Simone *et al*., 2002; Clement *et al*., 1993; Pohl and Genderen, 1998; Ma, 2001). Kalluri *et al*. (2003) compared the characteristics of different Earth observing satellite instruments that have potential use in application development for decision makers at the state/local and tribal level.

In all these satellite-based environmental monitoring activities, land cover/use, desertification monitoring, wildland fire events are three important topics. These three topics were selected as the case studies in this thesis.

1-2. Land cover

Land cover is an important variable in many Earth system processes (**Fig. 1-4**). Many general circulation and carbon exchange models require the vegetation cover as a boundary layer necessary to run the model (Sellers *et al*., 1997). Vegetation also represents an important natural resource for humans and other species, and quantifying the types and extent of vegetation is important to resource management and issues regarding land cover change (Townshend, 1992). The multitemporal coverage provided by satellite data facilitates the use of remote sensing images to monitor changes in land cover and land use over time.

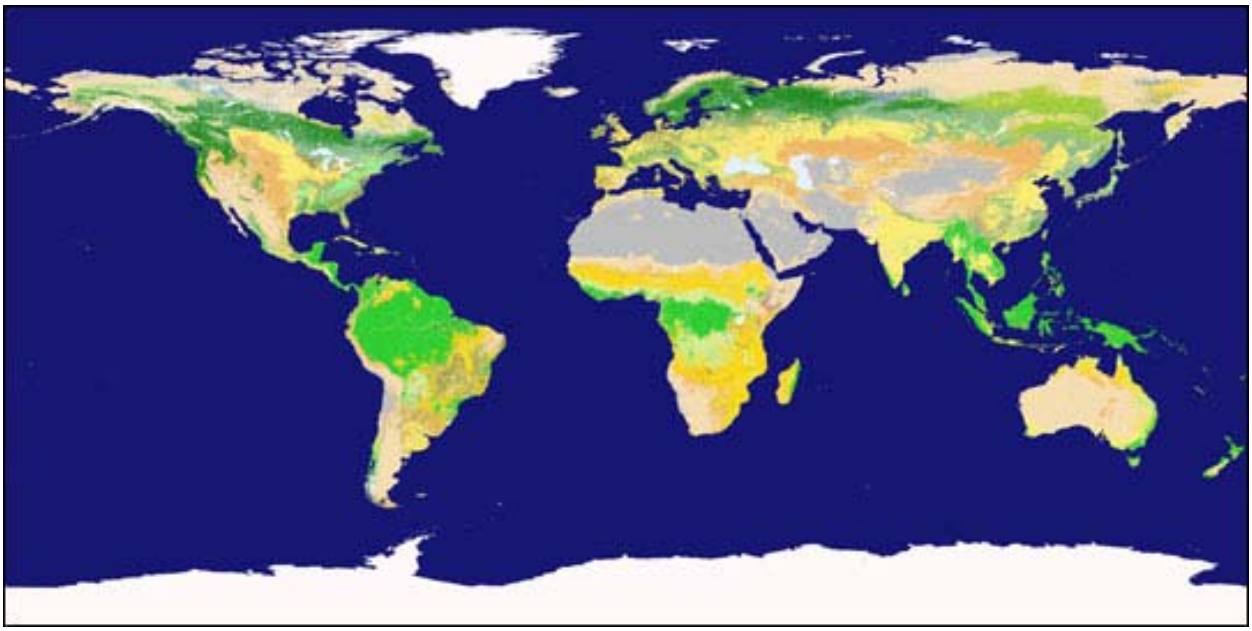

Fig. 1-4. Land cover is an important issue of Earth environment. This figure shows the distribution of forest (green), shrub (brown), desert (grey), grass and crops (yellow), ice (white) etc. on the Earth.

With increasing frequency, remotely sensed data sets have been used to classify global as well as regional and local land cover. The primary goals in developing these land cover products are to meet the needs of the modelling community and to attempt to better understand the role of human impacts on Earth systems through land cover conversions. Recent work in classifying regional, continental and global land cover has seen the application of multi-temporal remotely sensed data sets, which describe vegetation dynamics by viewing their phenological variation throughout the course of a year (Verhoef *et al*., 1996; Cihlar, 2000; DeFries and Townshend, 1999). Some continental scale classifications of land cover were produced using this approach (e.g. Tucker *et al*. 1985; Townshend *et al*., 1987; Stone *et al*., 1994). For global land cover, DeFries and Townshend had derived a one by one degree map (DeFries and Townshend, 1994) and as well as an 8 km map using AVHRR data (DeFries *et al*., 1998). The current global land cover products are much finer in resolution (Dickinson, 1995). As the resolutions of global data sets become finer, the ability to monitor short-term human-induced land cover changes has increased. Sensors such as the MODIS have resolutions sufficient enough to allow for global depictions of land cover change. Establishing a global baseline for land cover at 1 km is an important step to understand how change can be depicted with newer sensors.

A 1 km resolution data set employing AVHRR data has been developed based on the recommendations from the International Geosphere Biosphere Programme (IGBP) for use in global change research (Townshend, 1992). Loveland *et al*. (2000) had produced a 1 km resolution global land cover layer with 17 classes, named the IGBP DISCover product, where each continent was classified separately and then stitched together. They used 12 monthly Normalized Difference Vegetation Index (NDVI) values in an unsupervised clustering algorithm that was supplemented with ancillary data analysis. (To measure and map the density of green vegetation across the Earth's landscapes, scientists use satellite sensors that observe the distinct wavelengths of visible and near-infrared sunlight that is absorbed and reflected by the plants. Calculating the ratio of the visible and near-infrared yields a number from minus one -1 to plus one +1 named as Normalized Difference Vegetation Index. An NDVI value of zero means no green vegetation and close to +1 such as 0.8-0.9 indicates the highest possible density of green leaves). The University of Maryland (UMD) produced global land cover classification with 14 classes (Hansen *et al*., 2000). The Boston University produced global land cover using both IBGP and UMD legend (Friedl *et al*., 2002; Strahler *et al*., 1999). The European Joint Research Center has coordinated the application of SPOT VEGETATION to map global land cover in a resolution of 1 km.

1-3. Desertification

Desertification refers to land degradation in arid, semi-arid, and dry sub-humid areas resulting from climatic variations and human activities. In the definition proposed by the UN Convention on Desertification (UNCOD), desertification is considered the result of a series of natural and

anthropogenic processes, leading to gradual environmental degradation or loss of the land's biological or economic productivity (UNEP, 1994). Since UNCOD held in 1977 desertification has variously been viewed as one of the most pressing environmental issues affecting human kind (UNEP, 1987). The increasing rate of desertification on a global scale is one of the most pressing concerns among environmental scientists and laymen since it implies a clear manifestation of climatic change processes and human interaction on the environment (Collado *et al*., 2002). Desertification has been widely represented in the media and discussed by politicians, and has been seen as a major cause of human problems (**Fig. 1-5**): By the UNEP classification system, 41% of the Earth's land area is hyper-arid, arid, semi-arid or dry sub-humid (UNEP, 1992). UNEP estimated that 69% of the drylands, excluding the hyper-arid deserts, were already moderately to severely degraded by 1992 (Dregne *et al*., 1991). Of the more than 900 million inhabitants of drylands 135 million are considered at risk of collapse of their traditional land-use systems and episodic mass starvation continues to be a problem in Africa (Lean, 1998). According to UNEP over-grazing of rangelands is the most serious cause of desertification, accounting for 93% of the total 3,560,000 ha of degraded dryland and 55% of the total $42 US billion per year of foregone income (Kassas, 1995).

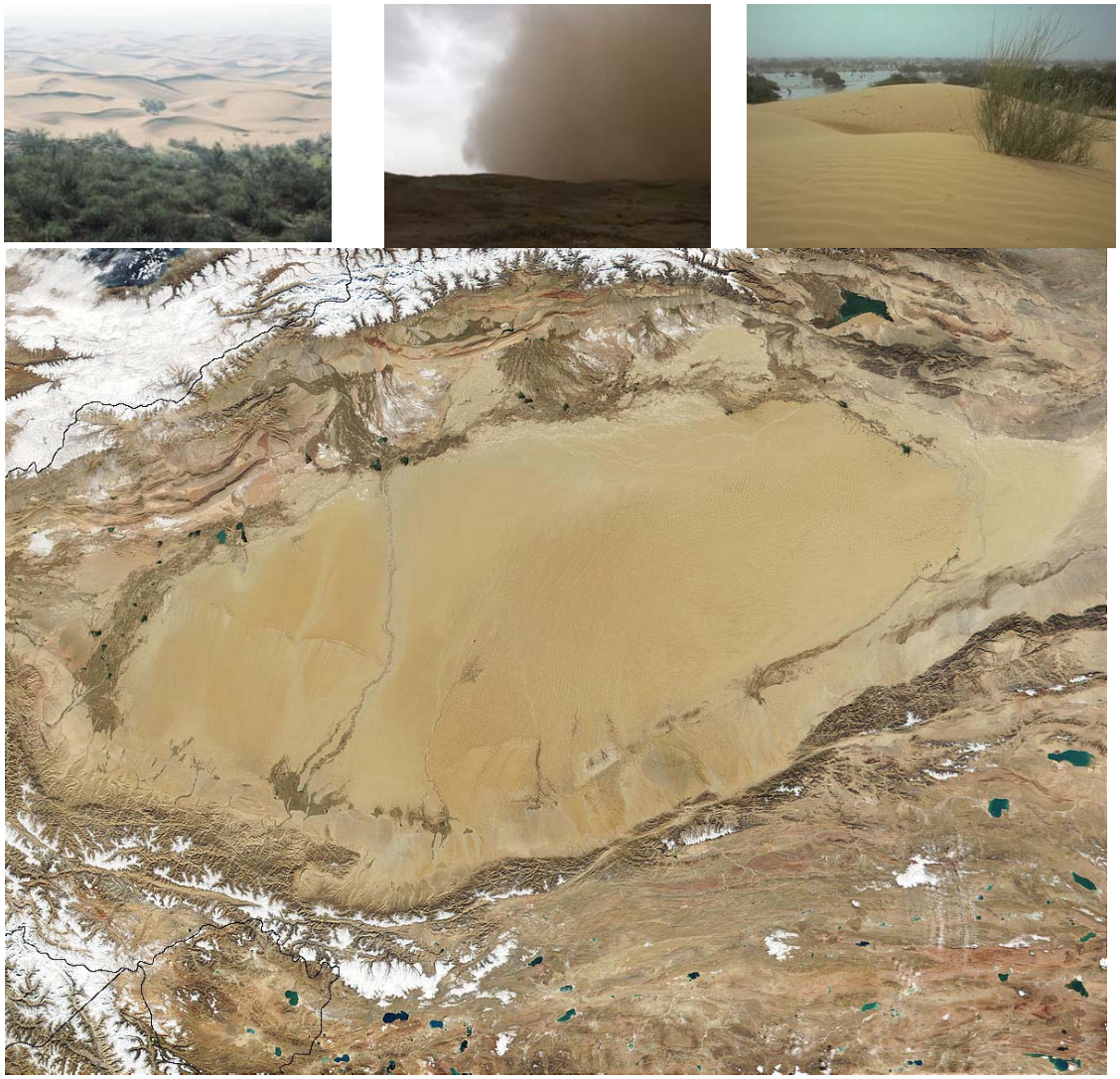

Fig. 1-5. Desertification is a serious environmental problem around the world.

While standard methods for undertaking such measurements are imperfect or expensive it has been demonstrated that, besides airborne systems for individual surveys on local to regional scale, several geostationary and polar-orbiting satellites (e.g., METEOSAT/GOES, NOAA-AVHRR, Landsat, SPOT-HRV and -VEGETATION, IKONOS) are available which operate in the reflective and emissive domain and offer a considerable potential. The various data sources available through remote sensing offer the possibility of gaining environmental data over both large areas and relatively long-time periods. Remote sensing systems, and in particular Earth observation satellites, provide significant contributions to desertification assessment and monitoring, particularly by providing methodological pathways for scaling up the results of field investigations and by supplying the spatial information needed for regional scale analysis of the relationships between climate change, land degradation and desertification processes. It seems obvious that the identification of degraded areas in the sense of environmental inventories provides the fundamental basis for better understanding the processes of land degradation and desertification in their spatial context.

A wide range of processing techniques are available to discriminate changes in multitemporal data (Jensen, 1996). These properties enable the use of satellite remote sensing for monitoring trends of land degradation as well as to identify and characterize sand dunes and their temporal dynamism in the study of desertification (Verbyla, 1995; Chen *et al*., 1998; Smith *et al*., 1990a, b; Paisley *et al*., 1991; Tucker *et al*., 1991, 1994). The monitoring has been mainly based on the analysis of a time series of spectral vegetation indices (VIs). VIs are arithmetic transformations of spectral bands that emphasize vegetation over soil signals (Sellers, 1989). Usually, the red and infrared reflectances are combined (Tucker, 1979; Bannari *et al*., 1995) since in the red the vegetation strongly absorbs incident radiation (up to 90%, caused by the leaf pigments) while in the infrared green leaves are highly reflective due to leaf structure. This strong reflectance contrast is only observed in green vegetation, since bare soils present a similar reflectance in both bands (Mulders, 1987). In arid regions, multitemporal analysis of VIs have been applied to monitor soil degradation associated with cattle grazing (e.g. Pickup and Chewings, 1994), as well as to follow seasonal trends in vegetated dunes, discriminating the most degraded ones (Jacobberger and Hooper, 1991). There have also been some attempts to establish global scale models, relating temporal evolution of VI data to rainfall seasonality (Kerr *et al*., 1989). This approach has made it possible to monitor temporal changes in the desert boundary of the Sahel from the NOAA meteorological satellite (e.g. Tucker *et al*., 1991, 1994).

1-4. Fire

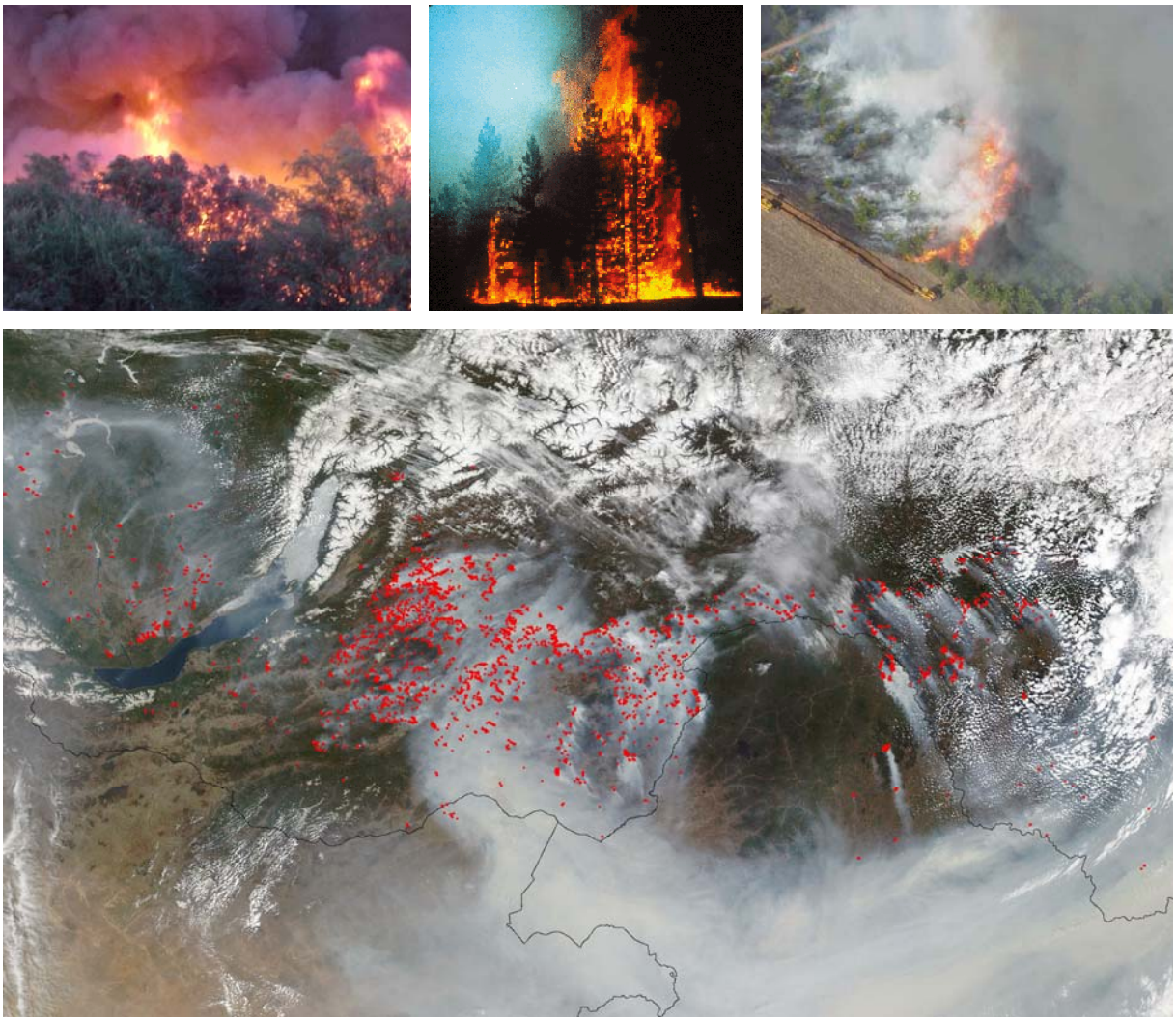

Fig. 1-6. Fire is an important ecological factor influencing Earth environment

In the past decades wildfires are becoming an increasingly important ecological factor which significantly influences the Earth's environment and climate change. Fire is an important process within a significant number of terrestrial biomes, and the release of gases and particulate matter during biomass burning is an important contributor to the chemical reactions and physical processes taking place in the atmosphere (**Fig. 1-6**). Fires change the physical state of the vegetation, affect energy exchange, affect biodiversity and release a variety of harmful greenhouse gases into the atmosphere, which strongly influence chemical processes within the troposphere (Andreae, 1991; Barbosa *et al*., 1999b). In tropical regions, biomass burning has been shown to strongly influence regional and global distributions of tropospheric ozone and has been related to acid deposition (Crutzen and Andreae, 1990). In boreal forests, fire affects the flow of energy between the atmosphere and ground layer dramatically, and there is a dependence on the melting and formation of permafrost and the occurrence of fire, which in turn has a strong influence on the hydrology of these sites (Brown, 1983). On a global scale, fires are known to contribute significantly to the release of gases and aerosols into the

atmosphere, and to be a major disturbance to the vegetation cover. Biomass burning contributes up to 50%, 40% and 16% of the total emissions of anthropogenic origin for carbon monoxide, carbon dioxide and methane respectively (Grégoire *et al*., 2003). The detection of fires and the assessment of their impacts on the vegetation are important to monitor and to model and predict global climate change (Page *et al*., 2002; Molion, 1991).

Satellite remote sensing is able to provide essential information useful in fire monitoring and management as well as damage assessment. Remotely sensed data and techniques have been widely used to detect active fires and extract the desirable information of fire location, fire area extent, land cover types burnt by fire and geographical distribution of fires (Domenikiotis *et al*., 2002). Dwyer *et al*. (1999) demonstrated that satellite remote sensing is an efficient way for the detection of fire occurrence over a range of temporal and spatial scales which allow a detailed characterization of seasonal and inter-annual patterns of fire activity. Several techniques have been developed for using visible, infrared and thermal data to detect and map active fires and burn scars (Cahoon *et al*., 1992, 1994; Kasischke and French, 1995a; Ahern *et al.*, 2000). Many satellite sensors such as AVHRR, MODIS, Advanced Along-Track Scanning Radiometer [A(A)TSR], SPOT VEGETATION and European Remote-Sensing Satellite (ERS) are applied in burnt area identification (Kaufman *et al*., 1998; Arino *et al*., 2001; Stroppiana *et al*., 2002; Tansey, 2002; Kasischke, 1993; Roy *et al*., 2002; Siegert and Rücker, 2000; Simon, 2002).

Two general categories of products (Fire hot-spot detection and burn area maps) are typically derived in fire monitoring and assessment by satellites. The spectral density distribution of the vegetation fires whose temperature varies from 500 up to 1200 K occurs in the mid-wave infrared (MIR) wavelength region at 3-5 μm. According to Wien's displacement law, 3-5μm is the main channel for fire hotspot detection. Optical burnt scar mapping is normally based on the reflectance change after the vegetation is burnt. Many studies were already conducted in the burnt area detection by AVHRR (e.g. Razafimpanilo *et al*., 1995; Barbosa *et al*., 1999a; Kasischke *et al*., 1993; Kasischke and French, 1995; Domenikiotis *et al*., 2002), MODIS (e.g. Roy *et al*., 2002), Landsat (e.g. Pereira and Setzer, 1993; Díaz-Delgado *et al*., 2003; Hudak *et al*., 2004; Bowman *et al*., 2003; Scholes *et al*., 1996). The use of contextual algorithms that combines hot-spot detections with burnt area maps can improve the detection of active fires and area burnt estimation (Eva and Flasse, 1996). Fraser *et al*. (2000) presented a concise and thorough review of AVHRR fire detection and mapping work and describe a hybrid technique they have developed for fire mapping in Canada. Soja *et al*. (2004) and Sukhinin *et al.* (2004) derived the fire frequency, distribution, and area burnt in Siberia using AVHRR based on the similar hybrid technique.

Besides the optical data, SAR data are also widely used for fire scar mapping. One of the benefits of using SAR satellite for fire scar monitoring is that the microwave energy penetrates cloud cover. SAR backscatter intensity and interferometric coherence have been used in forest mapping and monitoring (e.g. LeToan *et al*., 1996; Wegmuller and Werner, 1995; Stussi *et al*, 1997). These tests to analyse variations in radar image intensity associated with forest fires have been done in the boreal region (Kasischke *et al*., 1992; Bourgeau-Chavez *et al*, 1993; Kasischle *et al*., 1994; Dwyer *et al*. 2002; Bourgeau-Chavez *et al*., 1997; Ranson *et al*., 2002), in Mediterranean landscapes (Gimeno *et al*., 2002a, Gimeno *et al*., 2002b; Gimeno *et al*., 2003) and in the tropical rain forest (LeToan *et al*., 1996; Siegert *et al*., 1995; Kuntz *et al*., 1999; Siegert and Hoffmann, 2000). All of them found differences in the backscatter between undisturbed and fire-disturbed areas. Originally it was hypothesized that the increase in radar backscatter within the burnt regions was due to an increase in dihedral scattering between tree trunks and the ground surface. However, latter experiments concluded that the differences in radar backscatter depend on the level of damage to the vegetation cover, and on the soil moisture, surface roughness, and topography (Kasischke *et al*., 1994).

1-5. Summary

Unprecedented pressure on the physical, chemical and biological systems of the Earth results in environment problems locally and globally (Singh, 1996), therefore the detection and understanding of environmental change is very urgent (Parr *et al*., 2003), which indicates long-term environmental data are required and needed to update frequently. With the main advantages of global observation, repetitive coverage, multispectral sensing and low-cost implementation, satellite remote sensing technology is a promising tool for monitoring environment, especially in developing countries where natural resources is depleted, environment is changing faster, environmental awareness is poor, environmental investment is insufficient, ground access is sometimes difficult and updated map is normally unavailable (Wehrmeyer and Mulugetta, 1999; Centeno, 2002).

The analysis of satellite images acquired by different satellites with different spatial resolution and spectral sensitivity may provide increased interpretation capabilities and more reliable results since data with different characteristics are combined and can achieve improved accuracies and better inference about the environment than could be achieved by the use of a single sensor alone (Simone *et al*., 2002; Clement *et al*., 1993; Pohl and Genderen, 1998; Ma, 2001).

The prospect of multi-sensor application to environmental monitoring is enhanced by more and more new satellite sensors which have been or will be available for Earth observations (**Fig. 1-7**). For example, ENVISAT, launched in 2002, carries ten sophisticated optical and radar instruments to

provide continuous observation of the Earth's land, atmosphere, oceans and ice caps. The largest single instrument onboard ENVISAT, Advanced Synthetic Aperture Radar (ASAR), ensures continuity of data after ERS-2, while the Medium Resolution Imaging Spectrometer (MERIS) measures the solar radiation reflected by the Earth at a ground spatial resolution of 300 m in visible and near infrared 15 bands with global coverage of the Earth every 3 days. The Advanced Along Track Scanning Radiometer (AATSR), another sensor onboard ENVISAT, is to establish continuity of the ATSR-1 and ATSR-2 data sets of precise sea surface temperature (SST), but it can also be used for wildland fire detection. In addition to these sensors onboard ENVISAT, the VEGETATION sensor, which is operational since April 1998, is conceived to allow daily monitoring of terrestrial vegetation cover through remote sensing at regional to global scales. The first VEGETATION instrument is part of the SPOT 4 satellite and a second payload, VEGETATION 2, is now operated onboard SPOT 5. Besides all these new European satellites and sensors, there are still other new sensors orbiting in space. ASTER, an imaging instrument that is flying on TERRA satellite launched in December 1999 as part of NASA's Earth observing system, is used to obtain detailed maps of land surface temperature, emissivity, reflectance and elevation. MODIS instrument provides high radiometric sensitivity in 36 spectral bands ranging in wavelength from 0.4 μm to 14.4 μm. The first MODIS instrument is integrated on the TERRA spacecraft. The second MODIS flight instrument is integrated on the AQUA spacecraft which was successfully launched on 4 May 2002. All these instruments (ASAR, MERIS, AATSR, VEGETATION, ASTER, MODIS etc.) are offering unprecedented looks at terrestrial, atmospheric, and ocean phenomenology for a wide and diverse user communities. These sensors differ in the spatial, spectral, temporal dimension and width swath. How to combine these satellite data as well as the conventional sensors (e.g. Landsat, AVHRR) for environmental monitoring needs to be investigated. The objective of this thesis is to demonstrate the potential of multi-sensor satellite data to monitor the environment in developing countries. Land cover assessment in Salonga national park, desertification monitoring in North China, and tropical/boreal forest fire monitoring and impact assessment in Indonesia/Siberia are specially emphasized in this thesis.

Salonga national park, an isolated region hardly accessible on ground, is a protection area for different animal species, especially the ape. In spite of its importance to natural conservation, little was known about the spatial distribution of vegetation types and human impacts, and the ongoing war impede the ground survey. Can we use multisource data to assess the land cover in a cost-effective way?

China is one of the developing countries with vast desertified areas and desertification is very serious (Zha and Gao 1997). Considering the labour costs and financial constraints, multi-scale remote sensing monitoring system is needed (Li and Zhou, 2000). This means that the area at risk of desertification should be firstly identified from large scale area, and then these areas are analyzed in detail (Lin and Zhou, 2000; Sun and Chen, 2000; Sun and Zhou, 2000). Using a full year time series

daily SPOT VEGETATION images with ground resolution of 1 km, can we identify the prior area? Is such multi-scale monitoring system feasible?

Indonesia and Siberia are two regions greatly affected by wildland fires. However, because of the could/haze, satellite overpass, fire spread dynamics, and ground resolution, the burnt area detection and impact assessment may not be satisfactory. Can we use the available data from those new sensors to identify the burnt area and assess the fire impact more efficiently ?

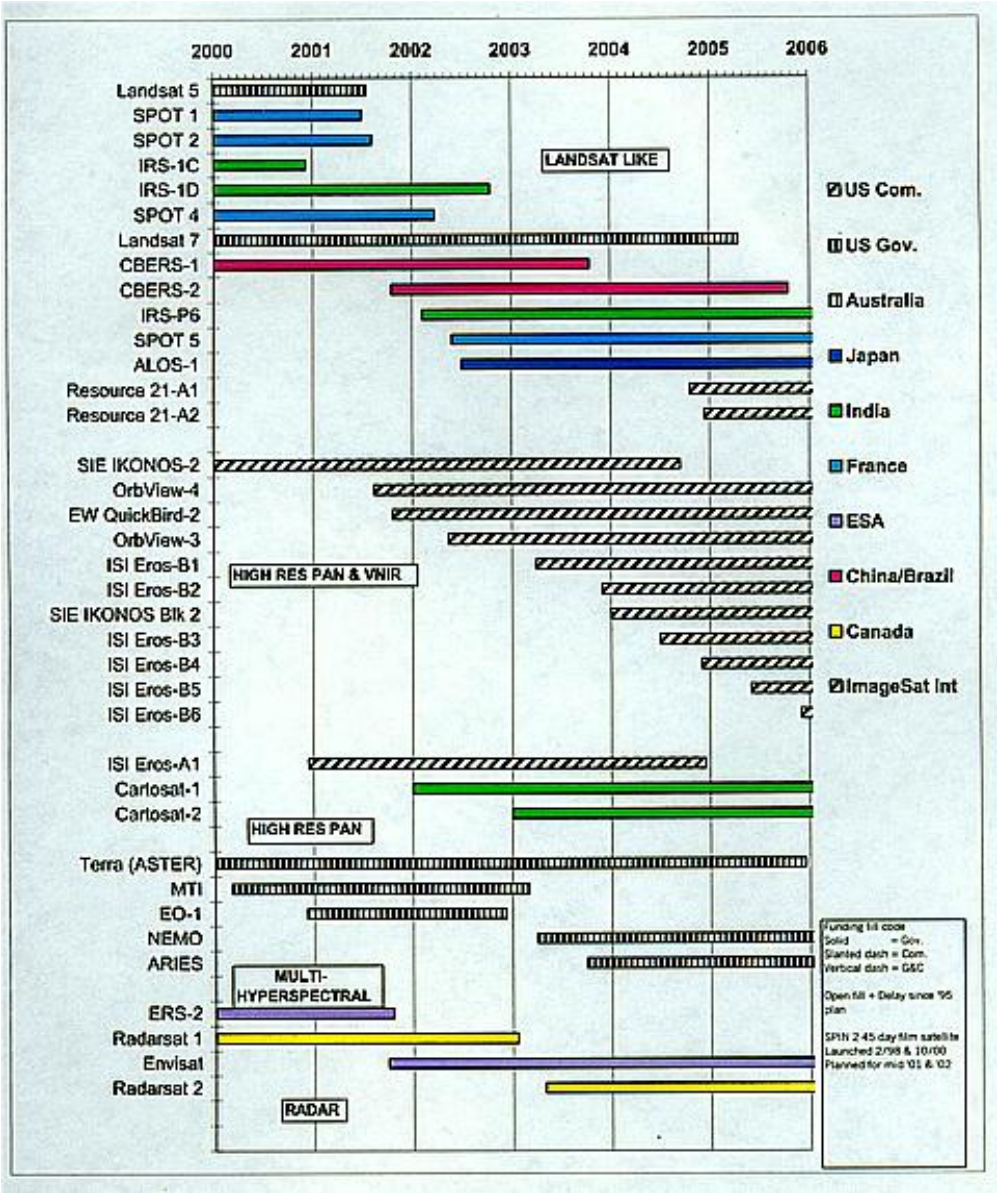

Fig. 1-7. Satellite names of the principal vehicles from 2000 through 2006 (modified from Stoney, 2002)

In this thesis, **Chapter 2** shows the combination of multi-sources data as optical high resolution Landsat satellite images, Global Position System signals, continuous aerial video, and digital photos for mapping and evaluating the Salonga national park in Congo of Africa. **Chapter 3** shows the time series SPOT VEGETATION with coarse resolution of 1 km and the ASTER images with higher

resolution as well as Landsat images for land cover mapping optimised for desertification monitoring in North-China. **Chapter 4** firstly investigates the characteristics of single ASAR and MERIS for fire scar detection, secondly investigates the potential of European ENVISAT multi-sensor of MERIS, AATSR, ASAR for tropical forest fire event monitoring and impact assessment in tropical Indonesia, and then finally applies these multi-sensor technology to the disastrous boreal forest fire event of 2003 around East and West Lake Baikal in Siberia.

1-6. References

Ahern, F. J., Epp, H., Cahoon, D., French, N. & Kasischke, E. (2000). Using Visible and Near-Infrared Satellite Imagery to Monitor Boreal Forests, in Kasischke, E. K. & Stocks, B. (eds), *Fire, Climate Change, and Carbon Cycling in the Boreal Forest*, pp 312 – 330, New York: Springer Verlag.

Andreae, M. O. (1991). Biomass burning: its history, use, and distribution and its impaction environmental quality and global climate. In Levine, J. S. (Ed.), *Global Biomass Burning*, pp. 3-21, Cambridge, MA: The MIT Press.

Arino, O., Simon, M., Piccolini, I., Rosaz, J.M. (2001). The ERS-2 ATSR-2 world fire atlas and the ERS-2 ATSR-2 world burnt surface atlas projects. *Proceedings of the 8th ISPRS conference on Physical Measurement and Signatures in Remote Sensing*, Aussois, 8-12 January 2001.

ASRAR, G., and DOKKEN, D. J., 1993, EOS Reference Handbook (Greenbelt; MD: NASA).

Bannari, A., Morin, D., Bonn, F. & Huete, A.R. (1995). A review of vegetation indices. *Remote Sensing Reviews, 13,* 95-120.

Barbosa, P.M., Gregoire, J.-M. & Pereira, J.M.C. (1999a). An algorithm for extracting burned areas from time series of AVHRR GAC data applied at continental scale, *Remote Sensing of Environment, 69,* 253-263.

Barbosa, P.M., Grégoire, J.-M., Stroppiana, D. & Pereira, J.M.C. (1999b). An assessment of fire in Africa (1981-1991): burnt areas, burnt biomass and atmospheric emissions. *Global Biogeochemical Cycles, 13 (4),* 933-950.

Boles, S., Xiao, X., Liu, J., Zhang, Q., Munkhtuya, S., Chen, S. & Ojima, Dennis. (2004). Land cover characterization of Temperate East Asia using multi-temporal VEGETATION sensor data. *Remote Sensing of Environment, 90* , 477-489.

Bourgeau-Chavez, L. L., Harrell, P. A., Kasischke, E. S. & French, N. H. F. (1997). The detection and mapping of Alaskan wildfires using a spaceborne imaging radar system, *International Journal of Remote Sensing, 18,* 355-373.

Bourgeau-Chavez, L.L., Kasischke, E.S. & French, N.H.F. (1993). Detection and interpretation of fire disturbed boreal forest ecosystems in Alaska using space born SAR data*, Proceeding of the Topical Symposium on Combined Optical-Microwave Earth and Atmosphere Sensing,* Albuquerque, New Mexico, New York: IEEE.

Bowman, D.M.J.S., Zhang, Y., Walsh A. & Williams, R. J. (2003). Experimental comparison of four remote sensing techniques to map tropical savanna fire-scars using Landsat-TM imagery, *International Journal of Wildland Fire, 12(4),* 341-348.

Brown, R. J. E. (1983). Effects of fire on the permafrost ground thermal regime. In Wein, R. W. & Maclean, D. A. (Ed.), *The Role of Fire in Northern Circumpolar Ecosystems* (pp. 97-110). New York: John Wiley & Sons.

Cahoon, D. R., Stocks, B. J., Levine, J. S., Cofer, W. R. & Chung, C. C. (1992). Evaluation of a technique for satellite-derived area estimation of forest fires, *Journal of Geophysical Research, 97,* 3805-3814.

Cahoon, D. R., Stocks, B. J., Levine, J. S., Cofer, W. R. & Pierson, J. M. (1994). Satellite analysis of the severe 1987 forest fires in northern China and southeastern Siberia, *Journal of Geophysical Research, 99(D9),* 18,627-18,638.

CEES, 1992, Our Changing Planet: The FY 1992 U.S. Global Change Research Program. Committee on Earth and Environmental Sciences (Washington, D. C.: National Science Foundation).

Centeno J.C. (2002). *Developing Countries, Population and the Environment.* South center (An organization of developing countries) Bulletin 41, 2002. http://www.southcentre.org/info/southbulletin/bulletin41/bulletin41.pdf

Cihlar, J. (2000). Land cover mapping of large areas from satellites: Status and research priorities. *International Journal of Remote Sensing, 21,* 1093– 1114.

Clement, V., Giraudon, G., Houzelle, S. & Sandakly, F. (1993). Interpretation of remotely sensedimages in a context of multisensor fusion using a multispecialist architecture. *IEEE Transactions on Geoscience and Remote Sensing, 31(4),* 779-791.

Chen, Z., Elvidge, C. D. & Groenveld, D. P. (1998). Monitoring of seasonal dynamics of arid land vegetation using AVIRIS data. *Remote Sensing of Environment, 65,* 255-266.

Collado, A. D., Chuvieco, E. & Camarasa, A. (2002). Satellite remote sensing analysis to monitor desertification processes in the crop-rangeland boundary of Argentina. *Journal of Arid Environments, 52,* 121-133.

Colwell, J. E. & Sadowski, F. (1993). Past patterns as a guide for future forest management. *Earth Observation Magazine, 2(2),* 46-48.

Crutzen, P. & Andreae, M. (1990). Biomass burning in the tropics: Impact on atmospheric chemistry and biogeochemical cycles, *Science, 250,* 1669-1678.

DeFries, R., Hansen, M., Townshend, J. R. G. & Sohlberg, R. (1998). Global land cover classifications at 8 km spatial resolution: The use of training data derived from Landsat Imagery in decision tree classifiers, *International Journal of Remote Sensing, 19,* 3141-3168.

DeFries, R. S. & Townshend, J. R. G. (1994). NDVI-derived land cover classification at global scales. International Journal of Remote Sensing, 15, 3567-3586.

DeFries, R. S., & Townshend, J. R. G. (1999). Global land cover characterization from satellite data: From research to operational implementation? *Global Ecology and Biogeography, 8,* 367– 379.

Diaz-Delgado, R., Lloret, F. & Pons, X. (2003). Influence of fire severity on plant regeneration by means of remote sensing imagery. *International Journal of Remote Sensing, 24 (8),* 1751-1763.

Dickinson, R. E. (1995). Land processes in climate models, *Remote Sensing of Environment, 51,* 27-38.

Domenikiotis, C., Dalezios, N. R., Loukas, A. & Karteris, M. (2002). Agreement assessment of NOAA/AVHRR NDVI with Landsat TM NDVI for mapping burned forested areas, *International Journal of Remote Sensing, 23,* 4235–4246.

Dregne, H., Kassas, M. & Rosanov, B. (1991). A new assessment of the world status of desertification. *Desertification Control Bulletin, 20*, 6-18.

Dwyer, E., Pereira, J.M.C., Grégoire, J.-M. & DaCamara, C.C. (1999). Characterization of the spatio-temporal patterns of global fire activity, *Journal of Biogeography, 27,* 57-69

Dwyer, E, Stocks, B.J. & Arino, O. (2002). Burn scar mapping in Canada using ERS time series data, *Earth Observation Qurterly*, No70 Jan 2002, pp. 10-11. Esa, Nordwijk, Netherlands.

Ehlers, M. (1991). Multisensor image fusion techniques in remote sensing. *ISPRS Journal of Photogrammetry and Remote Sensing, 46(1),*19-30.

Ehrlich, D., Estes, J. E. & Singh, A. (1994). Applications of NOAA AVHRR 1-km data for environmental monitoring. *International Journal of Remote Sensing, 15 (1),* 145-61.

Eva, H. & Flasse, S. (1996). Contextual and multiple-threshold algorithms for regional active fire detection with AVHRR data, Remote Sensing Reviews, 14(4), 333-351.

Fraser, R. H., Li, Z. & Landry, R. (2000). SPOT VEGETATION for characterizing boreal forest fires, *International Journal of Remote Sensing, 21(18),* 3525-3532.

Freeman, P. H. & Fox, R. (1994). *Satellite Mapping of Tropical Forest Cover and Deforestation: A Review with Recommendations for USAID*. Arlington, VA: Environment and Natural Resources Information Center, DATEX.

Friedl, M. A., McIver, D. K., Hodges, J. C. F., Zhang, X. Y., Muchoney, D., Strahler, A. H., Woodcock, C. E., Gopal, S., Schneider, A., Cooper, A., Baccini, A.,Gao, F., Schaaf, C. (2002). Global land cover mapping from MODIS: algorithms and early results. *Remote Sensing of Environment, 83,* 287-302.

Gimeno M., San-Miguel, J., Barbosa P. & Schmuck G. (2002a). Using ERS-SAR images for burnt area mapping in Mediterranean landscapes, In Viegas (Ed.), *Forest Fire Research & Wildland Fire Safety*. Rotterdam: Millpress, ISBN 90-77017-72-0. available at *http://natural-hazards.jrc.it/documents/fires/2002-publications/MGimeno%20et%20al.pdf*

Gimeno, M. San-Miguel-Ayanz, J., Barbosa, P.M. & Schmuck, G. (2002b). Burnt area mapping from ERS-SAR time series using the principal components transformation. *SPIE 9th International Symposium on Remote Sensing,* Capsis Beach Hotel and Conference Center, Aghia Pelagia, Crete, Greece, 22-27 September 2002.

Gimeno, M., San-Miguel-Ayanz, J. & Liberta, G. (2003). Evaluation of a RADARSAT-1 data for identification of burnt areas in Southern Europe. *Proceedings of EARSeL General Symposium*, Ghent, Belgium, 5-7 June 2003.

Goward, S. N. (1989). Satellite bioclimatology. *Journal of Climate 2,* 710-20.

Grégoire, J. M., Tansey, K. & Silva, J.M.N. (2003). The GBA2000 initiative: developing a global burned area database from SPOT-VEGETATION imagery, *International Journal of Remote Sensing, 24,* 1369-1376.

Haack, B. & Bechdol, M. (1999). Multisensor remote sensing data for land use/cover mapping. *Computers, Environment and Urban Systems, 23(1),* 53–69.

Hall D.L. & Llinas J. (1997). An introduction to multisensor data fusion, Proceeding *IEEE 85 (1)*, 6–23.

Hansen, M. C., DeFries, R. S., Townshend, J. R. G., & Sohlberg, R. (2000). Global land cover classification at 1 km spatial resolution using a classification tree approach. *International Journal of Remote Sensing, 21,* 1331– 1364.

Hobish, M. K. (2002). Earth Systems Science - Earth Science Enterprise and the EOS Program. http://rst.gsfc.nasa.gov/Front/tofc.html

Hudak, A.T., Fairbanks, D.H.K. & Brockett, B.H. (2004). Trends in fire patterns in a southern African savanna under alternative land use practices. *Agriculture, Ecosystems and Environment, 101*, 307-325.

IGBP (1992). *Improved Global Data for Land Applications, IGBP Report 20,* International Geosphere Biosphere Programme, Stockholm.

Jacobberger, P. A. & Hooper, D. M. (1991). Geomorphology and reflectance patterns of vegetation-covered dunes at the Tsodilo Hills, north-west Botswana. *International Journal of Remote Sensing, 12,* 2321-2342.

Jacobson, H. K. & Price, M. F. (1990). *A Framework for Research on the Human Dimensions of Global Environmental Change*. Barcelona: Human Dimensions of Global Environmental Change Programme.

Jensen, J.R. (1996). *Introductory Digital Image Processing: A Remote Sensing Perspective*. Upper Saddle River, NJ: Prentice-Hall. 379 pp.

Kalluri, S., Gilruth, P. & Bergman, R. (2003). The potential of remote sensing data for decision makers at the state, local and tribal level: experiences from NASA's Synergy program. *Environmental Science & Policy, 6,* 487-500.

Kasischke, E. S., Bourgeau-Chavez, L. L., French, N. H. F., Harrell, P. A. & Christensen, N. L. (1992). Initial observations on using SAR to monitor wildfires scars in boreal forest, *International Journal of Remote Sensing, 13,* 3495-3501.

Kasischke, E. S., Bourgeau-Chavez, L. L. & French, N. H. F. (1994). Observations in ERS-1 SAR image intensity associated with forest fires in Alaska,*IEEE transactions on geoscience and remote sensing, 32,* 206-210.

Kasischke, E. S., & French, N. H. F. (1995a). Locating and estimating the areal extent of wildfires in Alaskan boreal forests using multiple-season AVHRR NDVI composite data, *emote Sensing Environment 51,* 263-275.

Kasischke, E. S., French, N. H. F., Harrell, P., Christensen, N. L., Ustin, S. L. & Barry, D. (1993). Monitoring of wildfires in boreal forests using large area AVHRR NDVI composite image data*, Remote Sensing of Environment, 45,* 61-71.

Kassas, M. (1995). Desertification: A general review. *Journal of Arid Environments 30,* 115-118.

Kaufman, Y. J., Justice, C. O. & Flynn, L. P. *et al.* (1998). Potential global fire monitoring from EOS-MODIS,*Journal of Geophysical Research, 103,* 32,215-32,238.

Kerr, Y., Imbernon, J., De Dieu, G., Hautecoeur, O., Lagouarde, J. P. & Seguin, B. (1989). NOAA-AVHRR and its use for rainfall and evapotranspiration monitoring. *International Journal of Remote Sensing, 10,* 847-854.

Kuntz, S., Siegert, F. & Ruecker, G. (1999). ERS SAR Images for tropical rainforest and land use monitoring: change detection over five years and comparison with Radarsat and JERS SAR images. In *Proceedings of the International Geoscience and Remote Sensing Symposium 1999 (IGARRS),* IEEE Geoscience and Remote Sensing Society, Piscataway.

Lean, G. (1998). *Down to Earth: A Simplified Guide to the Convention to Combat Desertification*. UNSO, Geneva, Switzerland.

LeToan, T., Ribbes, F., Hahn, T., Floury, N. & Wasrin, U. R. (1996). Use of ERS-1 SAR data for forest monitoring in South Sumatra, *Proceeding 1996 International Geoscience Remote Sensing symposium,* 842-844.

Lilesand, T. M. & Kiefer, R. W. (1994). *Remote Sensing and Image Interpretation, 3rd edn*. New York: John Wiley & Sons.

Lin, J., & Zhou, W. D. (2000). A summary of desertification monitoring of China. In desertification monitoring center of ministry of forestry (Ed.), *Research of Desertification Monitoring Technique in China* (pp.1-6). Beijing: China Forestry Science Press (264 pp.) (in Chinese).

Loveland, T. R., Reed, B. C., Brown, J. F., Ohlen, D. O., Zhu, Z., Yang, L.,& Merchant, J. W. (2000). Development of global land cover characteristics database and IGBP DISCover from 1 km AVHRR data. *International Journal of Remote Sensing, 21,* 1303– 1330.

Ma B. (2001). *Parametric and Nonparametric Approaches for Multisensor Data Fusion*.PhD thesis in The University of Michigan.

Molion, L.C.B. (1991). Amazonia: burning and global climate impacts, In Levine, J.S. (Ed.), *Global Biomass Burning: Atmospheric, Climatic and Biospheric Implications*, pp.457-462, MIT Press: Cambridge, MA.

Mulders, M. A. (1987). *Remote Sensing in Soil Science*. Amsterdam: Elsevier. pp.

Oldfield, F. & Dearing, J. A. (2003). The role of human activities in past environmental change. In Alverson, K. D, Bradley, R. S. &, Pedersen, T. F. (Ed.), *Paleoclimate, Global Change and the Future* (pp. 143-162).Berlin, Heidelberg: Springer-Verlag.

Page S.E., Siegert F., Rieley J.O., Boehm H-D.V. & Jaya A. (2002). Carbon released during peatland fires in Central Kalimantan, Indonesia in 1997,*Nature, 420,* 61-65

Paisley, E.C.I., Lancaster, N., Gaddis, L. R. & Greelye, R. (1991). Discrimination of active and inactive sand from remote sensing: Kelso Dunes, Mojave Desert, California. *Remote Sensing of Environment, 37*, 153-166.

Parr, T.W., Sier, A. R. J., Battarbee, R.W., Mackay, A. & Burgess, J. (2003). Detecting environmental change: science and society perspectives on long-term research and monitoring in the 21st century. *The Science of the Total Environment, 310,* 1-8.

Pereira, M. & Setzer, A. (1993). Spectral characteristics of deforestation fires in NOAA/AVHRR images, *International Journal of Remote Sensing, 14,* 583-587.

Pickup, G. & Chewings, V. H. (1994). A grazing gradient approach to land degradation assessment in arid areas from remotely-sensed data. *International Journal of Remote Sensing, 15,* 597-617.

Pohl C. & Genderen, J. L. (1998). Multisensor image fusion in remote sensing: concepts, methods and applications. *International. Journal of Remote Sensing, 19(5),* 823- 854.

Ranson, K.J. , Kovacs, K., Sun, G. & Kharuk, V. I. (2002). Fire Scar Detection using JERS, ERS and Radarsat Data in the Boguchany Area, Eastern Siberia. CEOS-SAR01-073, http://forest.gsfc.nasa.gov/SMP/PDF/CEOS073.PDF

Razafimpanilo, H., Frouin, R., Iacobellis, S.F. & Somerville, R.C.J. (1995). Methodology for estimating burned area from AVHRR reflectance data, *Remote Sensing of Environment, 54,* 273-289.

Roy, D., Lewis, P. & Justice, C. (2002). Burned area mapping using multi-temporal moderate spatial resolution data - a bi-directional reflectance model-based expectation approach, *Remote Sensing of Environment, 83,* 263-286.

Running, S. W., Justice, C. O., Salomonson, V., Hall, D., Barker, J., Kaufman, Y. J., Strahler, A. H., Huete, A. R., Muller, J.-P., Vanderbilt, V., Wan, Z.-M., Teillet, P., & Carneggie, D. (1994). Terrestrial remote sensing science and algorithms planned for EOS/MODIS. *International Journal of Remote Sensing, 15*(17), 3587-3620.

Scholes, R. J., Kendall, J. & Justice, C. O. (1996). The quantity of biomass burned in Southern Africa. *Journal of Geophysical Research, 101,* 23667-23676. Sellers, P. J., Dickinson, R. E., Randall, D. A., Betts, A. K., Hall, F. G., Mooney, H. A., Nobre, C. A., Sato, N., Field, C. B. & Henderson-Sellers, A. (1997). Modeling the exchanges of energy, water, and carbon between continents and the atmosphere, Science, 275, 502-509.

Sellers, P. J. (1989). Vegetation-canopy spectral reflectance and biophysical processes. In: Asrar, G. (Ed*.), Theory and Applications of Optical Remote Sensing*, pp. 297-335. New York: Wiley. 734 pp.

Siegert, F. & Hoffmann, A.A. (2000). The 1998 forest fires in East Kalimantan (Indonesia), *Remote Sensing of Environment, 72(1),* 64-77.

Siegert, F., Kuntz, S., Streck, C. & Bergbauer, B. (1995). Land use planning and monitoring in Indonesia using ERS-1 RADAR data. *Proceeding of International Conference on Remote Sensing and GIS for Environmental Resources Management –The Indonesian – European Experience*, Jakarta, Indonesia, 6-8 June 1995.

Siegert, F. & Rücker, G. (2000). Use of multitemporal ERS-2 SAR images for identification of burned scars in South-East Asian tropical rain forest, *International Journal of Remote Sensing, 21(4),* 831-837.

Simon, M. (2002). *GLOBSCAR Products Qualification Report.* ESA-ESRIN, Frascati, Italy.

Simone, G., Farina, A., Morabito, F. C., Serpico, S.B. & Bruzzone, L. (2002). Image fusion techniques for remote sensing applications. *Information Fusion, 3,* 3–15.

Singh, A. (1996). Further possibilities through UNEP for promoting the role of developing countries in conduct of ground-based experiments in support of utilization of global satellite data. *Advanced Space Research, 17(8),* 101-104.

Smith, M.O., Ustin, S.L., Adams, J.B. & Gillespie, A.R. (1990a). Vegetation in deserts: I. A regional measure of abundance from multispectral images. *Remote Sensing of Environment, 31*, 1-26.

Smith, M.O., Ustin, S.L., Adams, J.B. & Gillespie, A.R. (1990b). Vegetation in deserts: II. Environmental influences on regional vegetation. *Remote Sensing of Environment, 31,* 27-52.

Soja, A. J., Sukhinin, A. I., Cahoon, D. R., Shugart, H. H. & Stackhouse P.W. (2004). AVHRR-derived fire frequency, distribution and area burned in Siberia, *International Journal of Remote Sensing,25,* 1939-1960

Stone, T. A., Schlesinger, P., Houghton, R. A. & Woodwell, G. M. (1994). A map of the vegetation of South America based on satellite imagery. *Photogrammetric Engineering and Remote Sensing, 60,* 541-551.

Stoney W.E., Remote sensing in the 21st century: outlook for the future. The International Geoscience and Remote Sensing Symposium (IGARSS), Singapore, August 7, 1997, Updated: July, 2002). http://rst.gsfc.nasa.gov/Sect21/Sect21_1.html

Strahler, A., Muchoney, D., Borak, J., Friedl, M., Gopal, S., Lambin, E., & Moody, A. (1999). MODIS Land Cover Product Algorithm Theoretical Basis Document (ATBD), Version 5.0, NASA EOS-MTPE Documentation, NASA, Washington, DC. 66 pp.

Stroppiana, D., Pinnock, S., Pereira, J. M. C., & Gregoire, J. M. (2002). Radiometric analysis of SPOT-VEGETATION images for burnt area detection in Northern Australia. *Remote Sensing of Environment, 82,* 21- 37.

Stussi, N., Liew, S. C., Kwoh, L. K. & Lim, H. (1997). Landcover classification using ERS-SAR/INSAR data over tropical areas, *Proceeding 1997 International Geoscience Remote Sensing Symposium.* pp. 813-815.

Sukhinin, A. I., French, N.H.F., Kasischke, E.S., Hewson, J. H., Soja, A. J., Csiszar, I. A., Hyer, E. J., Loboda, T., Conard, S. G., Romasko, V. I., Pavlichenko, E. A., Miskiv, S. I. & Slinkina, O. A. (2004). Satellite-based

mapping of fires in Russia: new Products for fire management and carbon cycle studies, *Remote Sensing of Environment, 93,* 546– 564.

Sun, S. H., & Chen, J. W. (2000). China national desertification monitoring, In desertification monitoring center of ministry of forestry (Ed.), *Research of Desertification Monitoring Technique in China* (pp.96-107). Beijing: China Forestry Science Press (264 pp.) (in Chinese).

Sun, S. H., & Zhou, C. X. (2000). The basic frame for formulating the technical scheme of China national desertification monitoring. In desertification monitoring center of ministry of forestry (Ed.), *Research of Desertification Monitoring Technique in China* (pp.49-54). Beijing: China Forestry Science Press (264 pp.) (in Chinese).

Tansey, K.(2002). Implementation of regional burnt area algorithms for the GBA2000 initiative, *Publications of the European Commission (20532)*, Luxembourg.

Townshend, J. R. G. (1992). *Improved Global Data for Land Applications: A Proposal for a New High Resolution Data Set. Report No. 20*, (Stockholm, Sweden: International Geosphere-Biosphere Program).

Townshend, J. R. G., Justice, C. O. & Kalb, V. T. (1987). Characterization and classification of South American land cover types using satellite data, *International Journal of Remote Sensing, 8,* 1189-1207.

Tucker, C. J. (1979). Red and photographic infrared linear combinations for monitoring vegetation. *Remote Sensing of Environment, 8,* 127-150.

Tucker, C. J., Dregne, H. E. & Newcomb, W. W. (1991). Expansion and contraction of the Sahara Desert between 1980 and 1990. *Science, 253*, 299-301.

Tucker, C.J., Newcomb, W.W. & Dregne, H.E. (1994). AVHRR data sets for determination of desert spatial extent. *International Journal of Remote Sensing, 15,* 3547-3565.

Tucker, C. J., Townshend, J. R. G. & Goff, T. E. (1985). African land-cover classification using satellite data, *Science, 227*, 369-375.

UNCED (1992). *Rio Declaration on Environment and Development---Agenda 21*. Available at http://habitat.igc.org/agenda21/

UNEP (1987). *Sands of Change*. UNEP Environmental Brief 2. Nairobi: UNEP. 4 pp.

UNEP (1992). *World Atlas of Desertification*. London: Edward Arnold. 69 pp.

UNEP (1994). *United Nations Convention to Combat Desertification in Those Countries Experiencing Serious Drought and/or Desertification, Particularly in Africa.* Geneva: United Nations Environment Programme for the Convention to Combat Desertification (CCD), Interim Secretariat for the CCD. 71 pp.

Urquhart, N. S., Paulsen, S. G. & Larsen, D. P. (1998). Monitoring for policyrelevant regional trends over time.*Ecology Application, 8,* 246 –257.

Varshney P.K. (1997). Multisensor data fusion. *Electronics and Communication Engineering Journal*, *9,* 245–253.

Verbyla, D. (1995). *Satellite Remote Sensing of Natural Resources*, Boca Raton: Lewis Publishers. 224 pp.

Verhoef, W., Meneti, M. & Azzali, S. (1996). A clour composite of NOAAAVHRR NDVI based on time series analysis (1981-1992). *Internationa Journal of Remote Sensing, 17,* 231-235.

Verstraete, M.M., Pinty, B. & Myneni, R.B. (1996). Potential and limitations of information extraction on the terrestrial biosphere from satellite remote sensing. *Remote Sensing of Environment 58,* 201-214.

Wegmuller, U. & Werner, C. L. (1995). SAR interferometric signatures of forest, *IEEE transactions on geoscience and remote sensing, 33,* 1153-1161.

Wehrmeyer, W. & Mulugetta, Y. (1999). *Growing Pains: Environmental Management in Developing Countries.* Greenleaf Publishing Ltd.

Zha, Y., & Gao, J. (1997). Characteristics of desertification and its rehabilitation in China. *Journal of Arid Environments,37(3),* 419-432.

CHAPTER 2---MULTISOURCE DATA COMBINATION FOR THE ASSESSMENT OF SALONGA NATIONAL PARK

The Salonga National Park (SNP) is the second largest tropical forest national park in the world and represents the largest area of protection for the bonobo apes. Up-to-date maps on land cover and vegetation status are not available and little is known about the spatial distribution of vegetation types and human impacts. The objective was to rapidly assess the current status of the SNP, especially its vegetation, and investigate the possible human impacts by shifting cultivation, logging and mining. SNP is located in a remote area and access on ground was very difficult due to dense forests and extensive swamps, satellite remote sensing images, aerial video and Global Position System (GPS) technologies were used to this study with the support of the Geographical Information System (GIS). Seven Enhanced Thematic Mapper images of Landsat were classified by the combination of automatical classification and visual on-screen delineation in an established GIS. Eighteen GPS coordinates of interest points determined from Landsat images were selected in GIS for guiding the actual 1000 km flight route in aerial survey. The aerial video system time was synchronized to the GPS track of the flight route for positioning the digital video sequence used in accuracy assessment. Results show that the forest in the SNP is in very good condition. 98.5% of the SNP itself was covered by undisturbed, pristine evergreen lowland and swamp forests. No logging or mining activities were detected. However many human related land covers were found around the park and this indicates the SNP is currently under the threat from human beings.

2-1. Introduction

Salonga National Park (SNP) is located in the center of the Congo basin of the Democratic Republic of Congo and it lies in a large section of the central basin of the Zaïre River in Bandundu and Kasaï equatorial regions (1°00'S-3°20'S and 20°00'E-22°30'E), a very isolated region mainly accessible by water transport (**Fig. 2-1**). SNP is the second largest tropical forest national park in the world (next to the Tumucumaque Mountains National Park in Brazil which covers 38,700 km^2) and represents the largest area of protection for the bonobo apes. This park was created in 1970 and became inscribed on the United Nations Educational, Scientific and Cultural Organization (UNESCO) “World Natural Heritage List” in 1984 and “List of World Heritage Sites in Danger” in 1999.

Fig. 2-1. Location of Salonga National park. It is located in the center of the Democratic Republic of Congo as well as in the Bonobo range and represents the largest area of protection for the Bonobo apes. Source: http://www.zoosociety.org/Conservation/Bonobo/BCBI/Salonga.php

The park covers about 36,000 km^2 in two sectors of approximately equal size, separated by a corridor of about 45 km (Van Krunkelsven, 2001). The altitude of SNP is 350 meters to 700 meters rising from west to east. The climate is typically continental equatorial, hot and humid with mean annual precipitation of 2000 mm over most of the reserve, falling to 1800 mm in the south, and a slightly drier season from June to August. Rains are mostly downpours. Average relative humidity is 86%, regularly reaching saturation at night, but maintaining 77% mostly during the day. Temperatures are stable with daily mean variations from 20°C at night to 30°C during the day. Mean annual temperature is 24.5°C. Three types of landscape characterize the SNP: low plateau, river terraces, and high plateau. Rivers in the west of the north sector are large and meandering with marshy banks. On the higher ground in the east, valleys are deeper, and rivers may run below cliffs of up to 80 m. The south sector includes the watershed between the basin of the Luilaka, Lokoro, and Lukeni. Equatorial forest covers most of the area, varying in composition according to the geomorphology. The principal forest types are swamp, riverine, and dry-land forests. Evergreen ombrophile forest is dominated by well-developed stands of *Gilbertiodendron dewevrei*. Semi-deciduous forest covers almost all areas between the rivers, most frequently comprising *Staudtia stipitata*, *Polyalthia suavaeoleus*, *Scorodophloeus zenkeri*, *Anonidium mannii* and *Parinari glaberrimum*. Pioneer or transitory communities are found along riverbanks, including *Macaranga lancifolia* and *Harungana madagascariensis*.

SNP is the habitat of many endemic endangered species (Dupain *et al*., 1996). The most prominent animal species in the SNP is the bonobo chimpanzee *Pan paniscus* which is endemic to the Democratic Republic of Congo and is listed as highly vulnerable in the IUCN/SSC Action Plan for African Primate Conservation (Oates, 1986), endangered in the IUCN Red Data Book (Baillie and Groombridge, 1996), protected by Congolese and international laws and listed as Class A of the

African Convention (Dupain *et al*., 2000). Bonobo species are only found in central Africa and the SNP is the only area in bonobo territory that is at least theoretically protected by law and represents the largest potential area of protection for bonobos (**Fig. 2-1**).

The bonobo population density in SNP is only 1.15 bonobos per km^2 (Krunkelsven, 2001), but it is still higher than the densities of 0.45 and 0.43 respectively for Yalosidi (Uehara, 1988) and Lilungu (Sabater Pi and Vea, 1990), which are situated about 100 km east and 150 km northeast from the northern sector of the park. Bonobos prefer dry primary forest as the type of habitat (Horn, 1975; Kano, 1984) and they avoid secondary forests for nest building (Fruth, 1995). However, the bonobos themselves and their living environment are currently influenced by human activities.

In the area limited by the Congo stream and the rivers south of the SNP, the population of the bonobo in the northern half was as high as 54,000 in 1980s (Kano, 1984). However the population of the species might have declined to less than 5,000 individuals in 1990s (Thompson-Handler *et al*., 1995). In the Lomako forest, which is 200 km north of the SNP, at least two different kinds of threats decimated the populations of the bonobos (Dupain *et al*., 2000). One was the more intense hunting from indigenous inhabitants who were concentrating on commercial bush meat hunting as an alternative to the loss of their agricultural economy. To survive there was an increasing migration into the forest where they established permanent settlements, start small-scale cultivation, and hunt for bush meat. This tendency towards remigration into the forest from the more densely inhabited border areas because of the deteriorating of economic prospects, is a general phenomenon throughout Congo and other parts of Africa (Macgaffey, 1991; Pearce and Ammann, 1995; Goodall, 1996). The second was the increased commercial hunting from exotic people who entered the area. The population of the bonobos in the north part, except in the most impenetrable forest area, seemed to be decimated because of hunting. In contrast in the south-central part, where there was almost no hunting, there was still a rather large bonobo population (Dupain *et al*., 2000). As a consequence of the hunting, the smoked bush meat as well as live bonobo infants were exchanged for clothes, soap, bullets, medicines, and other goods in the market place of Lomako (Dupain *et al*., 2000). More important is that not only the bonobo is suffering from a quickly growing hunting pressure, but also seven other species of primates: *Cercopithecus ascanius*, *C. neglectus*, *C. wolfi*, *Cercocebus aterrimus*, *Colobus angolensis*, *Galago demidovi*, and *Allenopithecus nigroviridis* (Thompson-Handler *et al*., 1995). In addition, Wilkie *et al*. (1992) and Oates (1994) reported the former lumber roads of abandoned concessions helped to make remote areas more accessible.

The above mentioned bonobo status related to vegetation type and human activities indicate the importance of knowing the area and spatial distribution of land cover and land use. However, in spite of the importance of SNP to protect the different animal species especially the ape, up-to-date maps

were not available and little was known about the spatial distribution of vegetation types and human impacts influencing the wildlife status. Currently there are almost no management and park guard capacities available for most of the SNP area. The Institut Congolais pour la Conservation de la Nature (ICCN) officials in Kinshasa, as the wildlife management authority, received no reports from the park guards regarding wildlife status because many of the park guards fled to Kinshasa when the war started in 1998 and still remained there after this study was finished. The management capacities had been destroyed and ICCN personnel had been unable to monitor or control the park. The objective of this survey was a rapid assessment of the current status of the SNP, especially its vegetation and possible human impacts by shifting cultivation, logging and mining, and provide baseline maps in different scales for 1.) assisting the demarcation of the SNP area, 2.) an ecological monitoring system to be established, and 3.) improving SNP management (buffer zone management, park development) and ecological surveys (habitat mapping, biodiversity surveys etc.). Different land covers, especially the vegetation type and the human-related land features such as shifting cultivation and disturbed forest, needed to be investigated exactly. To better understand the human influence on this park, the investigation area was extended outside and the mapping of important features such as big rivers and agriculture around the SNP was also taken into account. Because the SNP is located in a remote area and access on ground to this area is very difficult due to dense forests and extensive swamps, the survey was therefore mainly based on the evaluation of satellite imagery. A Geographical Information System (GIS) was set up for managing and analyzing different sources data. To assess the accuracy of the mapping result a field and an aerial survey was conducted using Global Position System (GPS) technology and digital video recording.

2-2. Materials and methods

Seven cloud-free Landsat Enhanced Thematic Mapper (ETM) 7 imageries, all acquired in the year 2002, were chosen for this study (**Table 2-1**).

Table 2-1. Procured Landsat ETM scenes description

Path-Row	Date (DD, MM, YY)	Data description
179-60	18.8.2002	Band 1 (0.450-0.515 μm), 2 (0.525-0.605 μm), 3 (0.630-0.690 μm), 4 (0.750-0.900 μm), 5 (1.550-1.750 μm), and 7 (2.090-2.350 μm) at resolution of 30 meters; Band 6 (10.400-12.500 μm) at 60 meters; Panchromatic band (0.520-0.900 μm) at 15 meters.
179-61	18.8.2002	
179-62	23.2.2002	
178-61	15.1.2002	
178-62	15.1.2002	
177-61	25.2.2002	

First, geocorrection and reprojection were applied to each Landsat scenes in a unified Universal Transmercator projection with the WGS-84 Geodetic datum. Second, radiometric correction was done

to minimize differences between neighboring and successive orbits and a seamless image mosaic of the SNP area was produced.

The land cover/land use map was produced by a combined procedure of supervised classification and visual on-screen delineation. Landsat band 1 was excluded from the image processing because the haze that covered the acquisitions significantly influenced the data in shorter wavelengths. Resolution merge is a technique that combines a high spatial resolution data additively with the high spectral resolution image for producing high resolution, multispectral imagery (Schowengerdt, 1980). Landsat ETM sensor data have one panchromatic band with higher spatial resolution of 15 m (**Table 2-1**). Therefore Landsat bands 2-5 were resampled to a higher spatial resolution of 15 meters based on the panchromatic band using resolution merge algorithm and then were used for the classification process. Automatical classification using threshold value was applied to the mosaiced image for identifying some lands such as savanna and water, however most of the classification had to be done in a color image (combination: R5G4B3) using on-screen delineation method because haze in the image mosaic impeded any pixel-based classification procedures. The scale of on-screen delineation was set as 1:30,000 in GIS to achieve a mapping scale of 1:50,000. Small rivers/streams and roads are digitized as line themes. Mapping included the assessment of 1.) vegetation cover (year 2002) and natural features (rivers, lakes etc), 2.) current land use, human impact (logging, shifting cultivation etc.) and 3.) infrastructure (public and logging roads, settlements).

To validate the land cover and assess the classification accuracy derived from the satellite images, a field and an aerial survey were conducted from Feburary 3-17, 2003. During the field survey all major vegetation types were visited on foot with the support of GPS (**Fig. 2-2**). Different forest types typical for much of the SNP had been accessed on ground near the base camp. It was a 20 km hike from Ipope to the base camp (**Fig. 2-2** left). The trail crossed several large grasslands colonized by termites and two large swampy tracts along the Lokoro and some other rivers. Ecosystem and forest types as well as soil characteristics (wet soil, dry soil, nutrient poor sand soils, etc.) were recorded along the field survey. Approximately 300 photographs were taken for documentation. However the region covered by the survey was not big enough for the whole SNP, so an aerial survey was also conducted. In remote and inaccessible areas as the SNP, an aerial survey is more efficient and cheaper than ground-based methods.

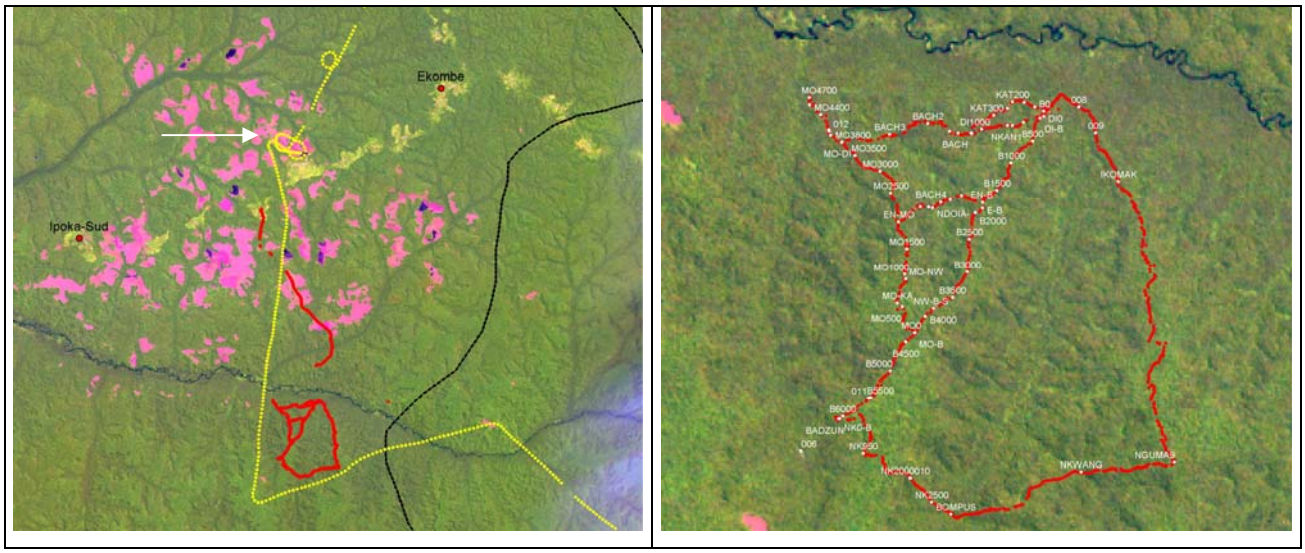

Fig. 2-2. Ground survey for verifying the land cover discrimination. Left: Ipope and Lokoro river. 5,4,3 band combination showing evergreen lowland forest (green), shifting cultivation (yellow-bright green) and grasslands (purple). Red lines: GPS track of field survey; yellow line: GPS track of aerial survey, black line: NP boundary according to Central African Regional Program for the Environment (CARPE). On the right side there are the GPS tracks of biodiversity transects. White arrow: air strip. Length of GPS recorded transects: approx. 30 km.

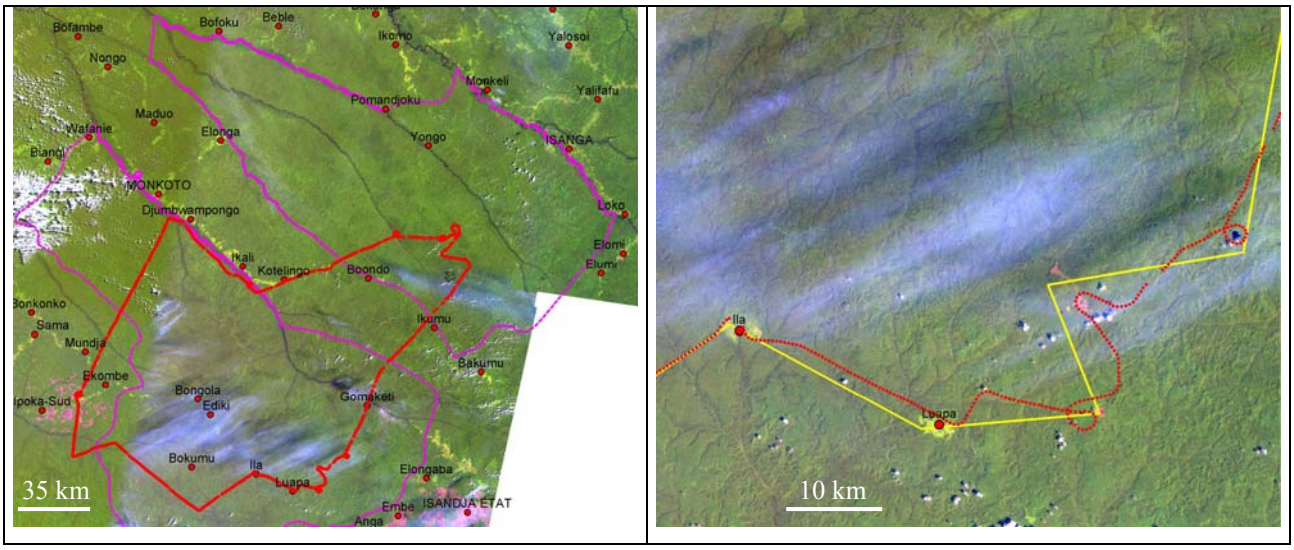

Fig. 2-3: GPS recording of the aerial survey (red line in left) and a section (right) of the planned (yellow) and actual (red) flight path.

The aerial survey allowed inspecting representative samples for each major class and some unclear features from the air, e.g. areas which were suspected as mining activities. The flight route was planned in laboratory with the satellite image as reference before the airplane took off. The coordinates of interest points in flight route were visually determined using the georeferenced and mosaiced landsat satellite image. The flight route was intently determined in a such a way that all

typical lands could be guaranteed for checking. Altogether 18 points coordinates were selected and the route linked by these 18 points was stored in GIS for the planned aircraft track in a line theme format.

Before the airplane took off, one video camera was fixed in the right side of airplane with the view angle being approximately 45° to the earth surface. The system time of one GPS instrument and this digital video camera were synchronized. When the actual aerial survey was implemented, the position signal of the airplane was recorded by this onboard GPS instrument in "continuous track" mode in every 5 seconds. The GPS coordinates, as well as the time, were timely imported to the laptop GIS system, in which the satellite image mosaic, the land cover map and the planned flight route were stored. By displaying on-line the current GPS recorded position on the satellite image and the planned flight track, it was possible to adjust the flight path and to visually compare the satellite image with the real world situation. **Fig. 2-3** shows the GPS recorded track of the aerial survey (left) and a section of the planned (yellow) and actual (red) flight path.

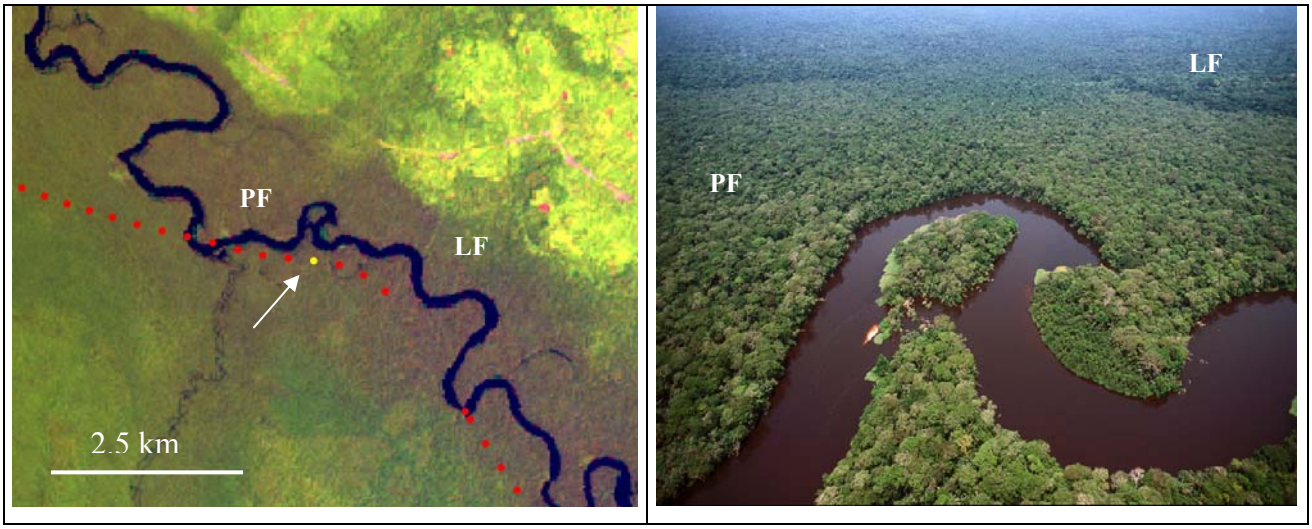

Fig. 2-4. Identifying specific geographic locations in the satellite image (left, R5G4B3) and at the same time in the digital video sequence (right). Note the sharp boundary of permanently inundated forest (PF) and mixed lowland forest (LF). This GPS point (yellow) superimposed with the satellite image indicates the same location on the right digital video scene because the GPS recorded time are the same as the recorded time of the digital video sequence.

Totally the route of the aerial survey covered approximately 1,000 km. Flight height above the surface was usually 300-500 meters. In some areas we went down to 200 meters to get close up views of the land feature. The right view along the flight was documented by digital video (4 hours). This recorded video material was used to validate the classification and assess the accuracy in laboratory. First, 361 video sequences (approximately every 2 minutes) were chosen for visual interpretation. It was intently guaranteed that the time of each chosen video sequence was also recorded in the GPS track database so that it could be exactly positioned by the GPS. In visual video interpretation the center parts of these video sequences were used. Second, the GPS point that had the same time as this video sequence

was identified, and the classification of the location, which was perpendicular to the flight direction and 1-2 km distant to this GPS point, was compared to the video sequence interpretation. **Fig. 2-4** shows one example of satellite and the video sequence.

2-3. Results

Both the Landsat satellite image mosaic, which provided the vivid landscape qualitatively, and the land cover map, which provided the detailed information quantitatively, were produced. Four different products were designed from the initial 1:50,000 classification with the minimum distance of 0.5 mm in map sheet: 1.) Satellite image map of the SNP, scale 1:400,000 (**Fig. 2-5,** top), 2.) land cover and land use map of the SNP, scale 1:400,000 (**Fig. 2-5**, bottom), 3.) land cover and land use map of the northern part of the SNP, scale 1:100,000, and 4.) land cover and land use map of the southern part of the SNP, scale 1:100,000. In land cover and land use product, those land features related to human activities around the SNP were also included, because they are an important indicator for showing the human influence on the SNP. The area and percent of each land cover/use class are shown in **Table 2-2**.

Table 2-2. Different land cover and their area within and around the SNP

No	Class names	Area within the SNP(ha)	Area around the SNP (ha)
1	Mixed lowland forest	1,386,576	x
21	Mixed lowland forest (dark signature in ETM)	25,919	x
4	Lowland forest on plateau	781,031	x
5	Lowland forest in valleys	778,067	x
2	Swamp forest	25,580	x
3	Palm swamp forest	736	x
6	Lowland forest, Riverine seasonally inundated	107,355	x
7	Lowland forest, Riverine permanently inundated	86,813	x
8	Dry grasslands, savanna	150	52,575
9	Wetland	2,529	x
10	Regenerating forest	20,447	11,312
11	Strongly degraded forest, bushland	3,237	2,715
12	Agriculture (shifting cultivation)	8,454	213,815
13	Libeke within the National Park (wet grassland)	26	x
33	Esobe within the National Park (dry grassland)	380	x
14	Disturbed forest (possibly mining, logging or natural)	1,435	x
15	Bare soil, cleared land	6	158

No	Class names	Area within the SNP(ha)	Area around the SNP (ha)
16	Plantation*	0	173
18	Clouds	88,014	x
19	River	11,562	x
20	Lake	167	x
30	unmapped	8,672	x
Sum		**3,337,156**	**x**

Landsat image (**Fig. 2-5**, top) shows the vegetation in both the north part and south part is well protected. However the transitional zone between the North and the South is influenced by shifting cultivation. Land cover classification (**Fig. 2-5**, bottom) shows most of the vegetation found in the SNP is lowland forest. Riverine forest distribute along the bigger rivers crossing the SNP. These rivers make up the only infrastructure enabling access to the park. The current vegetation status of SNP is in good condition: totally 98.5% inside the SNP is covered by undisturbed, pristine evergreen lowland and swamp forests. Very few villages can be found in SNP, however many relatively big villages were found around the park boundary and these villages are surrounded by areas of shifting cultivation. No logging or mining activity could be detected. In the southern section some small villages of shifting cultivators are located along the footpath from Ipope to Anga. The accessibility to SNP by river and the surrounding human residential areas around SNP indicate this park is easy to be influenced by human activities. Few villages detected within the SNP indicate the conceived policy of transmigrating the local people outside of the SNP is feasible (Schoonbroodt, 1987).

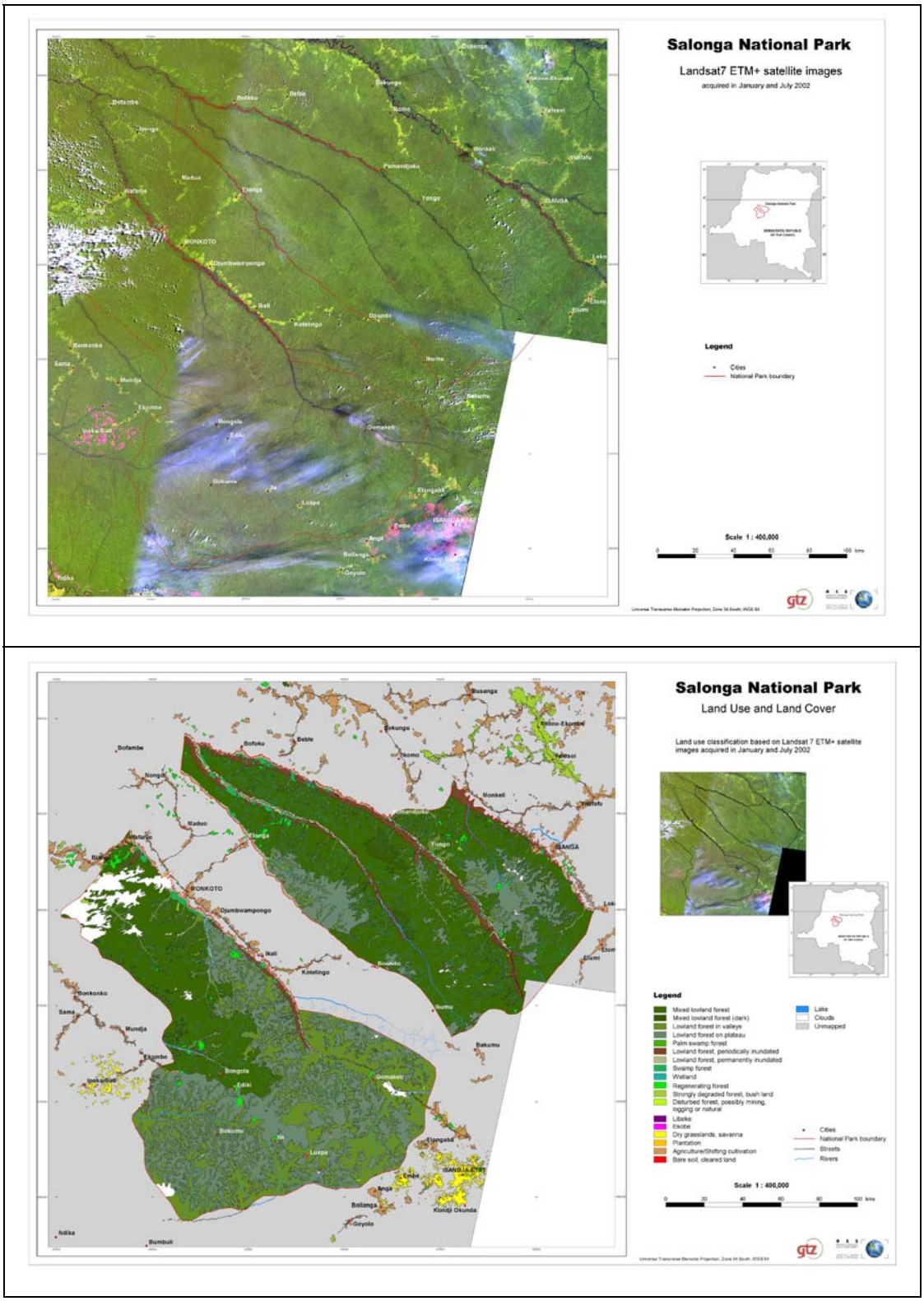

Fig. 2-5. The overview illustration of Satellite image map (top, R5G4B3) and the classification map of the Salonga NP (bottom) showing the overall pattern of land cover/use.

In addition, only some small areas of secondary forest were found within the park, which indicates the current vegetation is good for bonobos because they avoid secondary forests for nest building

(Fruth, 1995). “Libeke” and “Esobe” are two unique features in this SNP which are from local language representing important land to wildlife activities.

The result of accuracy assessment is shown in a Pivot table (**Table 2-3**). Class 3 (palm swamp forest), 14 (disturbed forest), 15 (bare soil) and 16 (plantation) were not found along the aerial survey track. For all other classes random sample points ranging from 2 to over 100 were taken for accuracy assessment. Since class 10 (regenerating forest) and 11 (strongly degraded forest) are almost non-existent within the SNP, very few random sample points could be respectively adopted. Most difficult was the discrimination of class 1 (mixed lowland forest) from class 5 (lowland forest in valleys) as well as class 4 (lowland forest on plateau) from class 1 (mixed lowland forest). Overall classification accuracy for class 1 was 81.3% and for class 4 (lowland forest on plateau) was 84.7%. Class 1 (mixed lowland forest) was assigned to lowland forests on undulating relief with a slightly darker green signature in band combination (R5G4B3) of the Landsat image mosaic while class 4 was assigned to lowland forests on flat plateaus with almost no relief. Class 4 (lowland forest on plateau) has a bright green signature in band combination 5, 4, 3 of the Landsat image mosaic. Permanently and periodically inundated forests could be discriminated clearly from all other forest and vegetation types. 100 % accuracy was recorded for classes 8 (grasslands/savanna) and 12 (agriculture).

Table 2-3. Pivot table of the accuracy assessment based on aerial survey

Ground observation / Classified class	**1**	**2**	**4**	**5**	**6**	**7**	**8**	**9**	**10**	**11**	**12**	**13**	**Sum**
1 Mixed lowland forest	**91**		7										98
2 Swamp forest		**10**											10
4 Lowland forest on plateau	2		**50**										52
5 Lowland forest in valleys	18		1	**58**									77
6 Riverine forest, seasonal					**23**								23
7 Riverine forest, permanent	1			1	2	**39**							43
8 Dry grasslands, savanna							**12**						12
9 Wetland								**5**					5
10 Regenerating forest									**2**				2
11 Degraded forests, bush land			1							**3**			4
12 Agriculture											**30**		30
13 Libeke, 33 Esobe												**5**	5
Sum	112	10	59	59	25	39	12	5	2	3	30	5	**361**

Note: The class code represents the same class name as in Table 2-2.

The field survey showed that all forest types that had clear differences in signature in the Landsat ETM images could be discriminated in the field. On the other hand there were no vegetation types that were not recognized in Landsat ETM except probably small patches of palm swamp forest. Small sedge meadows (less than 2 ha area) along the rivers were visible in Landsat and were mapped together with suspected small patches of palm swamp forest. We visited two areas of suspected illegal logging or mining, but in both cases no human activity could be observed. We believe that these signatures represent natural erosion or animal activities, e.g. by elephants.

2-4. Summary and discussion

A high resolution land cover map was unavailable for Salonga NP before this study while many coarse resolution satellite data had been used extensively to map global or regional land cover (DeFries and Townshend, 1999; Cihlar, 2000). The GLC2000 land cover map of Africa (http://www.gvm.sai.jrc.it/glc2000/Products) used SPOT VEGETATION sensor data with ground resolution of 1 km and only three different kinds of vegetation types in SNP were detected: closed evergreen lowland forest, swamp forest and forest mosaics. In the Tropical REsources and Environment monitoring by Satellite (TREES) map there are only two classes detected: lowland moist forest and secondary forest mosaic (Achard *et al*., 2001). The U.S. Geological Survey produced the global land cover classification for the International Geosphere–Biosphere Programme (IGBP) with 17 classes (Loveland *et al*., 2000). The University of Maryland (UMD) produced global land cover classification with 14 classes (Hansen *et al*., 2000). The Boston University produced global land cover using both IBGP and UMD legend (Strahler *et al*., 1999; Friedl *et al*., 2002). However due to the coarse spatial resolution these data are of limited use for monitoring the status of Salonga NP.

The result of this study is the first detailed information on land cover and land use in the SNP and surrounding areas. Shortly after this study finished in March of 2003, another land cover dataset produced from visual interpretation of digitally enhanced LANDSAT TM images (Bands 4,3,2) acquired mainly in the year 2000-2001 by "Africover" (see http://www.africover.org/download/documents/Short_Project_description_en.pdf) was released in October 2003. This land cover classes had been developed using the FAO/UNEP international standard LCCS classification system and the scale is 1:200,000. These two land cover datasets enhanced the monitoring and management capability of the SNP.

During the workshop in Kinshasa and further discussions we found that the boundary provided by CARPE that was used for the SNP land cover map is not correct in several locations (about 20% of its length). The CARPE boundary does not agree with new information based on maps provided by ICCN and the original law text (Ordonnance No 70/318 dated on 20.11.1970, unpublished). It is therefore suggested to integrate this new information and update the boundary and the missing land covers

accordingly and then to serve as reference for all coming activities related to the protection and management of the SNP. In addition a second task was considered as highly important and valuable for the future work of ICCN and other interested institutions: the assignment of names to all rivers visible in the satellite image according to information derived from detailed maps. This will greatly facilitate the planned demarcation missions, and all field survey teams can be equipped with print outs of satellite image maps showing correctly assigned river and village names as well as land cover.

2-5. Acknowledgements

Special thanks to GTZ (German Society for technical cooperation) and ICCN (the Institut Congolais pour la Conservation de la Nature) for financial support on this study. The help from Dr. Barbara Fruth and Gottfried Hohmann is also appreciated.

2-6. References

Achard, F., Eva, H. & Mayaux, P. (2001). Tropical forest mapping from coarse spatial resolution satellite data: production and accuracy assessment issues. *International Journal of Remote Sensing, 22,* 2741-2762.Baillie, J. & Groombridge, B. (1996). 1996 IUCN Red List of Threatened Animals. IUCN Gland. Switzerland. 378 p.

Cihlar, J. (2000). Land cover mapping of large areas from satellites: Status and research priorities. *International Journal of Remote Sensing, 21,* 1093– 1114.

DeFries, R. S., & Townshend, J. R. G. (1999). Global land cover characterization from satellite data: From research to operational implementation? *Global Ecology and Biogeography, 8,* 367– 379.

Dupain, J., Van Krunkelsven, E. & Van Elsacker, L. (1996). Bonobo in situ. Iyema. Update No. 1. 1 June, EEP-Newsletter.

Dupain, J., Van Krunkelsven, E., Van Elsacker, L. & Verheyen, R. F. (2000). Current status of the bonobo (Pan paniscus) in the proposed Lomako Reserve (Democratic Republic of Congo). *Biological Conservation,94*, 265-272.

Friedl, M. A., McIver, D. K., Hodges, J. C. F., Zhang, X. Y., Muchoney, D., Strahler, A. H., Woodcock, C. E., Gopal, S., Schneider, A., Cooper, A., Baccini, A.,Gao, F., Schaaf, C. (2002). Global land cover mapping from MODIS: algorithms and early results. *Remote Sensing of Environment, 83,* 287-302.

Fruth, B. (1995). *Nests and Nest Groups in Wild Bonobos (Pan paniscus): Ecological and Biological Correlates.* PhD Thesis. Shaker. Aken.

Goodall, J. (1996). Foreword: conserving great apes. In McGrew, W.C. & Marchant, T. (Eds.), *Nishida, Great Ape Societies*. . Cambridge: Cambridge University Press.

Hansen, M. C., DeFries, R. S., Townshend, J. R. G., & Sohlberg, R. (2000). Global land cover classification at 1 km spatial resolution using a classification tree approach. *International Journal of Remote Sensing, 21,* 1331– 1364.

Horn, A. (1975). Adaptations of pygmy chimpanzee (Pan paniscus) to forests of Zaire basin, *American Journal of Physical Anthropology, 42*, 307.

Kano, T. (1984). Distribution of pygmy chimpanzees (Pan paniscus) in the Central Zaire Basin. *Folia primatologica, 43,* 36-52.

Kano, T. (1992). *The Last Ape Pygmy Chimpanzee Behavior and Ecology*. Stanford: Stanford University Press.

Loveland, T. R., Reed, B. C., Brown, J. F., Ohlen, D. O., Zhu, Z., Yang, L.,& Merchant, J. W. (2000). Development of global land cover characteristics database and IGBP DISCover from 1 km AVHRR data. *International Journal of Remote Sensing, 21,* 1303– 1330.

MacGaffey, J. (1991). *The Real Economy of Zaire: the Contribution of Smuggling and other Unofficial Activities to National Wealth*. London:James Curry.

Oates, J. F. (1986). *Action Plan for African Primate Conservation:1986-1990*. IUCN/SSC Primate Specialist Group. New York: Stony Brook.

Oates, J. F. (1994). Africa's primates in 1992: conservation issues and options, *American Journal of Primatology, 34,* 61-71.

Pearce, J. & Ammann, K. (1995). *Slaughter of the Apes*. London: WSPA.

Sabater P., J. & Vea, J. (1990). Nest building and population estimates of the bonobo from Lokofe-Lilungu-Ikomaloki region of Zaire. *Primate Conservation, 11,* 43-47.

Schoonbroodt, A. (1987). Motifs de la création et historique ancien du Parc National de la Salonga. In: Premier séminaire international sur la gestion et l'avenir du Parc National de la Salonga. Institut Zairois pour la Conservation de la Nature Mbandaka. Zaire. 39-40. (in French).

Schowengerdt, R. A. (1980). Reconstruction of multispatial, multispectral image data using spatial frequency content. *Photogrammetric Engineering & Remote Sensing, 46,* 1325-1334.

Strahler, A., Muchoney, D., Borak, J., Friedl, M., Gopal, S., Lambin, E., & Moody, A. (1999). MODIS Land Cover Product Algorithm Theoretical Basis Document (ATBD), Version 5.0, NASA EOS-MTPE Documentation, NASA, Washington, DC. 66 pp.

Thompson-Handler, N., Malenky, R. K. & Reinartz, G. E. (1995). *Action Plan for Pan paniscus: Report on Free-ranging Populations and Proposals for their Preservation*. Zoological Society of Milwaukee County. Wisconsin: Milwaukee.

Uehara, S. (1988). Grouping patterns of wild pygmy chimpanzees (Pan paniscus) observed at a marsh grassland amidst the tropical rain forest of Yalosidi. Republic of Zaire. *Primates, 29*, 41-52.

Van Krunkelsven, E. (2001). Density estimation of bonobos (Pan paniscus) in Salonga National Park, Congo. *Biological Conservation, 99,* 387-391.

Wilkie, D. S., Sidle, J.G. & Boundzanga, G. C. (1992). Mechanized logging, market hunting and bank loan in Congo. *Conservation Biology, 6,* 570-580.

CHAPTER 3---LAND COVER CLASSIFICATION OPTIMIZED TO DETECT AREAS AT RISK OF DESERTIFICATION IN NORTH CHINA BASED ON SPOT VEGETATION IMAGERY

Monitoring of desertification processes by satellite remote sensing is an important task in China and other arid regions of the world. A full year time series of SPOT VEGETATION images with 1 km spatial resolution was used to produce a land cover map with special emphasis on the detection of sparse vegetation as an indicator of areas at risk of desertification. The study area covered 2000 x 3500 km in North China extending from boreal forests to the Gobi desert to the Tibet high plateau. A classification approach for different land cover types with special emphasis on sparse vegetation cover was developed which was able to resolve problems related to seasonal effects and the highly variable natural conditions. The best classification results were obtained by exploiting seasonal effects detectable in time series of optimized Normalized Difference Vegetation Index images calculated from 10-day composites. The result of the land cover classification suggests that 1.60 Million km^2 are areas at risk of desertification. Due to the wide swath and sensitivity to vegetation growth SPOT VEGETATION imagery should be very useful to detect large scale dynamics of environmental changes and desertification processes.

3-1. Introduction

According to the definition of the United Nations Convention to Combat Desertification (UNCCD), 'desertification' means land degradation in arid, semi-arid and dry sub-humid areas resulting from various factors, including climatic variations and human activities. China is one of the countries with vast desertified areas and desertification is a serious problem in many regions of the country (Zha and Gao, 1997). Almost 60% of its population is living in areas at risk covering approximately 3.327 Million km^2 in 13 provinces and autonomous regions mainly in the North of China (CNC-UNCCD, 1996). The desertification by wind erosion has exceeded the total area of arable lands in China and the most seriously wind-eroded areas are mainly spread out in desert areas in Xinjiang, Qinghai, Gansu province as well as Inner-Mongolia and Tibet autonomous regions. CNC-UNCCD (1996) estimated that 13 Million ha. of arable lands had been threatened by disasters of wind and sand storms; about 100 Million ha of steppe, desert steppe and pasture lands had been seriously degraded due to the desertification caused by wind erosion and sand drifts; thousands of water conservation facilities and irrigation systems had been threatened. Desertification causes a direct economic loss estimated between US$2–3 billion while the associated indirect loss is 2–3 times more (Zha and Gao, 1997).

Neighbouring to the North of China, Mongolia has the same desertification problem. It has been estimated that more than 78% of the total territory of Mongolia is under the risk of desertification, of which nearly 60% is classed as highly vulnerable, and this problem has arisen since 1990 as the number of livestock has increased (Yang *et al*., 2004).

Desertification in China is caused by both environmental settings and inappropriate human activities including overcultivation, overgrazing, construction of transportation routes, and excessive gathering of fuelwood and plant species for medicinal purpose (CNC-UNCCD, 1996; Zha and Gao, 1997). Nevertheless, deserts are expanding and desertification processes have accelerated in many regions in the past two decades: the annual area of desertification increased from 1560 km^2 in 1950-60s to 2460 km^2 in 1990s (CMA, 2002).

Frequent sandstorms which are a direct consequence of desertification are observed in North China. The areas most seriously affected by sandstorms are located in the arid and semi-arid middle-latitude regions (CMA, 2002). Eight large sandstorms were observed in the 1960s, 13 in 1970s, 14 in 1980s and 20 in 1990s. In March 2002 the most violent sandstorm ever observed since the 1990s affected over 1,400,000 km^2 of land and 130 Million people. Almost half of recently reclaimed wastelands became the major source for this sandstorm. Sandstorm affecting Hebei province in 2002 originated from about 250,000 km^2 of degraded and discarded arable land and not from the Gobi desert as perceived by most people (CMA, 2002). Wang *et al*. (2004) found that dust storms were highly correlated with human activities and climate change, while real deserts contributed only marginally to the observed dust storms.

To combat desertification China has taken many measures (Yang, 2004; Zha and Gao, 1997; Guo *et al*., 1989). The most famous program is called “Three-North forest shelter belts”. The “Three-North” region consists of three sub regions: Northeast, North, and Northwest of China covering 3.89 Million km^2, almost 40 percent of the country’s territory. Although the project has brought amelioration of ecosystems in some areas, desertification and soil erosion have worsened in much of the northern part of the country (Yang, 2004).

Continuous monitoring is required to understand the processes leading to desertification. Since the area is so vast remote sensing is required to support programs that combat desertification (Wang *et al*., 2000). Remote sensing has been applied to monitor desertification in Asia, to map land cover/land use and to ascertain indicators for desertification (Crépeau *et al*., 2000; Kharin, *et al*., 1999; Tsunekawa, 2000a, 2000b). NOAA Advanced Very High Resolution Radiometer (AVHRR) Normalized Difference Vegetation Index (NDVI) data have also been used with some success to assess the condition of the vegetation in arid and semi-arid regions (Bastin *et al*., 1995; Prince, 1991; Tripathy *et*

al., 1996; Tucker *et al*., 1991; Weiss *et al*., 2001). Collado *et al*. (2002) and Ghosh (1993) demonstrated the application of high resolution satellite data such as Landsat TM, Landsat MSS, and IRS-I, ISS-II to investigate desertification processes.

Historically, ground surveys are conducted to collect desertification information in China, and this method is gradually replaced by small-scale aerial photographs interpretation. Since the emergence of space-borne remote sensing, satellite images have been utilized to delineate the extent of desertified areas (Zha and Gao, 1997). Geographical Information System (GIS) and remote sensing were used to prepare maps of soil degradation in the Loess plateau that is the region most seriously affected by soil erosion in the world (CNC-UNCCD, 1996). Long (2000) applied an AVHRR time series NDVI for monitoring desertification in China and described the growing season of different vegetation types as well as the relation between NDVI and the degree of soil erosion. Zhong and Qu (2003) compiled the 'Modern Dynamical Changes Map of Sand Deserts in China' at a scale of 1:500,000 using aerial photographs and TM images. Liu *et al*. (2004) used Landsat TM to assess the grassland degradation. Currently it is not feasible to use high resolution satellite imagery to monitor large regions like the Three-North shelter belt because of high costs, effort and data unavailability. Therefore a multi-scale remote sensing monitoring approach is proposed in which coarse resolution satellite imagery should be used to monitor large scale processes and to identify "hotspots" of change, i.e. desertification, and then these areas should be analyzed using higher resolution satellite data (Lin and Zhou, 2000; Sun and Chen, 2000; Sun and Zhou, 2000).

In this paper, the characteristics and usefulness of low resolution SPOT VEGETATION satellite imagery for desertification assessment and monitoring were investigated. A land cover classification approach optimized to detect sparse vegetation cover was developed, because these are likely areas at risk of desertification. The overall objective was to find out whether SPOT VEGETATION is useful to identify areas at risk of desertification over large areas such as Northwest China and whether it could be used in a multi-scale desertification monitoring system.

3-2. Material and methods

Study site

The study site (**Fig. 3-1**) covers an area from 86°00'E to 119°00'E in longitude and from 49°00'N to 35°00'N in latitude (2000 x 3500 km, 7 Million km^2). The land cover types vary greatly in this vast area, including evergreen forest, deciduous forest, agricultural areas in which crops are grown once or twice a year, shrubland, grassland and barren deserts like Gobi. Land cover variability is strongly influenced by the monsoon climate system and elevation. The monsoon circulation creates a strong seasonality in precipitation: availability, the amount, and the spatial distribution of the annual precipitation is controlled by several sources and prevailing winds (Xue, 1996). The majority of annual precipitation falls in the warm summer season in association with the arrival of the monsoon. Summer is also the time of the critical growing season when vegetation activity is at its maximum. Elevation, varying from sea level to over 6000 meters, also has great effects on land cover: several sizable mountain ranges and the north part of the Tibet Plateau are located within the study site. With the influence of the continental monsoon climate and altitude, the study site can be divided into three climate zones, i.e. the humid and semi-humid subtropical zone, the arid and semi-arid temperate zone, and the Tibet Plateau zone.

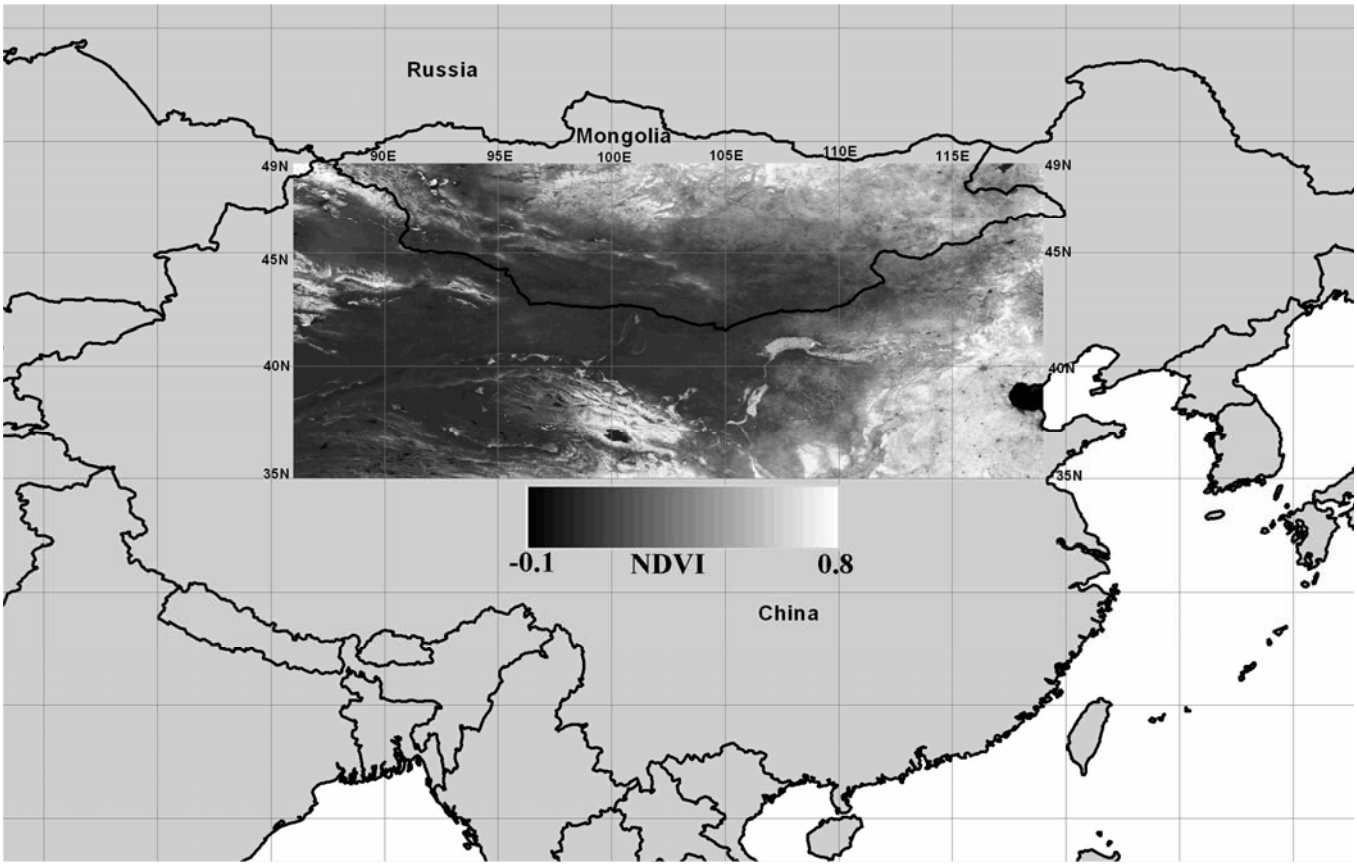

Fig. 3-1. The study area in 86°00'E - 119°00'E and 49°00'N - 35°00'N. Annual Maximal NDVI as background image.

For the classification, the type of forest canopy density (open/closed), seasonal forest types (evergreen/deciduous) and leaf type (needleleaf/broadleaf) as well as different seasonal types of agriculture besides general features such as water bodies, urban area, and permanent snow/ice were discriminated. A class of "mixed grassland and agriculture" was also considered because this indicates an important transitional ecological zone and is seriously affected by desertification (Pei, 1999). Most important was the identification of sparsely vegetated areas that are most fragile and are in peril of desertification. The sparsely vegetated areas were defined as land whose vegetation (herbaceous or shrub) cover is between 10% and 40%. Land with less than 10% vegetation cover was classified as non-vegetated area in this study.

Image processing and classification

A time series of SPOT VEGETATION images acquired in the year 2000 with daily coverage of the study site was provided by Joint Research Center (JRC) within the framework of the GLC2000 initiative. The 365 images were co-registered to an uniform geographical Latitude/longitude projection based on WGS84 spheroid with a pixel size of 0.0089285714 degrees. The data set included four spectral bands (blue, red, NIR, MIR), four view geometries angles (VZA, VAA, SZA, SAA) and one status map (**Table 3-1**).

Table 3-1. SPOT VEGETATON daily data set

Data set	Description
B_0	Blue 0.43-0.47 μm
B_2	Red 0.61-0.68 μm
B_3	NIR 0.78-0.89 μm
B_4	MIR 1.58-1.75 μm
SM (Status Map)	Radiometric quality for 4 bands, land/water, ice/snow and cloud status
VZA, VAA	View Zenith Angle and View Azimuth Angle
SZA, SAA	Solar Zenith Angle and Solar Azimuth Angle

Cloud cover, snow/ice, MIR stripes and directional effects disturbed the quality of single day SPOT VEGETATION images (Passot, 2000). Cloud and snow/ice were eliminated using the information of the band Status Map (SM). MIR stripes were identified and eliminated using an averaging by 7x7 filter. Directional effects were eliminated using the Bidirectional Reflectance Distribution Function (BRDF) model of Roujean *et al*. (1992). 10-day composites were calculated by the maximal NDVI method (Holben, 1986). The time series NDVI data was improved by the Harmonic Analysis of NDVI Time Series (HANTS) algorithm (Roerink *et al*., 2000). The annual

maximal NDVI for the year 2000 was calculated using the maximal value of the 36 NDVI 10-day composites.

Training sites were selected based on Advanced Spaceborne Thermal Emission and Reflection (ASTER) imagery and GPS-recorded field observations. Subsequently the land cover was classified in four steps:

1.) water bodies and permanent snow/ice were visually identified in the 10-day composites using the GTOPO Digital Elevation Model (DEM) as reference. Urban areas were digitized from a NDVI combination (R: NDVI of June, G: July and B: August) which was superimposed by the city GIS layer of Digital Chart of the World (DCW).

2.) vegetated and non-vegetated areas were separated based on threshold values: if the annual maximal NDVI was less than 0.116, then the pixel represented non-vegetation, and if larger than 0.26, then it belonged to vegetation. In the range from 0.116 and 0.260, the annual maximal NDVI criteria was not sufficient to discriminate sparse vegetation from non-vegetated land unambiguously because the NDVI of sparse vegetation is influenced by signals from the soil (Edwards *et al*., 1999). Therefore the following criteria were used for identifying vegetated area: a pixel was vegetation if (a) the NDVI was maximal between June to September (when the majority of annual precipitation occurs) and (b) the standard deviation of the NDVI from April to October (Weiss *et al*., 2001) was higher than a threshold of 0.19.

3.) non-vegetated areas were classified into stone/rock (Gobi) and sand desert based on single day cloud-free SPOT VEGETATION image.

4.) Vegetated areas were classified based on the seasonal variation of the NDVI and ancillary data (**Fig. 3-2**). Agricultural areas with two or more harvests were identified using their unique characteristic of more than one NDVI peak. To separate forested areas, shrub and grasslands, the ISODATA classification was applied on three NDVI images of August (peak growing season), May (beginning of growing season) and March (non-growing season). These areas were then further specified using the China forest belt map to discriminate deciduous and needle forest types (Hou, 1988), the map of the agricultural-grazing transition zone to identify the mixed grasslands/agriculture (Pei, 1999) and the GTOPT DEM to identify agriculture (one harvest) in lowland areas.

The classification accuracy was assessed using a random sampling scheme: a point GIS layer within the coverage of 17 ASTER (The ASTER reflectance retrieving is described in **Appendix 2**) and 8 Landsat images was created with a distance between neighboring points being 0.1 degree in longitude and latitude. Totally 2941 reference points were selected, only 37 were cloud covered in the reference images. All points were visually interpreted in the ASTER and Landsat images and compared to the classification result.

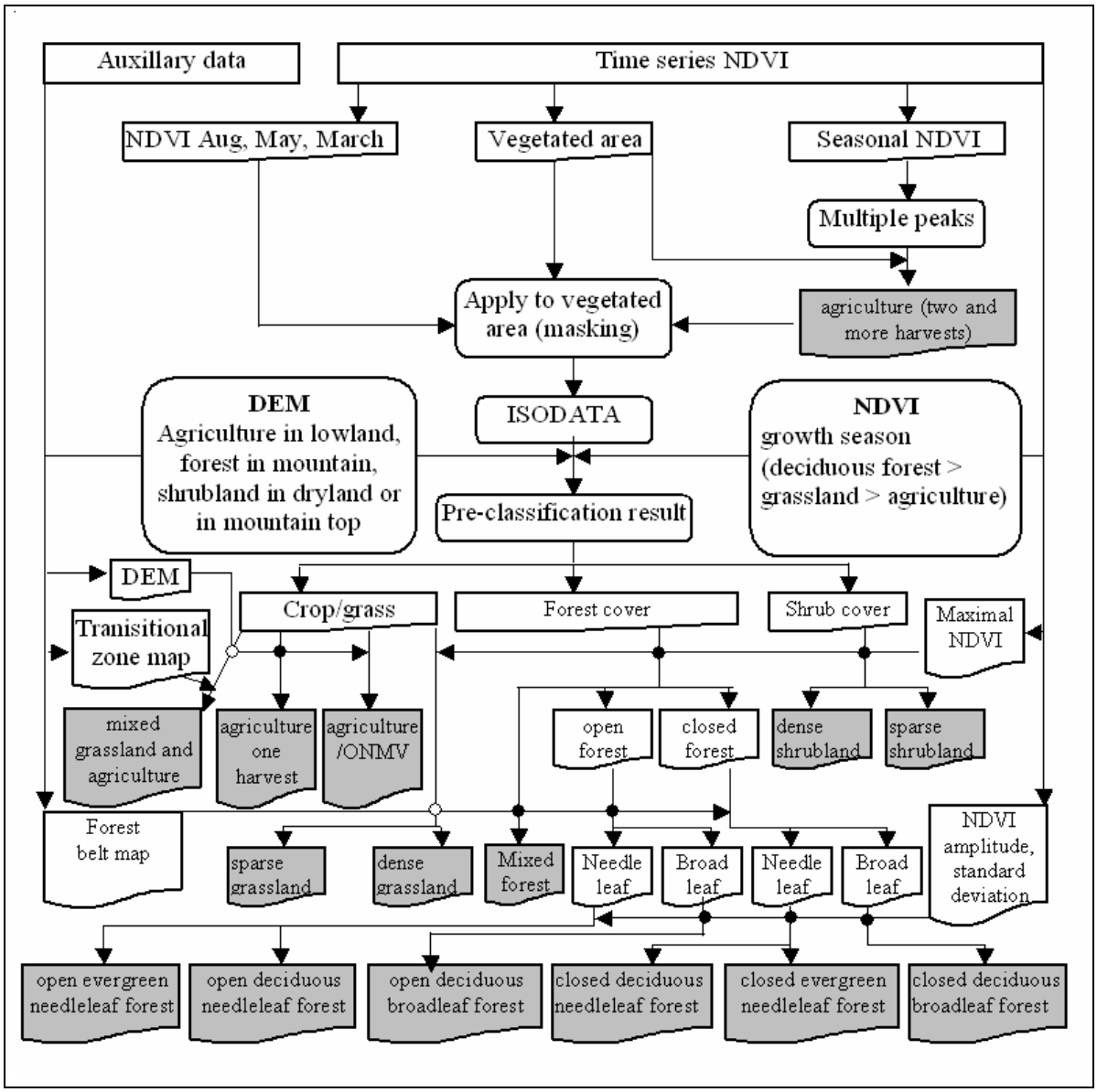

Fig. 3-2. Flowchart diagram of the vegetation classification. The vegetated area is a result of the discrimination of vegetation and non-vegetation (see text). ONMV is the abbrevation of "other natural mixed vegetation". The shading indicate the final classification.

3-3. Results

The annual maximal NDVI allowed to discriminate vegetated and non-vegetated areas. **Fig. 3-1** shows that large areas of the study site are desert. Large areas in the western part of the study area had very low NDVI values indicating the Taklamakan, Tengger, Muus deserts. High NDVI values were found in the Southeastern humid and semi-humid regions, the boreal forest belt in Mongalia, some mountain ranges in Xinjiang province and the land around Lake Qinghai. In the Northwest part of the study sites, the annual maximal NDVI of agriculture was obviously higher than the surrounded sparse vegetation or desert, and the agriculture there could be easily discriminated. After comparing the result of the annual maximal NDVI with the available ASTER imagery, it was found that the annual

maximal NDVI could be used to discriminate the dense/sparse shrubland, dense/sparse grassland as well as open/closed forest.

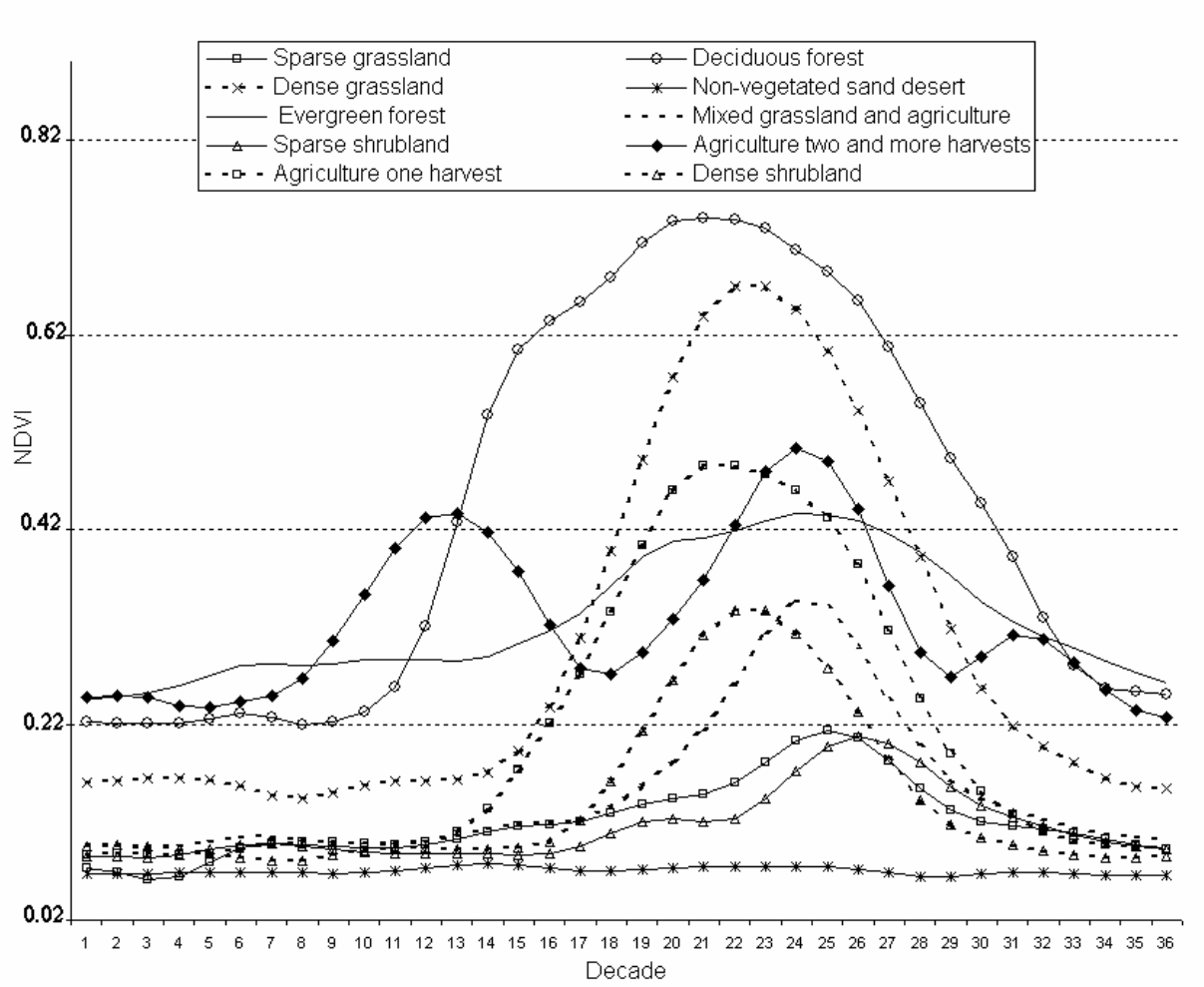

Fig. 3-3. Time series scaled NDVI of selected training sites.

The NDVI time series of the 10-day composites showed a distinct seasonal pattern for different vegetation types (**Fig. 3-3**) while the NDVI of non-vegetated areas (sand desert and Gobi) showed low, stable values throughout the year. The NDVI of vegetated areas began to increase in May and decreased again in October with a peak in July and August, which conforms to vegetation growth in North China (Hou, 1988). In the Southeast of the study area, agricultural areas with two or more harvests showed more than one NDVI peak while all other vegetation classes had only one peak. This NDVI signal conforms to the agricultural practice in North China: Winter wheat starts to grow in March and is ready for harvest in June, while other crops begin to grow in July and are ready for harvest in October. In addition, the NDVI time series revealed considerable differences between forest types during summer (the peak of growing season) and winter (non-growing season): the NDVI of evergreen forest was higher than that of deciduous forest in winter, while it was lower in summer (June to September). The higher NDVI value of deciduous forest during summer indicates the greater chlorophyll content of the canopy, which was also observed by Boles *et al*. (2004). Therefore the annual NDVI amplitude (the difference of annual maximal NDVI and annual minimal NDVI) and the

coefficient of variation of the NDVI values could be used to discriminate evergreen forest and deciduous forest. **Fig. 3-3** also shows the lengths of the growing season were different between agriculture (one harvest), deciduous forest and grassland: The length of the growing season of deciduous forest was longer than that of grassland, and grassland longer than that of agriculture. Since these results well represented natural processes (Groten and Ocatre, 2002), these properties were used to discriminate different land cover types. It was found that the NDVI of sparse vegetation varied with the seasonal change of photosynthetic activity, increasing at the beginning of June, peaking in August and decreasing again in September, while non-vegetated areas did not show such a temporal pattern. This difference was used to separate vegetated and non-vegetated land by the standard deviation.

Fig. 3-4a shows the result of the land cover classification. Stone and sand deserts are located in the western part of the study site ranging from the Northwest to Southeast. Sparse grassland and sparse shrubland are mainly distributed next to sand or stone deserts. Dense grassland, dense shrubland, and mixed agriculture/grassland are distributed next to sparse grassland/shrublands. To the East and South are forests on mountain ridges, and agricultural areas in the Eastern plains. This spatial pattern, i.e. the gradual increase of vegetation density from Northwest to Southeast and from deserts, to sparse and then dense vegetation, suggests that the sparse grassland/shrubland class might be a buffer against the invasion of the desert into agricultural areas. **Fig. 3-4a** also shows that crops are planted mainly in valleys, river basins or well-watered oasis surrounded by sparse vegetation and deserts. In some areas, especially the Loess plateau and in Northern Tibet, deserts were found in landscapes dominated by sparse grass- and shrubland. This indicates that previously sparsely vegetated areas had been converted into desert by desertification processes.

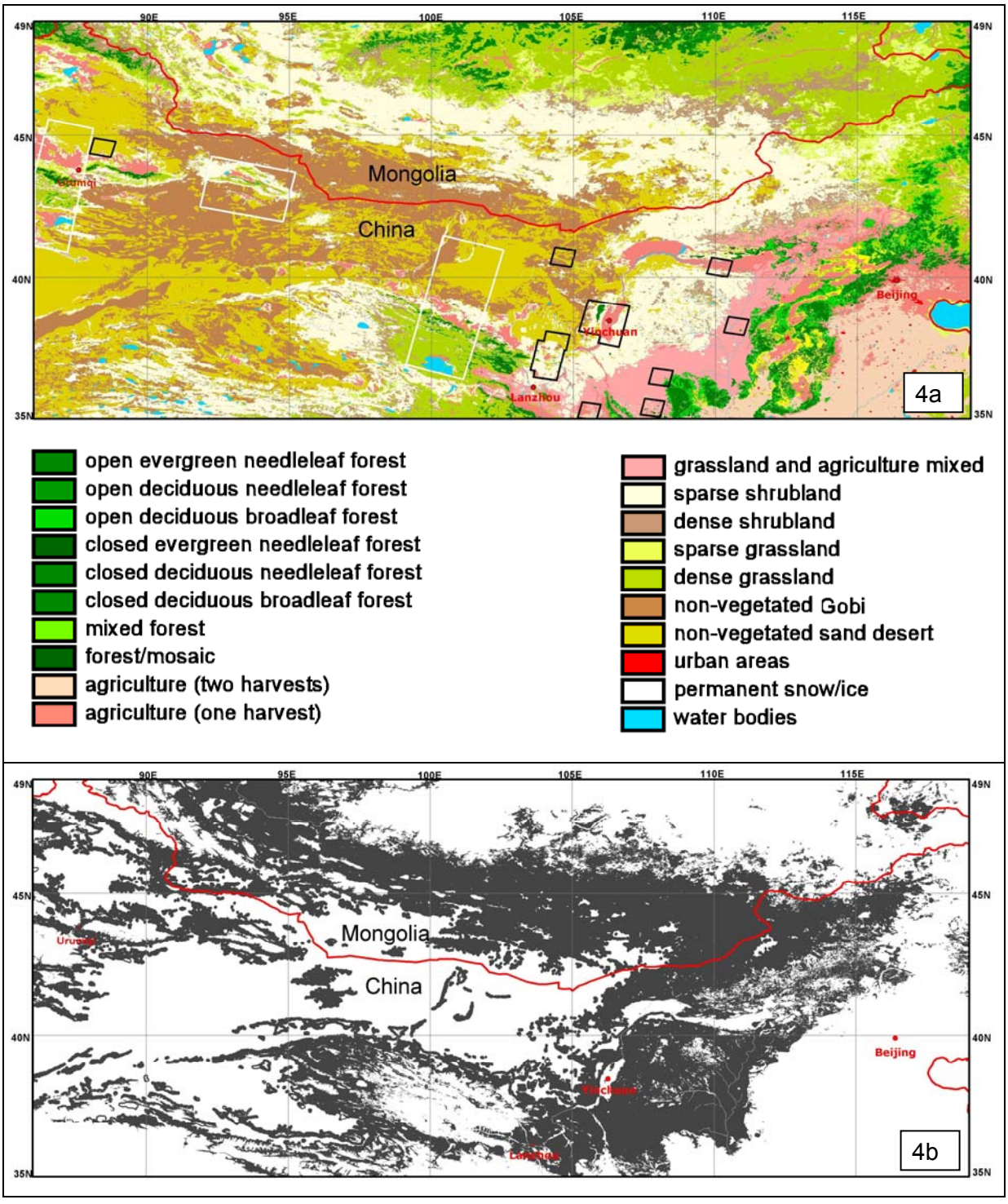

Fig. 3-4. Land cover classification derived from year 2000 SPOT VEGETATION (a) and desertification risk area (b). Black and white polygons in 4a are respectively ASTER and landsat ETM coverage for accuracy assessment. Black areas in 4b are identified as desertification risk area.

Table 3-2. Classification result in km^2 and % of the total area

Class code	Class name and description	km^2	Area (%)
1	open evergreen needleleaf forest (Dominated by evergreen needleleaf woody vegetation with canopy cover between 15% and 40% and height exceeding 2 m)	17,113	0.26
2	open deciduous needleleaf forest (Dominated by deciduous needleleaf woody vegetation with canopy cover between 15% and 40% and height exceeding 2 m)	60,192	0.90
3	open deciduous broadleaf forest (Dominated by deciduous broadleaf woody vegetation with canopy cover between 15% and 40% and height exceeding 2 m)	89,480	1.34
4	closed evergreen needleleaf forest (Dominated by evergreen needleleaf woody vegetation with canopy cover more than 40% and height exceeding 2 m)	28,375	0.43
5	closed deciduous needleleaf forest (Dominated by deciduous needleleaf woody vegetation with canopy cover more than 40% and height exceeding 2 m)	68,942	1.04
6	closed deciduous broadleaf forest (Dominated by deciduous broadleaf woody vegetation with canopy cover more than 40% and height exceeding 2 m)	111,494	1.67
7	mixed forest (Dominated by mixed tree type with canopy cover more than 40% and height exceeding 2 m)	8,648	0.13
8	forest/mosaic (A mosaic of forest and other vegetation; no one comprises more than 60%)	81,992	1.23
9	agriculture (two and more harvests) (Land dedicated to the production of crops with two or more seasons during the year)	279,770	4.20
10	agriculture (one harvest) (Land dedicated to the production of crops with only one season during the year)	328,161	4.93
11	mixed grassland with agriculture (A mosaic of cropland and natural herbaceous vegetation; no one comprises > 60%)	256,118	3.85
12	sparse shrubland (Wood vegetation less than 2 m in height and shrub canopy between 10% and 40%)	1,547,322	23.24
13	dense shrubland (Wood vegetation less than 2 m in height and shrub canopy cover more than 40%)	304,598	4.57
14	sparse grassland (Land with the herbaceous cover less than 40%, tree and shrub cover less than 10%)	322,616	4.85
15	dense grassland (Land with herbaceous cover more than 40%, tree and shrub cover less than 10%)	911,979	13.70
16	non-vegetated Gobi (Areas of exposed and consolidated soil, rocks that never have more than 10% vegetated cover during any time of the year)	1,035,626	15.55
17	non-vegetated sand desert (Areas of exposed and unconsolidated soil, sand that never have more than 10% vegetated cover during any time of the year)	1,124,256	16.88
18	urban areas (Covered by buildings and other human-made structures)	4,565	0.07
19	permanent snow/ice (Lands under snow/ice cover throughout the year)	16,139	0.24
20	water bodies (Oceans, seas, reservoirs, lakes and rivers)	61,055	0.92
Sum		**6,658,441**	**100**

Table 3-2 shows the quantitative result of the land cover classification. A large area of about 2.16 Million km^2 of stone (Gobi) and sand desert cover approximately 32.5% of the total area. Only about 5.5% of the total area is covered by forest and 9.1% are under agricultural use. Mixed grassland/shrubland covers approximately 3.9%. Water bodies and permanent snow/ice are important water sources in the area and cover only 0.92% and 0.24 respectively. 46.36% of the total area are covered by shrubland and grassland with almost 61% being sparse shrub and grassland. Sparse vegetation was mainly located in South Mongolia, the Loess plateau and the North slope of the the Tibet plateau. Small amounts of them were found around the oasis and at the top of high mountains.

Table 3-3. Accuracy assessment

Class Code*	Reference totals	Classified totals	Number correct	Producer accuracy (%)**	Users accuracy (%)***	Kappa Coefficients****
1	25	24	24	96.00	100.00	1.0000
2	21	19	15	71.43	78.95	0.7879
3	4	4	4	100.00	100.00	1.0000
4	8	8	8	100.00	100.00	1.0000
5	8	7	6	75.00	85.71	0.8567
6	2	2	2	100.00	100.00	1.0000
9	28	17	15	**53.57**	88.24	0.8812
10	290	312	268	92.41	85.90	0.8433
11	94	103	81	86.17	78.64	0.7793
12	637	585	501	78.65	85.64	0.8161
13	134	47	40	**29.85**	85.11	0.8439
14	82	61	54	**65.85**	88.52	0.8819
15	325	398	297	91.38	74.62	0.7143
16	563	556	489	86.86	87.95	0.8505
17	612	693	554	90.52	79.94	0.7459
19	8	8	8	100.00	100.00	1.0000
20	63	60	58	92.06	96.67	0.9659
Total	**2904**	**2904**	**2424**	**-**	**-**	**-**

Overall Classification Accuracy = 83.47%, Overall Kappa Statistic = 0.8030

* The meaning of class code is the same as table 3-2.

**Producer accuracy measures the probability of a reference site being correctly classified.

*** User accurace is an indication of the probability that a site classified in the image actually represents that class on the ground.

**** Kappa Coefficient measures how well the classification performed compared to the probability of randomly assigning points to their correct categories.

The overall accuracy of the classification result was 83.47% (**Table 3-3**). The user accuracy was more than 74%. In some instances the producer accuracy was low: agriculture (two or more harvests) 53.57%, dense shrubland 29.58% and sparse grassland 65.85%. These errors occurred mainly in the transitional zone from agriculture to grazing. Out of 134 reference points for dense shrubland, 16 and 72 were classified as agriculture and dense grassland respectively. Out of 82 reference points for sparse grassland, 15 points were classified as sparse shrubland. This shows the agriculture, grassland and shrubland were not well discriminated. This might relate to a similar seasonal variation in plant growth and spectral reflectance of the biomass. The density of plant growth (dense grass-shrubland / sparse grass-shrubland) that is especially important for the risk assessment was very well distinguished. As can be seen in table 3-3, the user accuracy of sparse shrubland and sparse grassland are up to 85.64% and 88.52% respectively.

Due to highly variable rainfall events and increasing human pressure the landscapes covered by sparse, drought adapted vegetation are most seriously affected by desertification (RG-SCDC, 1998). Four major risk areas were potentially of the interests: 1.) the surroundings of oases which are damaged by excessive fuelwood collection; 2.) the lower reaches of the interior rivers which are affected by inappropriate water utilization; 3.) the overgrazed land in semi-arid regions; and 4.) the transitional zone from agriculture to grazing (Pei, 1999; RG-SCDC, 1998). Sand and stone deserts, as well as sparsely vegetated high mountains, were formed a long time ago and are more-or-less stable ecosystems, where very few people live. These ecosystems were excluded from the risk assessment. Of greatest interest is the buffer zone next to the deserts because these areas are most sensitive to desertification (Sun and Chen, 2000). Areas at risk of desertification were defined as all sparsely vegetated areas consisting of the classes of sparse grassland, sparse shrubland, mixed grassland/agriculture and all land within a 10 km wide zone next to the classes sand desert and Gobi. Mountain areas higher than 4500 meters in Tibet plateau and 2500 meters in all other regions and water bodies as well as some isolated small sparsely vegetated areas which are not located in the arid, semi-arid and dry sub-humid zone were excluded.

According to these definitions approximately 1.60 Million km^2 at significant risk of desertification was estimated, in which China and Mongolia account for about 60% (0.96 Million km^2) and 40% (0.64 Million km^2) respectively (**Fig. 3-4b).** These areas are located mainly in the south of Mongolia, the west of Inner-Mongolia in China, the Loess plateau, the north of the Tibet plateau, and the surroundings of oases and mountains in Xinjiang province. Large areas belonge to the main grazing regions and the transition zone between agriculture and grazing. The areas at risk extend from Northwest to Southeast, corresponding to the dominant wind direction in the area, indicating that wind

might be a driving force for desertification. **Fig. 3-4b** also shows that desertification spans across international boundaries, which makes internationally coordinated action programs mandatory.

3-4. Discussion

Vegetation cover is a common criterion to assess desertification, especially if remote sensing is used (Zha and Gao, 1997). The NDVI, which is calculated from red and near infrared red bands, was very useful to assess the land cover in arid areas. Compared with the mono-temporal NDVI of August, which is a critical month during growing season (Long, 2000), the annual maximal NDVI proved to be more useful to detect sparse vegetation because vegetation growth in arid and semi-arid environments is usually highly rainfall dependent (Nicholson *et al*., 1990) and peaks in NDVI values coincide with the vegetation response to occasional rainfall events (Schmidt and Karnieli, 2000). In addition the growing season and the climate vary strongly across such a large area (2000 x 3500 km).

Although many studies have demonstrated the usefulness of the NDVI in arid and semi-arid environments (e.g. Malo and Nicholson, 1990; Peters and Eve, 1995; Peters *et al*., 1997; Liu *et al*., 2004), the influence of background signal from the soil is a particular problem which deteriorates the classification accuracy (Edwards *et al*., 1999; Weiss *et al*., 2004). It was found that sparse vegetation covers with less than 10% coverage, which is normally categorized as severely desertified land (Zha and Gao, 1997), were difficult to detect by SPOT VEGETATION. Other vegetation indices such as the perpendicular vegetation index (PVI), the soil-adjusted vegetation index (SAVI) and the transformed soil-adjusted vegetation index (TSAVI) may perform better in this case.

There are quite disparate figures reported for the area at risk of desertification in China. Zhu and Cui (1996) accounted the desertified land in China to be 1.1 Million km^2 while Zhou and Pu (1996) estimated 2.2 Million km^2 and Guo et al. (1989) estimated 1.3 Million km^2. The differences can be mainly attributed to different definitions of desertification and the degree of desertification (Zha and Gao, 1997). The extent of desertified land estimated by different authors converges at around 0.334 Million km^2 if the revised international definition of desertification by Rhodes (1991) is adopted (Zha and Gao, 1997) and at 0.371 Million km^2 if the UN definition of desertification is adopted (Yang et al., 2004). Our estimation of the China part in the study area is about 0.96 Million km^2, which is significantly larger. Major reasons for this discrepancy are that 1.) sparse vegetation was identified and not desertified land itself. Some regions with sparse vegetation such as those in the high Tibet plateau are natural and have almost no risk of s desertification, and 2.) our estimate includes ‘desertification′’ and ‘vulnerability to desertification’, which should be distinguished (Rhodes, 1991). On the other hand, desertified land in the sub-humid zone mapped by RG-SCDC (1998) and Zha and Gao (1997) was not detected in our product. This is probably related to more dense vegetation growth due to better water availability in sub-humid zones. Generally, the spatial pattern of our map agrees well with the

map of RG-SCDC (1998) and Zha and Gao (1997). In Mongolia Yang *et al.* (2004) reported that 78% of the territory (approximately 1.22 Million km^2) is under the risk of desertification, of which about 0.73 Million km^2 are highly vulnerable. Our estimate of 0.64 Million km^2, which was derived from 82% of the whole Mongolia, is little different from this number of 0.73.

The result of our study supports the analysis of desertification because it provides information on the land cover across a very large area. This should help scientists and relevant authorities to determine priority areas for ground surveys and high resolution remote sensing. Especially in areas which are difficult to access on ground such as the Tibet plateau, information from coarse resolution satellites can be an important information source. Nevertheless, SPOT VEGETATION can be used to assess the type of vegetation, but not the causes of desertification. This requires ground surveys or high resolution remote sensing.

By analyzing a full year time series of SPOT VEGETATION imagery, important parameters such as the length of growing season, the coefficient of variation of different land covers, and the NDVI amplitude could be derived. These parameters can be used to monitor intra-annual changes of the ecosystem and to improve the land cover classification as discussed by Boles *et al*. (2004). Furthermore, in arid regions vegetation can vary inter-annually in response to climatic conditions change (Okin *et al*., 2004). The study of precipitation change from 1956-2000 within our study sites (Gong *et al*., 2004) suggests future work utilizing inter-annual comparison. 'Desertification' refers not only to the expansion of existing deserts but also the slow degradation of fertile land by the gradual loss of soil productivity or thinning out of the vegetation cover. Through the analysis over several years SPOT VEGETATION imagery was expected to be very useful to monitor large scale desertification processes (Tucker *et al*., 1991) and to assess the condition of the vegetation cover (Weiss *et al*., 2004). Additionally SPOT VEGETATION imagery can be used to analyze the origin, development and propagation of large-scale sand storms.

The major restriction of the SPOT VEGETATION system lies in its coarse resolution of 1 km at nadir viewpoint, which limits its use for a detailed analysis of boundary changes between different land covers such as grass, shrubland and desert. In developing countries such as China where extremely large and highly inaccessible areas have to be monitored regularly, the collection and analysis of high resolution satellite imagery is not operational because of high data costs and effort. Therefore, conventionally ground based methods are used to monitor desertification in China (Lin and Zhou, 2000): Representative sample sites are selected and monitored by long-term ground observation or by high resolution remote sensing images. The results derived from these sample plots are then used to extrapolate to the whole area. A multi-scale monitoring system is mandatory in this case (Lin and Zhou, 2000). The whole country will be monitored by coarse resolution satellite imagery such as

SPOT VEGETATION or by medium resolution satellite imagery such as TERRA/AQUA MODIS or ENVISAT MERIS, while the most endangered areas, i.e. hotspot areas, will be monitored by high resolution satellite imagery such as Landsat ETM or TERRA ASTER. In such a system, coarse and medium resolution imagery with daily coverage could provide data on large scale environmental changes, which then will be analyzed in detail using higher resolution satellite imagery. Our study showed that it was possible to derive important parameters linked to desertification from SPOT VEGETATION imagery. This information can be used to detect "hotspots" of desertification, which then can be analyzed in more detail by high resolution satellite imagery (Liu *et al*., 2004). Such a multi-scale monitoring system based on SPOT VEGETATION imagery is of interest not only to China, but to all those developing countries where desertification is an urging problem and whose financial resources are limited.

3-5. Acknowledgements

The author would like to acknowledge Hans-Juergen Stibig and Etienne Bartholome, both at the JRC (Joint Research Center of the European Union), for providing the SPOT VEGETATION data in the framework of the GLC2000 initiative. Many thanks also to Rene Beuchle for his advice.

3-6. References

Bastin, G. N., Pickup G. & Pearce, G. (1995). Utility of AVHRR data for land degradation assessment: a case study. *International Journal of Remote Sensing, 16(4),* 651-672.

Boles, S., Xiao, X., Liu, J., Zhang, Q., Munkhtuya, S., Chen, S. & Ojima, Dennis. (2004). Land cover characterization of Temperate East Asia using multi-temporal VEGETATION sensor data. *Remote Sensing of Environment, 90,* 477-489.

CMA (China meteorological administration) (2002). Comprehensive description of China Duststorm, available at *http://www.duststorm.com.cn* (in Chinese).

CNC-UNCCD (China national committee for the implementation of the UN convention to combat desertification) (1996). China national action programmes to combat desertification. *http://www.unccd.int/actionprogrammes/asia/national/2000/china-eng.pdf*

Collado, A. D., Chuvieco, E. & Camarasa, A. (2002). Satellite remote sensing analysis to monitor desertification processes in the crop-rangeland boundary of Argentina. *Journal of Arid Environments, 52,* 121-133.

Crépeau, C., Bennouna, T., & Bicheron, P. (2000). Vegetation action and demonstration plan for desertification monitoring in Senegal and China. *VEGETATION 2000 Symposium, 3-6 April 2000* (pp.437-442). Italy: Belgirate.

Edwards, M. C, Wellens, J., Al-Eisawic, A. (1999). Monitoring the grazing resources of the Badia region, Jordan, using remote sensing. *Applied Geography, 19 (4),* 385-398.

Ghosh, T. K. (1993). Environmental impacts analysis of desertification through remote sensing and land based information system**.** *Journal of Arid Environments, 25(1),* 141-150.

Gong, D.Y., Shi, P.J. & Wang, J.A. (2004). Daily precipitation changes in the semi-arid region over northern China. . *Journal of Arid Environments,* 59, 771–784.

Groten, S. M. E., & Oatre, R. (2002). Monitoring the length of the growing season with NOAA. *International Journal of Remote Sensing*, 23, 2797-2815.

Guo, H., Wu, D. & Zhu, H. (1989). Land restoration in China. *Journal of Applied Ecology, 26*, 787–792.

Holben, B. N. (1986). Characteristics of maximum-value composite images from temporal AVHRR data. International Journal of Remote Sensing*, 7,* 1417-1434.

Hou, X. Y. (1988). *The Nature and Ecology Regionization of China and the Agriculture Development Strategy*. Beijing: Science Press (154pp.) (in Chinese).

Kharin, N., Tateishi, R.& Harahsheh, H. (1999). *Degradation of the Drylands of Asia*, Chiba University.

Lin, J., & Zhou, W. D. (2000). A summary of desertification monitoring of China. In desertification monitoring center of ministry of forestry (Ed.), *Research of Desertification Monitoring Technique in China* (pp.1-6). Beijing: China Forestry Science Press (264 pp.) (in Chinese).

Liu Y., Zha, Y., Gao, J. & Ni, S. (2004). Assessment of grassland degradation near Lake Qinghai, West China, using Landsat TM and *in situ* reflectance spectra data *International Journal of Remote Sensing,, 25(20),* 4177-4189.

Long, J. (2000). Desertification monitoring and estimation from AVHRR data in China. In Desertification monitoring center of ministry of forestry (Ed.), *Research of Desertification Monitoring Technique in China* (pp.55-60). Beijing: China Forestry Science Press (264 pp.) (in Chinese).

Malo, A. R. & Nicholson, S. E. (1990). A study of rainfall and vegetation dynamics in the African Sahel using Normalized Difference Vegetation Index. *Journal of Arid Environments 19,* 1–24.

Nicholson, S. E., Davenport, M. L. & Malo, A. R. (1990). A comparison of vegetation response to rainfall in the Sahel and East Africa using Normalized Difference Vegetation Index from NOAA-AVHRR, *Climate Change, 17,* 209-241.

Okin, G.S. & Roberts, D.A. (2004). Remote sensing in arid regions: challenges and opportunities. In Ustin, S.L. (Ed.), *Manual of Remote Sensing,* 3rd ed. Vol. 4, (pp 111-146), John Wiley and Sons, New York.

Passot, X. (2000). VEGETATION image processing methods in the CTIV. *VEGETATION 2000 Symposium, 3-6 April 2000* (pp.15-22). Italy: Belgirate.

Pei, X. F. (1999). *Optimal Farming System in the Typical Agriculture-Grazing Transitional Area*. Beijing: Commission on integrated survey of natural resources of Chinese Academy of Sciences (PhD thesis, 119pp.) (in Chinese).

Peters, A. J., Eve, M. D. (1995). Satellite monitoring of desert plant community response to moisture availability. *Environmental Monitoring and Assessment 37,* 273–287.

Prince, S.D. (1991). Satellite remote sensing of primary production: comparison of results for Sahelian grasslands 1981-1988. *International Journal of Remote Sensing,, 12,* 1301-1311.

Rhodes, S.L. (1991). Rethinking desertification: what do we know and what have we learned? *World Development, 21,* 1137–1143.

RG-SCDC (Research group of 'Study on combating desertification/land degradation in China') (1998). *Study on Combating Desertification/Land Degradation in China*. Beijing: China Environment Science Press (164 pp.)

Roerink, G. J., Menenti, M. & Verhoef, W. (2000). Reconstructing cloudfree NDVI composites using Fourier analysis of time series. *International Journal of Remote Sensing, 21 (9),* 1911–1917.

Roujean, J. L., Leroy, M. & Deschamps, P. Y. (1992). A bidirectional reflectance model of the earth's surface for the correction of remote sensing. *Journal of .Geophysics Research, 97*, 20455-20468.

Schmidt, H., Karnieli, A. (2000). Remote sensing of the seasonal variability of vegetation in a semi-arid environment. *Journal of Arid Environments, 45,* 43–59.

SSCC (State Science Commission of China).(1994). *China's Agenda21-White Paper on China's Population, Environment and Development in the 21st Century*. Beijing: China Environment Science Press (192 pp.), english version available at *http://www.acca21.org.cn/indexe6.html*

Sun, S. H., & Chen, J. W. (2000). China national desertification monitoring, In desertification monitoring center of ministry of forestry (Ed.), *Research of Desertification Monitoring Technique in China* (pp.96-107). Beijing: China Forestry Science Press (264 pp.) (in Chinese).

Sun, S. H., & Zhou, C. X. (2000). The basic frame for formulating the technical scheme of China national desertification monitoring. In desertification monitoring center of ministry of forestry (Ed.), *Research of Desertification Monitoring Technique in China* (pp.49-54). Beijing: China Forestry Science Press (264 pp.) (in Chinese).

Tripathy, G. K., Ghosh T. K. & Shah S. D. (1996). Monitoring of desertification process in Karnataka state of India using multi-temporal remote sensing and ancillary information using GIS. *International Journal of Remote Sensing, 17(12),* 2243-2257.

Tsunekawa, A.(2000a). Methodologies of desertification monitoring and assessment. W*orkshop of the Asia regional thematic programme network on desertification monitoring and assessment(TPN1) (provisional edition)*, *28-30 June 2000* (pp.44-55). Japan: Tokyo, UNU.

Tsunekawa, A. (2000b). Research activities in Japan: Relevant to desertification monitoring and assessment. W*orkshop of the Asia regional thematic programme network on desertification monitoring and assessment(TPN1) (provisional edition), 28-30 June 2000* (pp.178-186). *Japan: Tokyo, UNU.*

Tucker, C. J., Dregne, H. E. & Newcomb, W. W. (1991). Expansion and contraction of the Sahara Desert between 1980 and 1990. *Science, 253*, 299-301.

Wang, X., Dong, Z., Zhang, J. & Liu, L. (2004). Modern dust storms in China: an overview. *Journal of Arid Environment, 58*, 559–574.

Wang G. S., Sun S.H, Liao Y. P. & Zhang, Y. X. (2000). Study on remote sensing monitoring and information of sand strom disaster , In desertification monitoring center of ministry of forestry (Ed.). *Research of Desertification Monitoring Technique in China* (pp. 186-193). Beijing: China Forestry Science Press (264 pp.) (in Chinese).

Weiss, E., Marsh, S.E. & Pfirman, E.S. (2001). Application of NOAA-AVHRR NDVI time-series data to assess changes in Saudi Arabia's rangelands. *International Journal of Remote Sensing, 22(6)*, 1005-1027.

Weiss, J. L., Gutzler, D. S., Coonrod, J. E. A. & Dahm, C. N. (2004). Long-term vegetation monitoring with NDVI in a diverse semiarid setting, central New Mexico, U.S.A.. *Journal of Arid Environments, 58,* 248-271.

Xue, Y. (1996). The impact of desertification in the Mongolian and the Inner Mongolian grassland on the regional climate. *Journal of Climate, 9,* 2173– 2189.

Yang, H. (2004). Land conservation campaign in China: integrated management, local participation and food supply option, *Geoforum, 35*, 507-518.

Yang X., Rost, K.T, Lehmkuhl, K., Zhu. Z. & Dodson J. (2004). The evolution of dry lands in northern China and in the Republic of Mongolia since the Last Glacial Maximum. Quaternity *Internation, 118–119*, 69–85.

Zha, Y., & Gao, J. (1997). Characteristics of desertification and its rehabilitation in China. *Journal of Arid Environments,37(3),* 419-432.

Zhong, D. & Qu, J. (2003). Recent developmental trend and prediction of sand deserts in China. *Journal of Arid Environments, 53,* 317–329.

Zhu, Z. & Cui, S. (1996). Distribution patterns of desertified land and assessment of its control measures in China. *China Environmental Science, 16,* 328–334. (in Chinese)

Zhou, J. & Pu, L. (1996). Rustic opinions on concept of desertification and its practical significance. *Journal of Arid Environments,16,* 191–195.

CHAPTER 4---MULTI-SENSOR SATELLITE DATA FOR FIRE MONITORING AND IMPACT ASSESSMENT IN INDONESIA AND SIBERIA

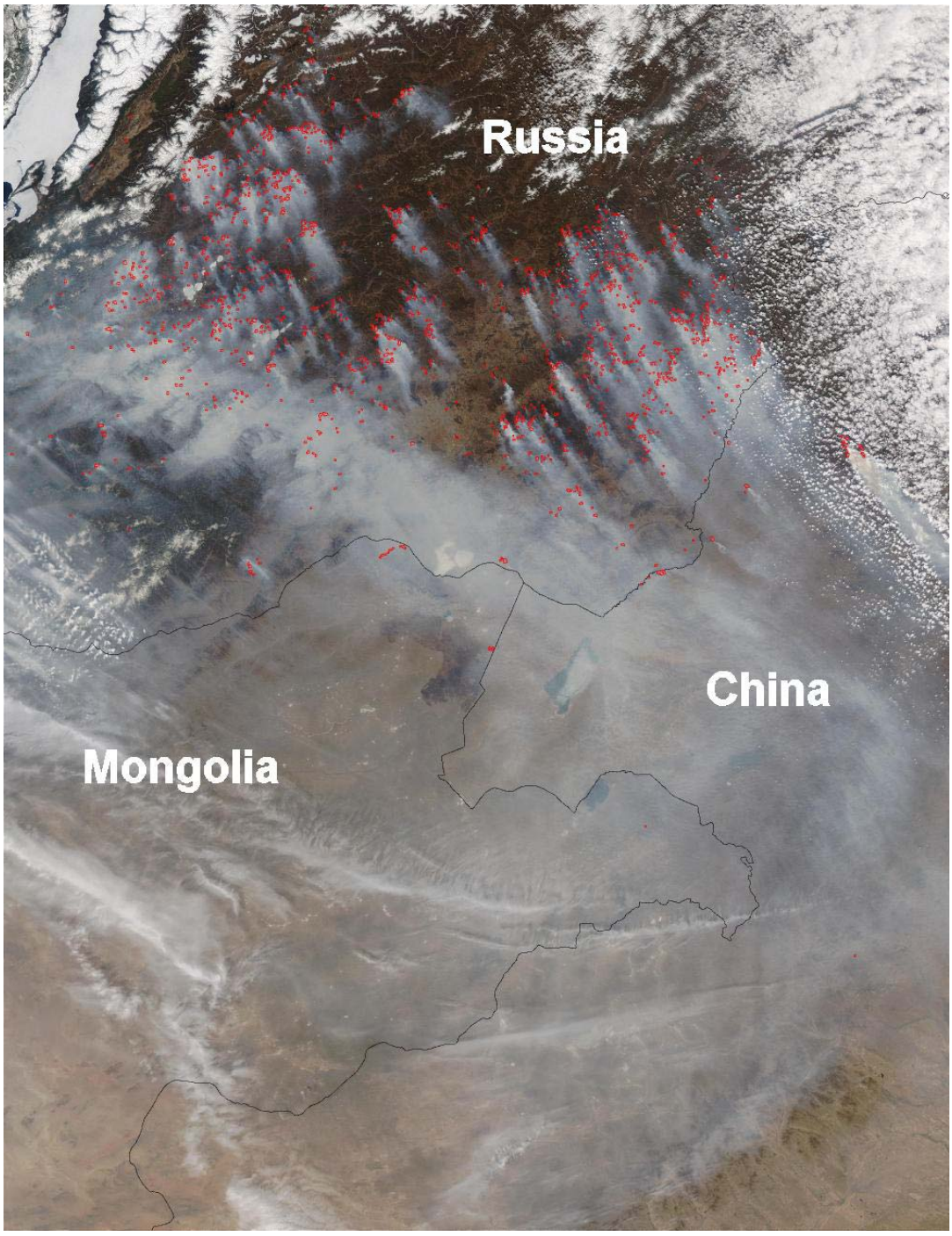

CHAPTER 4.1---OBSERVATION OF SIBERIAN FIRE-DISTURBED FORESTS IN ENVISAT ASAR WIDE SWATH IMAGES

Recurrent wildfires strongly affect the boreal ecosystem in Siberia and probably contribute to global warming by the release of significant amounts of carbon. Current fire monitoring activities in Russia are based on the detection of high temperature events by the NOAA-AVHRR instrument and the assessment of fire scars from spectral reflectance images. However, AVHRR sensor does not provide sufficient detail for a reliable analysis of the burnt area and fire impact due to its low spatial resolution. In addition, a persistent cloud cover and dense haze from burning fires impedes all other higher resolution optical satellite sensors. Active microwave sensors such as that onboard the European ENVISAT satellite overcome these problems. The Wide Swath Mode (WSM) of the ASAR instrument with a spatial resolution of 150 meters would be ideal for operational burnt area mapping over the vast territory of Russia. The objective of this paper was to investigate the performance of this instrument in fire-disturbed forests in south Siberia, where extensive forest fires occurred in 2003. It was found that 1.) the ASAR WSM backscatter signal was sensitive to fire disturbance; 2.) the backscatter change correlated mainly with snow-melt and rainfall; and 3.) the backscatter signal varied as a function of the incidence angle with a higher backscatter occurring at shallower incidence angles. These results suggest that ASAR WSM data can be used for operational fire impact monitoring in boreal forests of Siberia. However multi-temporal datasets are required, because environmental conditions strongly influence the backscatter signal.

4.1-1. Introduction

Siberian forests contain roughly half the world's growing stock volume of coniferous forest, making them an economically and ecologically precious resource (Nilsson and Shvidenko, 1998). Wildfire disturbance is common and is an integral part of the boreal Eurasian ecosystem (Goldammer and Furyaev, 1996). Some recent studies imply that fires in Russia might contribute to global warming by releasing large amounts of carbon (Kasischke and Stocks, 2000; Conard *et al*, 2002; Kajii *et al*., 2002; Van der Werf *et al*., 2004). In recent years the forest fire situation has become more serious (Goldammer, 2003; Sukhinin, 2003). In 2003, an extreme fire event occurred East of Lake Baikal (Siegert *et al*., 2004). The repeated occurrence of large-scale fire disasters and the presumable release of huge amounts of carbon prompt for accurate information on the burnt area and the damages to the vegetation. However, current assessments are not satisfactory due to the unavailability of enough data (Soja *et al*, 2004) and hence the fire regime is not well understood in Russia.

The enormous extent and the remoteness of much of boreal Russia require remote sensing technology for fire detection and monitoring. Currently operational fire monitoring is based on NOAA (National Oceanic and Atmospheric Administration)-AVHRR (Advanced Very High Resolution Radiometer) hotspots detection and the analysis of the spectral channels 1, 2 and 5. The low spatial resolution of the NOAA AVHHR instrument leads often to a significant over- or underestimation of the burnt area (Kasischke and French, 1995; Kasischke and Bruhwiler, 2003). Persistent cloud cover during summer when most fires occur (Warren *et al*., 1986) and dense haze from burning fires impede medium resolution optical sensors such as the Moderate Imaging Spectrometer (MODIS) and the MEdium Resolution Imaging Spectrometer (MERIS). Synthetic Aperture Radar (SAR) overcomes these problems.

The applicability of SAR imagery for fire scar mapping in boreal ecosystems was investigated extensively (Landry *et al*. 1995; French *et al*. 1996; French *et al*. 1999; Liew *et al*. 1999; Bourgeau-Chavez *et al*. 2002). Fire scars as detected by the European Remote Sensing Satellite (ERS) SAR were 3-6 dB brighter than adjacent unburnt forest (Kasischke *et al*., 1992). This increase was explained by the removal of the tree canopy by fire, exposure of rough ground surfaces and increased soil moisture (Kasischke *et al*., 1994; French *et al*., 1996; Bourgeau-Chavez *et al*., 1997). The increase in soil moisture was attributed to a decreased surface albedo and melting of the permafrost layer as well as lowered evapotranspiration (Brown, 1983; Dyrness and Norum, 1983; Viereck, 1983).

In addition, it was found that the incidence angle is critical in determining the relative brightness of the backscatter (French *et al*., 1999). They found that the signature of burnt areas in one site in C-HH imagery changed strongly as a function of incidence angle.

Layover and shadowing in steep mountainous regions, wetlands and seasonal conditions are disturbing factors which limit the applicability of SAR imagery to detect fire scars (Bourgeau-Chavez *et al*., 1997). The small difference in backscatter between burnt versus unburnt areas in Quebec was attributed to the intensity of fire (high versus low severity), small increase in ground moisture post-burn and wetlands (Bourgeau-Chavez *et al*., 2002). To overcome these problems Bourgeau-Chavez *et al*. (1997) composited three dates of ERS imagery to allow the fire scars to be detected in mountains by canceling out the effects of local incidence angles. Gimeno *et al*. (2002) tried to overcome the layover and shadowing problem by classifying the image into positive and negative slopes. Bourgeau-Chavez *et al*. (2002) found that multi-temporal SAR imagery sometimes allows better distinction between fire scars and wetlands, but a combination of SAR and multi-spectral data are likely to be necessary in wetland regions for reliable fire scar mapping.

In March 2002 the European Space Agency (ESA) launched ENVISAT, an advanced polar-orbiting Earth observation satellite. The Advanced Synthetic Aperture Radar (ASAR) on board ENVISAT operates at C-band with a frequency of 5.331 GHz. Compared to ERS Active Microwave Instrument (AMI), ASAR is a significantly advanced instrument employing a number of new technological developments which allow extended performance (European Space Agency, 2002a). ASAR was designed to operate in five different modes (Global Monitoring Mode, Wave Mode, Image Mode, Alternating Polarization Mode and Wide Swath Mode). In the Wide Swath Mode (WSM) the ScanSAR technique provides images with 405 km swath width at a medium geometric resolution of 150 meters (range and azimuth spacing is approximately 75 m) in HH or VV polarization with the repeat circle of 3 days. The incidence angles range from 16 to 44 degrees.

Due to its cloud and haze penetrating capability and its wide swath ASAR WSM should be useful to complement existing fire monitoring systems in the vast boreal ecosystems of the Russian Federation. The objective of our research was to investigate the capability of the ASAR WSM to detect fire disturbances in Siberian forests. A time series of backscatter images were analyzed to investigate temporal variations of backscatter of known fire scars and the influence of different incidence angles on the backscatter signal.

4.1-2. Materials and Methods

The study site is located East of Lake Baikal in a region covering 400 x 200 km, centered at 118°E and 54°30'N where fire occurred repeatedly between 1999 and 2003. SRTM digital elevation data shows that the site has a relatively flat undulating relief. To discriminate the disturbance of forest canopy by fire from other potential causes such as logging or storm, MODIS hotspot data, NOAA AVHRR fire products, multi-temporal Landsat quicklooks and ENVISAT MERIS images were comprehensively used. Weather data available from the station of Tungokochen and Tupik were used to assess snow-melt and rainfall events. Climate data of 2003 indicate that the maximum precipitation occurred from June to August. The permafrost map of Russia shows that the study site is located within the type of “>90% continuous”. The forest type in this region is mainly larch with little dwarf shrubs in the East. Most of the area is sparsely populated and covered by more or less intact forest.

Seven multi-look scenes (number of range looks and Azimuth looks are respectively 7 and 3) of ENVISAT wide swath SAR data were processed and analyzed (**Table 4.1-1**). The ASAR-WSM (level 1) images were first speckle filtered using the gamma map algorithm to reduce noise. The backscatter value in dB was calculated from the digital number (European Space Agency, 2002b) using equation

1:

$$\delta^0_{i,j}[dB] = 10 \bullet \log_{10}\left[\frac{DN^2_{i,j}}{K} \sin(\alpha_{i,j}) \right] \qquad for \quad i = 1.....L \quad and \quad j = 1....M \qquad (1)$$

where $\delta i,j^0$[dB] is the backscatter at image line and column "i, j", K is absolute calibration constant which was determined from the ASA-WSM header file, $DN_{i,j}$ is the pixel intensity value at image line and column "i, j", $\alpha_{i,j}$ is the incidence angle at image line and column "i, j" interpolated from header file and L and M are number of image lines and columns.

Table 4.1-1. Local weather conditions under which the seven images were acquired

No	Date of 2003	Polariz-ation	Absolute Orbit Number	Temperature Description*	Rainfall Description in 2003*
1	January 19	V/V	4645	-21°C, snow covered and frozen	0 mm
2	March 27	H/H	5604	4.3°C, snow covered but began to melt	0 mm, but 2 mm on March 25 in snow form
3	April 12	H/H	5833	4.5°C, more snow melted	0 mm
4	May 11	H/H	6248	9.1°C, snow totally melted	0 mm
5	June 18	H/H	6792	20.8°C	1 mm, but 8.2 mm on June 16
6	July 4	H/H	7021	26.2°C	0 mm, total 24.8 mm on June 19-July 2
7	July 13	H/H	7150	28.1°C	0.7 mm, but 2 mm on July 9 and 0.7 mm on July 10

* Data source: weather station Tungokochen of Russia Federation (location: 53°34'N 115°34'E, altitude: 811 m).

To determine the month and year of fire disturbance, the following data sets were used: 1.) a time series Landsat ETM quicklook images acquired from 1999 to 2004; 2.) twelve MERIS images with a ground resolution of 300 meters; 3.) the MODIS MOD14A2 product which is a gridded 1 km composite of fire hotspots detected in each grid cell over an eight-day composite interval; and 4.) a time series of fire scar polygons derived from NOAA AVHRR images acquired from 1996 to 2003 in which each polygon had been assigned the time of fire occurrence (Anatoly Sukhinin, personal

communication). Optical Landsat quick look images and MERIS images were visually interpreted for fire scar boundaries. All the data sets were georeferenced and co-registered.

The same histogram stretching parameters were applied to the time series of ASAR WSM images to investigate fire scar visibility over time. Sites for fire scars burnt in 1999 ("burnt 1999"), in 2000 ("burnt 2000"), in 2002 ("burnt 2002"), in 2003 ("burnt 2003") and unburnt forests were selected and mean backscatter values were calculated. To study the influence of different incidence angles, fire scars of 2002 in an ASAR wide swath image acquired in July 2003 were compared.

4.1-3. Results

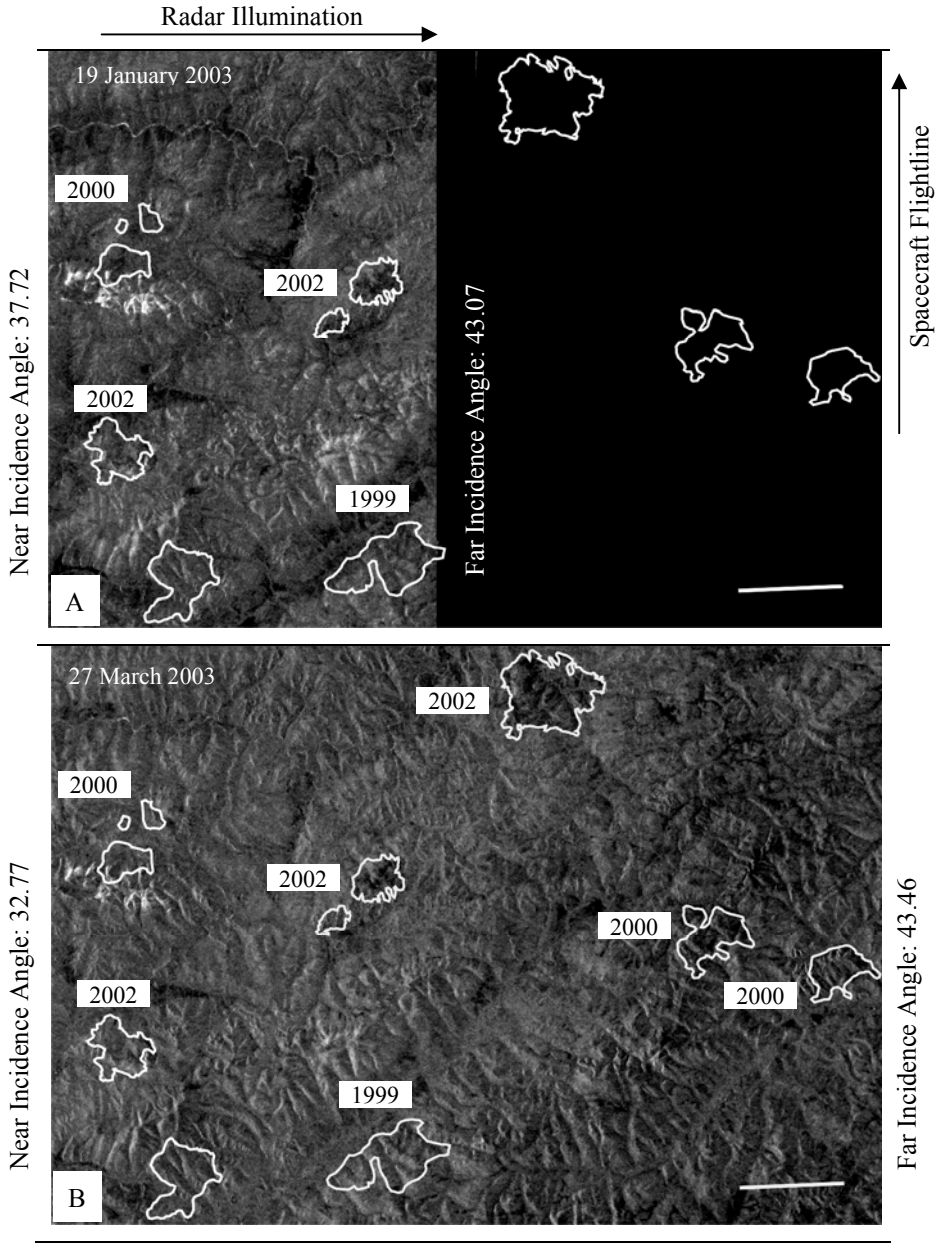

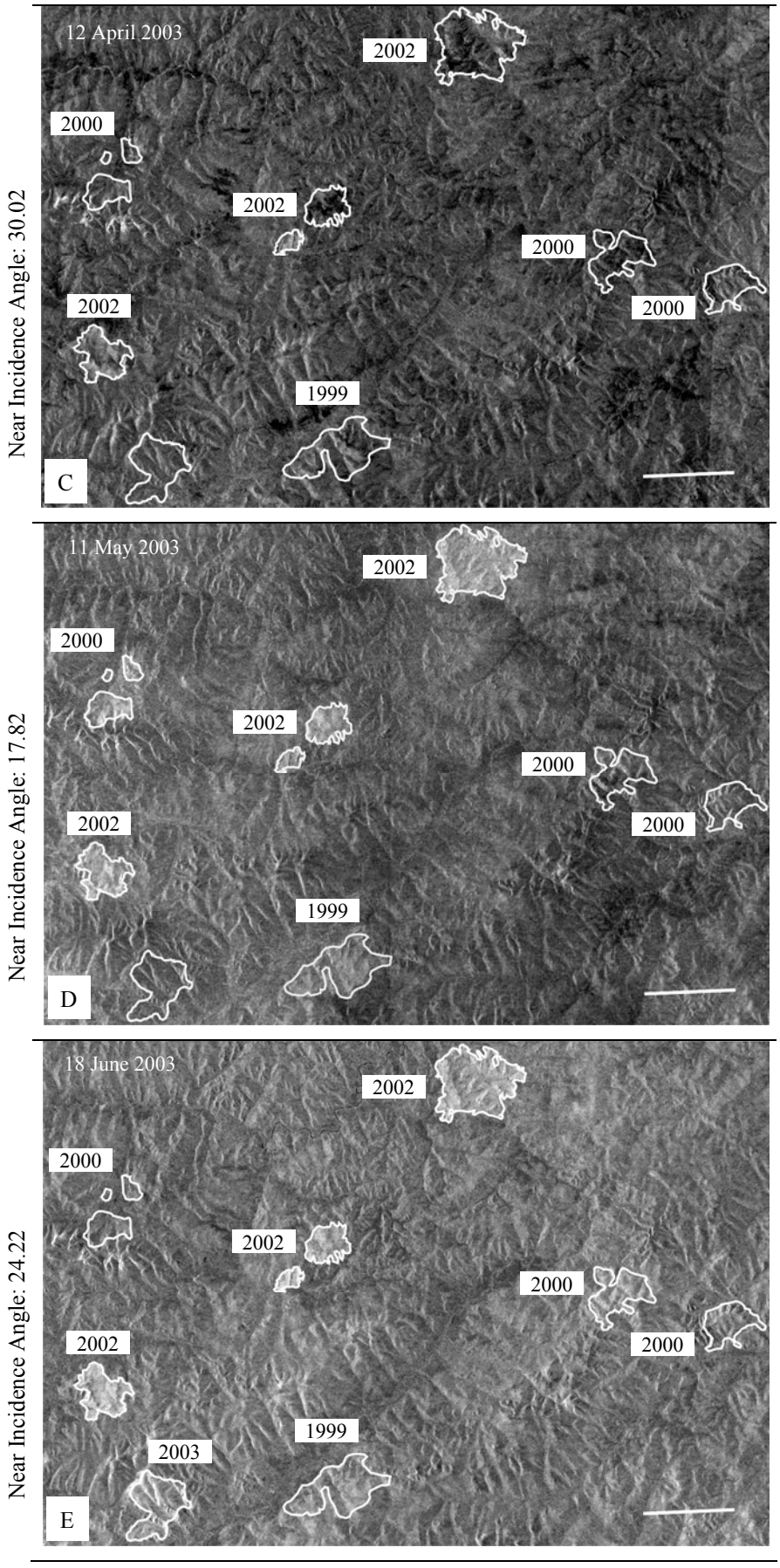
12 April 2003
2002
2000
2002
2000
2002
2000
1999
C
Near Incidence Angle: 30.02
Far Incidence Angle: 40.71
11 May 2003
2002
2000
2002
2000
2002
2000
1999
D
Near Incidence Angle: 17.82
Far Incidence Angle: 28.51
18 June 2003
2002
2000
2002
2000
2002
2000
1999
2003
E
Near Incidence Angle: 24.22
Far Incidence Angle: 34.91

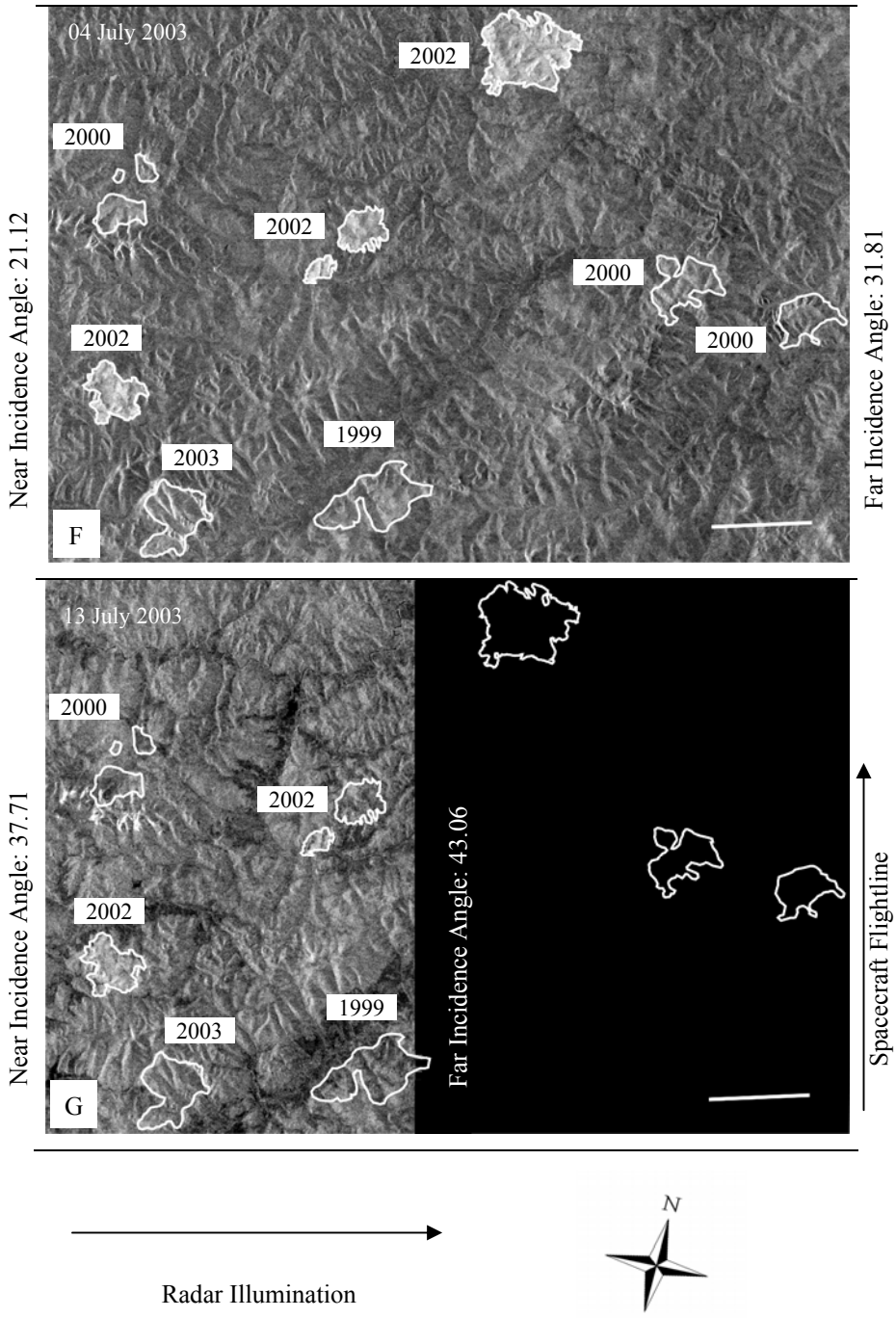

Fig. 4.1-1. The visibility of fire scars of different years varies in this time series of ASAR WSM images. No big fires occurred in 2001. Bar: 20 km

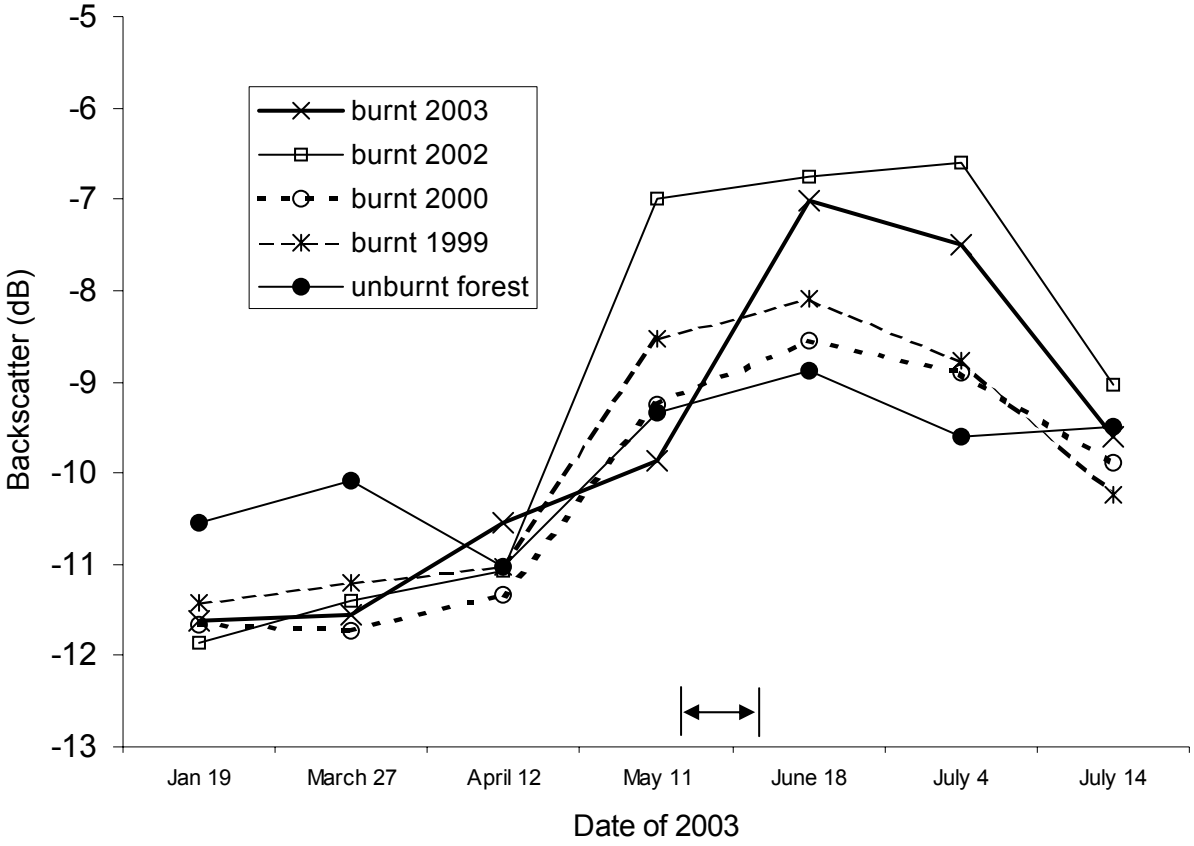

Fig. 4.1-2. Time series mean backscatter values of burnt forest and unburnt forest. The backscatter values of the unburnt forest are higher than those of burnt area before April whilst lower after April. Compared to unburnt forest, the difference of "burnt 1999" and "burnt 2000" is smaller than "burnt 2002". The "burnt 2003" (fire occurred between 18 May 2003 and 9 June 2003, the arrow above the X axis indicates the burning time) agrees with the unburnt forest before 11 May 2003 whilst agrees with the "burnt 2002" after 18 June 2003. Note the standard deviations of fire scars of different years are high (see Table 4.1-2).

The visibility of fire scars that were burnt in different years and unburnt forest is shown in **Fig. 4.1-1.** Their temporal backscatter mean values and standard deviations are shown in **Table 4.1-2** and **Fig. 4.1-2**. The time series shows that the visibility of fire scars burnt in 2002 varied significantly over time. From January to March, fire scars are almost invisible and have lower backscatter values than unburnt forest. In mid-April the backscatter signal starts to increase. In May, June and July the backscatter is significantly higher than that of unburnt forest. In Mid-July the fire scars are almost invisible again. The mean backscatter values of fire scars are 1.3-1.4 dB lower than these of unburnt forest from mid-January to end of March, but 2-3 dB higher from mid-May to early July. In mid-July the backscatter difference decreases to 0.4 dB (no data was available for the period from August to December). Landsat quick looks and MERIS images indicated that during the first two acquisitions (Fig. 4.1-1A and 1B) the fire scars were snow covered. The acquisition of April 12 (Fig. 4.1-1C)

represented a transitional period of snow-melt. Local weather data of temperature and rainfall in this period are shown in **Fig. 4.1-3**. In April the temperature was just above 0°C and snow had already begun to melt; after April 18 the temperature was permanently above 0° C and from June 14 to July 16 rainfall was recorded. This suggested that the observed backscatter change related to the snow-melt and rainfall. The snow-melt influence is specially represented in the acquisition of April 12 that was precisely during the transitional period of snow-melt: some fires scars are brighter than surrounding unburnt forest while others are darker.

Table 4.1-2. The backscatter mean and standard deviation of fire scars burnt in different years

Date of 2003	Unburnt forest		Burnt 1999		Burnt 2000		Burnt 2002		Burnt 2003	
	dB (Mean)	dB (std)	dB (Mean)	dB (std)	dB (Mean)	dB (std)	dB (Mean)	dB (std)	dB (Mean)	dB (std)
Jan. 19	-10.56	1.40	-11.43	2.20	-11.67	1.95	-11.85	1.48	-11.61*	1.17*
March 27	-10.09	1.61	-11.20	1.43	-11.73	1.71	-11.40	1.56	-11.56*	1.33*
April 12	-11.02	1.47	-11.02	1.86	-11.33	1.85	-11.08	2.10	-10.54*	1.36*
May 11	-9.34	1.52	-8.52	1.37	-9.26	2.07	-6.99	1.48	-9.87*	1.38*
June 18	-8.88	1.40	-8.08	1.34	-8.54	1.71	-6.76	1.68	-7.02	1.94
July 4	-9.59	1.49	-8.76	1.43	-8.90	1.81	-6.60	1.93	-7.51	2.10
July 13	-9.48	1.37	-10.24	2.00	-9.88	1.63	-9.04	1.63	-9.60	1.26

* still unburnt

The MODIS 8-day hotspots and AVHRR fire polygons indicated the fire scar labeled “burnt 2003” formed between 18 May 2003 and 9 June 2003. **Fig. 4.1-1** shows that it is not visible in the pre-fire image acquired on May 11 (Fig. 4.1-1D) whilst it is clearly visible in the post-fire image acquired on June 18 (Fig. 4.1-1E). **Table 4.1-2** and **Fig. 4.1-2** shows that the backscatter dramatically changes from –9.9 to –7.0 in the period of 11 May 2003 to 18 June 2003.

Fig. 4.1-1 also shows that fire scars that formed in 1999 and 2000 are difficult to discriminate from unburnt forest in 2003 imagery. In Fig. 4.1-1F the fire scars labeled “burnt 2002” and “burnt 2003” are clearly visible while the ones before (“burnt 1999” and “burnt 2000”) are difficult to discriminate. The backscatter values of “burnt 1999” and “burnt 2000” are only about 0.7-0.8 dB higher than unburnt forest, while “burnt 2002” and “burnt 2003” are 2-3 dB higher (**Fig. 4.1-2**). This might be due to more vegetation regrowth in the fire scars of “burnt 1999” and “burnt 2000”.

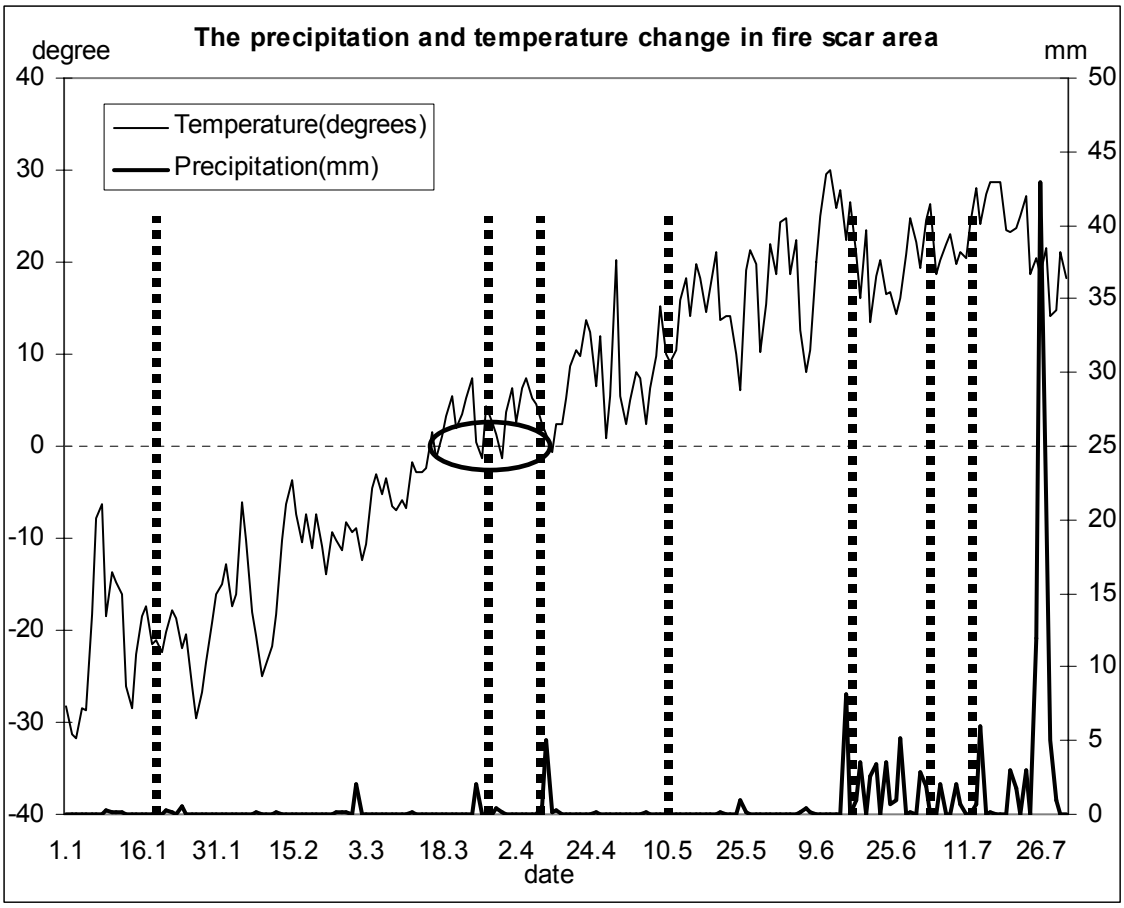

Fig. 4.1-3. Precipitation and temperature between January and July 2003. The dashed bars denote the ASAR WSM acquisitions (Jan 19, March 27, April 12, May 11, June 18, July 4, July 13 of 2003), the ellipse denotes the snow-melt period.

Rainfall events caused an increase in backscatter, however the acquisition of July 13, 2003 (Fig. 4.1-1F) did not fit into this pattern. Although the weather data (**Fig. 4.1-3)** indicated rainfall in this period, the fire scars were almost invisible. The invisibility was supposed to be correlated to the incidence angle. As can be seen in **Fig. 4.1-1**, fire scars burnt in 2002 were obviously brighter than adjacent unburnt forest in Fig. 4.1-1D, 1E and 1F when they were acquired under the shallower incidence angles about 20-30 degrees. In the acquisition of July 4 (Fig. 4.1-1G), the incidence angle was approximately 40 degrees. Since the weather data indicated some rain, the incidence angle was most likely the reason for the invisibility.

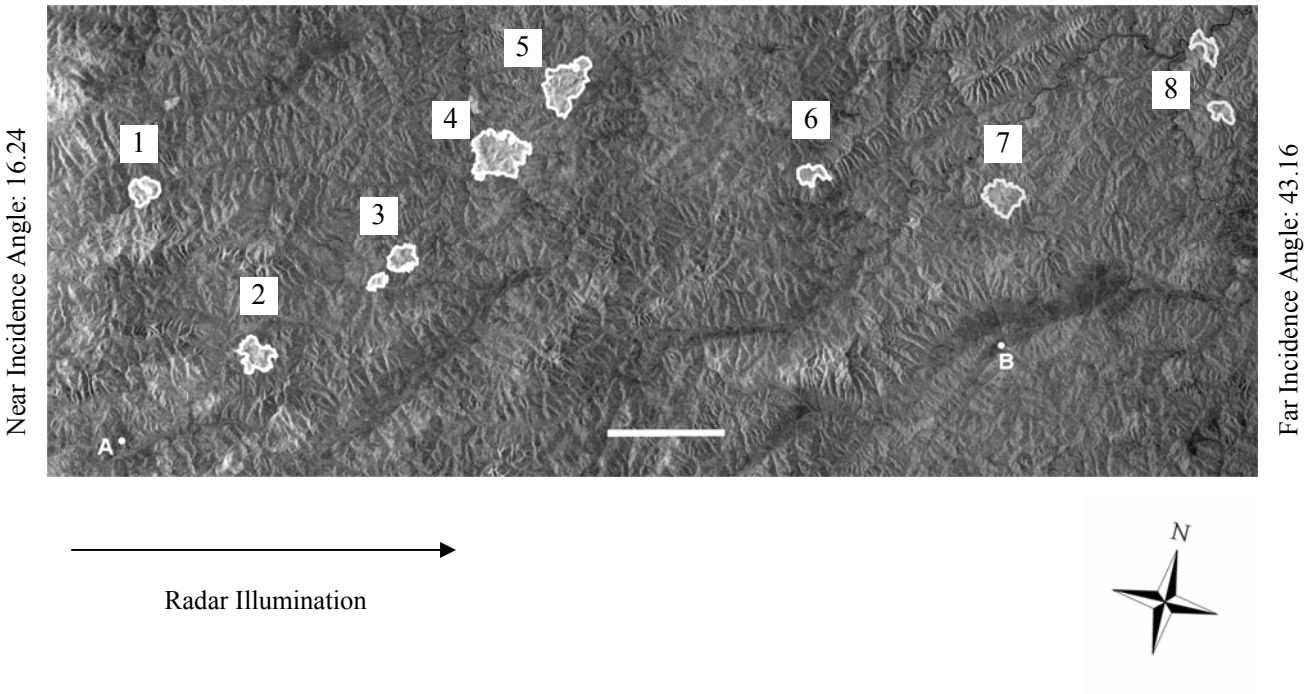

Fig. 4.1-4. Fire scars at different incidence angles (4 July 2003). The weather recorded by station Tupik (B) indicated 8, 0.3 and 12 mm rainfall on June 27, June 30 and July 2. Weather data of Tungokochen (A) indicated 5.1, 0.2, 2.9 and 1.9 mm rainfall on June 27, June 29, July 1 and July 2. Bar: 40 km

Table 4.1-3. The incidence angle and backscatter of fire scars formed in 2002

NO	Incidence angle	dB	MERIS NDVI*	Burning Date in 2002	Area (km^2)
1	19.230	-6.263	0.038	Aug 12-Aug 14	59.23
2	22.080	-6.406	0.023	Aug 06-Aug 16	86.62
3	25.233	-6.815	0.054	Aug 06-Aug 14	19.89
4	27.696	-6.465	0.019	Aug 05-Aug 16	211.91
5	29.121	-6.964	0.025	Aug 06-Aug 16	175.84
6	34.276	-7.840	0.022	July 21-Aug 14	42.11
7	37.961	-8.090	0.063	July 20-Aug 14	101.16
8	41.548	-8.413	0.056	July 21-Aug 15	81.34

*MERIS band 8 (0.68125 μm) and 14 (0.885 μm) were selected as red and NIR for this calculation.

To further investigate the influence of the incidence angle on fire scar visibility, several fire scars that all formed in a short period in 2002 were compared (**Fig. 4.1-4**) and were acquired on the same day under different incidence angles (**Table 4.1-3**). The weather station Tungokochen and Tupik indicated some rain. It was assumed that fire damage was similar in these fire scars, because the NDVI, which is related to fire severity (Chafer *et al*., 2004), varied very little. **Fig. 4.1-5** shows that the incidence angle had great effect on the backscatter of fire scars. With incidence angles ranging

from 19.2 to 41.5 degrees the backscatter values decreased from –6.3 to –8.4. The lower backscatter values of fire scars in the acquisitions of Jan 19, March 27 and April 12 (Fig. 4.1-1A, 1B and 1C) might also in part related to large incidence angles.

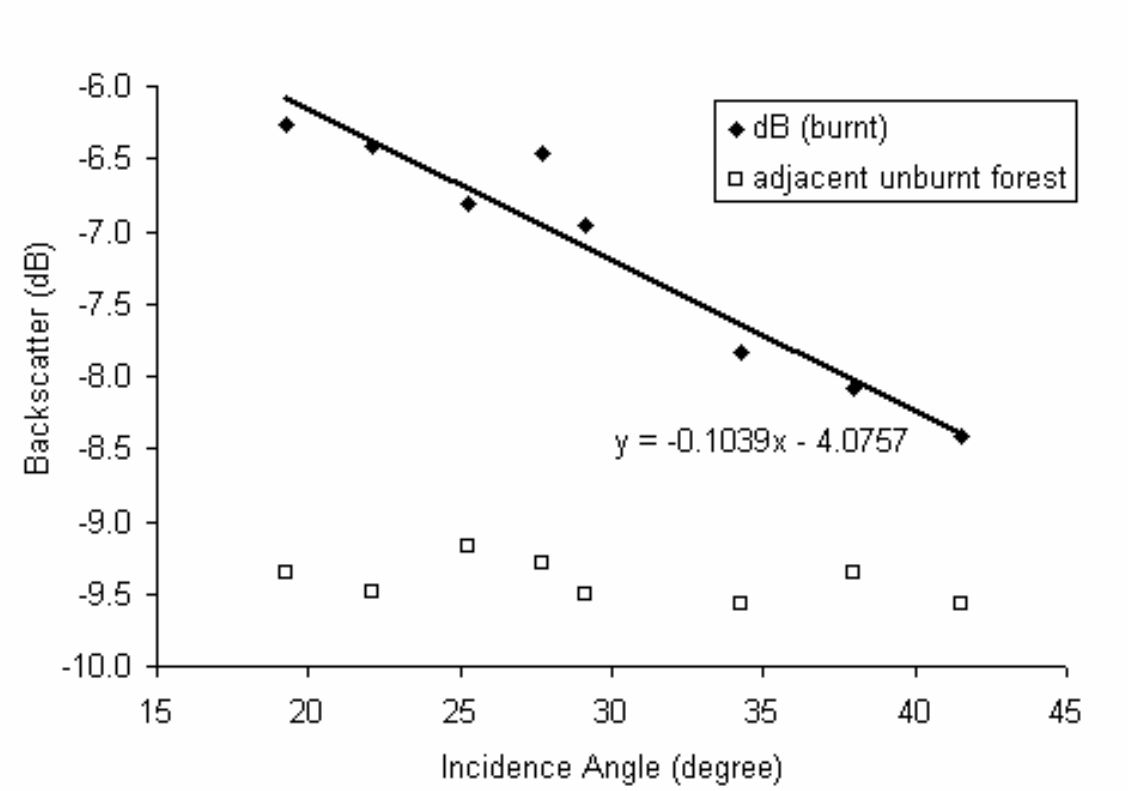

Fig. 4.1-5. Correlation of backscatter and incidence angle. The backscatters of the fire scars decreases by 0.1 dB for each degree in incidence angle whilst that of unburned forest not.

4.1-4. Discussion

Increased soil moisture in fire affected areas and the sensitivity of SAR to soil moisture are the main causes why backscatter features of fire scars were different from those of unburnt forest in ASAR WSM images in this boreal region. This relates to the facts that 1.) fire destroys and thus often removes large fractions of the vegetation and more solar energy can reach the ground, 2.) fire decreases the albedo of the ground thus increasing the amount of energy absorbed by the soil, and 3.) fire removes much of the dead organic matter that insulates the ground. This results in an increase in the moisture of soils in the permafrost zone during the initial years after a fire (Brown, 1983). In addition, in the microwave spectrum a change in moisture content generally provokes a significant change in the dielectric properties of natural materials. Increasing moisture is thus associated with an increased radar reflectivity (Lilesand and Kiefer, 1994). Since the ENVISAT ASAR instrument is operating in C-band wavelengths of 3.75-7.5 cm, at which the volume scattering of vegetation canopy predominates and surface scattering from the underlying soil is minimal, the backscatter signal is

mainly determined by vegetation canopy in undisturbed forests. However, if the canopy is largely removed by fire, the radar signal scattering becomes dominated by the ground layer.

The incidence angle is an important factor in monitoring soil moisture (Ulaby and Batlivala, 1976; Dobson and Ulaby, 1986). Our results show that the backscatter of fire scars varied as a function of the incidence angle with a higher backscatter correlated with smaller incidence angles. This observation confirms that of French *et al*. (1999) who used Radarsat SAR images.

Kasischke *et al*. (1992) found that in ERS SAR images of Alaska fire scars reflected 3-6 dB brighter than adjacent unburnt forest. In our study it was found that fire scars after one year had a backscatter signal 2-3 dB higher than the surrounding unburnt forest (mid-April to early July). The reason for this difference might relate to differences in forest types and fire behavior (e.g. more surface and less stand replacement burning in Russia) (Shvidenko and Goldammer, 2001; Conard *et al*., 2002; Soja *et al*., 2004). The observed backscatter corresponded well with local weather conditions of temperature and rainfall, which also agree with previous observations in which snow-melt in spring and rainfall were considered as the two factors determining the visibility of fire scars in SAR imagery (Bourgeau-Chavez *et al*., 1997). Using C-band ERS and Radarsat SAR imagery, Bourgeau-Chavez *et al*. (2002) found the fire scars in Canada and Russia had high backscatter values shortly after snow-melt in spring, low backscatter values as the ground dried out and high values again after rainfall events. These findings are confirmed by the seasonal visibilty of fire scars in our study.

The results show that fire scar detection using ENVISAT ASAR WSM imagery is influenced by several factors which are difficult to overcome as observed with other SAR systems. For operational burnt area mapping it is important to develop a consistent algorithm, but the variability of the backscatter signal, which is influenced by many environmental conditions, imposes a great barrier to the development of such algorithms. Our data provide some clues for burnt area detection. For example, snow-melt, rainfall and incidence angle can be exploited to improve fire scar detection through calculating the coefficient of variation (e.g. standard deviation) of each pixel in time series data as observered in tropical forest region (Siegert and Rücker, 2000). This, however, requires the continous image acquisition and the processing of large volumes of data.

Rainfall events influence the backscatter of ENVISAT ASAR differently in tropical and boreal forests. In Siberia environmental conditions result in high soil moisture conditions from May to July, thus making the detection of fire scars feasible. In contrast, we found in another study in tropical forests in Indonesia that rainfall decreased the capability of ASAR WSM to detect fire scars (Huang and Siegert, 2004). In the humid tropical zone ASAR was useful in detecting burnt areas because radar backscatter of fire scars was significantly lower than that from forests under dry weather conditions.

The reason for low backscatter in this case is a considerable increase of heat flux after destruction of the forest canopy which leads to a quick drying out of the soil layer in fire scars (Siegert and Rücker, 2000). These observations suggest that the local natural conditions must be considered to select the optimal data and algorithms for burnt area detection.

The wide swath of the ENVISAT ASAR (405 km) makes this instrument very useful for large scale assessments of fire impact and thus may help to better understand fire regime in Russia and improve carbon release estimates. ENVISAT ASAR could complement existing systems of fire monitoring because 1.) optical instruments are often impeded by clouds in tropical and boreal regions; 2.) area estimates based on the low resolution optical instruments such as AVHRR have significant uncertainties; and 3.) high resolution satellite systems are not operational for large scale monitoring due to limited data availability, excessive processing time and data costs.

The ENVISAT ASAR instrument was expected to be especially useful in the framework of a multi-resolution (spatial and spectral) monitoring system. In addition to the ASAR instrument, which also provides a high resolution mode, the European ENVISAT satellite operates the multispectral MERIS instrument with 300 meters resolution and the AATSR instrument with 1 km resolution. This makes ENVISAT an unique system because it is possible 1.) to acquire both optical data and radar data at the same time; 2.) to acquire images both during day and night; and 3.) to acquire high, medium and low spatial resolution imagery which allows for simultaneous multi-scale analysis. The capability of ENVISAT to acquire imagery with different instruments almost simultaneously will allow one to obtain a much more detailed picture on fire events than with any other satellite system.

4.1-5. Acknowledgements

The author would like to thank ESA/ESRIN for financial support and free data provision in the framework of ENVISAT AO 689. Thanks also to Chris Schmullius in Jena University for providing forest cover maps and Anatoly Sukhinin in Sukachev Institute of Forest Research Academy of Russia for providing the time series NOAA AVHRR fire products.

4.1-6. References

Bourgeau-Chavez, L. L., Harrell, P. A., Kasischke, E. S. & French, N. H. F. (1997). The detection and mapping of Alaskan wildfires using a spaceborne imaging radar system. *International Journal of Remote Sensing, 18,* 355-373.

Bourgeau-Chavez, L. L., Kasischke, E. S., Brunzell S. & Mudd J. P. (2002). Mapping fire scars in global boreal forests using imaging radar data. *International journal of remote sensing, 23(20),* 4211-4234.

Brown, R. J. E. (1983). Effects of fire on the permafrost ground thermal regime. In Wein, R. W. & Maclean, D. A. (Ed.), *The Role of Fire in Northern Circumpolar Ecosystems* (pp. 97-110). New York: John Wiley & Sons.

Chafer, C. J., Noonan, M. & Macnaught, E. (2004). The post-fire measurement of fire severity and intensity in the Christmas 2001 Sydney wildfires. *International Journal of Wildland Fire, 13(2),* 227–240.

Conard, S.G., Sukhinin, A.I., Stocks, B.J., Cahoon, D.R., Davidenko, E.P. & Ivanova, G.A. (2002). Determining effects of area burnt and fire severity on carbon cycling and emissions in Siberia. *Climatic Change 55,* 197-211.

Dobson, M. C. & Ulaby, F. T. (1986). Active microwave soil moisture research. *IEEE transactions on geoscience and remote sensing, 24,* 23–36.

Dyrness, C. T. & Norum, R. A. (1983). The effects of experimental fires on black spruce forest floors in interior Alaska. *Canadian Journal of forest research, 13,* 879-893.

European Space Agency (2000a). ENVISAT ASAR Product Handbook, Issue 1.1, 1 December, 2002. available at *http://envisat.esa.int/dataproducts/asar/CNTR2-6-1.htm*

European Space Agency (2000b). MERIS Product Handbook, August, 2002. available at *http://envisat.esa.int/pub/ESA_DOC/ENVISAT/MERIS*

French, N. H. F., Bourgeau-Chavez, L.L., Wang Y. & Kasischke, E. S. (1999). Initial observations of radarsat imagery at fire-disturbed sites in interior Alaska. *Remote Sensing of Environment, 68(1),* 89-94.

French, N. H. F., Kasischke, E. S., Bourgeau-Chavez, L. L. & Harrell, P. A. (1996). Sensitivity of ERS-1 SAR to variations in soil water in fire-disturbed boreal forest ecosystem. *International Journal of Remote Sensing, 17,* 3037-3053.

Goldammer, J. G. & Furyaev, V. V. (1996). *Fire in Ecosystems of Boreal Eurasia*. Dordrecht: Kluwer Academic Publishers.

Goldammer J. G. (2003). Wildland fire season 2002 in the Russian Federation: an assessment by the Global Fire Monitoring Center (GFMC). *International Forest Fire News (IFFN),28,* 2-14.

Huang, S. & Siegert, F. (2004). ENVISAT multisensor data for fire monitoring and impact assessment. *International Journal of Remote Sensing, 25(20),* 4411-4416.

Kajii Y., Kato S., Streets, D. G., Tsai N. Y., Shvidenko A., Nilsson S., Minko,M. P., Abushenko N., Altyntsev D. & Khodzer T. V. (2002). Boreal forest fires in Siberia in 1998: estimation of area and emissions of pollutants by AVHRR satellite data. *Journal of Geophysical Research, 107(D24),* 4745, doi:10.1029/2001JD001078.

Kasischke, E. S., Bourgeau-Chavez, L. L., French, N. H. F., Harrell, P. A. & Christensen, N. L. (1992). Initial observations on using SAR to monitor wildfires scars in boreal forest. *International Journal of Remote Sensing, 13,* 3495-3501.

Kasischke, E. S., Bourgeau-Chavez, L. L. & French, N. H. F. (1994). Observations in ERS-1 SAR image intensity associated with forest fires in Alaska. *IEEE transactions on geoscience and remote sensing, 32,* 206-210.

Kasischke, E. S., & French, N. H. F. (1995). Locating and estimating the areal extent of wildfires in Alaskan boreal forests using multiple-season AVHRR NDVI composite data. *Remote Sensing Environment 51,* 263-275.

Kasischke, E. S. & Stocks, B. J. (2000). *Fire, Climate Change and Carbon Cycling in the Boreal Forest.* New York: Springer-Verlag.

Kasischke, E. S. & Bruhwiler, L. P. (2003). Emissions of carbon dioxide, carbon monoxide, and methane from boreal forest fires in 1998. *Journal of Geophysical Researc*h,107(D1), 8146, doi:10.1029/2001JD000461.

Lilesand, T. M. & Kiefer, R. W. (1994). *Remote Sensing and Image Interpretation, 3rd edn*. New York: John Wiley & Sons.

Landry, R., Ahern, F. J. & O'Neil, R. (1995). Forest burn visibility on C-HH radar images. *Canadian journal of remote sensing, 21,* 204-206.

Liew, S. C., Khoh, L. K., Padmanabhan, K., Lim O. K. & Lim, H. (1999). Delineating land/forest fire burnt scars with ERS interferometric synthetic aperture radar. *Geopgysical Research letters, 26,* 2409-2412.

Gimeno M., San-Miguel, J., Barbosa P. & Schmuck G. (2002). Using ERS-SAR images for burnt area mapping in Mediterranean landscapes, In Viegas (Ed.), *Forest Fire Research & Wildland Fire Safety*. Rotterdam: Millpress, ISBN 90-77017-72-0.

Nilsson, S. & Shvidenko, A. (1998). Is sustainable development of the Russian forest sector possible? IUFRO Occasional Paper No. 11, ISSN 1024-414X, IUFRO Secretariat, Vienna, Austria. 76 pp.

Shvidenko, A. & Goldammer, J.G. (2001). Fire situation in Russia. International Forest Fire News, 24, 41-59.

Siegert, F., Huang, S., Goldammer, J. G. & Sukhinin, A. I. (2004). Exceptionally large fire damage and carbon release by large-scale wildfires in South-Siberia in 2003. In preparation.

Siegert, F. & Rücker, G. (2000). Use of multitemporal ERS-2 SAR images for identification of burned scars in South-East Asian tropical rain forest. *International Journal of Remote Sensing, 21(4),* 831-837.

Soja, A. J., Sukhinin, A. I., Cahoon, D. R., Shugart, H. H. & Stackhouse P.W. (2004). AVHRR-derived fire frequency, distribution and area burned in Siberia, *International Journal of Remote Sensing,25,* 1939-1960.

Sukhinin, A. I. (2003). The 2002 fire season in the Asian part of the Russian Federation: a view from space. *International Forest Fire News (IFFN), 28,* 18-28.

Ulaby, F. T. & Batlivala, P. P. (1976). Optimum radar parameters for mapping soil moisture, *IEEE Transactions on Geoscience and Remote Sensing,14*, 81–93.

Van der Werf, G. R., Randerson, J. T., Collatz, G, J., Giglio, L., Kasibhatla, P. S., Arellano A. F., Olsen, S. C. & Kasischke, E. S. (2004). Continental-scale partitioning of fire emissions during the 1997 to 2001 El Nino/La Niña period. *Science, 303,* 73-76.

Viereck, L. A. (1983). The effects of fire in black spruce ecosystems of Alaska and northern Canada. In Wein, R. W. & Maclean, D. A. (Ed.), *The Role of Fire in Northern Circumpolar Ecosystems* (pp. 201-220). New York: John Wiley & Sons.

Warren, S.G., Hahn, C.J., London, J., Chervin, R.M., & Jenne, R.L. (1986). Global distribution of total cloud cover and cloud type amounts over land. National Center for Atmospheric Research (NCAR) Tech. Note, NCAR/TN-273+STR, 29 pp. + 200 maps.

CHAPTER 4.2---FOREST FIRE SCAR DETECTION IN SIBERIA USING ENVISAT MERIS

Russia holds two-thirds of the world's boreal forest and it accounts for one of the largest reservoirs of terrestrial carbon. Fire is a common phenomenon in this ecosystem and the forest vegetation is well adapted to fire impact. In recent years the forest fire situation became critical in some parts of the Russian Federation: fires became more frequent and larger in size. However, the system presently used to record fire occurrence, the Advanced Very High Resolution Radiometer (AVHRR) satellite instrument with a resolution of 1 km, is not accurate enough for fire scar mapping and fire impact assessment. The Medium Resolution Imaging Spectrometer (MERIS) instrument onboard the European ENVISAT satellite might be a promising new alternative with its ground resolution of 300 m and global coverage of the Earth in three days in 15 different visible to near infra-red spectral bands. The objective of this study was to investigate the applicability of ENVISAT MERIS for fire scar mapping in Siberian forest ecosystems. The spectral reflectance of forest, fire scars and cloud shadows were anlaysed for all spectral bands, the burnt area was determined using maximal Normalized Difference Vegetation Index (NDVI) image composites, and the mapping accuracy was assessed. The analysis showed that 1.) the near infrared reflectance ranging from band 9 to band 15 decreased almost half after a forest fire; 2.) cloud shadows were the major source of error during automated fire scar mapping; 3.) maximal NDVI composition eliminated the cloud shadows disturbance; 4.) the accuracy of fire scar mapping was high with only 3% overestimation compared to high resolution ASTER imagery. Our results suggest that MERIS is a promising instrument for fire scar mapping, which supplements current fire monitoring systems based on the AVHRR and MODIS instruments.

4.2-1. Introduction

In the past three decades wildfires became an increasingly important ecological factor which significantly influences the earth's environment and climate change. Fires change the physical state of the vegetation, affect biodiversity and release a variety of harmfull greenhouse gases into the atmosphere (Andreae, 1991; Page *et al*., 2002; Andreae and Merlet, 2001; Van der Werf *et al*., 2004). In boreal forests, fire affects the carbon budget and the flow of energy between the atmosphere and ground layer, and there is adependence on the melting and formation of permafrost and the occurrence of fire, which in turn has a strong influence on the hydrology of these sites (Brown, 1983; Harden *et al*., 2000). Russia is a critical region because it holds two-thirds of the world's boreal forest, and with its peatlands it accounts for one of the largest reservoirs of terrestrial carbon (Alexeyev and Birdsey,

1994; Goldammer and Furyaev, 1996). The detection of fires and the assessment of their impacts on the vegetation are important to better understand and model possible impacts on climate change on a global scale.

In recent years the forest fire situation turned out to be exceptional in some parts of the Russian Federation (Smith *et al*., 2004; Goldammer, 2003). From 1980 to 1999, official Russian estimates of annual area burned ranged from 0.23 to 5.4 Million ha (. Shvidenko and Goldammer, 2001). More detailed surveys based on National Oceanic and Atmospheric Administration (NOAA)-(Advanced Very High Resolution Radiometer) AVHRR imagery showed that in 1998 more than 9 Million ha and in 2000 more than 13 Million ha have been burned (Kajii *et al*., 2002; Conard *et al*., 2002). In 2002 many fire-related parameters exceeded the 7-year average by several orders of magnitude: 10,252 forest fires were recorded in Asian Russia affecting a total of 11.7 Million ha, with the mean fire size of 1,143 ha (Sukhinin, 2003). In 2003, an even larger fire event was recorded. From mid-March till the end of July, thousands of uncontrolled forest fires burnt more than 20 Million ha West of Lake Baikal alone (Siegert and Huang, 2004).

Area estimates are still not satisfactory, especially for the Asian part of Russia: official Russia government statistics based on ground and aerial surveys on the burnt area differ by a factor of 1.5 to 10 with results from NOAA AVHRR satellite image analysis (Conard *et al*., 2002; Shvidenko and Nilsson, 2000; Cahoon *et al*., 1994; Soja *et al*., 2004); The annual burnt area ranges from a 47-year average estimate of 1.3 million hectares (Mha) (Korovin, 1996) to more than12 Mha (Conard and Ivanova, 1997).

Since wildfires in Russia often affect large and inaccessible regions satellite remote sensing is the only solution to assess the burnt area and fire impact (Kajii *et al*., 2002; Conard *et al*., 2002; Sukhinin, 2003; Soja *et al*., 2004). The AVHRR instrument is the most widely used sensor for fire monitoring and mapping. However, AVHRR was not designed for fire detection and therefore it is not optimally configured for this application. In particular, the most important band for fire detection, the mid-infrared thermal band at 3.7 μm, saturates at ~322K for AVHRR/2 (up to NOAA-14) (Csiszar and Sullivan, 2002) and ~335K for AVHRR/3 (NOAA-15 and onwards). These brightness temperatures are often reached when a small fraction of the pixel is covered by flaming fires. This makes it impossible to quantify fire size and energy from AVHRR for a broad range of fires. Also, small or low-intensity fires may not be detected due to sensor resolution and the response time (Point Spread Function) of the instruments (Cahoon *et al*., 2000). Therefore measurements by AVHRR tend to miss smaller fires and to underestimate the total area of large fires based on their perimeters (Kasischke and French, 1995; Kasischke and Bruhwiler, 2003). Zhang *et al.* (2003) used SPOT VEGETATION imagery with a ground resolution of 1 km to

detect fire scars in Russia and their results showed that a burnt area of 2 km^2 or larger was reliably detected but the size was underestimated by on average 18% when compared to Landsat-Enhanced Thematic Mapper (ETM). The Bi-spectral InfraRed Detection (BIRD)- Hot Spot Recognition System (HSRS) and the TERRA/AQUA Moderate Resolution Imaging Spectroradiometer (MODIS) sensors were purposely designed for hotspot detection and analysis. The MODIS instrument contains 36 spectral bands of which the five equivalent to those of the AVHRR have equal or better spatial resolution, saturation level, dynamic range and signal-to-noise ratio (Ichoku *et al.*, 2003). The BIRD satellite is a promising new instrument also for the detection of less intensely radiating fires such as in peatlands, but it is not yet operational (Wooster *et al*., 2003; Siegert *et al*., 2004).

Low resolution systems such as MODIS, NOAA AVHRR, and SPOT VEGETATION cover large areas in short periods of time, however the results are not accurate enough and tend to under- or overestimate the burnt area. Multispectral satellites with high spatial resolution like Landsat ETM or SPOT 5 would allow a significantly improved accuracy for fire scar mapping, however they are of limited use if large areas have to be surveyed considering data costs, processing time and labour.

In March 2002, the European Space Agency (ESA) launched ENVISAT, an advanced polar-orbiting Earth observation satellite which provides measurements of the atmosphere, ocean, land and ice. The Medium Resolution Imaging Spectrometer (MERIS) is one of ten sensors on ENVISAT recording visible and near-infrared radiation reflection across a range of 15 programmable spectral bands. Its spatial resolution is either 1200 or 300 metres. In another study we investigated the applicability of ENVISAT MERIS, Advanced Along-Track Scanning Radiometer (AATSR) and Advanced Synthetic Aperture Radar (ASAR) for fire scar mapping in Indonesia and found this multi-sensor dataset supplements existing technologies (Huang and Siegert, 2004). However, at that time only the reduced 1200 meters resolution of MERIS was available. In this study the full resolution MERIS data with 300 meters for fire scar mapping in Siberia were investigated. Specific objectives were 1.) to investigate the usefullness of the ENVISAT MERIS instrument for fire scar mapping in a boreal forest ecosystem, 2.) to assess the significance of fire induced reflectance changes in all MERIS bands, 3.) to identify the main disturbing factors and error sources for automated fire scar mapping and possible solution and 4.) to determine the accuracy of the system compared to higher resolution satellite systems like Advanced Spaceborne Thermal Emission and Reflection (ASTER).

4.2-2. Materials and Methods

The research area was located to the East of Lake Baikal and to the North of Mongolia and China extending approximately 700 km in North-South direction and 800 km in West-East direction (**Fig.**

4.2-1). The climate is continental and recorded climate data indicate that the maximum precipitation falls from June through August. Most of the area is sparsely populated and covered by more or less intact mountain tagai coniferous larch and pine forests. In the Southern part forests blend into dryland steppe and some cropland are found along valleys. Shuttle Radar Topography Mission (SRTM) digital elevation data show that the site has a relatively flat undulating relief. Fires occurred in previous years, especially in 2000.

MERIS and ASTER

The MERIS instrument measures the solar radiation reflected by the Earth at a ground spatial resolution of 300 m in 15 spectral bands in the visible and near infrared spectrum (**Table 4.2-1)**. The revisit time of MERIS is approximately three days. MERIS products are available at two spatial resolutions: Full Resolution (FR) with a resolution at subsatellite point 300 m and Reduced Resolution (RR) with a resolution at subsatellite point 1200 m.

Table 4.2-1. The spectral coverage of MERIS instrument

No.	Band centre (nm)	Band width (nm)	Application
1	412.5	10	Yellow substance and detrital pigments
2	442.5	10	Chlorophyll absorption maximum
3	490	10	Chlorophyll and other pigments
4	510	10	Suspended sediment, red tides
5	560	10	Chlorophyll absorption minimum
6	620	10	Suspended sediment
7	665	10	Chlorophyll absorption and fluorescence reference
8	681.25	7.5	Chlorophyll fluorescence peak
9	708.75	10	fluorescence reference, atmosphere corrections
10	753.75	7.5	Vegetation, cloud
11	760.625	3.75	O2 R- branch absorption band
12	778.75	15	Atmosphere corrections
13	865	20	Vegetation, water vapour reference
14	885	10	Atmosphere corrections
15	900	10	Water vapour, land

Source: European Space Agency (2002).

The ASTER instrument has 14 bands arranged in three subsystems: 1.) VNIR (visible and near infrared bands 1, 2, and 3 from 0.55 to 0.80 μm) with 15 m resolution, 2.) SWIR (short wave infrared bands 4, 5, 6, 7, 8, and 9 from 1.65 to 2.4 μm) with 30 m resolution and 3.) TIR (thermal infrared bands 10, 11, 12, 13, and 14 from 8.3 to 11.32 μm) with 90 m resolution. ASTER was designed to obtain detailed maps of land surface temperature, emissivity, reflectance and elevation (Yamaguchi *et al*., 1998). The ASTER reflectance retrieving is described in **Appendix 2.**

MERIS pre-processing

The MERIS data used in this study were level 1 products with full resolution of 300 m (MER-FR-1P). They were firstly corrected using SMILE and SMAC algorithms provided by the BEAM software which can be downloaded for free from http://envisat.esa.int/services/beam/. MERIS is measuring the reflected sun light using Charged Coupled Device (CCD). This technology causes small variations of the spectral wavelength of each pixel. These disturbances result in visual artefacts and reduced accuracy. The SMILE algorithm allows to calculate corrected radiances from ENVISAT MERIS level 1 products. The SMAC algorithm implements the simplified method for atmospheric correction as described in (Rahman and Dedieu, 1994). The practical application of such a simplified model is to invert the radiative transfer equation, and to calculate the surface reflectance from satellite measurements. When the SMAC algorithm was implemented, the parameters of the surface pressure, the ozone content, the water vapour content, and the aerosols were required for input. These parameters came from the European Centre for Medium-term Weather Forecast (ECMWF) and were embedded in each MERIS header. Preliminary cloud masks were applied to each MERIS image. All MERIS surface reflectance images were then coregistered and imported into a Geographical Information System (GIS) for quantitative analysis and comparison with other datasets.

Fire scar mapping

In boreal ecosystems fire often destroys and thus removes a large portion of the vegetation layer as well as much of the dead organic matter covering the soil (French and Kasischke, 1996). In addition fire decreases the albedo of the ground (Brown, 1983). It was first investigated to what extent these significant changes of the ground surface properties could be detected by a reflectance change in each of the 15 MERIS bands.

Test site A (shown in **Fig. 4.2-1**) was about 26,645 km^2 in size near to the city of Ust-Karenqa with the center longitude and latitude being 117.103E and 54.391N. For this site several Landsat quick look images and a time series of MODIS and AVHRR hotspots were available. Several fires occurred in August 2002 resulting in five large fire scars and in 2003 another fire event occurred between April and June (shown in **Fig. 4.2-3(e))**.

Totally 16 MERIS color images were produced using different band combinations and displayed for visual inspection and analysis. Forest, grassland, and lakes were easily discriminable using appropriate band combination such as R6G10B1 and R6G5B2. In all band combinations it was difficult to discriminate fire scars and cloud shadows. The typical training sites of forest fire scars, unburnt forests and cloud shadows in a MERIS image were visually identified (shown in **Fig. 4.2-3(a)**). In total 8 training sites for fire scars, 8 for unburnt forest and 7 for cloud shadows were selected.

Based on the findings of reflectance analysis, the cloud shadows were eliminated by composing the two MERIS acquisitions of July 12, 2003 and August 6, 2003 using the maximal Normalized Difference Vegetation Index (NDVI) algorithm. The acquisition of August 6, 2003 was first relatively calibrated to the acquisition of July 12, 2003 using histogram matching and then the NDVI of both MERIS images was calcuated using the following formula (European Space Agency, 2002):

$$NDVI = \frac{\rho_{G\ 885}^{nir} - \rho_{G\ 681.25}^{red}}{\rho_{G\ 885}^{nir} + \rho_{G\ 681.25}^{red}} \quad (1)$$

where $\rho_{G\ 885}^{nir}$ is band 14 of MERIS and $\rho_{G\ 681.25}^{red}$ is band 8 of MERIS. The two MERIS acquisitions (July 12, 2003 and August 6, 2003) and the composed image were classified using band 1, band 8 and band 14 based on the Iterative Self-Organizing Data Analysis Technique (ISODATA) algorithm. Four classes were assigned: vegetation, burnt area, clouds and cloud shadows.

Accuracy assessment

The accuracy of the burnt area assessment based on MERIS imagery was compared to results obtained from high resolution multispectral ASTER imagery. The accuracy assessment was done in test site B (size: 25,200 km^2, shown in **Fig. 4.2-1**) for which a series of almost cloud-free ASTER images (13 July 2003) acquired only one day apart from the MERIS acquisition were available (12 July 2003). Disasterous fires occurred in the area in spring 2003. The burnt area in both MERIS and ASTER imagery was determined by manual on-screen digitizing because this approach is straight forward and more accurate than automated fire scar mapping techniques.

MERIS colour images of different band combinations (R6G10B1; R6G5B2) were digitally enhanced and imported into GIS for visual on-screen digitizing of fire scars. 7 ASTER scenes acquired on 13 July 2003 were coregistered and imported into GIS for visual on-screen image interpretation of fire scars using band combination Red: band 3, 0.81 µm; Green: band 2, 0.66µm; Blue: band 1, 0.56 µm. 11 sample sites without cloud cover in both sensors were selected (**Fig. 4.2-1**) and analyzed.

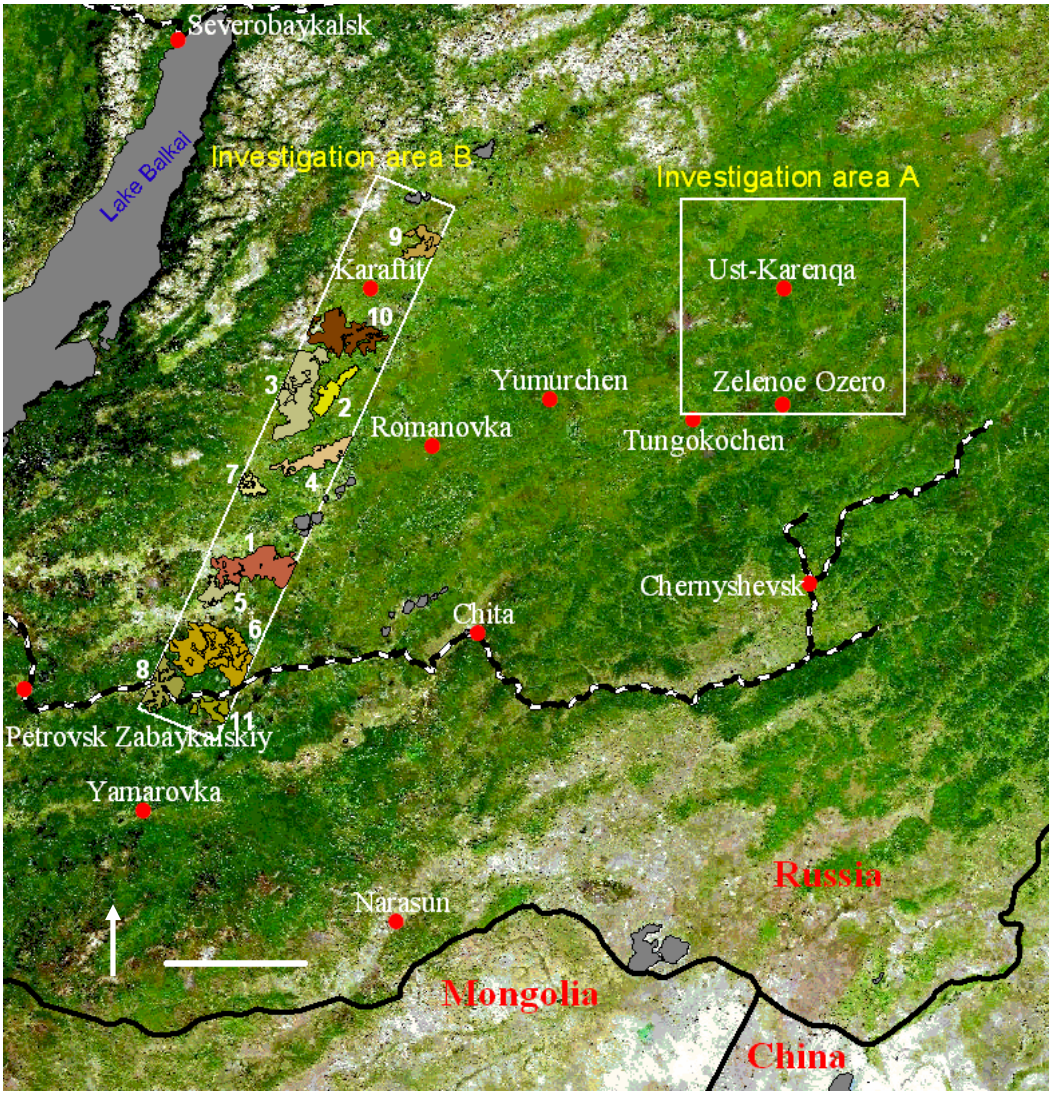

Fig. 4.2-1. The study area in South Siberia to the east of Lake Baikal and to the North of Mongolia and China. The background image shows a multitemporal MODIS composite of one month images acquired between August 20, 2002 and September 20, 2002. Forests (green) cover most of the region, grass and shrub (beige) and deserted land (white) cover the southern regions. The area is sparsely populated, few roads and one railway give access to the area. Spetral reflectance of forest, fire scars and cloud shadows were analyzed in area A (see text) and comparison with ASTER imagery was done in area B (see text). 2002 fire scars are visible as brown signatures near area A and to the Southwest of area B. Bar: 100 km.

4.2-3. Results

Reflectance analysis

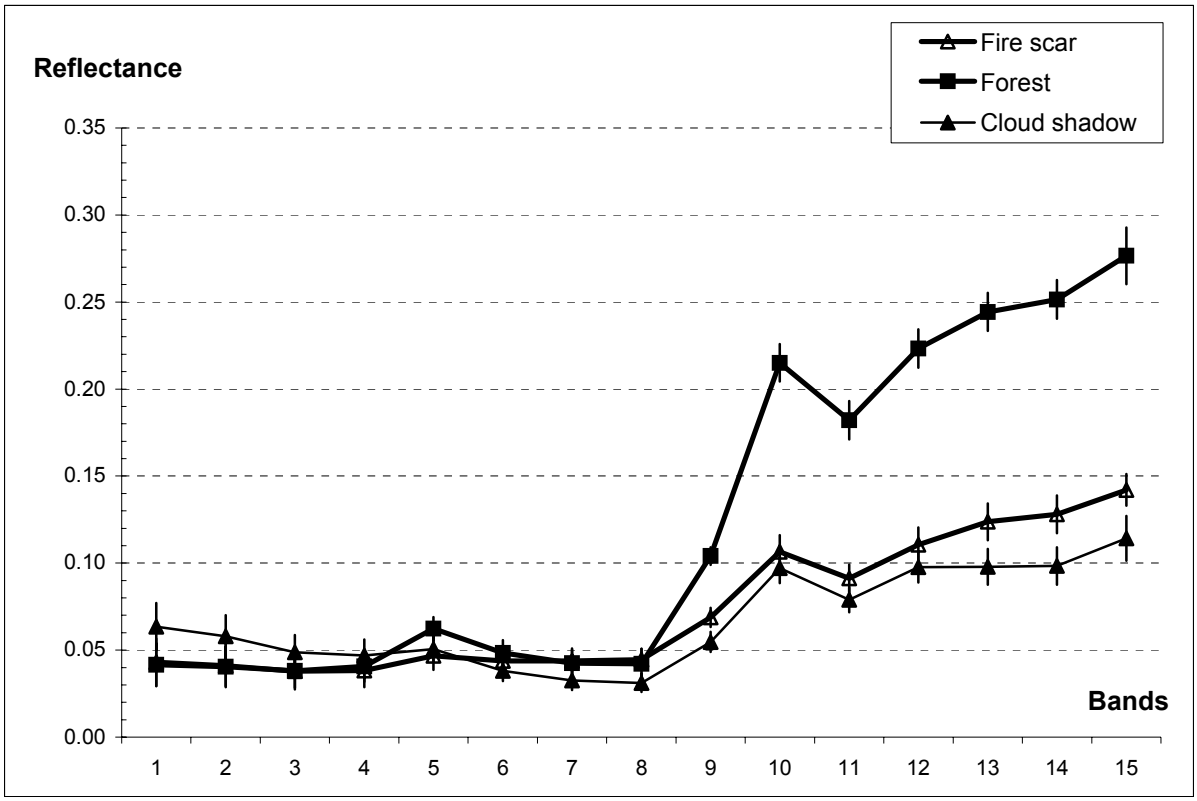

Fig. 4.2-2. Reflectance signals in a MERIS image for all bands of forest, fire scars and cloud shadows. Vertival bars: average deviation.

The result of the reflectance analysis for three different classes, forest, fire scars and cloud shadows, is shown for all 15 MERIS bands in **Fig. 4.2-2**. The reflectance was low in band 1-8 and similar for all three classes. In band 9-15 the reflectance of fire scars and cloud shadows differed very litte with about 3% maximum in band 13-15. The mean reflectance in band 9-15 of forest was significantly higher than that of fire scars and cloud shadows. These reults show that after fire disturbance the reflectance of forest in bands 1-8 changed very little whereas the reflectance in bands 9-15 decreased almost by half. This indicates the reflectance of forest is sensitive to fire disturbance probably due to biomass loss and albedo change and fire scars can be clearly discriminated from forest.

A problem was cloud shadows which had a very similar reflectances as fire scars in all 15 bands. Although the reflectances of fire scars in band 13, 14, and 15 were slightly higher than those of cloud shadows, this difference was not significant enough to clearly discriminate both.

Fire scar mapping

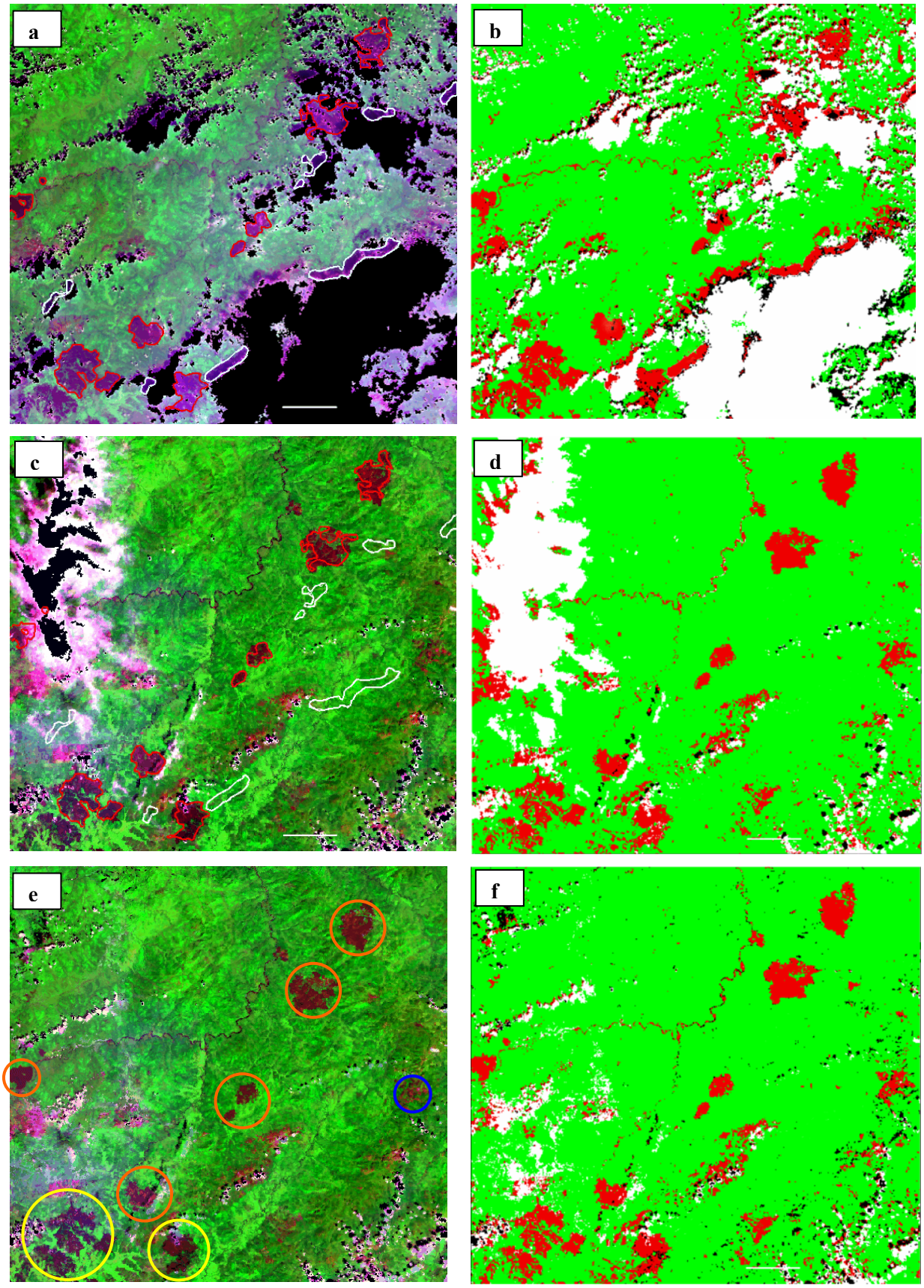

Fig. 4.2-3. MERIS images and classification results. (a): MERIS acquired 12 July 2003, band combination R8G14B1; (b): classification result of (a); (c): MERIS acquired 6 August 2003, band combination

R8G14B1; (d): classification result of (c); (e): Composite image of (a) and (c), band combination R8G14B1; (f): classification result of (e). In (a) and (c), white polygons are training sites for cloud shadows while the red polygonds indicate training sites for fire scars; In (e), red circles indicate fire scars formed in 2002, yellow in 2003 and blue in 2000; In (a), (c), and (e) the cloud mask (black), residual cloud/haze (white), vegetation (green) and fire scars (brown) are clearly visible. In (b), (d), and (f) green represents vegetation, red fire scars, white clouds and black cloud shadows. Bar:20 km.

Fig. 4.2-3 shows two MERIS acquisitions and the corresponding ISODATA classification results. The unambiguous discrimination of fire scars was impossible in both acquisitions of 12 July 2003 (**Fig. 4.2-3(a)**) and 6 August 2003 (**Fig. 4.2-3(c)**) because fire scars have very similar spectral refelctance to cloud shadows. Using the ISODATA algorithm it was not possible to correctly separate cloud shadows and fire scars.

Vigorous green vegetation such as forest absorbs incoming radiation in the red part of the spectrum and reflects in the near infrared part, whereas clouds have larger reflectance in the visible than in the near infrared. The NDVI, which is obtained as the difference of reflectances between red and near infrared bands normalized by the sum of those two bands, was therefore used to remove clouds when compositing multitemporal images (Fernandez *et al*., 1997). Furthermore, the NDVI should be useful to remove cloud shadows as well because the analysis showed the reflectance of cloud shadows was similar to that of forest in bands 1-8 but only half in band 9-15.

The NDVI composite of the two acquisitions is shown in **Fig. 4.2-3(e)**. In the composite image most clouds and cloud shadows have been successfully removed as expected. The ISODATA classification result is shown in **Table 4.2-2.** The accuracy of the burnt area detected in single acquisitions (12 July 2003 and 6 August 2003) was influenced by cloud shadows.

Table 4.2-2. ISODATA classification result of two single day MERIS acquisitions (12 July 2003 and 6 August 2003) and the maximal NDVI composite

Type	**12 July 2003 (km^2)**	**6 August 2003 (km^2)**	**Composite (km^2)**
Vegetation	15165	20413	22528
Cloud	7482	3653	1321
Cloud shadows	1267	139	593
Burnt area	2731	2439	2201
Total area	**26645**	**26645**	**26645**

Accuracy assessment

To assess the quality of the MERIS instrument for fire scar detection, the results were compared with high resolution multispectral ASTER imagery with 15 meters spatial ground resolution in VNIR bands. An area where large forest fires occurred and for which almost could-free ASTER and MERIS images had been acquired only one day apart from each other was selected. This guaranteed the correct recognition of the same fire scars in both data sets. 11 fire scars sites with a total size of about 740,000 ha have been visually identified in both data sets and compared quantitativley to each other. **Fig. 4.2-4** shows the same fire scar in the MERIS (left) and the ASTER (right) image. Generally there was a good agreement between the two sensors, however, fire scars detected in MERIS showed much less spatial detail than that in the ASTER image. Especially small fragments of unburnt forest were not detectable in the MERIS image.

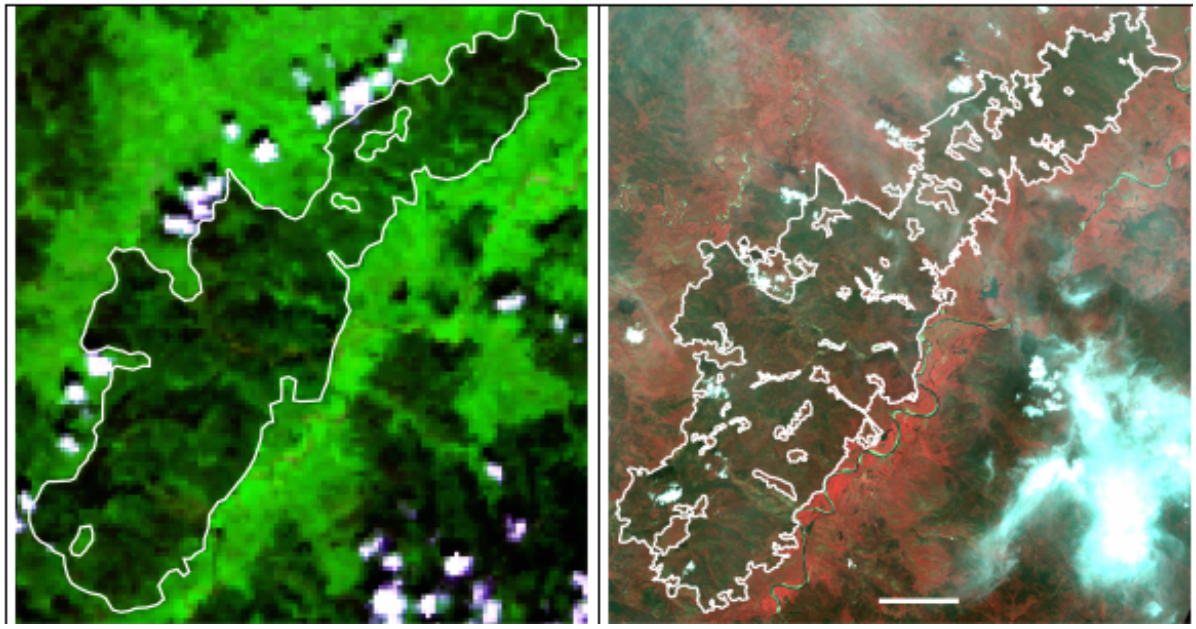

Fig. 4.2-4. Fire scars as digitized in a MERIS image (left, acquired on 12 July 2003) and an ASTER image (right, acquired on 11 July 2003). bar: 5 km

The result of the comparison is shown in **Table 4.2-3**. The area of the sample sites ranged from 20,000 ha to about 140,000 ha. Fire scars mapped in the ASTER imagery were overestimated in MERIS imagery in 7 sites with maximal 5.13% and underestimated in 4 sites with maximal –6.48%. On the average there was a slight overestimate of 2.2%, primarily due to the fact that small unburnt forest patches were not detectable in the lower resolution MERIS imagery.

Next is to investigate whether there is a correlation between the burnt area visible in high resolution ASTER imagery and medium resolution MERIS imagery. The result of the regression analysis is shown in **Fig. 4.2-5**. The coefficient R^2 equal to 0.9979 suggests that fire scars detected in MERIS and

ASTER imagery were highly correlated. The regression equation of y = 1.0299x indicates that the bias of the burnt area detected by MERIS is slightly shifted from the burnt area detected by ASTER.

Table 4.2-3. Quantitative comparison of fire scars detected in MERIS and ASTER imagery

Sites NO	MERIS Fire scar (Ha)	ASTER fire scar (Ha)	Relative Bias (%)
1	107,313	103,727	3.34
2	38,404	36,435	5.13
3	130,701	124,825	4.50
4	55,985	53,979	3.58
5	28,909	30,781	-6.48
6	139,595	134,402	3.72
7	19,352	18,596	3.91
8	56,535	59,418	-5.10
9	35,562	35,889	-0.92
10	100,546	98,525	2.01
11	27,873	28,003	-0.47
Sum	**740,775**	**724,580**	2.19

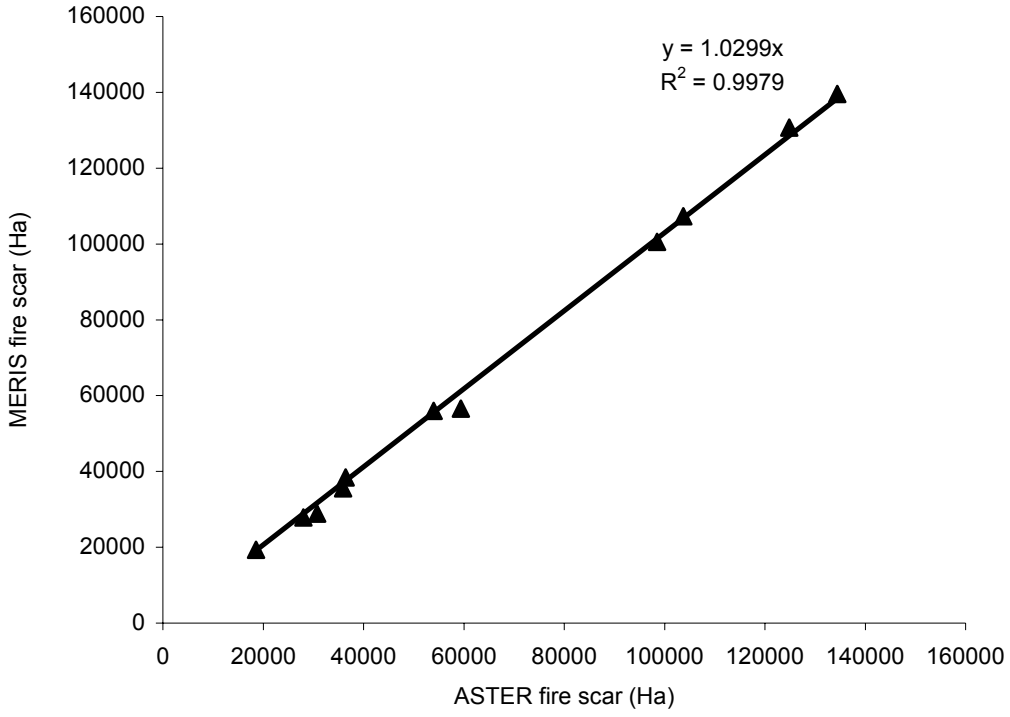

Fig. 4.2-5. The regression curve for fire scar areas determined in ASTER and MERIS imagery. y = 1.0299x where y refers to MERIS and x to ASTER.

4.2-4. Discussion

Two categories of fire products can be derived by satellite remote sensing: detection of active fires (hot-spots) and burnt areas. Hotspot detection is usefull for fire monitoring and active fire management, whereas the accurate assessment of burnt areas and fire impact on the vegetation are required to assess ecosystem disturbance and carbon release.

Hotspots are normally detected via their increased spectral signature in the Middle Infrared Red (MIR) spectral region (3.4-4.2μm) as reviewed in detail by Robinson (1991). Instruments used for hotspots detection include the NOAA-AVHRR, ERS/ENVISAT-A(A)TSR, TERRA/AQUA-MODIS, and BIRD.

In contrast to active fires that last for as short as a few hours, burn scars generally last from a few weeks to several months and even several years, and therefore potentially allow a more reliable detection through satellite remote sensing (Li *et al*., 2004). In boreal ecosystems like in Russia burnt scars are typically warmer than surrounding unburnt areas, so thermal infrared bands are useful in discriminating burn boundaries (Sukhinin *et al*., 2004). Li *et al.* (2004) reported that smoke particles with typical sizes on the order of 0.2 μm affected short-wavelength combination of 0.66, 0.55, and 0.47 μm more than long-wavelength combination of 2.13, 1.24, and 1.64 μm in burnt area identification, and thus the burn scars were better discriminated using the individual two channels of MODIS images centered near 1.24 and 2.13 μm. Zhang *et al.* (2003) also found that SPOT VEGETATION channel of 1.58-1.75μm also decreased following a fire event and could be used for burnt area identification.

Since MERIS only covers the spectral region ranging from 0.4125 to 0.900 μm, these findings can not be applied to MERIS imagery. Because NIR reflectance generally drops markedly after a fire, the remote detection of newly burnt areas is commonly based on Near InfraRed (NIR) reflectance thresholding, or observation of a significant NIR reflectance change (Zhang *et al*., 2003; Fraser *et al*., 2000; Stroppiana *et al*., 2002; Ahern *et al*., 2000). Many fire scar mapping activities using NOAA AVHRR imagery are based on the decrease of the NDVI after a fire event (Kasischke and French, 1995; Fernandez *et al*., 1997; Barbosa *et al*., 1999). Zhang *et al.* (2003) also regarded a significant fall in NIR reflectance between pre- and post-fire image dates as their primary method for mapping burned areas with SPOT VEGETATION.

Our results confirm these observations. A significant decrease (almost 50%) in the MERIS NIR bands 9-15 after fire impact was also found. The NIR reflectance drop can be used for fire scar mapping using MERIS imagery. Compared with others sensors, MERIS has more than 7 bands in NIR

spectral range and thus this higher spectral resolution might provide even more information on burn scars.

Several factors obstruct reliable fire scar mapping such as clouds, haze, and cloud shadows. Usually clouds are easily discriminable from land cover features because of their high reflectance in the visible and near infrared spectral region, but fire scars hidden under clouds will not be detected, thus leading to an underestimation of the burnt area. In addition, the spectral characteristics of cloud shadows were very similar to that of fire scars, so cloud shadows were easily recognized as fire scars in automated classification procedures. This leads to an overestimate of the burnt area. It was found that the maximal NDVI composite algorithm was useful to remove errors caused by cloud shadows. Errors still may occur due to the fact that MERIS band 8 (0.68125 μm) used for the NDVI is often contaminated by the scattering from smoke particles and haze (Li *et al*., 2004; Roy *et al*., 1999).

Kasischke *et al.* [1993] found that AVHRR NDVI composite images were useful to assess wildfire impacts in boreal forests. However, the coarse resolution of the AVHRR sensor (1-4 km) resulted in significant errors of burnt area estimates and tended to underestimate the total area of large fires in boreal regions (Kasischke and French, 1995; Kasischke and Bruhwiler, 2003). Similarly it was found that SPOT VGT underestimated the size of the burnt area by between 3% and 62% in Russia (Zhang *et al*., 2003) whereas it overestimated the size of burnt areas in Canadian forests by an average of 71% when compared to Landsat ETM (Fraser *et al*., 2000).

It was found that MERIS performed significantly better than NOAA AVHRR and SPOT VEGETATION. Burnt areas were only slightly overestimated (3%) when compared to high resolution ASTER imagery. This result suggests that MERIS might be very useful for fire scar mapping over large areas. However, our study was limited to only a few data sets in a specific geographic region. Results might be different in other regions and ecosystems with different fire regimes. More studies are required to validate these findings.

For example, it has been realized that both the issues related to and the methods used to monitor biomass burning in boreal forest are quite different than those for savannas and tropical forests (French *et al*., 1996). Fire events in boreal forest are often very large and leave a distinct scar which is clearly detectable through differences in surface reflectance. Fire events in tropical forests are often relatively small in size and less destructive. As a consequence fire scars in tropical forests are often not very distinct and fast vegetation regrowth makes their detection later even more difficult (Siegert *et al*., 2001). This differences prompt for detailed studies in tropical and sub-tropical regions for comparison.

Since MERIS is only one of three instruments onboard the European ENVISAT satellite which can be used for fire monitoring and impact assessment, ENVISAT will significantly improve our knowledge of the role of fire in the global ecosystem. In addition to MERIS multispectral data, ENVISAT acquires radar data with the ASAR instrument at wide swath mode (150 meters) and alternating polarization mode precision image at higher resolution of 30 meters as well as AATSR data at 1 km resolution. ASAR can be used to map fire scars when cloud and haze impede any optical sensors (Huang and Siegert, 2004) and AATSR is the successor of the Along Track Scanning Radiometer (ATSR) instrument onboard of ERS-1/2, which was successfully used to record fire hotspots (Arino *et al*., 2001). The capability to acquire data at different spectral and spatial resolutions simultaneoulsy allows to get a much more detailed picture of a fire event than with any other satellite system and makes ENVISAT a unique system for fire science.

4.2-5. Acknowledgements

The author would like to thank Chris Schmullius in Jena university for providing forest cover maps. Special thanks to Mr Andreas Langner for helping process the image.

4.2-6. References

Ahern, F. J., Epp, H., Cahoon, D., French, N. & Kasischke, E. (2000). Using Visible and Near-Infrared Satellite Imagery to Monitor Boreal Forests, in Kasischke, E. K. & Stocks, B. (eds), *Fire, Climate Change, and Carbon Cycling in the Boreal Forest*, pp 312 – 330, New York: Springer Verlag.

Alexeyev, V. A., Birdsey, R. A. (1994). *Carbon in Ecosystems of Forests and Peatlands of Russia*. Krasnoyarsk, Syberia: Jove Loony: 170 p.

Andreae, M. O. (1991). Biomass burning: its history, use, and distribution and its impaction environmental quality and global climate. In Levine, J. S. (Ed.), *Global Biomass Burning*, pp. 3-21, Cambridge, MA: The MIT Press.

Andreae, M. O. & Merlet, P. (2001). Emission of trace gases and aerosols from biomass burning, *Global Biogeochemical Cycles, 15,* 955-966.

Arino, O., Simon, M., Piccolini, I., Rosaz, J.M. (2001). The ERS-2 ATSR-2 world fire atlas and the ERS-2 ATSR-2 world burnt surface atlas projects. *Proceedings of the 8th ISPRS conference on Physical Measurement and Signatures in Remote Sensing*, Aussois, 8-12 January 2001.

Barbosa, P.M., Gregoire, J.-M. & Pereira, J.M.C. (1999a). An algorithm for extracting burned areas from time series of AVHRR GAC data applied at continental scale, *Remote Sensing of Environment, 69,* 253-263.

Brown, R. J. E. (1983). Effects of fire on the permafrost ground thermal regime. In Wein, R. W. & Maclean, D. A. (Ed.), *The Role of Fire in Northern Circumpolar Ecosystems* (pp. 97-110). New York: John Wiley & Sons.

Cahoon, D. R., Stocks, B. J., Levine, J. S., Cofer, W. R. & Pierson, J. M. (1994). Satellite analysis of the severe 1987 forest fires in northern China and southeastern Siberia, *Journal of Geophysical Research, 99(D9),* 18, 627-638.

Cahoon, D. R., Stocks, B. J., Alexander, M. E., Baum, B. A. & Goldammer, J. G. (2000). Wildland fire detection from space: theory and application. In Innes, J. L., Verstraete, M. M. & Beniston, M. (Ed.) *Biomass Burning and its Inter-Relationships with the Climate System* (pp. 151-169). Dordrecht: Kluwer Academic Publishers.

Conard, S.G., Sukhinin, A.I., Stocks, B.J., Cahoon, D.R., Davidenko, E.P. & Ivanova, G.A. (2002). Determining effects of area burnt and fire severity on carbon cycling and emissions in Siberia, *Climatic Change 55,* 197-211.

Conard, S.G. & Ivanova, G.A. (1997). Wildfire in Russian boreal forests–potential impacts of fire regime characteristics on emissions and global carbon balance estimates, *Environmental Pollution, 98(3),* 305-313.

Csiszar, I. & Sullivan, J. (2002). Recalculated pre-launch saturation temperatures of the AVHRR 3.7 mm sensors on board the TIROS-N to NOAA-14 satellites, *International Journal of Remote Sensing, 23,* 5271-5276.

European Space Agency. (2002, August). MERIS Product Handbook [online]. Available: http://envisat.esa.int/pub/ESA_DOC/ENVISAT/MERIS

Fernandez, F., Illera, P. & Casanova, J. L. (1997). Automatic mapping of surfaces affected by forest fires in Spain using AVHRR NDVI composite image data, *Remote Sensing of Environment 60*, 153–162.

Fraser, R. H., Li, Z. & Landry, R. (2000). SPOT VEGETATION for characterizing boreal forest fires, *International Journal of Remote Sensing, 21(18),* 3525-3532.

French, N. H. F., Kasischke, E. S., Johnson, R. D., Bourgeau-Chavez, L. L., Frick, A. L. & Ustin, S. L. (1996). Estimating fire-related carbon flux in alaskan boreal forests using multi-sensor remote sensing data. AGU Chapman Conference on Biomass Burning and Climate Change. *http://www.cstars.ucdavis.edu/papers/pdf/frenchetal1996a.pdf*

Goldammer, J. G. & Furyaev, V. V. (1996). *Fire in Ecosystems of Boreal Eurasia*. Dordrecht: Kluwer Academic Publishers.

Goldammer J. G. (2003). Wildland fire season 2002 in the Russian Federation: an assessment by the Global Fire Monitoring Center (GFMC), *International Forest Fire News (IFFN),28,* 2-14.

Harden, J.W., Trumbore, S.E., Stocks, B.J., Hirsch, A., Gower, S.T., O'Neill, K.P. & Kasischke, E.S. (2000). The role of fire in the boreal carbon budget," *Global Change* Biology, 6, S174–S184.

Huang, S. & Siegert, F. (2004), ENVISAT multisensor data for fire monitoring and impact assessment, *International Journal of Remote Sensing 25(20),* 4411–4416.

Ichoku, C., Kaufman, Y., Giglio, L., Li, Z., Fraser, R.H., Jin, J.-Z. & Park, W. M. (2003). Comparative analysis of daytime fire detection algorithms using AVHRR data for the 1995 fire season in Canada: Perspective for MODIS, *International Journal of Remote Sensing 24*, 1669-1690.

Kajii Y., Kato S., Streets, D. G., Tsai N. Y., Shvidenko A., Nilsson S., Minko,M. P., Abushenko N., Altyntsev D. & Khodzer T. V. (2002). Boreal forest fires in Siberia in 1998: estimation of area and emissions of pollutants by AVHRR satellite data, *Journal of Geophysical Research, 107(D24),* 4745, doi:10.1029/2001JD001078.

Kasischke, E. S., & French, N. H. F. (1995). Locating and estimating the areal extent of wildfires in Alaskan boreal forests using multiple-season AVHRR NDVI composite data, *remote Sensing of Environment 51,* 263-275.

Kasischke, E. S. & Bruhwiler, L. P. (2003). Emissions of carbon dioxide, carbon monoxide, and methane from boreal forest fires in 1998, *Journal of Geophysical Researc*h,107(D1), 8146, doi:10.1029/2001JD000461.

Kasischke, E. S., French, N. H. F., Harrell, P., Christensen, N. L., Ustin, S. L. & Barry, D. (1993). Monitoring of wildfires in boreal forests using large area AVHRR NDVI composite image data*, Remote Sensing of Environment, 45,* 61-71.

Korovin, G. N. (1996). Analysis of the distribution of forest fires in Russia. In Goldammer, J.G. & Furyaev, V. V. (Ed.), *Fire in Ecosystems of Boreal Eurasia,* pp. 112–128. Dordrecht, Boston, London: Kluwer Academic Publishers.

Li, R.R, Kaufman, Y.J., Hao, W.M., Salmon, J.M. & Gao, B.C. (2004). A technique for detecting burn scars using MODIS Data, *IEEE IEEE transactions on geoscience and remote sensing, 42*, 1300-1308.

Page S.E., Siegert F., Rieley J.O., Boehm H-D.V. & Jaya A. (2002). Carbon released during peatland fires in Central Kalimantan, Indonesia in 1997,*Nature, 420,* 61-65

Rahman, H., Dedieu, G. (1994). SMAC: a simplified method for the atmospheric correction of satellite measurements in the solar spectrum,*International Journal of Remote Sensing* 15(1), 123-143.

Robinson, J. M. (1991). Fire from space : Global fire evaluation using infrared remote sensing, *Internation journal of remote sensing, 12,* 3-24.

Roy, D., Lewis, P. & Justice, C. (2002). Burned area mapping using multi-temporal moderate spatial resolution data - a bi-directional reflectance model-based expectation approach, *Remote Sensing of Environment, 83,* 263-286.

Shvidenko, A. & Goldammer, J.G. (2001). Fire situation in Russia, *International Forest Fire News 24,* 41-59.

Shvidenko, A. Z. & Nilsson, S. (2000). Fire and the Carbon Budget of Russian Forests. In Kasischke, E. & Stocks, B. (Eds.), *Ecological Studies 138 - Fire, Climate Change and Carbon Cycling in the Boreal Forests,* pp. 289–311. New York: Springer- Verlag.

Siegert F., Huang S., Goldammer J. G. & Sukhinin A. I.. Exceptional carbon release by large-scale wildland fires in Siberia in 2003, *Global Biogeochemical Cycles* (submitted)

Siegert, F, Zhukov, B., Oertel, D., Limin, S., Page, S.E. & Rieley, J.O. (2004). Peat fires detected by the bird satellite, *International Journal of Remote Sensing*, 25(16), 3221-3230.

Siegert, F., Rücker G., Hinrichs A. & Hoffmann A. (2001). Increased fire impacts in logged over forests during El Niño driven fires, *Nature, 414,* 437-440.

Smith, L.C., MacDonald, G.M., Velichko, A.A., Beilman, D.W., Borisova, O.K., Frey, K.E., Kremenetski, K.V. & Sheng, Y. (2004). Siberian peatlands a net carbon sink and global methane source since the early holocene, *Science, 303,* 353-356.

Soja, A. J., Sukhinin, A. I., Cahoon, D. R., Shugart, H. H. & Stackhouse P.W. (2004). AVHRR-derived fire frequency, distribution and area burned in Siberia, *International Journal of Remote Sensing,25,* 1939-1960

Stroppiana, D., Pinnock, S., Pereira, J. M. C., & Gregoire, J. M. (2002). Radiometric analysis of SPOT-VEGETATION images for burnt area detection in Northern Australia. *Remote Sensing of Environment, 82,* 21- 37.

Sukhinin, A. I. (2003). The 2002 fire season in the Asian part of the Russian Federation: a view from space. *International Forest Fire News (IFFN) 28,* 18-28.

Sukhinin, A. I., French, N.H.F., Kasischke, E.S., Hewson, J. H., Soja, A. J., Csiszar, I. A., Hyer, E. J., Loboda, T., Conard, S. G., Romasko, V. I., Pavlichenko, E. A., Miskiv, S. I. & Slinkina, O. A. (2004). Satellite-based mapping of fires in Russia: new Products for fire management and carbon cycle studies, *Remote Sensing of Environment, 93,* 546– 564.

Van der Werf, G. R., Randerson, J. T., Collatz, G, J., Giglio, L., Kasibhatla, P. S., Arellano A. F., Olsen, S. C. & Kasischke, E. S. (2004). Continental-scale partitioning of fire emissions during the 1997 to 2001 El Nino/La Niña period. *Science, 303,* 73-76.

Wooster, M.J., Zhukov, B. & Oertel, D. (2003). Fire radiative energy for quantitative study of biomass burning: derivation from the BIRD experimental satellite and comparison to MODIS fire products, *Remote Sensing of Environment 86,* 83–107.

Yamaguchi, Y., Kahle, A., Tsu, H., Kawakami, T. & Pniel, M. (1998). Overview of advanced spaceborne thermal emission and reflection radiometer (ASTER). *IEEE transactions on geoscience and remote sensing,* 36(4):1062- 1071.

Zhang Y. H., Wooster, M. J., Tutubalina O. & Perry, G.L.W. (2003). Monthly burned area and forest fire carbon emission estimates for the Russian Federation from SPOT VGT, *Remote Sensing of Environment, 87,* 1-15.

CHAPTER 4.3---ENVISAT MULTISENSOR DATA FOR FIRE MONITORING AND IMPACT ASSESSMENT

The European ENVISAT satellite provides both optical and radar measurements of the Earth surface. In this chapter, three ENVISAT instruments were used to investigate the extent and impact of the forest and peatland fires which devasted large areas in Central Kalimantan, Indonesia in 2002. Reduced spatial resolution MERIS imagery was used to identify simple land cover features and smoke plumes. Fire hotspots were detected by band 3.7 µm in AATSR night time acquisitions, and burnt areas were detected by ASAR wide swath radar imagery acquired before and after the fire event. The capability of ENVISAT to acquire data from different sensors simultaneoulsy or within a short period of time greatly enhances the possibilities to monitor fire occurrence and assess fire impact.

4.3-1. Introduction

The El Niño episode in 1997/98 caused an unusually long dry season across South East Asia, which boosted the spread of thousands of forest fires. Millions of hectares of tropical rainforests and peat swamp forests were destroyed and huge amounts of carbon were released into the atmosphere (Siegert et al., 2001; Page et al., 2002; Taconi, 2003). In 2002 a weak El Niño caused another drier than usual year and again hundreds of fires were observed in Central Kalimantan.

Considering the importance of forest and peatland fires for global climate change, this fire event was chosen to qualitatively investigate the potential of the new ENVISAT environmental satellite for fire monitoring. The objective of this study was to investigate and demonstrate the capability of ENVISAT to detect forest fires and fire impact by exploiting its sophisticated combination of instruments.

Multiple acquisitions of the Advanced Along Track Scanning Radiometer (AATSR), the MEdium Resolution Imaging Specrometer (MERIS) and the Advanced Synthetic Aperture Radar (ASAR) product, ASA-WSM-1P wide swath mode standard image and ASA-APP-1P alternating polarization mode precision image, on ENVISAT were used to detect fire hotspots and fire scars. The major advantage of the ENVISAT system is that all three instruments can record data almost simultaneously, thus, delivering a more detailed picture on a fire event than any other satellite system. The results were compared to established fire detection instruments such as the Moderate Resolution Imaging Spectroradiometer (MODIS), NOAA's Advanced Very High Resolution Radiometer (AVHRR) and field data.

4.3-2. Methods

The study area was located in the province of Central Kalimantan on the island of Borneo, Indonesia. It is characterized by extensive lowlands supporting a natural vegetation of peat swamp forests. In recent decades human activity such as logging and agriculture and recurrent fires have severely disturbed this fragile ecosystem. In 2002 hundreds of fire hotspots were observed by the NOAA receiving station operated by FFPMP-Forest Fire Prevention Management Project, the global daily MODIS fire product and the BIRD satellite (Siegert et al., 2004). Field data on land cover and land use was collected before the fires. During and after the fires the occurrence and extent of fire scars and fire impact were recorded within a distance of 50 km from Palangkaraya in areas accessible by car or boat. All observations were recorded by GPS and imported into the GIS to allow comparison with satellite imagery. An assessment of the burned area of 2002 based on Landsat ETM imagery was used for validation.

The AATSR sensor is characterized by three thermal bands at 3.7, 10.8 and 12 μm wavelengths and four reflected visible/near infrared bands. The instrument has 1 km spatial resolution at nadir view. The available night time acquisitions were used to detect fire hotspots. Pixel values saturated in band 3.7 μm were classified as fire hotspots (red colour in **Fig. 4.3-1B**). The accuracy of the AATSR derived hotspots was compared to the MODIS fire product and NOAA AVHRR hotspots downloaded (http://ffpmp2.hp.infoseek.co.jp/English/ and http://rapidfire.sci.gsfc.nasa.gov/production/). All data sets were georeferenced to UTM projection and imported into a GIS in order to allow the comparison of the different data sets.

MERIS is a 68.5˚ field-of-view pushbroom imaging spectrometer that measures the solar radiation reflected by the Earth at a ground spatial resolution of 300 m in 15 spectral bands in the visible and near infra-red. MERIS allows global coverage of the Earth in 3 days. In autumn 2002 only the reduced spatial resolution MERIS data in level 1b with 1200 m ground spatial resolution were available. The NIR bands which are sensitive to biomass change were chosen to detect fire scars. To identify the origin of smoke plumes blue band (band 1) was used because haze is better visible in the shortwave spectrum. Colour images were prepared using band 6 as red, band 10 as green and band 1 as blue to visualize the vegetation cover and haze produced by the fires.

ASAR, a cloud penetrating SAR instrument, operating at C-band, was designed to operate in six different modes ranging from alternating polarisations and from high to medium spatial resolution swath modes for regional and global monitoring. In this study the wide swath mode product (approximately 150 m ground range and 150 m azimuth) and alternating polarisation mode radar images (approximately 30 m ground range and 30 m azimuth) in level 1b, ASA-WSM-1P and ASA-APP-1P were evaluated. The ASAR image were first speckle filtered using the Gamma Map filter to

remove the noise. Brightness was then adjusted to compensate for near to far range effects. To detect fire scars a Principle Component Analysis (PCA) was applied to two radar image pairs acquired before and after the fire event. The second component depicts the differences between the two multitemporal radar images and thus indicates change caused by fire (Siegert and Rücker, 2000). RGB colour composites were produced for fire scar detection using the second component as red and the two, pre-fire and post-fire, images as green and blue respectively.

4.3-3. Results

12 AATSR scenes, 6 MERIS scenes, 8 ASAR WSM and 2 ASAR APP images were analysed. At that time it was not possible to record all sensors within a single day. However, in one instance shown in **Fig. 4.3-1,** MERIS and AATSR data only one day apart were available. More than 20 smoke plumes are visible in the MERIS image and thick haze covers the whole Northern section. There is a clear correlation between the smoke plumes visible in MERIS and AATSR hotspots as shown in **Fig. 4.3-1B**. NOAA and MODIS hotspots are shown for comparison. 126 hotspots were identified by AATSR, 337 by NOAA AVHRR and 321 by MODIS. The difference in hotspot numbers between the different instruments relates 1.) to the fact that MODIS and NOAA (acquired on the same day) were acquired two days earlier than the AATSR image and 2.) smoke and clouds were more dense during the AATSR acquisition (dark areas in **Fig. 4.3-1B**). GPS recorded fire locations (August 24, 2002, shown in **Fig. 4.3-2C**) were compared with the occurrence of smoke plumes visible in a MERIS image acquired on the same day as the fires were recorded on ground. Out of 15 fires observed on ground (red in **Fig. 4.3-2C**), 10 fire locations could be identifed by their smoke plumes and fire scars in the MERIS colour image product. Four fires could not be confirmed because thick smoke covered the area, one fire had no smoke plume in the MERIS image.

No acquisition of AATSR were available for 24th of August 2002 to be compared with GPS recorded fire locations accessed on ground. The comparsion of hotspots detected in an AATSR image acquired on September 19, 2002 (**Fig. 4.3-1B**) with burnt areas detected in a Landsat ETM image shows that almost all AATSR hotspots coincide with fire scars. Fire scars not detected by AATSR relate to fires damage which occurred after or before 19th September.

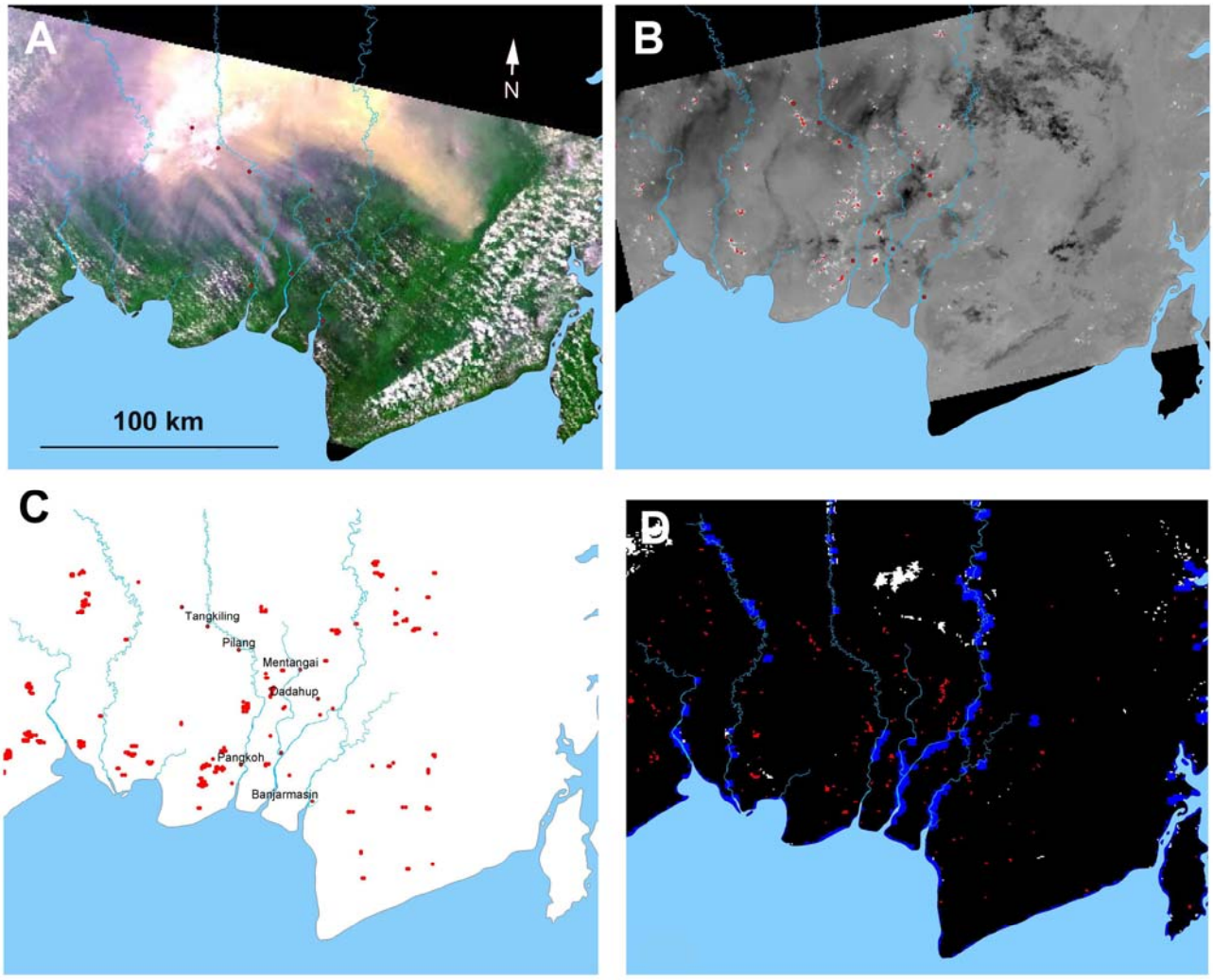

Fig. 4.3-1. MERIS colour image and hotspots detected by satellite different sensors. Fig. 4.3-1A: MERIS reduced spatial resolution (18.9.2002); Fig. 4.3-1B: AATSR night time acquisition (19.9.2002); Fig. 4.3-1C: NOAA AVHRR hotspots (17.9.2002) and Fig. 4.3-1D: MODIS hotspots (17.9.2002).

In ASAR WSM wide swath images burnt scars are clearly visible due to a reduced backscatter. Under dry weather conditions (**Fig. 4.3-2A**) as they prevailed during August and September 2002, deforested, burnt and agricultural areas have low backscatter while forests have intermediate backscatter values. Cities, villages and even small transmigrator houses (10 x 5 m) are well visible in ASAR WSM images with a spatial resolution of 150 m. GPS recorded fire locations were compared with fire scars detected in ASAR WSM images. Out of 15 burnt areas 10 were detectable in a multitemporal ASAR WSM image (**Fig. 4.3-2C**). This example demonstartes that in ASAR imagery fire scars are only visible in areas on siliceous sandy substrates with low soil moisture, while fire scars on swampy peatland are not detectable (indicated by red arrows in **Fig. 4.3-2C**). The pre and post-fire images used for the PCA colour composite were acquired in September and December 2002. Since rainy weather conditions prevailed in December the fire scar detection capability of the ASAR instrument became blurred, which confirms previous results (Siegert and Rücker, 2000).

An ASA-APP-1P radar image with high spatial resolution was compared to a Landsat ETM derived land cover map. It was found that ASA-APP-1P imagery with HV polarisation allowed better discrimination of forest and deforested areas than HH polarisation. In **Fig. 4.3-2D** all areas with low backscatter correspond to fire scars and/or low vegetation (grass and bushland). Unfortunately ASAR-APP images acquired before and after the fire event were not received. However, similarly as ERS-1 and ERS-2 imagery this high resolution data set was expected to allow very detailed analyses of burnt areas and fire impact.

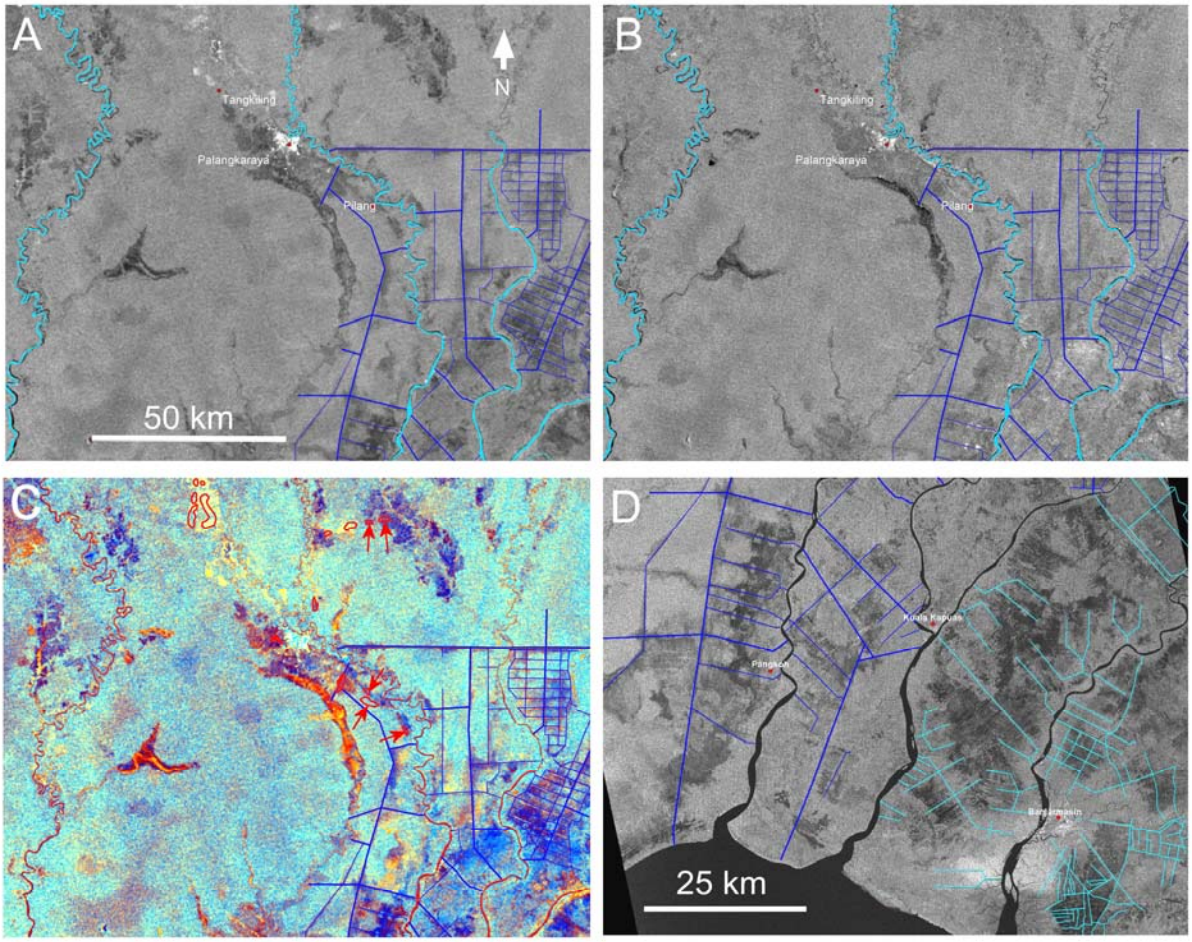

Fig. 4.3-2. ENVISAT radar images and change detection. Fig. 4.3-2A: ASAR product ASA-WSM-1P (28.9.2002); Fig. 4.3-2B: ASAR product ASA-WSM-1P (7.12.2002); Fig. 4.3-2C: Applying PCA to two ASA-WSM-1P images acquired on 28.9.2002 and 7.12.2002, then creating the colour image using component two (Red) and the two images (Green and Blue). Burnt scars are visible in yellow and pale orange. Red polygons indicate GPS recorded fire scars. Red arrows indicate fire scars not detected by ASAR due to wet soil conditions. Fig. 4.3-2D: ASAR ASA-APP-1P image with HV polarisation (25.9.2002).

4.3-4. Discussion and conclusion

This chapter describes some preliminary, mostly qualitative observations of the multi-sensor capability of the European ENVISAT satellite. ENVISAT's ASAR instrument which is able to pierce through haze, smoke and clouds was found very usefull in detecting fires and burnt areas. During active burning all optical sensors are of limited use for fire detection and timely fire impact assessment due to the release of haze and smoke by the fire. Similarly as it was shown for tropical regions using ERS-1/2 SAR images, ENVISAT ASAR images had a lower radar backscatter than forested areas, especially under dry weather conditions (Rücker and Siegert, 2000). Compared to high resolution radar data such as ERS with spatial resoultion of 25 m, ASAR WSM with the medium spatial resolution of 150 m can be used for regional fire monitoring and impact assessment. However, the capability of detecting the fire scar decreases under rainy weather conditions, and fire scars on swampy peatland with high soil moisture are not detected. This indicates the optical sensor data are indispensible for accurate impact assessment in wetland zones.

The high spatial resolution ASAR image product was found to be useful in detecting towns and villages and even individual houses. This ability to map settlements might be useful in assessing future fire risk since many fires are started by settlers clearing land for cultivation (Taconi, 2003). Also visible in ASAR imagery was the extensive network of canals that have been made to drain the peat swamps. These artificial canals drain the water from the humid peat swamps vulnerable to fire (Page et al., 2002). With a high spatial resoultion of 30 m similar to ERS, APP data is very useful for detailed fire impact assessments. The nearly simultaneous acquisition of both high and medium resolution radar data, i.e. the ASA-WSM and ASA-APP, in the same orbit should support fire monitoring and assessment in both spatially and temporally.

MERIS with a reduced spatial resolution of 1200 m was found to be useful for large scale fire scar mapping and to identify smoke plumes The reduced spatial resolution MERIS image product supplements existing real time monitoring capabilites because of the global coverage of the Earth in only 3 days. Sources of smoke plumes could be spotted in AATSR night time acquisitions. However clouds and thick smoke interfere with these two optical sensors limiting their application. The low spatial resolution of 1200 m may lead to an underestimate of the burnt area similarly as NOAA AVHRR. The full resolution MERIS data with a spatial resolution of 300 m was not available at that time. It is expected that this data set is much better suited for fire scar mapping and can be applied at regional level.

AATSR night acquisitions detected hotspots which were also clearly visible as smoke plumes in MERIS images. Each AATSR hotspot group coincide with fire scars of Landsat ETM. However due

to the coarse spatial resolution of 1 km the AATSR instrument may not detect small or low-intensity fires similarly as MODIS (Siegert et al., 2004) and AVHRR (Cahoon et al. 2000).

The capability of ENVISAT to acquire imagery with several different instruments almost simultaneously allows to get a much more detailed picture on a fire event than with any other satellite system. Major advantages are that ENVISAT is able to acquire 1.) both optical data and radar data, 2.) images both during day and night, 3.) a combination of high, medium and low spatial resolution imagery which allows for simultaneous multi-scale analysis and 4.) multiple bands covering different spectral wavelengths. These special characteristics make ENVISAT very suitable for fire monitoring and fire impact assessment in different regions with varying natural conditions and during different weather conditions at both local and regional level. The different ENVISAT intruments can be useful within the framework of a multiscale fire monitoring system in which low and medium resolution imagery is used for large scale active fire monitoring and impact assessement and high resolution ASAR data can be used for a rapid analysis of fire impact already during and shortly after the fire event.

4.3-5. Acknowledgements

The author would like to thank ESA/ESRIN for financial support and free data provision by ESA in the framework of ENVISAT AO 689. Field data collection was done by Adi Jaya, University of Palangkaraya and was funded by the EU 5th Framework Programme (INCO-DEV project STRAPEAT). Special thanks also to Miss Annette Bechteler for providing the Landsat ETM fire scar data.

4.3-6. References

Cahoon, D. R., Stocks, B. J., Alexander, M. E., Baum, B. A. & Goldammer, J. G. (2000). Wildland fire detection from space: theory and application. In Innes, J. L., Verstraete, M. M. & Beniston, M. (Ed.) *Biomass Burning and its Inter-Relationships with the Climate System* (pp. 151-169). Dordrecht: Kluwer Academic Publishers.

Page S.E., Siegert F., Rieley J.O., Boehm H-D.V. & Jaya A. (2002). Carbon released during peatland fires in Central Kalimantan, Indonesia in 1997,*Nature, 420,* 61-65.

Rücker, G. & Siegert, F. (2000). Burn scar mapping and fire damage assessment using ERS-2 SAR images in East Kalimantan, Indonesia. International Archives of Photogrammetry and Remote Sensing 2000 vol 33, 17– 21 August 2000 (Netherlands: Amsterdam), pp. 1287-1293.

Siegert, F. & Rücker, G. (2000). Use of multitemporal ERS-2 SAR images for identification of burned scars in South-East Asian tropical rain forest, *International Journal of Remote Sensing, 21(4),* 831-837.

Siegert, F., Rücker G., Hinrichs A. & Hoffmann A. (2001). Increased fire impacts in logged over forests during El Niño driven fires, *Nature, 414,* 437-440.

Siegert, F, Zhukov, B., Oertel, D., Limin, S., Page, S.E. & Rieley, J.O. (2004). Peat fires detected by the bird satellite, *International Journal of Remote Sensing, 25(16),* 3221 – 3230.

Taconi L. (2003). Fires in Indonesia: causes, costs and policy implications. Centre for International Forest Research Occasional Paper No. 38, ISSN 0854-9818, Indonesia.

CHAPTER 4.4---EXCEPTIONALLY LARGE FIRE DAMAGE BY LARGE-SCALE WILDFIRES IN SOUTHERN SIBERIA IN 2003

Vegetation fires significantly contribute to biogeochemical cycles and affect the composition and functioning of the global atmosphere. Exceptionally large forest fires were observed in Southern Siberia in 2003. Based on active fire measurements of the AVHRR and MODIS instruments and multispectral imagery from the MERIS and ASTER instruments, the spatial extent and fire impact within an area of 1,300,000 km^2 were investigated. 202,000 km^2 burnt in 2003, which is more than the total burnt area between 1996-2002. 71.4% of the burnt areas were forests, 11.6% wetlands and bogs. In total 32.2% of the forest cover has been burnt at least once from 1996 to 2003, 14% of the area has been affected at least twice by fire. Although fire is a common recurrent phenomenon in boreal ecosystems, these results suggest that the combined effects of climate extremes, stand-replacement fires, and inappropriate forestry practices will lead to deterioration of the carbon sequestration potential on some sites, thus to a net release of carbon to the atmosphere. The prompt release of carbon to the atmosphere contributed significantly to the so far unexplained high increase of the global atmospheric CO_2 concentration in 2003 by 2.54 ppm.

4.4-1. Introduction

Vegetation fires significantly contribute to biogeochemical cycles and affect the composition and functioning of the global atmosphere (Andreae and Merlet, 2001; Page *et al.*, 2002; Van der Werf *et al.*, 2004). Russia has the largest extent of boreal forest worldwide covering an estimated 8,250,000 to 8,960,000 km^2 and holding 28% of the world's terrestrial carbon in forests, wetlands and soils (Dixon *et al.*, 1994). Wildfire disturbance is common and an integral part of Eurasia's boreal forest ecosystems (Goldammer and Furyaev, 1996). Studies of large-scale wildland fires burning in Siberia and the Far East of the Russian Federation imply that fires in Russia might contribute significantly to the transfer of large amounts of carbon to the atmosphere and ecosystem deposits (e.g., Kasischke and Stocks, 2000; Shvidenko and Nilsson, 2000; Conard *et al.*, 2002; Kasischke and Bruhwiler 2003; Soja *et al.*, 2004a).

In recent years forest fire outbreaks have been exceptional in some parts of the Russian Federation (Goldammer, 2003). In 2002 more than 10,000 fires were recorded by NOAA (National Oceanic and Atmospheric Administration) - AVHRR (Advanced Very High Resolution Radiometer)

in the Asian part of Russia affecting more than 117,000 km^2, with a mean fire size of 11.43 km^2 (Sukhinin, 2003). Similar observations were made in 1998 and 2000 when 9000 and 130,000 km^2 were burned, respectively (Kajii *et al.*, 2002; Conard *et al.*, 2002). The observed trend towards the more frequent occurrence of years with large fire outbreaks emphasizes the need for accurate information on fire regime and carbon release (Goldammer and Stocks, 2000; Ahern *et al.*, 2001).

Current fire monitoring activities in Russia are mainly based on the detection of hotspots by the NOAA-AVHRR instrument and the assessment of fire scars from spectral reflectance images (Sukhinin, 2003). However, this widely used satellite sensor was not designed for fire detection and is therefore not optimally configured for this application. Small fires with low-energy release will not be detected because of sensor resolution, sensitivity and response time (Cahoon *et al.*, 1992). In addition, cloud coverage, fire plumes and the repeat cycle of satellite overpass limit the detection of all actual fires. The burnt area tends to be underestimated in Russian boreal due to the low resolution of the sensor (Kasischke and French, 1995; Kasischke and Bruhwiler, 2003; Soja *et al.*, 2004b). These factors have resulted in incomplete records of fire occurrence and thus figures on fire impact and carbon emission vary significantly (Kajii *et al.*, 2002; Simon, 2002; Sukhinin *et al.*, 2004). A hybrid algorithm that combines hotspot detections with burn scar maps was used to get a most complete set of historic fire maps, however, an initial validation indicates that the burned-area was underestimated (Sukhinin *et al.*, 2004).

2003 was an especially disastrous year for the Siberian forests. Thousands of fires were recorded between March and August in an area East of lake Baikal in South Siberia (110.27°E to 131.00°E and from 49.89°N to 55.27°N, blue polygon in **Fig. 4.4-1**). Thick haze covered the territories of the Russian Federation, Mongolia and China for weeks, with smoke plumes reaching as far as Japan and Alaska.

To overcome the limitations of the NOAA AVHRR system, data from other three different satellite systems were used to determine the burnt area more accurately: 1.) the Moderate Imaging Spectrometer (MODIS) onboard the TERRA satellite and the NOAA AVHRR with almost daily coverage and 1 km spatial resolution, 2.) multispectral images from the MEdium Resolution Imaging Spectrometer (MERIS) with 3 day revisit time and 300 m spatial resolution onboard the European ENVISAT satellite, and 3.) multispectral images from the Advanced Spaceborne Thermal Emission and Reflection Radiometer (ASTER) onboard the TERRA satellite with 16 day revisit time and 15 m spatial resolution.

The MODIS system provides the most accurate operational source for global monitoring of the occurrence, dynamics and spread of vegetation fires (Justice *et al.*, 2002; Kaufman *et al.,* 1998) and

the available AVHRR fire product provides the most complete set of historic fire maps (Sukhinin *et al.*, 2004), while multispectral images of the medium resolution MERIS and higher resolution ASTER instrument were used to assess the burnt area more accurately.

Since the area of fire occurrence in the Russian Federation was vast and because of limitations in data availability, the investigation was only focused on the region where most fires occurred in 2003. In addition to satellite-derived data, our analysis is based on official reports and an aerial survey of fire impact conducted in September 2003 in the region most affected by fires (Goldammer *et al.*, 2003) and a survey conducted in November 2004 by local staff of the Ministry of Natural Resources of the Russian Federation in Chita and Buryatia. To estimate the carbon release the Global Land Cover 2000 (GLC2000) vegetation map derived from SPOT VEGETATION and the Vegetation Continuous Field map derived from MODIS imagery were used (Bartalev *et al.*, 2003; Hansen *et al.*, 2003). The results of the 2003 fire season were compared to fire occurrence and burnt area for the years 1996 – 2002 derived from NOAA AVHHR data.

4.4-2. Materials and methods

Study site

The research area was located mainly East of Lake Baikal, ranging from 110.27°E to 131.00°E in longitude and from 49.89°N to 55.27°N in latitude (**Fig. 4.4-1**) with total area about 1,300,000 km^2. Climate is continental and recorded climate data indicates that the maximum precipitation falls from June through August. Most of the area is sparsely populated and covered by more or less intact coniferous forests interspersed with swampy wetlands. In the Southern part forests blend into dryland steppe and some cropland are found along the valleys. Digital Elevation data shows that the site has a relatively flat undulating relief.

MODIS hotspots and AVHRR fire products

The MODIS MOD14A2 product is a gridded 1 km composite of the most-confident hotspots detected in each grid cell over an eight-day composite interval. 32 scenes of MOD14A2 recorded between 14 March and 8 August 2003 were obtained from http://edcimswww.cr.usgs.gov. The images were reprojected into Albers conical equal-area projection and then spatially mosaiced. Each hotspot in the MOD14A2 product is assigned to one of the three fire confidence classes (low-confidence fire with value of 7, nominal-confidence 8 and high-confidence 9). All three values were considered as hotspots representing fire events in this study. The maximal value was chosen when compositing time series.

Production of the burned area product from NOAA AVHRR for the years 1996-2003 is a multi-step process, which includes a contextual fire detection algorithm (hot spot detection), creation

of fire polygons from adjoining fire detections, and mapping of post-fire burn scars. Adjacent and nearby fire pixels (within 3 to 4 pixels) were considered as belonging to the same fire event and aggregated to define a fire polygon. The coordinates of the center of the aggregated pixel polygon and area of the polygon were then calculated (Soja *et al.*, 2004b; Sukhinin *et al.*, 2004). For further analysis the AVHRR fire product was converted to raster format with each grid cell covering 1 km^2 in the albers conical equal-area projection.

MERIS and ASTER processing and burn scar mapping

MERIS measures the solar radiation at a ground spatial resolution of 300m with global coverage of the Earth in three days in 15 visible and near infra-red spectral bands, which are respectively centered at 0.4125, 0.4425, 0.490, 0.510, 0.560, 0.620, 0.665, 0.68125, 0.70875, 0.75375, 0.760625, 0.77875, 0.865, 0.885, 0.900 µm (http://www.envisat.esa.int/dataproducts/meris/CNTR.htm). Out of 16 MERIS acquisitions the most cloud free (12 July and 6 August 2003) were used for the burnt scar analysis. The images were geocorrected and reprojected into albers conical equal-area projection. MERIS colour images of different band combinations (Red: band 6, 0.6196 µm; Green: band 10, 0.7535 µm; Blue: band 1, 0.4125 µm; Red: band 6, 0.6196 µm; Green: band 5, 0.560 µm; Blue: band 2, 0.4425 µm) were digitally enhanced and imported into GIS for visual on-screen image interpretation of fire scars.

The ASTER instrument has 14 bands consisting of three subsystems: 1.) VNIR (visible and near infrared - 0.55 to 0.80µm) with 15-m resolution, 2.) SWIR (short wave infrared - 1.65 to 2.4 µm) with 30-m resolution and 3.) TIR (thermal infrared - 8.3 to 11.32 µm) with 90-m resolution. 7 ASTER scenes acquired on 13 July 2003 were geocorrected, reprojected and coregistered and imported into GIS for visual on-screen image interpretation of fire scars using band combination Red: band 3, 0.81 µm; Green: band 2, 0.66µm; Blue: band 1, 0.56 µm (The ASTER reflectance retrieving is described in **Appendix 2**). Old fire scars could be discriminated from recent fire scars by their spectral properties and Landsat ETM quick looks and were excluded from the analysis.

24 sample sites (11 for ASTER / MERIS and 13 for MERIS / MODIS-AVHRR) were selected according to 1.) whether recent and pre-2003 fire scars were distinguishable, and 2.) both MERIS and ASTER were cloud-free. The area of the MODIS hotspots and AVHRR were calculated within the respective MERIS fire scar polygon by assuming that a pixel covers the area of 1 km^2. The data were analyzed using a linear regression function.

Land cover data

The GLC2000 map (http://www.gvm.sai.jrc.it/glc2000/), the MODIS Vegetation Continuous Field map (http://modis.umiacs.umd.edu/) and the International Institute for Advanced Systems Analysis (IIASA) Russia wetland and vegetation spatial databases (http://www.iiasa.ac.at) were reprojected into Albers conical equal-area projection. Vegetation Continuous Field is a global data set which indicates biomass types, i.e. the proportion of woody vegetation, herbaceous vegetation and bare ground. A qualitative comparison of the MODIS Vegetation Continuous Field biomass map with the GLC2000 land cover map showed a good agreement between the total area and spatial distribution of high biomass and forests, and agreed also well with forested areas in ASTER and MERIS images. Both the MODIS hotspots composite and AVHRR fire product of 2003 were respectively used as masks to extract the burnt land cover types from the GLC2000 map, MODIS Vegetation Continuous Field map and IIASA datasets.

Ground and aerial surveys

Personal interviews with officials and statistical data collected by ground and aerial surveys, the official statistics of the Ministry for Natural Resources of the Russian Federation and the Aerial Forest Fire Protection Service *Avialesookhrana* were evaluated for the regions Irkutsk, Chita, Buryatia and Amur. Financial constraints for aerial fire assessments and political obstacles resulted in a severe underestimation of the area burned by Russian official sources. A validation mission was conducted by the Global Fire Monitoring Center in September 2003 flying two transects in Chita and Buryatia with an Antonov II (An-2) airplane and several ground surveys.

4.4-3. Results

128,546 spatially distinct hotspots were recorded by the MODIS instrument between 14 March and 8 August 2003 in the studied area, of which 2167 hotspots were of low-confidence, 57,539 of nominal-confidence and 68,840 of high-confidence (**Fig. 4.4-1)**. In the same region 157,554 pixels were identified as burnt by the NOAA AVHRR fire detection algorithm.

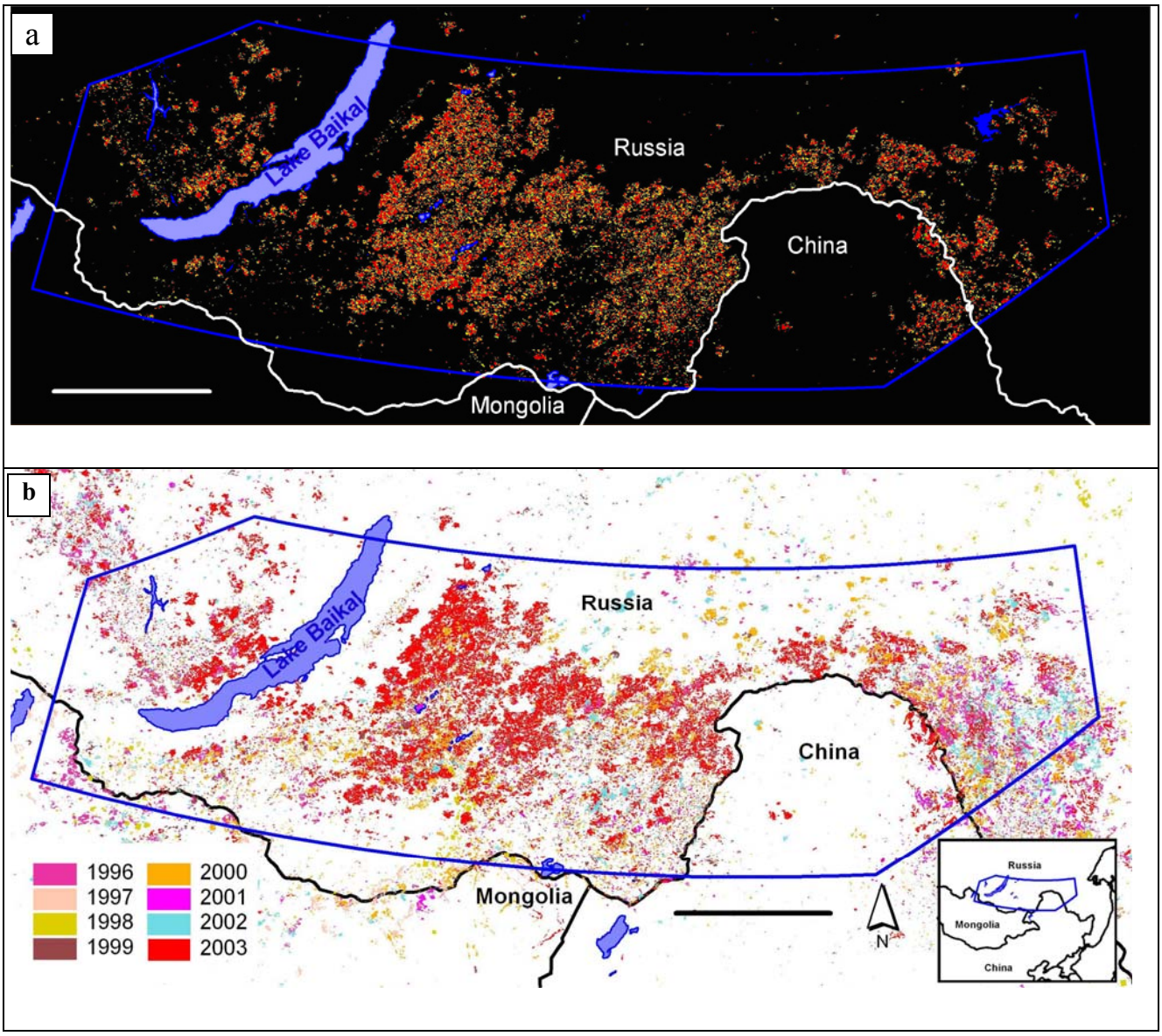

Fig. 4.4-1. Spatial distribution of MODIS hotspots recorded between 14 March and 8 August 2003 (a) and time series of NOAA AVHRR fire acquired between 1996 and 2002 (b). In Fig. 4.4-1a, Red: high-confidence fire, Yellow: nominal-confidence, Green: low- confidence. The blue outline indicates the area of investigation. Bar: 300 km.

Persistent cloud cover and orbit parameters did not allow observation of large areas with high resolution imagery shortly after the fires. Therefore a combination of high, medium and low resolution satellite imagery in which MODIS was used to record daily fire occurrence over large areas, while multispectral MERIS and ASTER imagery were used to determine the burnt area in cloud-free subsets of the studied area. Then the detailed results were extrapolated on burnt areas obtained from ASTER and MERIS to the full range covered by MODIS hotspot data.

In a first step fire scars in cloud-free sections of high resolution ASTER imagery were determined. Burnt areas were clearly identifiable and were visually delineated. Most burn scars were

large in size (average 66 km^2) and showed severe fire damage (**Fig. 4.4-2a**). Next the same burn scars in cloud-free sections in medium resolution MERIS imagery were identified. Also in MERIS imagery fire scars were clearly identifiable in bands R6G10B1 combination (**Fig. 4.4-2b**).

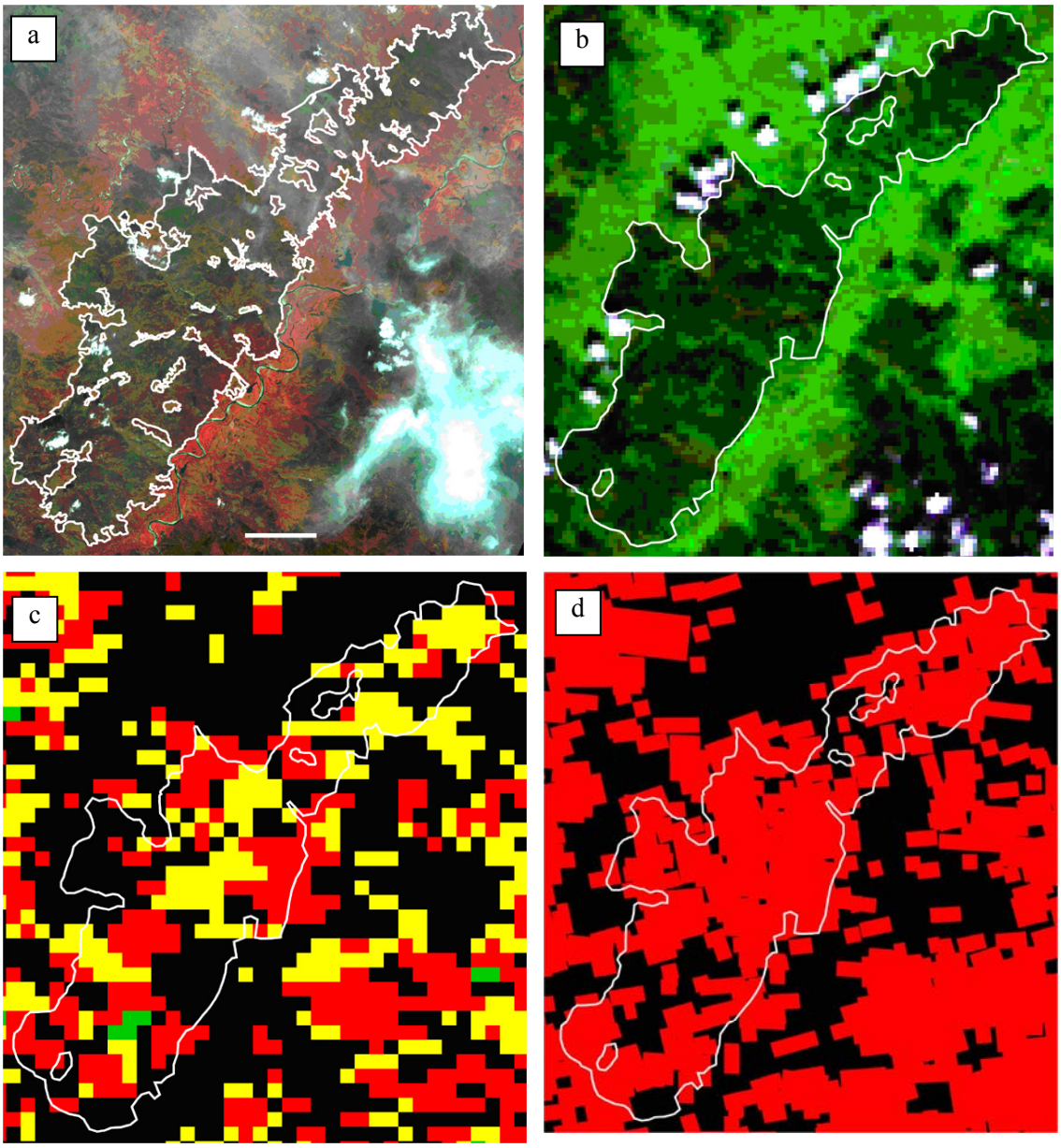

Fig. 4.4-2. Comparison of a fire scar as detected by (a) ASTER acquired 12 July 2003, RGB 6,10,1), (b) MERIS acquired 13 July 2003, RGB 3,2,1, (c) MODIS hotspots composite acquired between 14 March 2003 and 11 July 2003, and (d) AVHRR fire product of 2003. Bar: 5 km.

Then it was investigated whether there is a correlation between the burnt area visible in high resolution ASTER imagery and medium resolution MERIS imagery in order to be able to extend the area of investigation to the larger extent covered by MERIS. Fire scars detected by MERIS showed less spatial detail than the ASTER images and small fragments of unburnt forest were not visible (**Fig. 4.4-2a,b**). In a second step it was investigated if there is a correlation between the burnt area detected

by MERIS and covered by MODIS hotspots as well as NOAA AVHRR **(Fig. 4.4-2b, c, d, Fig. 4.4-3**). 11 fire scars of variable size visible in both ASTER and MERIS images and 13 fire scars visible in MERIS images and covered by MODIS hotspots as well as AVHRR fire were chosen to compare the burnt area detected by each instrument and to determine the respective errors.

There was a clear congruence between the four sensors. The regression curve for fire scars determined in ASTER and MERIS images showed a strong linear correlation (**Fig. 4.4-4a**), however, the burnt area detected by MERIS is slightly shifted from that detected by ASTER (approx 3%). This can be explained by the reduced spatial resolution of the MERIS sensor. The regression curve for MERIS and MODIS as well as for MERIS and NOAA AVHRR also showed strong linear regression (**Fig. 4.4-4b**). However, the burnt area was significantly underestimated by MODIS (approx 38%) and by AVHRR (approx 20%). This can be attributed to limitations of active fire detection by satellite such as frequent cloud cover typical for this region, dense haze from forest and peat fires, the speed of fire spread, sensor sensitivity and response time.

Taking into account the specific errors of the MERIS and MODIS system as well as AVHRR, the actual burnt area was 1.56 times larger than that derived from MODIS hotspots and 1.21 times larger than that derived from AVHRR fire products. These two factors were then used to estimate the total area which had been burnt between 14 March to 8 August 2003 on the basis of MODIS hotspots and total area burnt in 2003 on the basis of AVHRR fire products. Within an area of 1.3 Mio km^2, 202,000 km^2 had been burnt based on MODIS hotspots and 191,000 km^2 had been burnt based on AVHRR fire product (**Table 4.4-1).** The territories in China and Mongolia accounted for only 4.15% and 0.09% of the total burnt area. This is significantly more than previously reported for whole Russia: 110,000 km^2 in 2002, 117,000 km^2 in 1998, 140,000 km^2 in 1987 (Goldammer, 2003).

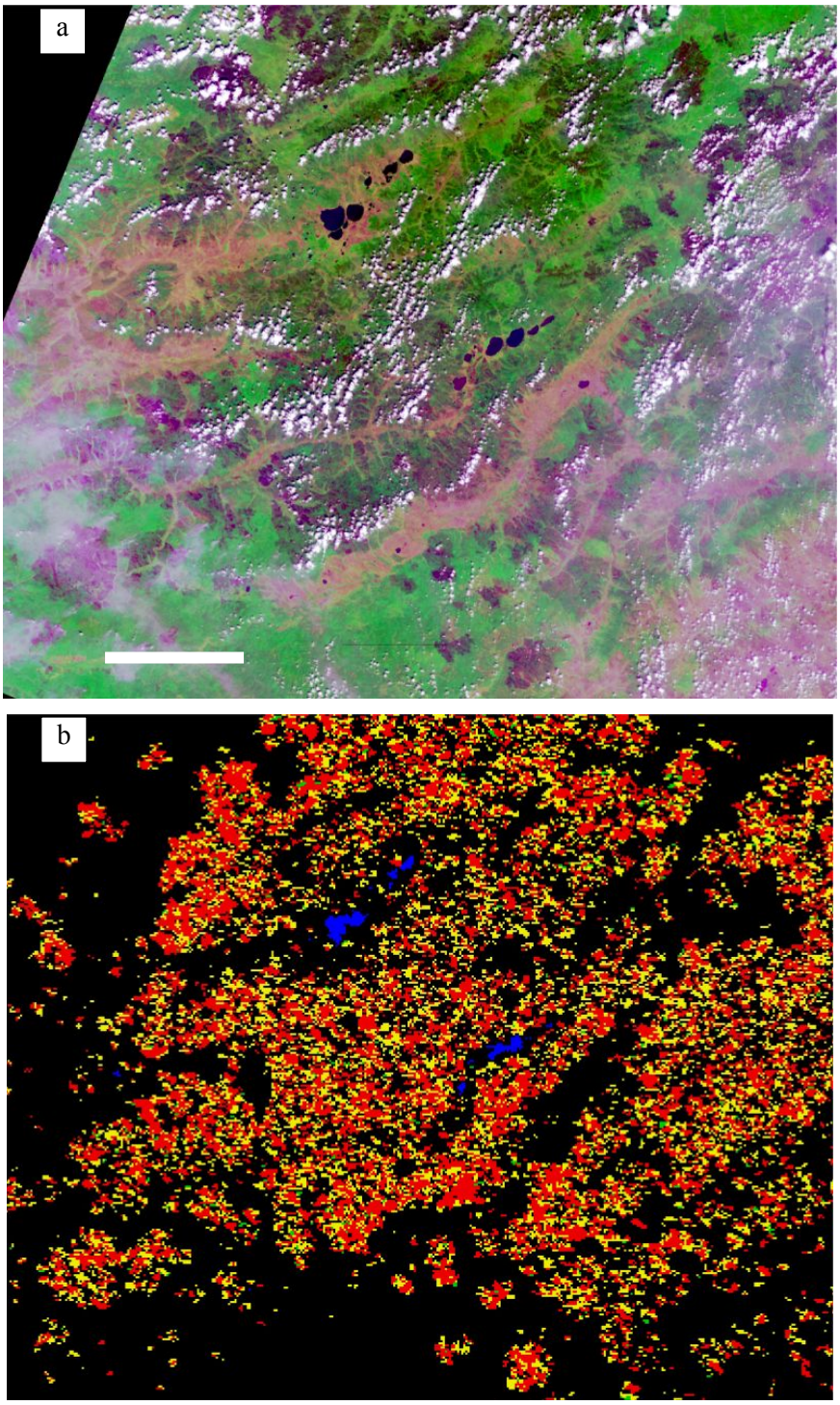

Fig. 4.4-3. Comparison of an MERIS image acquired 12 July 2003 (a) and the MODIS hotspots composite of 14 March 2003 to 11 July 2003 (b). Burnt areas and haze appear in purple colours in the MERIS RGB image (RGB 7,10,1). Bar: 50 km.

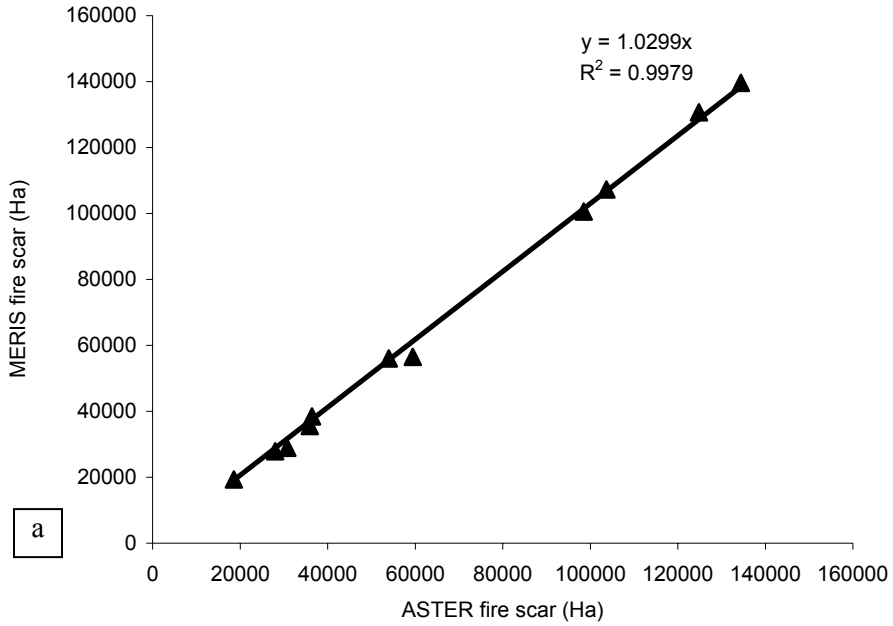

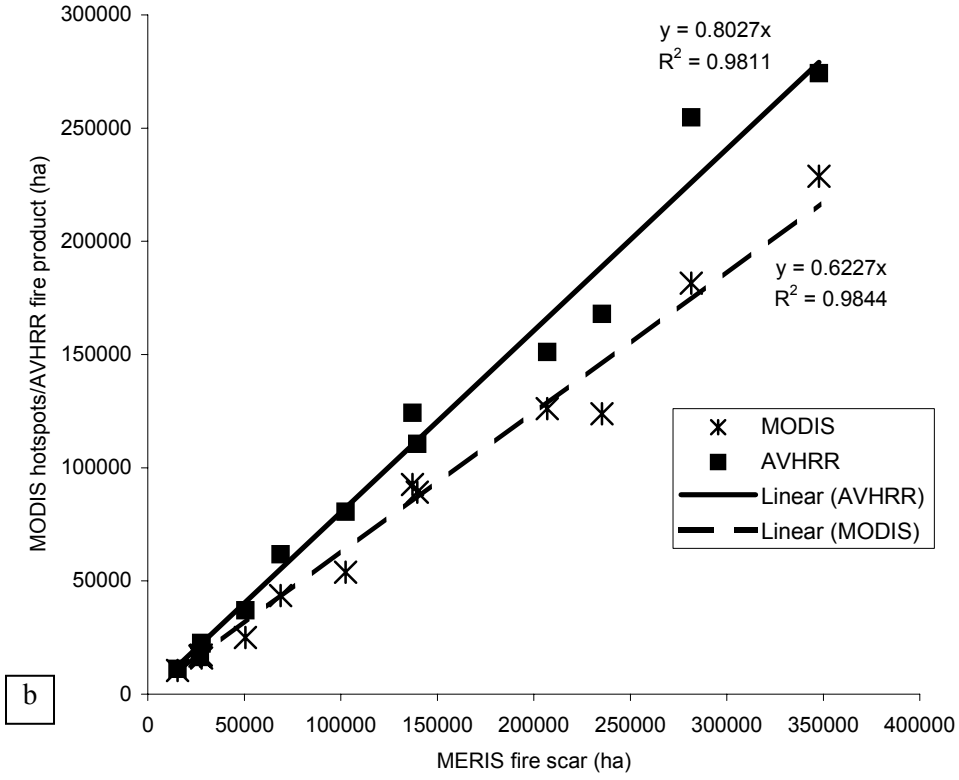

Fig. 4.4-4. Linear regression analysis for (a) MERIS and ASTER fire scars and (b) MODIS hotspots, AVHRR fire product and MERIS fire scars.

Table 4.4-1. Vegetation types affected by wildfires in the investigated region

GLC2000 land cover	MODIS hotspots 2003 (ha)[I]	MODIS hotspots 2003 (%)	AVHRR fire product2003 (ha) [II]	AVHRR fire product 2003 (%)
Evergreen Needle-leaf Forest	1,032,398	5.07	963,039	5.05
Deciduous Broadleaf Forest	1,462,296	7.38	1,202,256	6.31
Needle-leaf/Broadleaf Forest	375,228	1.86	391,435	2.05
Mixed Forest	301,958	1.43	305,041	1.60
Broadleaf/Needle-leaf Forest	929,290	4.67	942,227	4.94
Deciduous/Needle-leaf Forest	10,361,744	50.97	9,933,616	52.11
Subtotal Forests	**14,462,914**	**71.38**	**13,737,614**	**72.06**
Broadleaf deciduous shrubs	742,337	3.65	724,064	3.80
Needle-leaf evergreen shrubs	16,618	0.08	13,431	0.07
Humid grasslands	1,920,048	9.49	1,659,878	8.71
Steppe	127,185	0.64	113,135	0.59
Bogs and marshes	430,276	2.15	415,393	2.18
Subtotal Grasslands	**3,236,464**	**16.01**	**2,925,901**	**15.35**
Palsa bogs	7,176	0.04	7,260	0.04
Riparian vegetation	1,511	0.01	968	0.01
Barren tundra	0	0.00	0	0.00
Prostrate shrub tundra	5,571	0.03	3,146	0.02
Sedge tundra	2,266	0.01	2,178	0.01
Shrub tundra	29,459	0.15	25,168	0.13
Subtotal Tundra-wet	**46,013**	**0.24**	**38,720**	**0.20**
Recent burns (1996 – 1999)	367,108	1.83	326,095	1.71
Burns of year 2000	309,134	1.54	340,131	1.78
Subtotal Previously Burned	**676,242**	**3.37**	**666,226**	0.00
Croplands	759,144	3.76	694,903	3.65
Forest – Natural Vegetation complexes	82,241	0.44	85,063	0.45
Forest-Cropland complexes	121,048	0.64	117,733	0.62
Cropland-Grassland complexes	762,260	3.78	675,059	3.54
Subtotal Croplands	**1,724,693**	**8.62**	**1,572,758**	**11.74**
Others	80,730	0.38	122,815	0.64
Sum	**20,227,024**	**100**	**19,064,034**	**100**

Note: The area result of the spatial overlay of (I: MODIS hotspots; II: AVHRR fire products) and GLC2000 land cover was adjusted by the factor of (I: 1.56; II: 1.21) determined from linear regression analysis. It is simply assumed that the (I: MODIS; II: AVHRR) underestimation error is the same for each vegetation class.

To determine the significance of this fire event for the ecosystem and to estimate carbon-release, it was investigated which vegetation types had been affected by comparing the burnt area with the GLC2000 vegetation map. The intersection of all MODIS hotspots with this up-to-date vegetation map showed that 71.4% of the burnt area was forest, 9.5% were humid grassland and 2.15% bogs/marshes (**Table 4.4-1)**. The intersection of the burnt area with IIASA wetland layer showed that 71% of the burnt wetlands were peatlands, which represent a vast store of global carbon (Gorham, 1991) and can release significant amounts of carbon into the atmosphere if burnt (Bannikov, 2003). The MODIS Vegetation Continuous Field biomass map was used as another source to determine how much forest biomass had been burnt: 74.4% of the burnt area was covered by woody vegetation (tree cover more than 30%) which is slightly more than the forest area from the GLC2000 map (71.38%) and slightly less than the forest/woodland area from the IIASA vegetation map (77.6%).

For a better understanding of the fire regime, how much of the burnt area had been affected by fire in the years 1996-2002 was also investigated based on the available NOAA AVHRR data. Recurrent fires disturb forest regeneration, make forests more susceptible to fire and previous fire damage has to be considered in the calculation of carbon release. The burnt area detected by AVHRR hotspots varied greatly each year (**Table 4.4-2**). The total area burnt in 2003 (202,000 km^2 detected by MODIS and 191,000 km^2 detected by AVHRR) was significantly larger than the total area burnt in the same region from 1996-2002 (133,370 km^2).

Table 4.4-2. Burnt area detected by NOAA AVHRR between 1996-2002 and reburnt area in 2003

Year	AVHRR-hotspots area (km^2)	Reburnt area in 2003 (km^2)-MODIS [II]	Reburnt area in 2003 (km^2)-AVHRR [III]
1996	21,770	2,881	3,984
1997	3,201	406	491
1998	8,065	1,597	1,870
1999	15,699	2,536	3,079
2000	44,692	7,301	8,979
2001	9,997	1,319	1,582
2002	29,946	3,421	4,434
1996-2002			
Sum	133,370	19,461	24,419
Composited [I]	121,395	17,853	22,319

[I] Successive detected pixels in one location were counted only once

[II] AVHRR hotspots of each year were spatially overlaid with the MODIS hotspots of 2003

[III] AVHRR hotspots of each year were spatially overlaid with the AVHRR fire product of 2003

The comparison of the MODIS hotspot and AVHRR fire product of 2003 with the AVHRR hotspots of 1996-2002 showed that respectively 13.9% and 16.7% of the area had been affected by fire at least twice. 77.8 % of the reburnt area were forest/woodland, 11.7% grasslands and 11.4 % wetlands, of which 70.8% were peatlands.

The sum of all AVHRR hotspots acquired between 1996-2003 and all MODIS hotspots of 2003 showed that all together 303,731 km^2 have been burnt in the studied area. The intersection with the IIASA vegetation layer (vegetation status of 1995 and before) showed that 32.2 % of the forested area (720,779 km^2) has been burnt in the past eight years.

4.4-4. Discussion

Accurate estimates of the burnt area, fire impact on the vegetation, and carbon release are very important to assess the influence of fire on the ecosystem and global climate change. Due to the good geocorrection accuracy, the distribution of MODIS hotspots indicates the burnt location quite accurately and the daily availability allows detailed studies on fire dynamics and fire spread. However, MODIS hotspots are of limited use to assess burnt areas due to its coarse resolution of 1 km. Here it is shown that in combination with the medium resolution MERIS instrument on ENVISAT and the high resolution ASTER instrument on TERRA, it was possible to significantly improve the accuracy of burnt area assessments over extremely large territories. The inter-sensor correlation of low, medium, and high resolution satellite imagery was a straightforward, quick and efficient method to assess burnt areas on regional or even global scale. The intersection of the burnt area determined by MODIS hotspots and AVHRR fire polygons with pre-fire land cover data provided information on the type of vegetation which has been affected by fire. This in turn allowed us to approximately estimate the carbon released by this fire event, which was documented by another scientist in cooperation.

In 2003 nearly 15 x 10^6 ha of forested land have been burnt and in addition more than 2 x 10^6 ha of humid grasslands and bog sand marshes. Wildfires occur in this region in short intervals in forests and grasslands that are fairly well adapted to low- to medium-intensity surface fires. However, the analysis of MODIS hotspots and the NOAA AVHRR time series from 1996 to 2003 showed that a significant percentage of the land area has been affected by recurrent fires and 32.2 % of the forested area has been burnt in recent years. Cahoon *et al.* (1994) documented that 140,000 km^2 burned in Southeastern Siberia during the extended drought of 1987. A qualitative comparison with the NOAA-AVHRR-derived fire scar map of 1987 shows a strong overlap of burnt areas.

The inter-comparison of the areas burned in 2003 reveals that both MODIS and AVHRR underestimates the burnt area about 38% and 20% respectively, but the adjusted areas differ only approximately 6%. Since MODIS hotspots are provided free of charge via internet almost in real time,

it is more feasible to use MODIS to monitor the Southern Siberian wildland fire and assess the impact in a straightforward, quick and efficient way.

Recently released observations of atmospheric carbon dioxide concentrations at Mauna Loa indicate a dramatic and unexpected increase in carbon dioxide levels between 2002 and 2003 by 2.54 ppm (ABC, 2004; BBC 2004). A particularly significant Δ CO_2 of 3.4 ppm between August 2002 and August 2003 has been recorded. The increase in CO_2 was not uniform across the globe. Since the most recent increases were recorded in the absence of El Nino it has been speculated recently that the Northern Hemisphere hot summer of 2003 involving a larger than usual number of forest fires could have killed off vegetation and increased soil carbon release (BBC, 2004). Our study shows an exceptional large fire damage in Southern Siberia in 2003 which supports these findings and conjectures.

The region that is being studied is one where the albedo effects of forest clearing and regeneration may have a greater global effect than the carbon storage/release effects (Bonan *et al.*, 1992; Betts, 2000), and there was quantitative evidence of how wildfire history influences ecosystem carbon input, output, and sequestration in the boreal forest and the underlying soils (Wardle *et al.*, 2003). Furthermore, it is becoming more evident that peatlands in boreal Russia are of special importance in the context of climate change, because extensive data from Russia's Siberian lowland show peatlands are larger carbon stores than previously thought (Smith *et al.*, 2004). The haze plume which extended more than 4000 km for days suggests that substantial amounts of peat might have been burnt and an amount of carbon might be released as those Western Canadian spring-time fires burnt in peatland (Turetsky and Wieder, 2001; Turetsky *et al.*, 2002).

At least four factors are responsible for this exceptional fire event as observed by the Global Fire Monitoring Center: 1.) an extraordinary drought from August 2002 to May 2003 which was even more extreme than the last drought preceding the 1987 fire year in the Transbaikal Region. 2.) decreased fire management capabilities due to insufficient budgets for operation of the Aerial Forest Fire Protection Service *Avialesookhrana*. 3.) the depletion of China's forest resources and the increasing demand for timber products prompt the Chinese timber dealers to encourage local people to set arson fires to forest in order to increase the permissible salvage logging areas. Very few fires were recorded in China (**Fig. 4.4-1**). In addition, extensive illegal logging and timber export have been observed during two on-site inspection missions by the Global Fire Monitoring Center in Mongolia and the Russian Federation in August-September 2003. 4.) large-scale clearcuts from the 1990s have resulted in large areas dominated by pure grass stands. These lands are maintained by regular fires – a phenomenon that has been observed on a large scale in Mongolia and China

The repeated occurrence of severe fires in 1987 and during the investigated period from 1996 to 2003 affecting the same areas will lead to a gradual degradation of the otherwise fire-adapted pine-grass forest ecosystem. Ground and aerial reconnaissance conducted at the end of the 2003 fire season and an additional follow-up field survey in November 2004 revealed a high proportion of high-severity stand-replacement fires in 2003, which in combination with recurrent fires in short intervals and increased post-fire mortality due to combined fire and drought stress, and regional climate variability associated with extreme droughts such as in 2002-2003 are likely to result in the conversion of the forest ecosystem into grasslands and steppe. The analysis based on advanced remote sensing has shown that the area burned in the 2003 fire outbreak is one order of magnitude larger than that reported in official statistics. The increasing human pressure on Siberia's forest resources, coupled with recurrent fire and climate change, i.e. increasing occurrence of summer droughts, will reduce the carbon sequestration potential of this region.

4.4-5. Acknowledgements

Thanks to ESA-ESRIN for financial support and quick data provision, Don Cahoon for providing data for the comparative assessment of the 1987 fires, Chris Schmullius of University of Jena for providing forest cover maps, and the Max Planck Institute for Chemistry/Global Fire Monitoring Center for funding aerial and ground surveys in the Transbaikal region.

4.4-6. References

ABC (2004). Global warming fears heightened by carbon dioxide increase, 12 October, 2004, available at http://www.abc.net.au/am/content/2004/s1218111.htm

BBC (2004). Sharp CO_2 rise divides opinions, 11 October, 2004, available at http://news.bbc.co.uk/2/hi/science/nature/3732274.stm

Ahern, F., Goldammer, J. G. & Justice, C.O. (2001). *Global and Regional Vegetation Fire Monitoring from Space: Planning a Coordinated International Effort.* SPB Academic Publishing bv, Hague.

Andreae, M. O. & Merlet, P. (2001). Emission of trace gases and aerosols from biomass burning, *Global Biogeochemical Cycles, 15,* 955-966.

Bannikov, M. V., Umarova, A.B. & Butylkina, M.A. (2003). Fires on drained peat soils of Russia: causes and effects, *International Forest Fire News, 28,* 29-32.

Bartalev, S. A., Belward, A. S., Erchov, D. V. & Isaev, A. S. (2003). A new SPOT4-VEGETATION derived land cover map of Northern Eurasia, *International Journal of Remote Sensing, 24,* 1977–1982.Betts, R.A. (2000). Offset of the potential carbon sink from boreal forestation by decreases in surface albedo, *Nature, 408,* 187-190.

Bonan, G.B., Pollard, D. & Thompson, S. L.(1992). Effects of boreal forest vegetation on global climate, *Nature, 359*, 716-718.

Cahoon, D. R., Stocks, B. J., Levine, J. S., Cofer, W. R. & Chung, C. C. (1992). Evaluation of a technique for satellite-derived area estimation of forest fires, *Journal of Geophysical Research, 97,* 3805-3814.

Cahoon, D. R., Stocks, B. J., Levine, J. S., Cofer, W. R. & Pierson, J. M. (1994). Satellite analysis of the severe 1987 forest fires in northern China and southeastern Siberia, *Journal of Geophysical Research, 99(D9),* 18,627-18,638.

Conard, S.G., Sukhinin, A.I., Stocks, B.J., Cahoon, D.R., Davidenko, E.P. & Ivanova, G.A. (2002). Determining effects of area burnt and fire severity on carbon cycling and emissions in Siberia, *Climatic Change 55,* 197-211.

Dixon, R. K., Brown, S., Houghton, R. A., Solomon, A. M., Trexler, M. C. & Wisniewski, J. (1994). Carbon pools and flux of global forest ecosystems. *Science, 263,* 185-190.

Goldammer J. G. (2003). Wildland fire season 2002 in the Russian Federation: an assessment by the Global Fire Monitoring Center (GFMC), *International Forest Fire News (IFFN),28,* 2-14.

Goldammer, J. G. & Furyaev, V. V. (1996). *Fire in Ecosystems of Boreal Eurasia*. Dordrecht: Kluwer Academic Publishers.

Goldammer, J. G. & Stocks, B. J. (2000). Eurasian perspective of fire: dimension, management, policies, and scientific requirements. In Kasischke, E. S. & Stocks, B. J. (Eds.) *Fire, Climate Change, and Carbon Cycling in the Boreal Forest*, pp. 49-65. Springer-Verlag, Berlin-Heidelberg-New York.

Goldammer, J. G., Sukhinin, A. & Csiszar, I. (2003). The current fire situation in the Russian Federation: implications for enhancing international and regional cooperation in the UN framework and the global programs on fire monitoring and assessment. *http://www.fire.uni-freiburg.de/GlobalNetworks/BalticRegion/Russia%20Wildland%20Fires%202003%20GFMC%20Analysis.pdf.*

Gorham, E. (1991). Northern peatlands: role in the carbon cycle and probable responses to climatic warming, *Ecological Application. 1,* 182–195.

Hansen, M. C., DeFries, R. S., Townshend, J.R.G., Carroll, M., Dimiceli, C. & Sohlberg, R.A. (2003). Global percent tree cover at a spatial resolution of 500 meters: first results of the MODIS vegetation continuous fields algorithm, *Earth Interactions 7,* 1-10.

Justice, C.O, Giglio, L., Korontzi, S., Owens, J., Morisette, J.T., Roy, D., Descloitres, J., Alleaume, S., Petitcolin, F. & Kaufman, Y. (2002). The MODIS fire products, *Remote Sensing of Environment 83,* 244-262.

Kajii Y., Kato S., Streets, D. G., Tsai N. Y., Shvidenko A., Nilsson S., Minko,M. P., Abushenko N., Altyntsev D. & Khodzer T. V. (2002). Boreal forest fires in Siberia in 1998: estimation of area and emissions of pollutants by AVHRR satellite data, *Journal of Geophysical Research, 107(D24),* 4745, doi:10.1029/2001JD001078.

Kasischke, E. S. & Bruhwiler, L. P. (2003). Emissions of carbon dioxide, carbon monoxide, and methane from boreal forest fires in 1998,*Journal of Geophysical Researc*h,107(D1), 8146, doi:10.1029/2001JD000461.

Kasischke, E. S., & French, N. H. F. (1995). Locating and estimating the areal extent of wildfires in Alaskan boreal forests using multiple-season AVHRR NDVI composite data, *emote Sensing Environment 51,* 263-275.

Kasischke, E. S. & Stocks, B. J. (2000). *Fire, Climate Change and Carbon Cycling in the Boreal Forest.* New York: Springer-Verlag.

Kaufman, Y.J., Justice, C.O., Flynn, L.P., Kendall, J.D., Prins, E.M., Giglio, L., Ward, D.E., Menzel, W.P. & Setzer, A. W. (1998). Potential global fire monitoring from EOS-MODIS,*Journal of Geophysical Research, 103,* 32,215-32,238.

Page S.E., Siegert F., Rieley J.O., Boehm H-D.V. & Jaya A. (2002). Carbon released during peatland fires in Central Kalimantan, Indonesia in 1997,*Nature, 420,* 61-65

Shvidenko, A. Z. & Nilsson, S. (2000). Fire and the Carbon Budget of Russian Forests. In Kasischke, E. & Stocks, B. (Eds.), *Ecological Studies 138 - Fire, Climate Change and Carbon Cycling in the Boreal Forests,* pp. 289–311. New York: Springer- Verlag.

Simon, M. (2002). *GLOBSCAR Products Qualification Report.* ESA-ESRIN, Frascati, Italy.

Smith, L.C., MacDonald, G.M., Velichko, A.A., Beilman, D.W., Borisova, O.K., Frey, K.E., Kremenetski, K.V. & Sheng, Y. (2004). Siberian peatlands a net carbon sink and global methane source since the early Holocene, *Science, 303*, 353-356.

Soja, A.J., Cofer III, W.R., Shugart, H.H., Sukhinin, A.I., Stackhouse, P.R., McRae, D.J. & Conard, S.G. (2004a). Estimating fire emissions and disparities in boreal Siberia (1998 through 2002), *Journal of Geophysical Research,* in press.

Soja, A. J., Sukhinin, A. I., Cahoon, D. R., Shugart, H. H. & Stackhouse P.W. (2004b). AVHRR-derived fire frequency, distribution and area burned in Siberia, *International Journal of Remote Sensing,25,* 1939-1960

Sukhinin, A. I. (2003). The 2002 fire season in the Asian part of the Russian Federation: a view from space. *International Forest Fire News (IFFN) 28,* 18-28.

Sukhinin, A. I., French, N.H.F., Kasischke, E.S., Hewson, J. H., Soja, A. J., Csiszar, I. A., Hyer, E. J., Loboda, T., Conard, S. G., Romasko, V. I., Pavlichenko, E. A., Miskiv, S. I. & Slinkina, O. A. (2004). Satellite-based mapping of fires in Russia: new Products for fire management and carbon cycle studies, *Remote Sensing of Environment, 93*, 546– 564.

Turetsky, M.R. & Wieder, R.K. (2001). A direct approach to quantifying organic matter lost as a result of peatland wildfire, *Aanadian Journal of Forest Research, 31(2),* 363-366.

Turetsky, M.R., Wieder, R.K. & Vitt, D.H. (2002). Boreal peatland C fluxes under varying permafrost regimes, S*oil Biology & Biochemistr,34 (7)*, 907-912.

Van der Werf, G. R., Randerson, J. T., Collatz, G, J., Giglio, L., Kasibhatla, P. S., Arellano A. F., Olsen, S. C. & Kasischke, E. S. (2004). Continental-scale partitioning of fire emissions during the 1997 to 2001 El Nino/La Niña period. *Science, 303,* 73-76.

Wardle D.A., Hornberg, G., Zackrisson, O., Kalela-Brundin, M. & Coomes, D.A. (2003). Long-term effects of wildfire on ecosystem properties across an island area gradient, *Science, 300*, 972-975.

CHAPTER 5---SUMMARY AND DISCUSSION

Currently plenty of satellite data from hundreds of sensors (approximately 320) can be used. It may seem to be more than the demand from the Earth observing community. But actually none of the satellites will provide all of the data characteristics needed by the broad range of user requirements. The reasons of the need for satellite multi-sensor are due to the negative effects of the cloud cover, and the requirement of different ground resolution, different spectral region, different swath width, and different repeat period by the user. The shortcomings of one single sensor in these aspects can be compensated by multiple sensor combination.

The advantage of the multi-sensor satellite remote sensing lies in the combination of specific temporal, spatial and spectral characteristics of different satellite systems: In temporal dimension, environment change phenomenon continuously develops, and the users concern on different monitoring periods such as monthly or annual update, however, a satellite image is only a 'snapshot' of the Earth at a given time point; In the spatial dimension, users concern on diverse scale (global, regional, local) monitoring, however, high ground resolution data are too expensive over large area while low ground resolution data are not accurate enough; In spectral dimension (wavelengths), the same environment objects on the Earth's surface can be detected by both optical and radar sensor, however, they look quite different because the scattering or reflection mechanisms of electromagnetic waves are quite dependent upon wavelength. These three temporal, spatial and spectral characteristics make multi-sensor satellite data more useful than single sensor in environmental monitoring because multi-sensor data improve the monitoring capability in temporal, spatial and spectral dimensions. Taking the Siberia Fire as an example, the optical sensor of MODIS underestimated the burnt area because of coarse resolution of 1 km, sensitivity and response time, cloud coverage and the satellite overpass frequency, while MERIS and ASTER are more accurate because of their higher ground resolutions. However these optical sensors can not penetrate the cloud and smoke whilst microwave sensor of ASAR is able to do this. Taking these multi-sensor covering different spectral wavelengths with various ground resolution and diverse revisit time, it is more accurate to analyze the fire phenomenon in Siberia.

In multi-sensor satellite data for environmental monitoring, there are different kinds of data fusion techniques: 1.) Different ground resolution images are fused. For example, using the higher resolution PAN band to improve the resolution of other spectral bands; combining coarse resolution and fine resolution data in a multi-scale monitoring system. 2.) Multitemporal images are fused. For example, using images acquired in different periods to monitor the land cover change, to monitor the vegetation dynamics, or detect the fire spread etc. 3.) Images acquired in different spectral region are fused. For example, combining the visible and thermal bands to identify the fire hotspots; selecting

suitable bands to create best colorful images for identifying the expected target; retrieving important information from hyperspectral images; fusing optical images and radar images to improve the interpretation. 4.) Data with different file formats are fused. Besides remote sensing data in raster format, other data such as GIS layer in vector format, GPS signal in database format, text description in ASCII format, video sequence in animation format, or atlas in analog map are needed to help interpretation. How to combine these data with different formats to get the accurate result is important.

This thesis demonstrates different types of multi-sensor data applications in environmental monitoring. In **chapter 2** (land cover assessment in Salonga national park), Landsat 15 m Pan band and other 30 m spectral bands were combined to improve the spatial resolution; remote sensing raster data, GPS signal database, digital photos and continuous video sequence were fused to map and validate the land cover. The technique shown in this study demonstrated that the land cover and vegetation could be accurately assessed in a region which is unknown by people or inaccessible on ground if the satellite images, global position system and aero-video are well harmonized. This is important to such developing countries where baseline data are absent and war breaks out often. The results of this study show 98.5% of the national park itself was covered by undisturbed, pristine evergreen lowland and swamp forests. No logging or mining activities were detected. However, many human-related land covers were found around the park and this indicates that the Salonga national park is currently under the threat from human beings. According to the talk with the local staff, the derived maps are the first high-resolution land cover and land use products since the national park was established.

In **chapter 3** (desertification monitoring in North China), time series coarse resolution images were composited to monitor the temporal vegetation dynamics at large scale, while high resolution infrequent images and ground survey were used for validation. In processing multitemporal images, the cloud influence was eliminated using the Bidirectional Reflectance Distribution Function (BRDF) model, and the time series vegetation indices were improved by the Harmonic Analysis of NDVI Time Series (HANTS) algorithm. This multitemporal data fusion technique is useful in long-term environmental monitoring. The author used a full year of 2000 time series of SPOT VEGETATION images with 1 km spatial resolution to produce a land cover map with special emphasis on the detection of sparse vegetation as indicator for identifying areas at risk of desertification. The identified ‘hotspots’ can then be analyzed by higher resolution images. This technique demonstrates a framework of combining the low-cost coarse resolution images covering large area with high-cost fine resolution images covering sample plots. This combination would decrease the investment which is important in developing countries. The results presented show that within a satellite based multi-scale monitoring system SPOT VEGETATION imagery can be very useful to detect large scale dynamic environmental changes and desertification process. This helps establish a multi-scale environmental

monitoring system. To the author's knowledge, this research is very new in operational application of SPOT VEGETATION to desertification monitoring in China after the multi-scale monitoring system was proposed.

In **chapter 4** (fire monitoring and impact assessment), multi-sensor satellite data with different spectral region (optical and radar, visible and thermal), different ground resolution (15 m, 25 m, 150 m, 300 m, 1000 m) were demonstrated to derive the burnt area at large scale.

In **chapter 4.1**, a time series of ASAR wide swath images for investigating the temporal variation of fire scars' backscatter were analyzed. Multitemporal comparison was used to monitor fire-induced backscatter changes before and after a fire event. The backscatter changes of fire scars formed in different years were compared. The results show that ASAR WSM on ENVISAT is useful for operational burnt area mapping and monitoring in the boreal forests of Siberia. Until recently application of this technique in Russian boreal forests has not been done very often, and use of ENVISAT is also new and enlightening.

In **chapter 4.2**, the applicability of ENVISAT MERIS for fire scar mapping in Siberian forest ecosystems was investigated. The results show that MERIS is a promising instrument for fire scar mapping, which supplements current fire monitoring systems based on the AVHRR and MODIS instruments. Although the fact presented in this section that the NIR reflectance decrease almost half after fire event is well known based on similar analyses of other sensors, the MERIS analysis is still useful since there is little information available in literature about MERIS image.

In **chapter 4.3**, the first results on the performance of the ENVISAT satellite to detect wildland fires are presented. Three ENVISAT instruments were used to investigate the extent and impact of the forest and peatland fires in Indonesia. The results show that the capability of ENVISAT to acquire data from different sensors simultaneously or within a short period of time significantly enhances the possibilities to monitor fire occurrence and assess fire impact. To the author's knowledge, this is the first publication reported for ENVISAT multi-sensor potential in wildland fire detection.

In **chapter 4.4**, based on multiresolution satellite imagery (a combination of the TERRA ASTER, ENVISAT MERIS and TERRA MODIS instruments), the burnt area was rapidly assessed in very detail over a large area with the support of aerial and ground field surveys. The techniques demonstrated in this study show the inter-sensor correlation of low, medium, and high resolution satellite imagery is a straightforward, quick and an efficient method to assess burnt areas on regional or even global scale. The fire disaster of 2003 in Eastern-Siberia happened almost unnoticed from the

public. There is an unexpected increase in carbon dioxide levels between 2002 and 2003 by 2.54 ppm, especially a particular significant Δ CO2 of 3.4 ppm increase between August 2002 and August 2003, but the reason is not clear (ABC, 2004; BBC 2004). Some scientists are speculating that something unusual happened in Northern Hemisphere and fire might be a reason. This study shows an exceptional large fire damage in Southern Siberia in 2003 which supports these findings and conjectures. The main point is that recurrent wildland fires in Siberia threaten the largest extent of boreal forest worldwide and its carbon sequestration potential. It highlights the importance of the boreal ecosystem in Russia as carbon store and indicates the sensitive nature of this resource and its vulnerability to fire. The major finding is that recurrent fires in short intervals caused by increasing human pressure on Siberia's forest resources, coupled with fire and climate change will further degrade forests and thus reduce the carbon sequestration potential of this region.

It is shown from these studies that the investment of satellite data application to environmental monitoring can be decreased when multi-sensor satellite data are combined. This is very important to developing countries who have no adequate financial support for environmental monitoring.

Although the multi-sensor satellite data are advantageous because of the integrated information in spatial, temporal and spectral dimension, the indirect satellite measurements and thus uncertainties on environment phenomena as well as the undetectable environment cause are two main disadvantages in multi-sensor satellite application in environment monitoring.

The fundamental problem of remote sensing is to establish to what extent the radiation measurements made in space can in fact provide useful information and to design the tools and techniques for extracting such information. Satellite remote sensing observations are merely radiation measurements made hundreds of kilometers away from the targets of interest, and they are not direct samples of the observed phenomenon. However most users in environment monitoring are ultimately interested in some form of high level information, such as the temporal evolution of the spatial distribution of biomass burning. The dichotomy between the natures of the measured signals and of the variables of interest prompted a discussion of the feasibility of retrieving useful information on the variables of interest from the space measurements (Verstraete *et al*., 1996). The only way to ascertain exactly what information can be retrieved for environment monitoring from the satellite measurement (and therefore to determine the range of applicability of remote sensing) is to understand the physical processes that control or affect the emission of radiation at the source, its transfer within the relevant media, and its absorption in the detector (Verstraete *et al*., 1996). That is to say, when we use satellite technology to monitor the environment, we need to understand theoretically how the instrument is making the measurements and the possible sources of the measurement uncertainties, and the satellite measurements must be calibrated against reality to retrieve the useful information. However this

calibration is never exact and measurement uncertainty can be large, which make data interpretation sometimes difficult. Lack of personnel skilled in these technologies in remote sensing data were noted as one of the common barriers for adoption of satellite technology, especially in developing countries /regions (Kalluri *et al*., 2003). For one example in the fire monitoring case, we need to know the theory of wildland fire detection from space described by Cahoon *et al*. (2000) as well as the sensor's characteristics, and then the optimised algorithm for the corresponding sensor can subsequently be designed.

Another disadvantage of satellite is that satellite image can detect the environment change, but the cause of environment is difficult to detect from the space. Millette *et al*. (1995) showed 30 meter resolution satellite data can provide useful information associated with broad land management practices and land cover changes, but it was needed to be combined with ground truth fieldwork, and interviewing to provide an assessment of types and causes of environmental change. For one example in the desertification monitoring, we can identify the desertification risk area, but why the desertification develops on the region can only be ascertained by standard method such as ground survey and interviewing.

In spite of these two disadvantages, satellite technology are demonstrated very useful for environment monitoring in less developed countries/regions of North-China, Siberia, Africa Congo and Indonesia. The future of multi-sensor satellite application to environment monitoring in developing countries is challenging. For accurate interpretation on remote sensing images, it is important to knowing the satellite measurements and its' uncertainties (Verstraete *et al*., 1996). Further, the multi-sensor data fusion method is currently not satisfactory and still developing in the image processing communities (Pohl and Genderen, 1998; Ehlers, 1991). The lack of personnel skilled in multi-sensor satellite processing is the biggest barrier of environment monitoring in developing countries/regions, so the technology transfer from the developed countries is needed.

References

ABC (2004). Global warming fears heightened by carbon dioxide increase, 12 October, 2004, available at http://www.abc.net.au/am/content/2004/s1218111.htm

BBC (2004). Sharp CO_2 rise divides opinions, 11 October, 2004, available at http://news.bbc.co.uk/2/hi/science/nature/3732274.stm

Cahoon, D. R., Stocks, B. J., Alexander, M. E., Baum, B. A. & Goldammer, J. G. (2000). Wildland fire detection from space: theory and application. In Innes, J. L., Verstraete, M. M. & Beniston, M. (Ed.) *Biomass Burning and its Inter-Relationships with the Climate System* (pp. 151-169). Dordrecht: Kluwer Academic Publishers.

Ehlers, M. (1991). Multisensor image fusion techniques in remote sensing. *ISPRS Journal of Photogrammetry and Remote Sensing, 46(1),*19-30.

Kalluri, S., Gilruth, P. & Bergman, R. (2003). The potential of remote sensing data for decision makers at the state, local and tribal level: experiences from NASA's Synergy program. *Environmental Science & Policy, 6,* 487-500.

Millette, T. L., Tuladhar, A. R., Kasperson, R.E. & Turner, B. L. (1995). The use and limits of remote sensing for analysing environmental and social change in the Himalayan Middle Mountains of Nepal. *Global Environmental Change, 5(4),* 367-380.

Pohl C. & Genderen, J. L. (1998). Multisensor image fusion in remote sensing: concepts, methods and applications. *International. Journal of Remote Sensing, 19(5),* 823- 854.

Verstraete, M.M., Pinty, B. & Myneni, R.B. (1996). Potential and limitations of information extraction on the terrestrial biosphere from satellite remote sensing. *Remote Sensing of Environment 58,* 201-214.

APPENDIX

Appendix 1--- Some popular satellite sensors in land application

Instrument	Mission	Type	Measurements /application	Technical characteristics
AATSR Advanced Along-Track Scanning Radiometer	Envisat	Imaging multi-spectral radiometer (vis/IR)	Measurements of sea surface temperature, land surface temperature, cloud top temperature, cloud cover, aerosols, vegetation, atmospheric water vapour and liquid water content	*Waveband:* VIS-NIR: 0.555, 0.659, 0.865 μm, SWIR: 1.6 μm, MWIR: 3.7 μm, TIR: 10.85, 12 μm *Resolution:* IR ocean channels: 1 km x 1 km Visible land channels: 1 km x 1 km *Swath*: 500 km *Accuracy:* Sea surface temperature: <0.5K over 0.5 deg x 0.5 deg (lat/long) area with 80% cloud cover, Land surface temperature: 0.1K (relative)
ASAR Advanced Synthetic Aperture Radar	Envisat	Imaging radar	- Earth Observation - Site specific investigations - Land, sea, ice and ocean monitoring and surveillance	*Waveband:* active microwave C-Band .331 GHz *Operational Modes*: Image, Wide Swath, Wave, Alternating Polarisation, Global Monitoring *Geometrical Resolution:* Image mode: 30 m x 30 m Wide swath mode: 150 m x 150 m Global mode: 1 km x 1 km
ASTER Advanced Spaceborne Thermal Emission and Reflection Radiometer	Terra	High resolution imager	Surface and cloud imaging with high spatial resolution, stereoscopic observation of local topography, cloud heights, volcanic plumes, and generation of local surface digital elevation maps. Surface temperature and emissivity	*Waveband:* VIS&NIR: 3 bands in 0.52-0.86 μm *SWIR*: 6 bands in 1.6-2.43 μm, TIR: 5 bands in 8.125-11.65 μm *Resolution:* VNIR: 15 m, stereo: 15 m horizontally and 25 m vertical, SWIR: 30 m, TIR: 90 m *Swath:* 60km, *Accuracy:* VNIR & SWIR: 4% (absolute) TIR: 4K *Geolocation:* 7 m
ATSR-2 Along Track Scanning Radiometer - 2	ERS-2	Imaging multispectral radiometer (vis/IR)	Provides measurements of sea surface temperature, land surface temperature, cloud top temperature and cloud cover, aerosols, vegetation, atmospheric water vapour and liquid water content	*Waveband:* VIS-SWIR: 0.65, 0.85, 1.27, and 1.6 μm SWIR-TIR: 1.6, 3.7, 11 and 12 μm Microwave: 23.8, 36.5GHz (bandwidth of 400MHz) *Resolution:* IR ocean channels: 1 km x 1 km, Microwave near-nadir viewing: 20 km *Swath:* 500 km *Accuracy:* Sea surface temperature to <0.5 K over 0.5 deg x 0.5 deg (lat/long) area with 80% cloud cover Land surface temperature: 0.1 K
AVHRR/2 Advanced Very High Resolution Radiometer/2	NOAA-11, 12, 14	Imaging multi-spectral radiometer (vis/IR)	Provides measurements of land and sea surface temperature, cloud cover, snow and ice cover, soil moisture and vegetation indices. Data also used for volcanic eruption monitoring	*Waveband:* VIS: 0.58-0.68 μm, NIR: 0.725-1.1 μm, MWIR: 3.55-3.93 μm, TIR: 10.3-11.3 μm, 11.5-12.5 μm *Resolution:* 1.1 km *Swath:* 3000 km approx
AVHRR/3 Advanced Very High Resolution Radiometer/3	NOAA-15,16,M, N,N' METOP-1,2,3	Imaging multi-spectral radiometer (vis/IR)	Provides measurements of land and sea surface temperature, cloud cover, snow and ice cover, soil moisture and vegetation indices. Data also used for volcanic eruption monitoring	*Waveband:* VIS: 0.58-0.68 μm, NIR: 0.725-1.1 μm, SWIR: 1.58-1.64 μm, MWIR: 3.55-3.93μm, TIR: 10.3-11.3 μm, 11.5- 12.5 μm *Resolution:* 1.1 km *Swath:* 3000 km approx, Ensures full global coverage twice daily
ETM Enhanced Thematic Mapper	Landsat 7	High resolution imager	Measures surface radiance and emittance, land cover state and change (eg vegetation type). Used as multipurpose imagery for land applications	*Waveband* and *resolution* Band 1: 0.450 - 0.515 um Blue 30 m Band 2: 0.525 - 0.605 um Green 30 m Band 3: 0.630 - 0.690 um Red 30 m Band 4: 0.760 - 0.900 Near IR 30 m Band 5: 1.550 - 1.750 um Mid IR 30 m Band 6: 10.40 - 12.5 um Thermal 60 m Band 7: 2.080 - 2.35 um Mid IR 30 m Band 8: 0.52 - 0.92 um Pan *Swath*: 185 km
HRV High Resolution Visible Imaging	SPOT	High resolution imager		*Waveband* and *resolution* Multispectral mode 0.50 - 0.59 μm 20 m 0.61 - 0.68 μm 20 m 0.79 - 0.89 μm 20 m Panchromatic mode 0.51 - 0.73 μm 10m *Swath*: 60 km
HSRS Hot Spot Recognition Sensor	BIRD	Imaging multispectral radiometer (vis/IR)	Detection of hot spots (forest fires, volcanic activities, burning oil wells or coal seams)	*Waveband:* MWIR: 3.4-4.2 μm, TIR: 8.5-9.3 μm *Resolution:* 370 m *Swath:* 190 km

Instrument	Mission	Type	Measurements /application	Technical characteristics
Hyperion Hyperspectral Imager	NMP EO-1	Imaging multispectral radiometer (vis/IR)	Hyperspectral imaging of land surfaces	*Waveband:* TVIS-NIR: 400-1000 nm; NIR-SWIR: 900-2500 nm; 10nm spectral resolution for 220 bands *Resolution:* 30 m *Swath:* 7.5 km *Accuracy:* SNR: 10% refl target: vis 10-40, swir 10-20
MODIS Moderate-Resolution Imaging Spectro Radiometer	Terra, Aqua	Imaging multispectral radiometer (vis/IR)	Data on biological and physical processes on the the Earth surface and in the lower atmosphere, and on global dynamics. Surface temperatures of land and ocean, chlorophyll fluorescence, land cover measurements, cloud cover (day and night)	*Waveband:* VIS-TIR: 36 bands in range 0.4-14.4 μm *Resolution:* Cloud cover: 250 m (day) and 1000 m (night), Surface temperature: 1000 m *Swath:* 2330 km *Accuracy:* Long wave radiance: 100nW/m^2, Short wave radiance: 5%, Surface temperature of land: <1K, Surface temperature of ocean: <0.2K, Snow and ice cover: 10%
MERIS Medium-Resolution Imaging Spectrometer	Envisat	Imaging multi-spectral radiometer (vis/IR)	Main objective is monitoring marine biophysical and biochemical parameters. Secondary objectives are related to atmospheric properties such as cloud and water vapour and to vegetation conditions on land surfaces	*Waveband:* VIS-NIR: 15 bands selectable across range: 0.4-1.05 μm (bandwidth programmable between 0.0025 and 0.03 μm) *Resolution:* Ocean: 1040 m x 1200 m, Land & coast: 260 m x 300 m *Swath:* 1150 km, global coverage every 3 days *Accuracy:* Ocean colour bands typical S:N = 1700
SAR (RADARSAT) Synthetic Aperture Radar (CSA) C band	RADARSAT-1	Imaging radar	Provides all-weather images of ocean, ice and land surfaces. Used for monitoring of coastal zones, polar ice, sea ice, sea state, geological features, vegetation and land surface processes	*Waveband:* Microwave: C band: 5.3GHz, HH polarisation *Resolution:* Standard: 25 x28 m (4 looks), Wide beam (1/2):48-30 x 28 m/32-25 x 28 m (4 looks), Fine resolution: 11-9 x 9 m (1 look), ScanSAR (N/W): 50 x 50 m/ 100 x 100 m (2-4/4-8 looks), Extended (H/L): 22-19x28 m/ 63-28 x 28 m (4 looks) *Swath:* Standard: 100 km, Wide: 150 km Fine: 45 km, ScanSAR Narrow: 300 km ScanSAR Wide: 500 km Extended (H): 75 km Extended (L): 170km *Accuracy:* Geometric distortion: < 40m, Radiometric: 1.0 dB
SAR (RADARSAT-2) Synthetic Aperture Radar (CSA) C band	RADARSAT-2	Imaging radar	Provides all-weather images of ocean, ice and land surfaces. Used for monitoring of coastal zones, polar ice, sea ice, sea state, geological features, vegetation and land surface processes	*Waveband:* Microwave: C band 5.405 GHz: HH, VV, HV, VH polarisation includes fully polarimetric imaging modes, and leftand right-looking capability *Resolution:* Standard: 25 x 28 m (4 looks), Wide beam (1/2):48-30 x 28 m/ 32-25 x 28 m (4 looks), Fine resolution: 11-9 x 9m (1 look), ScanSAR (N/W): 50 x 50 m/ 100 x 100 m (2-4/4-8 looks), Extended (H/L): 22-19 x 28 m/ 63-28 x 28 m (4 looks) Ultrafine: 3 m *Swath:* Standard: 100 km (20-49deg), Wide beam (1/2): 165 km/ 150 km (20-31/ 31-39deg), Fine resolution: 45 km (37- 48deg), ScanSAR (W): 510 km (20-49deg), Extended (H/L): 75 km/170 km (50-60/ 10-23deg) Ultrafine: 10-20 km *Accuracy:* Geometric distortion: < 40 m, Radiometric: 1.0 dB
SAR (JERS)	JERS	Imaging radar	Map the topography and geological characteristics of the earth's surface. Also well suited to land based studies	Active L band *Swath width:* 75 km *Resolution:* 18 m x 18 m *Off nadir angle:* 35deg *Observation frequency:* 1,275MHz *Wavelength:* 235 mm
SAR (ERS)	ERS	Imaging radar	Meteorology, geology, vegetation change, crop monitoring, hydrology, land use, oeanography and glaciology	Active microwave sensor C band *Frequency:* 5.3 GHz *Wavelength:* 56 mm *Incidence Angle:* 23 deg (mid swath) *Polarisation:* VV *Swath width:* 100 km *Resolution*: 30 m (azimuth), 26.3 m (range)
SEVIRI Spinning Enhanced Visible and Infrared Imager	MSG-1, 2, 3	Imaging multi-spectral radiometer (vis/IR)	Measurements of cloud cover, cloud top height, precipitation, cloud motion, vegetation, radiation fluxes, convection, air mass analysis, cirrus cloud discrimination, tropopause monitoring, stability monitoring, total ozone and sea surface temparature	*Waveband:* VIS: 0.56-0.71 μm, 0.5-0.9 μm(broadband), NIR: 0.74-0.88 μm, SWIR 1.5-1.78 μm, SWIR: 3.48-4.36 μm, TIR: 5.35-7.15 μm, 6.85-7.85 μm, 8.3-9.1 μm, 9.38-9.94 μm, 9.8-11.8 μm, 11-13 μm, 12.4-14.46 μm *Resolution:* 1 km (at SSP) for one broadband visible channel HRV, 5 km (at SSP) for all other channels *Swath:* Full Earth disk *Accuracy*: Cloud cover: 10%, Cloud top height: 1 km, Cloud top temparature: 1 K, Cloud type: 8 classes, Surface temparature: 0.7-2.0 K, Specific humidity profile: 10%, Wind profile (horizontal component): 2-10 m/s, Long wave Earth surface radiation: 5 W/m^2

Instrument	Mission	Type	Measurements /application	Technical characteristics
TM Thematic Mapper	Landsat - 4, 5	High resolution imager	Measures surface radiance and emittance, land cover state and change (eg vegetation type). Used as multipurpose imagery for land applications	*Waveband:* VIS-TIR: 7 channels: 0.45-12.50 um *Resolution:* VIS-SWIR, 30 m; TIR: 120 m *Swath:* 185 km
VEGETATION	SPOT-4, 5	Imaging multi-spectral radiometer (vis/IR)	Data of use for crop forecast and monitoring, vegetation monitoring, and biosphere/ geosphere interaction studies	*Waveband:* Operational mode: VIS: 0.61-0.68 µm, NIR: 0.78-0.89 µm, SWIR: 1.58-1.75 µm, Experimental mode: VIS: 0.43-0.47 µm *Resolution:* 1.15 km at nadir - minimal variation for off-nadir viewing *Swath:* 2200 km
WAOSS-B Wide-Angle Opteoelectronic Stereo Scanner	BIRD	Imaging multispectral radiometer (vis/IR	Vegetation and Cloud coverage	*Waveband:* 1 x VIS: 600-670 nm, 1 x NIR: 840-900nm *Resolution:* 185 m *Swath:* 533 km
WiFS Wide Field Sensor	IRS-1C,D,P3,P4	Imaging multispectral radiometer (vis/IR)	Vegetation monitoring, environmental monitoring, drought monitoring, snow melt run-off forecasting, global green cover assessment, agro-climatic regional planning	*Waveband:* VIS: 0.62-0.68 µm NIR: 0.77-0.86 µm SWIR: 1.55-1.7µm (IRS P3 only) *Resolution:* 188 m *Swath:* 810 km
X-Band SAR X-Band Synthetic Aperture Radar	TerraSAR -X	Imaging radar	Provides images for monitoring of land surface and coastal processes and for agricultural, geological and hydrological applications. Instrument modes: Spotlight, Stripmap, ScanSAR	*Waveband:* Microwave: 9.6 GHz (X-band), 4 polarisation modes: HH, VV, HV, VH (selectable or twin) *Resolution:* Spotlight: 1, 2 m x 1-4 m, Stripmap: 3 m x 3-6 m, ScanSAR: 16m x 16m *Swath:* Spotlight: 5-10 km x 10 km, Stripmap: 30 km, ScanSAR: 100 km

Appendix 2---Image-based ground reflectance retrieval from the ASTER measurement

The different data of ASTER L1A and ASTER 1B need to be unified as quantitative ground reflectance from the digital number (DN) of the ASTER for improved interpretation and comparison. This appendix describes the algorithm to calculate the ground reflectance from ASTER 1A in the visible and near-infrared portion of the spectrum based on the experience of Landsat COST model. Sensor calibration, Sun elevation correction, Earth-Sun distance correction, and atmospheric correction are taken into account in the algorithm. The advantage of the developed algorithm is that no additional information other than those provided by the imagery itself is required.

Introduction

ASTER covers a wide spectral region with 14 bands from the visible to the thermal infrared with high spatial, spectral and radiometric resolution. It consists of three subsystems with different spatial resolution: VNIR (visible and near infrared - 0.55 to 0.80um) subsystem with 15-m resolution; SWIR (short wave infrared-1.65 to 2.4um) subsystem with 30-m resolution; and TIR (thermal infrared - 8.3 to 11.32um) subsystem with 90-m resolution (Yamaguchi *et al*., 1998). The bands are centered at approximately 0.56, 0.66, and 0.81 μm for the VNIR subsystem (with band passes of 0.08, 0.06, and 0.10 μm respectively); 1.65, 2.165, 2.205, 2.26, 2.330, 2.395 μm for the SWIR (with band passes of 0.10, 0.04, 0.04, 0.05, 0.07, and 0.07 μm); and 8.30, 8.65, 9.10, 10.60, 11.30 μm for the TIR (with band passes of 0.35, 0.35, 0.35, 0.70, and 0.70 μm). The bands and corresponding resolution are shown in **Table 1**.

Table 1. Spectral range and ground resolution for ASTER instruments

	VNIR	**SWIR**	**TIR**
Spectral Range	Band 1: 0.52 - 0.60 μm Nadir looking	Band 4: 1.600 - 1.700 μm	Band 10: 8.125 - 8.475 μm
	Band 2: 0.63 - 0.69 μm Nadir looking	Band 5: 2.145 - 2.185 μm	Band 11: 8.475 - 8.825 μm
	Band 3: 0.76 - 0.86 μm Nadir looking	Band 6: 2.185 - 2.225 μm	Band 12: 8.925 - 9.275 μm
	Band 3: 0.76 - 0.86 μm Backward looking	Band 7: 2.235 - 2.285 μm	Band 13: 10.25 - 10.95 μm
		Band 8: 2.295 - 2.365 μm	Band 14: 10.95 - 11.65 μm
		Band 9: 2.360 - 2.430 μm	
Ground Resolution	15 m	30m	90m

In remote sensing, any given digital image data set varies widely among sensors. Other things being equal, the radiance measured by any given system over a given object is influenced by such factors as changes in scene illumination, atmospheric conditions, viewing geometry, and instruments response characteristics. In the case of satellite sensing in the visible and near-infrared portion of the spectrum, it is often desirable to generate mosaics of images taken at different times or study the changes in the reflectance of ground features at different times or locations. In such applications, it is usually necessary to apply a Sun elevation correction and an Earth-Sun distance correction. The Sun elevation corrections accounts for the seasonal position of the Sun relatively to the Earth. Through this process, image data acquired under different solar illumination angles are normalized by calculating pixel brightness values assuming the Sun was at the zenith on each date of sensing. The correction is usually applied by dividing each pixel value in a scene by the sine of the solar elevation angle for the particular time and location of imaging. The Earth-Sun distance correction is applied to normalize for seasonal changes in the distance between the Earth and the Sun. The Earth-Sun distance is usually expressed in astronomical units. The irradiance from the Sun decreases as the square of the Earth-Sun distance. Furthermore, the influence of solar illumination variation is also compound by atmospheric effects. The "path radiance" effect introduces 'haze' in the imagery and reduces image contrast, so the haze compensation procedure should be designed to minimise the influence of 'path radiance' effect (Lillesand & Kiefer, 1994), and the image-based haze compensation (Chavez, 1996) has been widely used for this effect.

When comparing images from different sensors, image standardization is the fundamental step in putting image data from multiple sensors and platforms into a common radiometric scale, normalizing image pixel values for differences in Sun illumination geometry, atmospheric effects and instrument calibration. Proportional ground reflectance is the best unit for comparing the different sensors. First, the different instrument characteristics can be minimised; second, it compensates for different values of the exoatmospheric solar irradiances arising from spectral band differences; third, the atmosphere conditions when images are acquired at different times can be removed; and fourth, the satellite-Sun-object geometry influence to image information is decreased; fifth, Almost all of the canopy radiative transfer models that are used for inverting land surface biophysical parameters are based on surface reflectance(Liang *et al*., 2001).

ASTER L1B data are defined as "registered radiance at the sensor", however ASTER L1A data are defined as reconstructed, unprocessed instrument data at full resolution, and it consist of the image data, the radiometric coefficients, the geometric coefficients and other auxiliary data without applying the coefficients to the image data, thus maintaining original data values (Aster user handbook). The influence of scene illumination, atmospheric conditions, viewing geometry, and instruments response characteristics are therefore contained in ASTER L1A, which decreases the quality and limit the use.

In this study, the Landsat data were firstly converted to ground reflectance using the COST model whose details are described in the work of Chavez (1996), Markham & Barker (1986), and Moran *et al*. (1992) (http://support.erdas.com/downloads/models/user_models/user_model_2.html). Most of the ASTER data in the study are in L1A data and some of the data are in Level 1B data, and the comparison and interpretation between these two types data result in accuracy uncertainties, therefore they need to be unified. An algorithm was thus developed to retrieve the ground reflectance from the original satellite measurement of ASTER 1A based on the COST model experience of Landsat (Chavez, 1996). This algorithm is based on the parameters which are provided by the ASTER 1A data itself instead of other sources. It mainly consists of two steps: 1.) converting the DN of ASTER 1A to at-sensor radiance, namely converting ASTER L1A to ASTER L1B, and 2.) converting the at-sensor radiance to ground reflectance. In this method, the instruments response characteristics, scene illumination, viewing geometry, atmospheric conditions are considered.

Method

2.1 Instrument calibration--- Converting the DN of ASTER to at-sensor radiance

Radiometric correction data processing activity involved in many quantitative applications of digital image data is conversion of DNs to absolute radiance values. This operation accounts for the extraction form of the A-to-D response functions for a given sensor and is essential in applications where measurements of absolute radiance is required. ASTER 1A original DN can be converted to raw radiance using unit conversion coefficients which is defined as radiance per 1DN. Radiance (spectral radiance) is expressed in unit of W/(m^2•sr•μm), and the value can be obtained from DN values as follows,

$$\text{Radiance} = (DN_{value} - 1) \times \text{Unit conversion coefficient} \quad (1)$$

Unit conversion coefficients are provided by ASTER user handbook shown in **Table 2**. For each scene, specific conversion coefficients are bundled in each scene header file for its conversion.

Table 2. Unit conversion coefficients from ASTER bands and gain mode. Unit: (W/(m 2 *sr*μm)/DN)

Band No.	High gain	Normal gain	Low gain1	Low gain 2
1	0.676	1.688	2.25	N/A
2	0.708	1.415	1.89	N/A
3N	0.423	0.862	1.15	N/A
3B	0.423	0.862	1.15	N/A
4	0.1087	0.2174	0.290	0.290

Band No.	High gain	Normal gain	Low gain1	Low gain 2
5	0.0348	0.0696	0.0925	0.409
6	0.0313	0.0625	0.0830	0.390
7	0.0299	0.0597	0.0795	0.332
8	0.0209	0.0417	0.0556	0.245
9	0.0159	0.0318	0.0424	0.265
10	N/A	6.882×10^{-3}	N/A	N/A
11	N/A	6.780×10^{-3}	N/A	N/A
12	N/A	6.590×10^{-3}	N/A	N/A
13	N/A	5.693×10^{-3}	N/A	N/A
14	N/A	5.225×10^{-3}	N/A	N/A

Source: ASTER product user handbook

The resulted radiance from DN in equation 1 includes the radiometric artifacts (e.g. striping) caused from instrument system error. ASTER L1A data is bundled with the radiometric coefficients but without applying these coefficients to the image data. These coefficients can be extracted from Aster 1A itself and applied to correct the radiometric and produce the at-sensor radiance, which is an improved version of original radiance, using equations 2, 3 and 4.

To VNIR bands: $Lv = A_v * V / G_v + D_v$ (2)

To SWIR bands: $Ls = A_s * V / G_s + D_s$ (3)

To TIR bands: $Lt = C_0 + C_1 * V + C_2 * V * V$ (4)

Where V is each pixel DN value in 1A scene; Lv, Ls and Lt are at-sensor radiances for VNIR, SWIR and TIR channels respectively, Av; Gv and Dv are calibration coefficients for detectors of VNIR channels; As, Gs and Ds are calibration coefficients for detectors of SWIR channels; C_0, C_1 and C_2 are calibration coefficients for detectors of TIR channels. These coefficients are bundled with each band.

When the ASTER sensor acquire data from the Earth, scanned linear detector arrays for VNIR and SWIR subsystems are arranged one linear array for each band to obtain one line data in the cross-track, which means one line of image data of all VNIR/SWIR bands in the along-track direction are acquired by one detector because of pushbroom scanning method. For TIR subsystem ten detectors for each band are arranged to obtain ten lines in the cross-track direction for each scan period because of the whiskbroom scanning method. Therefore, when calibrating these bands using above equations, VNIR and SWIR detector calibrations are applied to each line in along-track direction; TIR detector calibration is repeatedly applied to every 10 lines in across-track direction. An Interactive Development Language (IDL) programming was developed to carry out the calibration. After the calculation, the level 1A raw digital numbers were converted to at-sensor radiance. TIR is used for

temperature instead of ground reflectance, so the followed processing is only applied to VNIR and SWIR.

2.2 Atmosphere correction--Converting the at-sensor radiance to ground reflectance

For relatively "clear" ASTER scenes, after the at-sensor radiance is calculated, it can be converted to a planetary or exoatmospheric reflectance through a normalization for solar irradiance using the below equation 5,

$$\rho_{AT\text{-}SENSOR} = \pi * d^2 * Lsat_{\lambda} / (ESUN_{\lambda} * \cos\theta) \quad (5)$$

where $\rho_{AT\text{-}SENSOR}$ is the anticipated at-sensor reflectance, Lsatλ is the at-sensor radiance resulted from radiometric correction processing; d is the Earth-Sun distance in astronomical units, which is presented in Table 3; θ is the Solar zenith angle in degrees which is a supplementary angle of solar elevation angle when the image were acquired. ESUNλ is the mean solar exoatmospheric spectral irradiance for ASTER which will be described later.

Table 3. Earth-Sun Distance in Astronomical Units for various days throughout a year

Julian Day	Distance	Julian Day	Distance	Julian Day	Distance	Julian Day	Distance	Julian Day	Distance
1	0.9832	74	0.9945	152	1.0140	227	1.0128	305	0.9925
15	0.9836	91	0.9993	166	1.0158	242	1.0092	319	0.9892
32	0.9853	106	1.0033	182	1.0167	258	1.0057	335	0.9860
46	0.9878	121	1.0076	196	1.0165	274	1.0011	349	0.9843
60	0.9909	135	1.0109	213	1.0149	288	0.9972	365	0.9833

Although the solar irradiance was normalised, the above converted reflectance still has the problem of atmospheric effect. Accurate atmospheric correction can remove the effects of changes in satellite-Sun geometry and atmospheric conditions (Teillet, 1992). Atmospherically corrected surface reflectance images improve the accuracy of surface type classification (Fraser *et al*., 1977; Kaufman, 1985) and are also a basis for estimating the radiation budget of the Earth (Kimes & Sellers, 1985). Full use of satellite data for agricultural resource management also requires atmospheric correction (Moran *et al*., 1990). However, the atmospheric correction for the VNIR and SWIR of the ASTER atmosphere team is based upon a LUT approach using results from a Gauss-Seidel iteration radiative transfer code (RTC) (ASTER user handbook), and this method currently assumes atmospheric scattering optical depths and aerosol parameters are known from outside sources. Using these parameters, a set of piecewise-linear fits are determined from the LUT that relate the measured at-sensor radiances to surface radiance and surface reflectance. The sources of this information are results from other AM-1 platform sensors such as the Multi-Angle Imaging Spectroradiometer (MISR) and

the MODIS or global assimilation model (GAM) results. Difficulties arise when these sources of information are not available. To the users of Aster 1A, collecting *in-situ* atmospheric measurements and radiometric transfer code (RTC) is normally difficult and more costly to implement. One popularly used means of atmospheric correction (Kaufman & Sendra, 1988; Kaufman *et al*., 2000; Liang *et al*., 1997; Teillet & Fedosejevs, 1995; Edirisinghe at al., 2001) in multispectral data is to observe the radiance recorded over target areas of essentially very low reflectance in the visible spectrum, namely dark-Object atmospheric correction method (Chavez, 1988).

The image-based atmospheric correction method based on Dark-Object theory can be used to remove the atmospheric effect, requiring no additional information other than that provided by the imagery. The first step of this method is to Compute haze correction coefficient for each band based on equation 6 (Chavez, 1996), and equation 7 is used to compute radiance of a dark object [assumed to have a reflectance of 1% by Chavez (1996) and Moran *et al*. (1992)] for each band.

$$L_{\lambda,HAZE} = L_{\lambda,MIN} - L_{\lambda,1\%} \quad (6)$$

in which

$$L_{\lambda,1\%} = 0.01 * ESUN_{\lambda} * COS^2 \theta / (\pi * D^2) \quad (7)$$

Where $L_{\lambda,MIN}$ is the corresponding radiance representing dark object, which normally has the lowest radiance, in the scene. The $l_{\lambda,min}$ choice will be the lowest value at the base of the slope of the histogram, where slope of the histogram begins to increase more dramatically.

After the haze correction coefficient is calculated, equation 8 instead of equation 5 is used to convert the at-sensor radiance to ground reflectance ρ_{GROUND} (Chavez, 1996):

$$\rho_{GROUND} = \pi * d^2 * (Lsat_{\lambda} - Lhaze_{\lambda}) / (ESUN_{\lambda} * \cos\theta * \cos\theta) \quad (8)$$

where the second cosθ in the equation is introduced for estimating the outgoing path of radiance affected by the atmosphere. In order to get the ground reflectance, the Exoatmospheric Spectral Irradiance (ESUNλ) for each ASTER VNIR and SWIR should be firstly produced. In our work, Solar Spectrum database used at the World Radiation Center was downloaded from ftp://ftp.pmodwrc.ch/pub/data/irradiance/spectral_irradiance/ and then they are used to calculate the ASTER Exoatmospheric Spectral Irradiance for each VNIR and SWIR channels. **Fig. 1** is the curve covering the ASTER VNIR and SWIR spectral range from this data source.

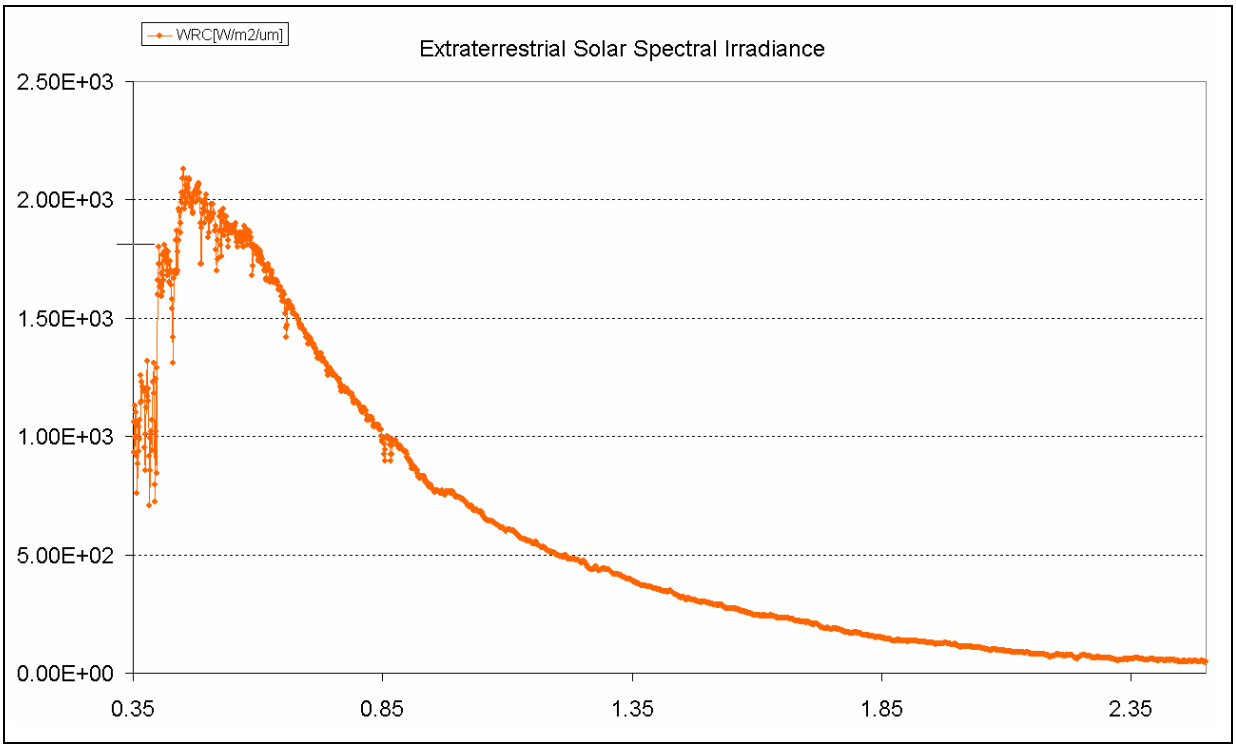

Fig. 1. The Exoatmospheric Spectral Irradiance curve (original data Source: WRC)

For each band, the Exoatmospheric Spectral Irradiance in this bandwidth was summarised and the mean value was calculated. The result is taken as the mean exoatmospheric Spectral Irradiance coefficient shown in **Table 4**.

Table 4. ASTER band and MEAN exoatmospheric Spectral Irradiance

Band NO.	Band width (μm)	WRC average ($W/m^2/um$)
VNIR01	0.52-0.60	1850
VNIR02	0.63-0.69	1560
VNIR3N	0.76-0.86	1110
VNIR3B	0.76-0.86	1110
SWIR04	1.600-1.700	233
SWIR05	2.145-2.185	80.1
SWIR06	2.185-2.225	74.7
SWIR07	2.235-2.285	68.7
SWIR08	2.295-2.365	60.0
SWIR09	2.360-2.430	57.3

3. Case study and result

The method described above is applied to the ASTER 1A archive. One ASTER 1A scene, which covers HeLan mountain of China acquired on 18 April 2001, has 4100 X 4200 DN value for VNIR

bands 1, 2 and 3N, and 2048 X 2100 DN value for SWIR bands 4, 5, 6, 7, 8 and 9; furthermore, 3 X 4100 coefficients for each VNIR and 3 X 2048 coefficients for each SWIR are bundled. The along-track direction is in the column, so each column would be converted using the same three coefficients (**Table 5**). TIR can not be used for the ground reflectance, but their radiometric correction is also shown in **Table 5**.

Table 5. The ASTER 1A data and the radiometric correction

Image dimension		Coefficientdimension		Data matrix	Radiometric correction method	Comments
Col	line	col	line			
4100	4200	3	4100	VNIRIMG[4100,4200] VNIRCOE[3,4100]	Lv(C,L)= VNIRIMG(C,L)*VNIRCOE(2,C)/ VNIRCOE(3,C)+ VNIRCOE(1,C)	Equation 2
2048	2100	3	2048	SWIRIMG[2048,2100] SWIRCOE[3,2048]	Ls(C,L)= SWIRIMG(C,L)*SWIRCOE(2,C)/ SWIRCOE(3,C)+ SWIRCOE(1,C)	Equation 3
700	700	3	10	TIRIMG[700,700] TIRCOE[3,10]	Lt(C,L)= TIRCOE(1,REST(L/10))+ TIRCOE(2, REST(L/10))*TIRIMG(C,L)+ TIRCOE(3, REST(L/10))* TIRIMG(C,L)* TIRIMG(C,L)	Equation 4 Rest calculates the rest of a division
*VNIR/SWIR data were scanned in pushbroom, TIR data were scanned in Whiskbroom; *The satellite flight direction is along column; *L(C,L) is the element of L matrix which column=C and line=L						

After this radiometric correction, the DN was converted to at-sensor radiance and the stripes in the original DN image will be removed. **Fig. 2** is one case which shows the improvement of the VNIR channel 1.

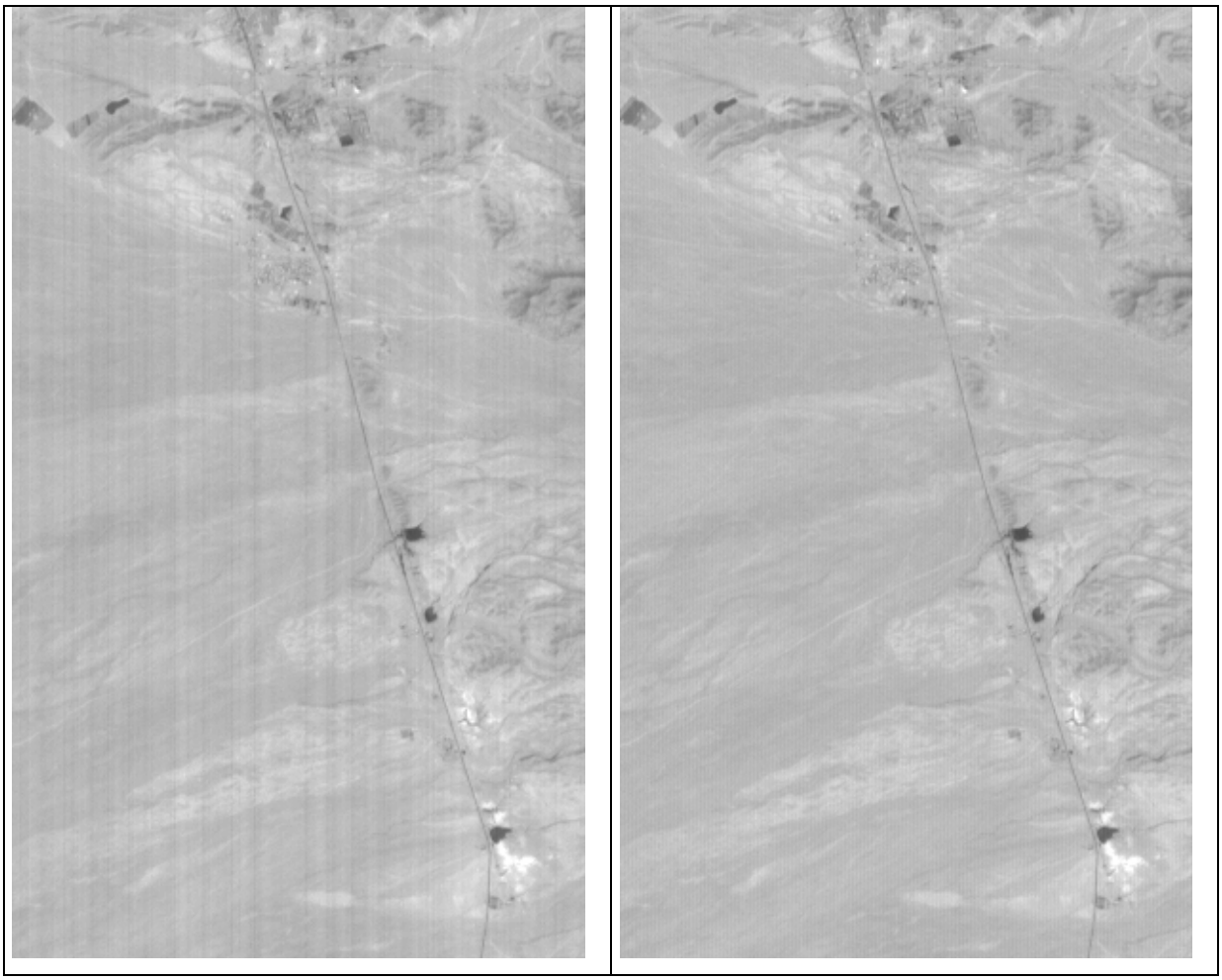

Fig. 2. The VNIR band 1 image (Comparison between before and after the calibration). The vertical stripe is removed after applying radiometric coefficients.

Equation 6 and 7 was used for converted the at-sensor radiance to ground reflectance. From **Table 3**, the Earth-Sun distance is about 1.0033, and the solar elevation angle 59.472389 from the header file was found. To determine the dark object at-sensor radiance, each band histogram was plotted and the value where slope of the histogram begins to increase dramatically was chosen for the $\mathbf{L_{\lambda,MIN}}$ in equation 6. **Fig. 3** shows the choice of 44.0754 as the $\mathbf{L_{\lambda,MIN}}$ for VNIR band 1.

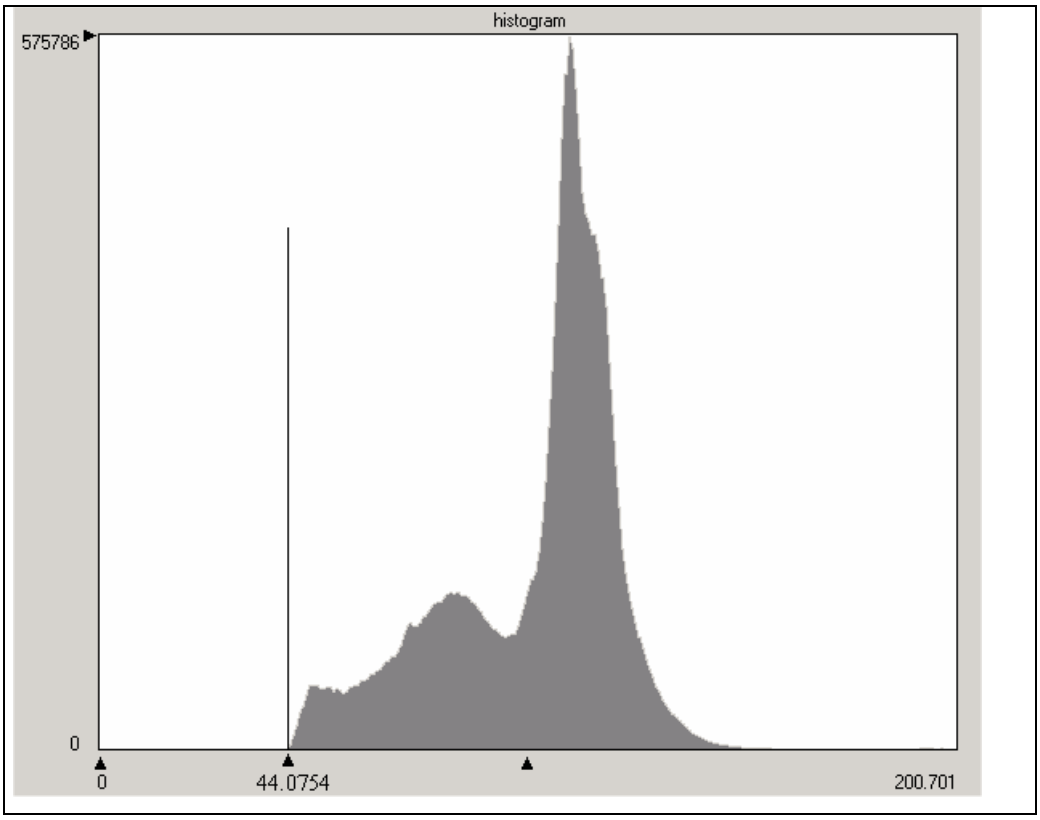

Fig. 3. The histogram of VNIR band1 for choosing the Lλ,min parameter

Table 6 summarized the relevant values in image-based atmospheric correction.

Table 6. Values used for image-based atmospheric correction of the case ASTER 1A scene acquired on April 18, 2001

	VNIR01 (0.52-0.60)	**VNIR02 (0.63-0.69)**	**VNIR03 (0.76-0.86)**	**SWIR04 (1.600-1.700)**	**SWIR05 (2.145-2.185)**	**SWIR06 (2.185-2.225)**	**SWIR07 (2.235-2.285)**	**SWIR08 (2.295-2.365)**	**SWIR09 (2.360-2.430)**
L~,min	44.0754	32.0838	38.3498	7.4959	2.3442	2.0245	1.8317	1.2868	1.1633
L~,1%	4.3406	3.6602	2.6044	0.5467	0.1879	0.1753	0.1612	0.1408	0.1344
L~,min -L~,1%	39.7348	28.4236	35.7454	6.9492	2.1562	1.8492	1.6705	1.1460	1.0288

After the Atmosphere correction, the influence of Atmosphere effect can be decreased, and the data quality can be improved. **Fig. 4** is the comparison between the at-sensor radiance color image and the ground reflectance color image.

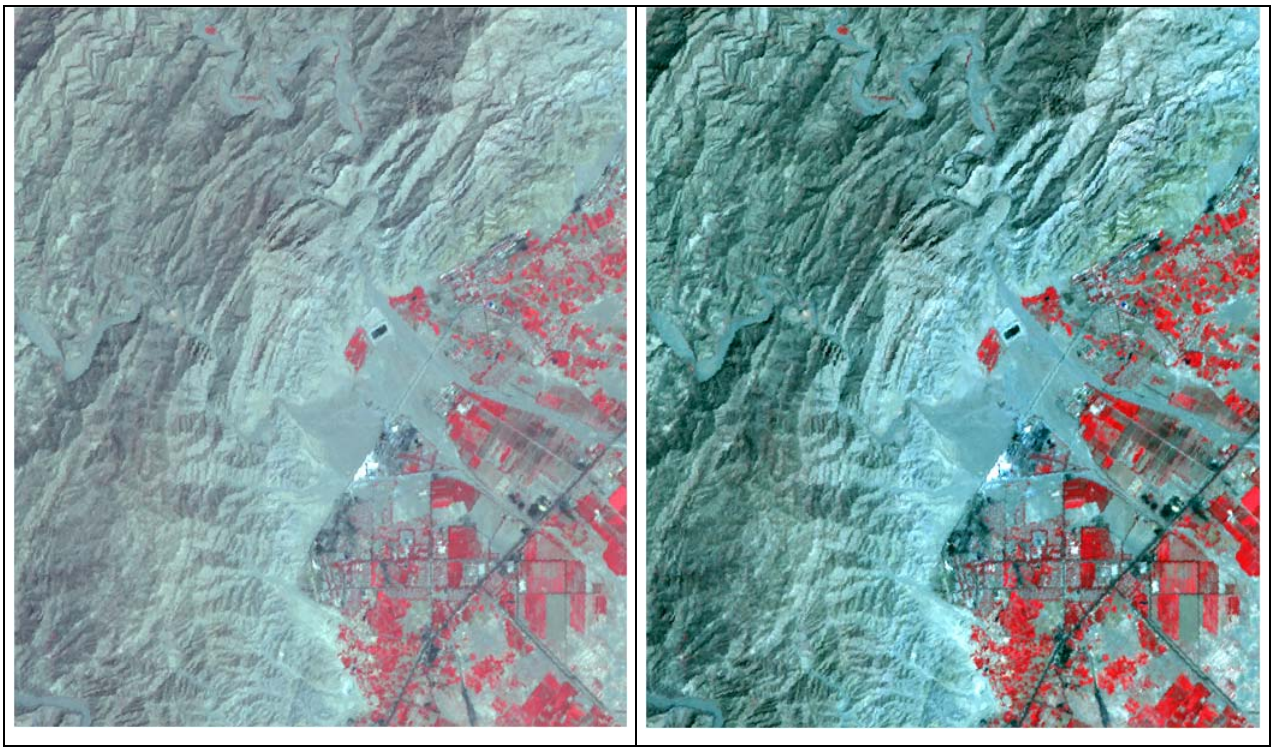

Fig. 4. The data quality improvement after calculating the ground reflectance from at-sensor radiance. Left is the ASTER VNIR at-sensor radiance color image (Red band3, Green band 2, Blue band 1), and right is the ASTER VNIR ground reflectance color image (Red band3, Green band 2, Blue band 1). Both image use standard-deviation histogram stretch.

4. Summary and discussion

With the characteristics of high spatial resolution, wide spectral range of visible, near IR, short wave IR and thermal IR, and stereo view in the same orbit, ASTER has provided information to complement data from other sensors to monitor the Earth. As a comparable radiometric scale, ground reflectance retrieval from ASTER is an important process for change detection using different sensors or mosaicing images taken at different times or locations. The factors such as instruments characteristics, viewing geometry, atmospheric conditions influence the satellite measurement of ASTER. The radiometric coefficients for each detector bundled with the original DN can be used to remove the stripes caused from the instrument characteristics. Solar elevation angle and Earth-Sun distance can be normalized using the solar angle and Earth-Sun distance for the particular time and location of imaging. To decrease the atmospheric conditions effect in ASTER, the haze compensation procedure is designed based on the dark-object atmospheric correction method. The advantage of the ground reflectance retrieval described above is that all the parameters adopted is easily available, thus the method is widely operational.

However, some points in the retrieval processing should be discussed here. In equation 8, the cosine of the solar zenith angle θ in the Chavez (1996) method for atmospheric correction is

introduced for estimating the outgoing path of radiance affected by the atmosphere. But some researches on Landsat TM/ETM$^+$ have indicated that cosθ overestimates the amount of outgoing radiance of affected by the atmosphere. This seems to be especially true when imagery was captured on especially clear days or when the solar zenith angle is high. The deviation of cosθ influence on ASTER correction was not studied in our work. Furthermore, the topography features also influence the satellite radiance, especially in the rugged mountainous area, because the flux of incident sunlight over a given area reaches a maximum when that area is oriented perpendicular to the Sun's rays. No matter the surface type or atmospheric conditions, if more light is incident upon a surface, more light will be scattered back into space (Reeder at al., 1999; Ekstrand, 1996). High-resolution digital elevation models provide a means to correct the data in a satellite image for the topographic effect. By calculating the slope and aspect of a surface, the Sun-surface-sensor orientation can be determined, and its effects can be estimated. ASTER provide a stereo pair of VNIR band 3, which can be used for extracting high resolution relative DEM and thus no other information is required for this topographic correction. The topographic influence was tried to correct based on the assumption that the surface is a lambertian, which reflects incident solar energy uniformly in all directions and that variations in reflectance are due to the amount of incident radiation, but the result always shows the overcorrection which occurs in areas with steep slopes oriented away from the Sun.

References

Chavez, P. S. (1988). An improved dark-object subtraction technique for atmospheric scattering correction of multispectral data. *Remote Sensing of Environment, 24,* 459-479.

Edirisinghe, A., Chapman, G. E. & Louis, J. P. (2001). A simplified method for retrieval of ground level reflectance of targets from airborne video imagery, *International Journal of Remote Sensing, 22(6),* 1127 – 1141.

Ekstrand, S. (1996). LANDSAT TM-based forest damage assessment: correction for topographic effects. *Photogrammetric Engineering & Remote Sensing, 62,* 151-161.

Fraser, R. S., Bahethi, O. P. & Al-Abbas, A. H. (1977). The effect of the atmosphere on the classification of satellite observations to identify surface features, *Remote Sensing of Environment*, *6,* 229-249.

Kaufman, Y. J. (1985). The atmospheric effect on the separability of field classes measured from satellites, *Remote Sensing of Environment, 18,* 21-34,.

Kaufman, Y. J. & Sendra, C. (1988). Automatic atmospheric correction, *International Journal of Remote Sensing, 9,* 1357–1381.

Kaufman, Y. J., Karnieli, A. & Tanre, D. (2000). Detection of dust over deserts using satellite data in the solar wavelengths, *IEEE Transaction on Geoscience and Remote Sensing, 38,* 525–531.

Kimes, D. S. & Sellers, P. J. (1985). Inferring hemispherical reflectance of the Earth's surface for global energy budgets from remotely sensed nadir or directional radiance values, *Remote Sensing of Environment, 18,* 205-223.

Liang, S., Fallah-Adl, H., Kalluri, S., JaJa, J., Kaufman, Y. & Town-shend, J. (1997). Development of an operational atmospheric correction algo-rithm for TM imagery, *Journal of Geophysical Research, 102,* 17 173–17 186.

Liang, S., Fang, H. & Chen, M. (2001). Atmospheric correction of Landsat ETM+ Land surface—Part I: methods. *IEEE transactions on Geoscience and remote sensing,39*, 2490-2498.

Moran, M. S., Jackson, R. D., Hart, G. F., Slater, P. N., Bartell, R. J., Biggar, S. F., Gellman, D. I. & Santer, (1990). Obtaining surface reflectance factors from atmospheric and view angle corrected SPOT-1 HRV data, *Remote Sensing of Environment,32,* 203-214.

Popp, T. (1995). Correcting atmospheric masking to retrieve the spectral albedo of land surface from satellite measurements, *International Journal of Remote Sensing,*16, 3483–3508.

Reeder, D., Bryant, E. & Birnie, R. (1999). Removing the topographic effect from digital satellite data, ERIM 13th International Conference on Applied Geologic Remote Sensing, Vancouver, Canada, March 3, 1999.

Smith, J. A., Lin, T. L. & Ranson, K. J. (1980). The Lambertian assumption and Landsat data. *Photogrammetric Engineering &Remote Sensing,46,* 1183-1189.

Teillet, P. M. (1992). An algorithm for the radiometric and atmospheric correction of AVHRR data in thesolar reflective, *Remote Sensing of Environment, 41,* 185-195.

Teillet, P. M. & Fedosejevs, G. (1995). On the dark target approach to atmo-spheric correction of remotely sensed data, *Canada Journal of Remote Sensing, 21,* 374–387.

ABBREVIATION

AATSR	Advanced Along-Track Scanning Radiometer
APP	Alternating Polarisation Precision
ASAR	Advanced Synthetic Aperture Radar
ASTER	Advanced Spaceborne Thermal Emission and Reflection
ATSR	Along Track Scanning Radiometer
AVHRR	Advanced Very High Resolution Radiometer
BIRD	Bi-spectral Infra-Red Detection
BRDF	Bidirectional Reflectance Distribution Function
C	Celsius, centigrade
CARPE	Central African Regional Program for the Environment
CCD	Charged Coupled Device
CO_2	Carbon Dioxide
DEM	Digital Elevation Model
DN	Digital Number
ECMWF	European Centre for Medium-term Weather Forecast
ENVISAT	Environmental Satellite
EOS	Earth Observing System
EROS	Earth Resources Observation System
ERS-1	European Remote-Sensing Satellite-1
ERS-2	European Remote-Sensing Satellite-2
ERTS	Earth Resources Technology Satellite
ESA	European Space Agency
ETM+	Enhanced Thematic Mapper Plus
FAO	Food and Agriculture Organization of the United Nations
GCP	Ground Control Point
GEMI	Global Environment Monitoring Index
GIS	Geographical Information System
GMS	Geostationary Meteorological Satellite
GPS	Global Positioning System
GTZ	GTZ (Deutsche Gesellschaft für technische Zusammenarbeit mbH)
HDF	Hierarchical Data Format
H	Horizontal
HIRS	High Resolution Infrared Radiation Sounder
HTE	High Temperature Events
ICSU	International Council of Scientific Unions
IDL	Interactive Development Language
IFOV	Instantaneous Field of View
IGBP	International Geosphere - Biosphere Programme
IIASA	International Institute for Advanced Systems Analysis
IPCC	Intergovernmental Panel on Climate Change
JERS-1	Japanese Earth Remote-sensing Satellite-1
Kg	Kilogram
Km	Kilometer
Landsat	Land Remote Sensing Satellite
LCCS	Land Cover Classification System
LUT	LookUp Table
MERIS	MEdium Resolution Imaging Spectrometer
MIR	Middle Infrared Red

MISR	Multi-Angle Imaging Spectroradiometer
MODIS	Moderate Resolution Imaging Spectroradiometer
MSG	Meteosat Second Generation
MSS	Multispectral Scanner (Landsat)
MVC	Maximal Value Composition
NASA	National Aeronautics and Space Administration (US)
NDVI	Normalized Difference Vegetation Index
NIR	Near InfraRed
NOAA	National Oceanic and Atmospheric Administration
OLS	Operational Linescan System
PAN	panchromatic
PCA	Principle Component Analysis
Radarsat	Canadian Synthetic Aperture Radar Satellite
ROI	Region of Interest
RMS	Root-Mean-Square
RTC	Radiative Transfer Code
SAA	Solar Azimuth Angle
SAR	Synthetic Aperture Radar
SeaWiFS	Sea-viewing Wide Field of View Sensor
SEVIRI	Spinning Enhanced Visible and Infrared Imager
SMAC	Simplified Method for Atmospheric Correction
SNP	Salonga National Park
SPOT	System Probatoire pour l'Observation de la Terre
SRTM	Shuttle Radar Topography Mission
SWIR	Short Wave Infrared
SZA	Solar Zenith Angle
TIR	Thermal InfraRed
TM	Thematic Mapper
TREES	Tropical Ecosystem Environment Observations by Satellites
TRMM	Tropical Rainfall Measuring Mission
UN	United Nations
UNCED	United Nations Conference on Environment and Development
UNCOD	United Nations Conference on Desertification
UNEP	United Nations Environment Programme
UNESCO	United Nations Educational Scientific, and Cultural Organization
USGS	United States Geological Survey
UTM	Universal Transverse Mercator
V	Vertical
VAS	Visible Infrared Spin Scan Radiometer Atmospheric Sounder
VCF	Vegetation Continuous Fiels
VI	Vegetation Index/Indices
VIRS	Visible and InfraRed Scanner
VIS	Visible
VNIR	Visible Near InfraRed
VAA	View Azimuth Angle
VZA	View Zenith Angle
WAOSS	Wide-Angle Optoelectronic Stereo Scanner
WRC	World Radiation Center
WSM	Wide Swath Mode

PUBLICATIONS

[1] Shengli Huang, Florian Siegert, 2004. ENVISAT multisensor data for fire monitoring and impact assessment. *International Journal of Remote Sensing, 25(20),* 4411–4416.

[2] Shengli Huang, Florian Siegert, 2004. Envisat ASAR wide swath backscatter dynamics of the Siberia boreal forest fire scar. In Proceedings of Envisat 2004 Symposium, Salzburg, Austria, 6-10 September, 2004.

[3] Florian Siegert, Shengli Huang, 2004. Large-scale forest fires in Siberia analysed by MODIS, MERIS and ASTER multiresolution satellite imagery. In Proceedings of Envisat 2004 Symposium, Salzburg, Austria, 6-10 September, 2004.

[4] Shengli Huang, Florian Siegert, 2004. Observation of Siberian fire-disturbed forests in ENVISAT ASAR wide swath images. *Remote Sensing of Environment*, (revised and re-submitted).

[5] Shengli Huang, Florian Siegert, Andreas Langner, 2004. Multisource data combination for the assessment on Salonga National Park. *International Journal of Applied Earth Observation and Geoinformation*, in preparation.

[6] Florian Siegert, Shengli Huang, Johann G. Goldammer and Anatoly I. Sukhinin, 2004. Exceptionally large fire damage and carbon release by large-scale wildfires in South-Siberia in 2003. *Global Biogeochemical Cycles,* in review.

[7] Shengli Huang, Florian Siegert, 2004. Land cover classification optimized to detect areas at risk of desertification in North China based on SPOT VEGETATION imagery, *Journal of Arid Environment,* in review.

[8]Envisat focuses on carbon-rich peat swamp forest fires, European Space Agency Press, 6 August 2003, available at http://www.esa.int/export/esaEO/SEMRA7YO4HD_index_0.html

CURRICULUM VITAE

Name: Shengli Huang **Date of birth**: 4 December 1972
Sex: male **Nationality**: Chinese
Email: huang@rssgmbh.com **Tel**: 0049-(0)89-48954766
Address: Am Schaeferanger 9 / 302, D-85764, Oberschleissheim, Germany

EDUCATION

10/2001-12/2004: Second PhD study of biology in 1.)Biology department and Geobio center of Munich University. Thesis title is "the potential of multi-sensor satellite data for applications in environmental monitoring with special emphasis on land cover mapping, desertification monitoring and fire detection". (munich of germany);

10/2000-12/2000: Special course "crop monitoring" in International Institute for Geo-information Science and Earth Observation. (Enschede of Netherlands);

9/1995-9/2000: Master and Doctor of ecology, in 1.) graduate school of University of Science and Technology of China & Chinese Academy of Sciences (CAS); 2.)Land resources division, commission for integrated survey of natural resources, State Planning Commission and CAS; 3.)Centre for earth sciences data and information network, institute of geographical sciences and natural resources research, CAS. The thesis title is "Ecological diagnosis information system for Chinese agriculture resources sustainable development". (Beijing of China);

9/1991-7/1995: Bachelor degree of geography, in geography department of Anhui Normal University. The thesis title is "Agriculture development and ecology restoration in subtropical mountain area of south Anhui province". (Anhui of China).

WORKING EXPERIENCES

10/2001-12/2004: Scientist, Remote Sensing Solutions GmbH, Munich, Germany.

8/2000-9/2001: Project manager, Beijing Huanqiu Mechanical & Electronic High Technology Co. Ltd.

9/1996-8/1997: Research assistant, Synthesis research center of Chinese Ecosystem Research Network, Chinese Academy of Sciences.

5/1995-7/1995: Teaching practice, the first middle school of Wuhu city, Anhui province;

COMPUTER SKILLS [1]-basic, [5]-very good

[1] GIS: ArcInfo[4], Arcview[5], Mapinfo[3], Genamap[1]
[2] Remote sensing: ENVI[5], Erdas Imagine[5], Ermapper[3], PCI[1], Ecognition [4]
[3] Database: Sybase[3], SQL[3]
[4] Programming language: IDL[3], C[4], Perl[4], Java[3]
[5] Network: HTML[4], VRML[4], CGI[4]
[6] Image processing: PhotoShop, PaintShopPro, 3D TerriVision, 3D Terragen
[7] Operating system: Windows, Sun Solaris Unix

LANGUAGES

Chinese [Native Language] English [Fluent] German [Basic]

PROJECT EXPERIENCES

5/2004-Present: land cover mapping and photosynthesis monitoring in Gabun of Africa.

My task: Classify Gabun and monitor the photosynthesis activity using multiresolution data of Landsat, MERIS and ASAR (IMP and WSM).

1/2003-11/2004: Envisat data investigation for fire events in Siberia and Indonesia.

My task: Comparing AATSR, AVHRR and MODIS hotspots in Indonesia; Processing ASAR (WSM and APP) for impact assessment; Investigating MERIS full resolution images and ASAR (WSM) backscatters for boreal fire scar detection; Investigating the relation among the MODIS hotspots, ASTER and MERIS and using these multisensor data for fire monitoring and carbon release estimation.

8/2002-10/2004: Hotspots detection in tropical forest.

My task: Combining different kinds of data (MODIS, BIRD, Landsat, GPS, GIS data and ground survey data) for monitoring the fire progress (based on hotspot detection) and fire damage (based on land cover change detection).

2/2004-4/2004: Information system for fire monitoring and assessment in Indonesia.

My task: Developing an ERDAS interface information system using Macro Language (EML) and Spatial Modeler Language (SML) for IFFM (http://www.iffm.org/). The main functions include: Projection conversion, cloud masking, NOAA hotspots automatical detection, Maximal NDVI composition.

11/2002-5/2003. Multiresolution 3D interactive information system.

My task: Developing a pilot system for integrating multiresolution data (Aerial photo, IRS, Landsat, MODIS, SPOT VEGETATION) into a 3D interactive system.

11/2002-5/2003: National park mapping in Salonga of Africa.

My task: Processing Landsat ETM data for classification and evaluating the classification accuracy with survey Video and on-site images (GPS supported).

10/2001-5/2003: Time series SPOT VEGETATION for land cover and desertification monitoring in North China.

My task: Processing 365 SPOT VEGETATION for time series 10-day composites images and NDVI; Developing an expert system for land cover classification and assessing the accuracy based on ASTER and GPS-supported ground survey; Identifying the risk area of desertification; IDL programming for calibrating ASTER 1A to ASTER1B and classifying HeLan mountain land cover based on objective-oriented Ecognition software.

4/1999-12/2000: Monitoring and management information system for 3-north protection forest of China.

My task: Invited by GTZ (Deutsche Gesellschaft fuer Technische Zusammenarbeit GmbH), consulting on user requirement investigation and analysis report; General system designing and technical supporting for applying Remote Sensing, GIS, DB, GPS, INTERNET to monitor and manage the protection forest resources change and ecological environment evaluation.

10/1997-8/2000: Information system for Chinese agricultural resources data sharing.

My task: Supervision on data quality; Developing information system (WEBGIS development using JAVA language, database querying using PERL language through CGI, Remote sensing model calculation in Client-Server mode, 3D visualisation based on VRML) for data sharing in INTRANET.

11/1996-1/2001 : Crop monitoring and yield estimation using Remote Sensing, GIS and GPS.

My task: Land resources survey and assessment; C-Language programming for China-formatted NOAA AVHRR 1B processing (Radiation-Correcting, Geo-correcting); Developing models of crop monitoring and yield estimation; Integrating the data of Remote sensing, GPS, GIS for implement.

10/1996-5/1998 : “Management information system for land resources of China based on 1:1M map”.

My task: Digitising, editing, projecting, matching 4 land maps in Arcinfo software; Establishing attribute database for corresponding land unit; Assisting in system development in Unix environment (AML language).

PUBLICATIONS AND REPORTS

[1] Shengli Huang, Florian Siegert, 2004. Envisat ASAR wide swath backscatter dynamics of the Siberia boreal forest fire scar. In Proceedings of Envisat 2004 Symposium, Salzburg, Austria, 6-10 September, 2004.

[2] Florian Siegert, Shengli Huang, 2004. Large-scale forest fires in Siberia analysed by MODIS, MERIS and ASTER multiresolution satellite imagery. In Proceedings of Envisat 2004 Symposium, Salzburg, Austria, 6-10 September, 2004.

[3] Shengli Huang, Florian Siegert, 2004. Observation of Siberian fire-disturbed forests in ENVISAT ASAR wide swath images. *Remote sensing of environment*, (revised and re-submitted).

[4] Shengli Huang, Florian Siegert, Andreas Langner, 2004. Multisource data combination for the assessment on Salonga National Park. *International Journal of Applied Earth Observation and Geoinformation*, in preparation.
[5] Florian Siegert, Shengli Huang, Johann G. Goldammer and Anatoly I. Sukhinin, 2004. Exceptionally large fire damage and carbon release by large-scale wildfires in South-Siberia in 2003. *Global Biogeochemical Cycles,* in review.
[6] Shengli Huang, Florian Siegert, 2004. ENVISAT multisensor data for fire monitoring and impact assessment. *International Journal of Remote Sensing*, 25(20), 4411–4416.
[7] Shengli Huang, Florian Siegert, 2004. Land cover classification optimized to detect areas at risk of desertification in North China based on SPOT VEGETATION imagery, *Journal of Arid Environment,* in review.
[8] Shengli Huang, Yue Yanzhen, 1998. Land resources grade evaluation of Anhui province under the support of geographyical information system. In: Poh-Chin Lai(ed.), Proceedings of international Conference on Modeling Geographical And Environmental Systems with GIS. Department of Geography, The Chinese University of HongKong, 363-367
[9] Shengli Huang, Jiulin Sun, 1998. Wheat area estimation through remote sensing and GIS. In: Poh-Chin Lai(ed.), Proceedings of international Conference on Modeling Geographical And Environmental Systems with GIS. Department of Geography, The Chinese University of HongKong, 722-727.
[10] Shengli Huang, Yanzhen Yue, 1998. Main technique of WebGIS for scientifical database. In: Li Wangping(ed.), Scientific Database And Information Technology. Science press, 199-203. (In Chinese)
[11] Shengli Huang, 1998. Establishment of the WWW information system for Chinese agriculture resource. *Computer Journal of China*, 23B. (In Chinese)
[12] Shengli Huang, Maoxin Wang, 1998. Radiation correction of AVHRR image. *Remote Sensing Information,* 52:20-22. (In Chinese)
[13] Shengli Huang, 1998. Land management information system using GIS and INTERNET. *China Land Science*, 12(5):39-41. (In Chinese)
[14] Shengli Huang, Jinming Hu, 2000. Quantitative evaluation of regional resources' advantage. *Resources Science,* 15(1):23-28. (In Chinese)
[15] Shengli Huang, Jinmin Hu, 2000. Analysis between population and ecology pressure of China. *Population, Resources and Environment of China,* 10(1):34-37. (In Chinese)
[16] Shengli Huang, 2000. Eco-environment Assessment of Agricultural Resources' Integrated Development. *Environment Sciences Research,* 10(1):45-48. (In Chinese)
[17] Shengli Huang, Forian Siegert. Report to IFFM project: Hotspot processing of NOAA AVHRR imagery in fire monitoring system in Indonesiea. March 2004
[18] Shengli Huang, Florian Siegert. Report to The Institut Congolais pour la Conservation de la Nature (ICCN): Assessment of land cover and land use in the Salonga National Park based on satellite imagery. March 2003.
[19] Shengli Huang, Florian Siegert. Report to Joint Research Center of EU: Global Land Cover mapping for the year 2000 (GLC2000)--North China. April 2003.
[20] Shengli Huang, Florian Siegert. Report to European Space Agency (ESA): Production of public relations material illustrating the multisensor fire monitoring capability of ENVISAT. November 2003. *Offer No: 08-03/ENVISAT-Siberia*
[21] Shengli Huang, Florian Siegert. Report to European Space Agency: Demonstration of the ENVISAT multisensor fire monitoring capability. June 2003. *Offer No: 08-02/ESA ENVISAT*
[22]Envisat focuses on carbon-rich peat swamp forest fires, ESA press, 6 August 2003, available http://www.esa.int/export/esaEO/SEMRA7YO4HD_index_0.html

PROFESSIONAL AFFILIATIONS

[1] IEEE Geoscience and Remote Sensing Society
[2] Deutsche Gesellschaft für Photogrammetrie, Fernerkundung und Geoinformation e.V. (German society of photogrammetry, remote sensing and geoinformation)

EHRENWÖRTLICHE VERSICHERUNG

Ich versichere hiermit ehrenwörtlich, dass die vorgelegte Dissertation von mir selbständig und ohne unerlaubte Beihilfe angefertigt ist.

München, den ....

(Unterschrift)

Erklärung

Hiermit erkläre ich, *

- dass ich mich anderweitig einer Doktorprüfung ohne Erfolg **nicht** unterzogen habe.

- dass ich mich mit Erfolg der Doktorprüfung im Hauptfach .....Ecology.....
und in den Nebenfächern .....Geography.....
bei der Fakultät für …….Geography and Natural Resources Research.....
der ..Chinese Academy of Sciences.....
(Hochschule/Universität)
unterzogen habe.

- dass ich ohne Erfolg versucht habe, eine Dissertation einzureichen oder mich der Doktorprüfung zu unterziehen.

München, den..... .....
(Unterschrift)

*) Nichtzutreffendes streichen